BULLETIN OF THE EARTHQUAKE RESEARCH INSTITUTE,
UNIVERSITY OF TOKYO. Vol. 39, Part 2. June, 1961.

東京大学
地震研究所彙報

第 39 号　第 2 册

昭和 36 年 6 月

目　次

論文及報告

頁

6. 地球熱学（第7報）海底地温勾配測定装置（英文）……上田誠也・友田好文・宝来一雄・金森博雄・淵秀隆 115
7. 火砕流堆積物の組織的性質（英文）……村井勇 133
8. レーリー波位相速度法による日本の地下構造の研究 第1報（英文）……安芸敬一 255
9. 御母衣爆破地震動観測による日本中部の地殻構造
第1部 御母衣爆破地震動の観測（英文）……爆破地震動研究グループ 285
10. 御母衣爆破地震動観測による日本中部の地殻構造
第2部 地殻構造について（英文）……三雲健・大塚道男・宇津徳治・寺島敦・岡田惇 327
11. 静岡県御前崎沖（御前岩）における波浪観測（序報）（邦文）……高橋竜太郎・羽鳥徳太郎 351

所　報

(The titles in occidental languages are given on the back cover.)

地震研究所彙報は，年4回定期に（ただし，第1号より第6号までは不定期に，第7号は3冊として刊行された），彙報別冊は不定期に刊行される．

この彙報に載せられた論文及び報告についての責任は，すべてその著者のみにある．

この彙報についての照会通信は，すべて東京大学地震研究所長にあてられたい．

The Bulletin is published quarterly. (Vols. 1-6 were published at irregular intervals and Vol. 7 consisted of three parts.)
Supplementary Volume is published at irregular interval.

The authors of the papers alone are responsible for the statements and opinions contained in their respective papers.

All communications relating to this Bulletin should be addressed to the Director of the Earthquake Research Institute, University of Tokyo, Japan.

Earthquake Research Institute, University of Tokyo
Address:
No. 1, Motofuji-cho, Bunkyo-ku,
Tokyo Metropolis, Japan.
Telephone: 921-3161-Extension 6506
Cable address: ZISINKEN, TOKYO.

東京大学地震研究所
所在地
東京都文京区本富士町一番地
電話 小石川 921—3161 (代) 構内 6506
電略 ブンケウ トウダイ ヂシン

Bulletin of the Earthquake Research Institute
Vol. 39 (1961), pp. 115-131

6. *Studies of the Thermal State of the Earth. The Seventh Paper: A Sea Bottom Thermogradmeter.*

By Seiya Uyeda and Yoshibumi Tomoda,

Earthquake Research Institute:

Ki-iti Hôrai and Hiroo Kanamori,

Graduate School, University of Tokyo

and

Hidetaka Futi,

Japan Meteorological Agency.

(Read December 20, 1960.—Received March 31, 1961.)

Summary

An apparatus for measuring the geothermal gradient in the sea bottom, or a sea bottom thermogradmeter, has been constructed. The apparatus consists of a probe containing two pairs of thermistors and a recorder set in a pressure tight and water proof steel container. Each of the pairs of the thermistors forms the two arms of an A.C. bridge. The other two arms of the bridge comprise a continuous potentiometer. Signals from the two A.C. bridges consisting of two pairs of thermistors and two potentiometers are separately amplified through amplifiers X and Y.

As the potentiometers rotate coaxially at the same speed as the recording drum, the phase angle of the output signal of the amplifier changes 180° when the potentiometer passes its balancing position. Therefore, as far as the phase angle is concerned, the output signal can be represented logically. It is the same for the output signal of the other amplifier. The output signals of the amplifiers X and Y are fed to an "and" gate circuit. The output signals of the gate circuit trigger the relay, and the contact of the relay makes or breakes when the potentiometers pass through their balancing positions, which give marks on the facsimile paper on the drum. Two pairs of thermistors give the temperature differences between the bottom and the top, and between the bottom and the middle point of the probe. The temperature differences ranging from 0°~2°C can be recorded on the paper with an accuracy of 0.001°C for about 2.5 hours.

Some preliminary experiments indicated that the apparatus will serve for determining the terrestrial heat flow through the sea bottom.

1. Introduction

Measurement of the terrestrial heat flow through the ocean floor has been carried out both in the Atlantic and Pacific Oceans[1),2),3)]. The pioneering work by Bullard, Maxwell and Revelle showed that the heat flow in the oceanic area is almost equal in amount to that in the continental area. This result, being in sharp disagreement with general expectations, seems to indicate that the mantle beneath the oceans may be quite different thermally from the mantle beneath the continents. More spectacular results have been reported by Herzen recently. Herzen's results for the south-eastern part of the Pacific showed a remarkable geographical distribution of the heat flow for which the only reasonable explanation appears to be the existence of thermal convection in the mantle[3),4)].

The Japanese Islands form one of the most active parts of the island arcs around the Pacific Ocean with regard to seismicity, volcanicity and recent orogenesis. In the hope of contributing to the clarification of the mechanism of these activities, we have conducted measuring activities of the terrestrial heat flow over the Japanese Islands since 1958[5),6),7)]. We have also wished to take measurements in the oceanic area surrounding Japan. Recently, the m.s. "Ryofu Maru" of the Japan Meteorological Agency has been equipped with a 13,000 m long tapered wire with a powerful winch and the Deep-Sea Research Committee has been organized by the Japan Society for the Promotion of Science[8)]. The Committee plans to measure the heat flow through the ocean floor as a part of its research project. The work was started in 1960 with the construction of the necessary instruments. The present report gives an account of thermogradmeter built to this end.

1) E. C. BULLARD, *Proc. Roy. Soc. A*, **222** (1954), 408.

2) E. C. BULLARD, A. E. MAXWELL and R. REVELLE, *Adv, Geophys., III* (1956), 153.

3) R. von. HERZEN, *Nature*, **183** (1959), 882.

4) T. RIKITAKE and K. HÔRAI, *Bull. Earthq. Res. Inst.*, **38** (1960), 403.

5) R. UYEDA, T. YUKUTAKE and I. TANAOKA, *Bull. Earthq. Res. Inst.*, **37** (1958), 251.

6) K. HÔRAI, *Bull. Earthq. Res. Inst.*, **37** (1959), 571.

7) S. UYEDA and K. HÔRAI, *Bull. Earthq. Res. Inst.*, **38** (1960), 421.

8) K. TERADA and H. FUTI, *Reports of Japanese Expeditions of Deep-Sea*, **1** (1960): *Oceanogr. Mag.* **11** (1960), 145.

2. General Description

The terrestrial heat flow, Q, may be obtained from measurements of the geothermal gradient, $\Delta T/\Delta h$, and the thermal conductivity, K, of the strata concerned, namely,

$$Q = K \cdot \Delta T/\Delta h \qquad (Q \text{ in cal/cm}^2\text{sec}, K \text{ in cal/cm sec deg. C}, T \text{ in deg. C and the depth } h \text{ in cm.})$$

The quantity $\Delta T/\Delta h$ at the sea bottom can be measured by thermistors placed in the tube penetrating vertically into the bottom. The constancy of the temperature at deep bottom[9] enables us to measure $\Delta T/\Delta h$ at the surface of the sea bottom, whereas $\Delta T/\Delta h$ on land has to be measured fairly

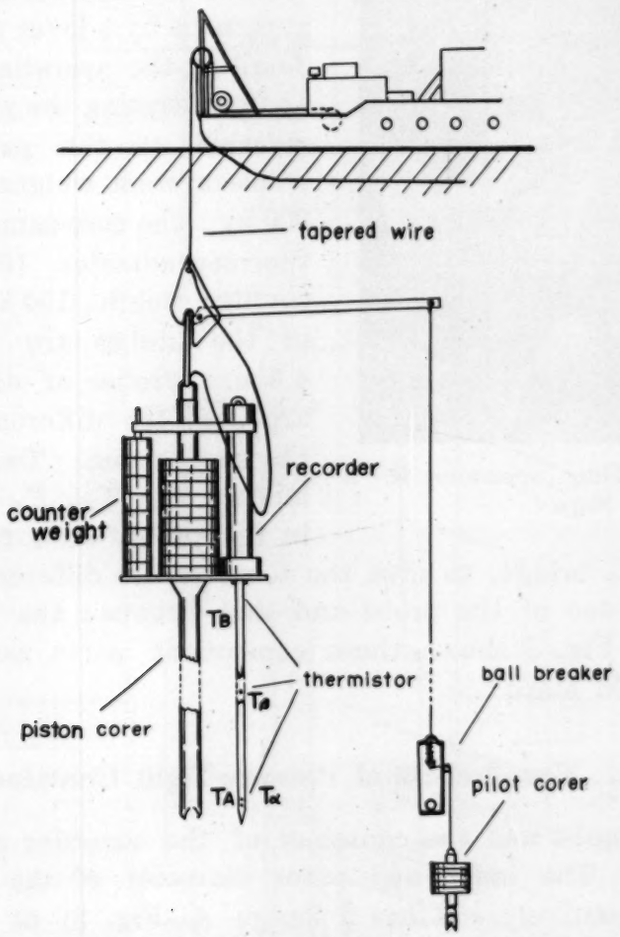

Fig. 1. Schematic diagram showing the operation of apparatus R. 1.

9) J. MASUZAWA, *presented at the annual meeting of Japan Oceanographical Society, November*, 1960 or W. S. WOOSTER and G. H. VOLKMANN, *Jour. Geophys. Res.*, **65** (1960), 1239.

deep below the surface. K is measured in laboratory by usual method[10] from the specimens of the bottom sediments obtained by a core-sampler.

The general layout of apparatus No. 1 (R. 1) is as shown in Fig. 1. The probe and the recorder are attachable to a piston-core-sampler, so that the core specimens can be obtained right on the spot, where the thermal gradient is measured, in one operation. To help in the penetration of the probe and the corer, the whole apparatus is allowed to fall freely for several meters when the pilot corer touches the bottom and unhooks the apparatus by a lever device. For the detail of the operation of unhooking and penetrating the probe readers are referred to the papers[11),12)]. The whole system weighs approximately 800 kg : the core-sampler 550 kg, the thermogradmeter 100 kg, and the counter weight 150 kg. The length of the probes are 1.5 m, 3 m and 4.5 m. Probes of different lengths are used for different conditions of the sea bottom. Two pairs of thermistors $T_A - T_B$, $T_\alpha - T_\beta$ are placed in the probe, each forming the two arms of an A.C. bridge, to give the temperature difference between the bottom and the top of the probe and that between the bottom and the middle point. Fig. 2 shows these component parts assembled aboard the m.s. "Ryofu Maru".

Fig. 2. Assembling apparatus R. 1. aboard the "Ryofu Maru".

3. The Probe and Pressure-Tight Container

The steel probe and the container of the recorder are as shown in Figs. 3 and 4. The inner and outer diameter of the probe is 15 mm and 25 mm respectively. It has a flange A (Fig. 3) at the top which presses the rubber packing B against the lid C. In order to accomplish

10) *loc. cit.*, (1) and (5).
11) *loc. cit.*, (1).
12) *loc. cit.*, (2).

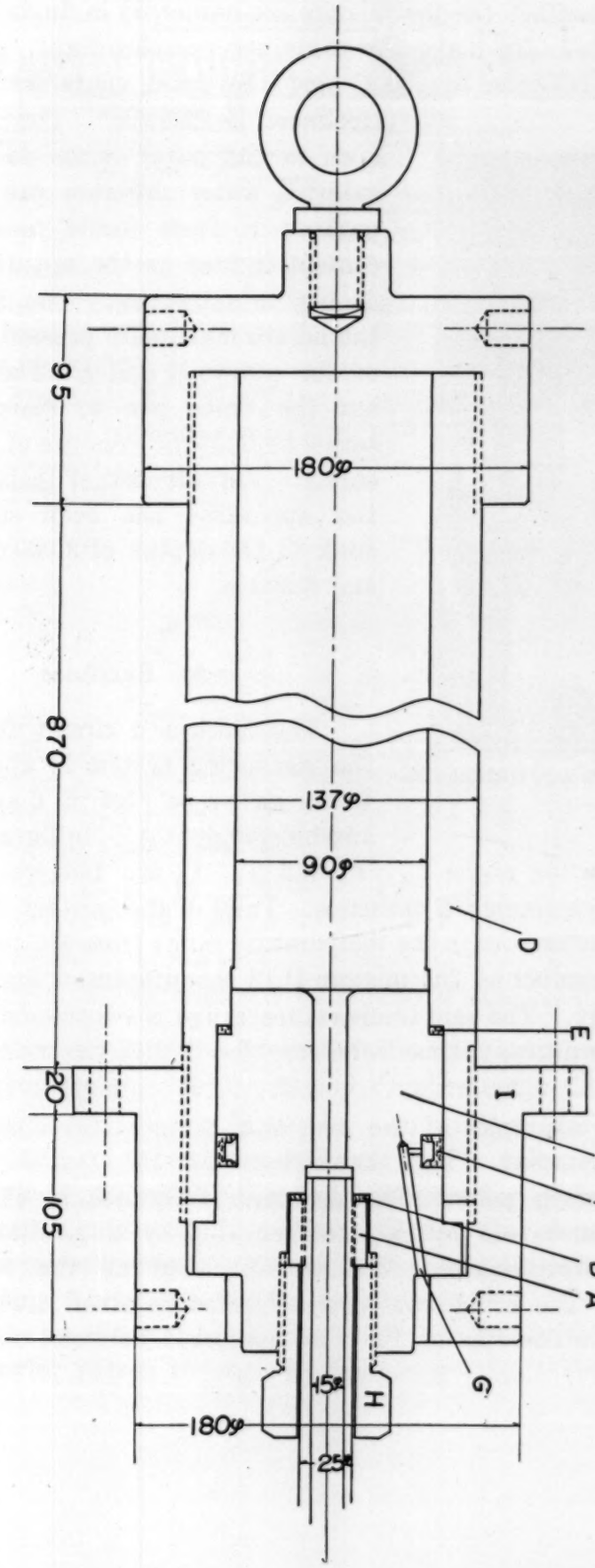

Fig. 3. Plan of the pressure-tight container of apparatus R. 1.

a better thermal contact the thermistors are immersed in fluidal paraphin which fills the tube. To make the container pressure-tight, packing E and F are placed between the lid C and the main container D whose thickness is 23.5 mm. The hole G is open to the outer space so that the external water pressure can push the packing F from inside to make the contact tighter as the apparatus sinks deeper into the sea. The probe and the lid are mannually pressed by means of the screws H and I. The container and the probe are to stand the external hydrostatic pressure of 1,000 bars safely. On our actual tests to date, the apparatus has been successfully sunk to the depths of 3,000 m, 5,040 m and 5,400 m.

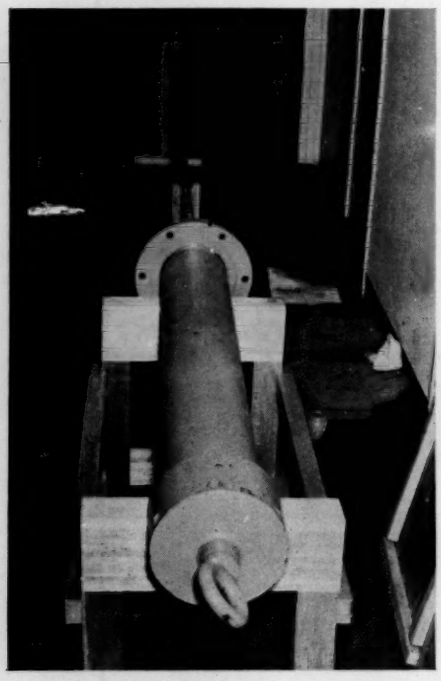

Fig. 4. The probe and container of apparatus R. 1.

4. Recorder

The block and circuit diagrams of the measuring system in apparatus R. 1. are shown in Figs. 5, 6 and 7. The two independent A.C. bridges, including the thermistors in the probe T_A, T_B and T_α, T_β are fed with a 400 c/s A.C. voltage from a single CR oscillator. Pairs of thermistors, having the same $\Delta R/\Delta T$ characteristics in the temperature range from 0°C to 4°C, were selected from a number of thermistors D 13 manufactured by the Nihon Electrical Company. The said temperature range is considered to include deep ocean temperatures: it has been reported that in the western Pacific the temperature at 5,000 m depth is 1.55 ± 0.10°C almost everywhere[13]. Fig. 7 shows the examples of the resistance-temperature characteristics of the thermistors used. The thermistors (52, 11), (12, 04), (03, 14), (05, 13) were used in pairs. The constant difference in the absolute values of resistance was roughly compensated by an additional carbon resistor connected in series. The resistance of all the temperature sensitive arms of the bridge was thus adjusted to about 3.0 kΩ at 0°C. A continuous potentiometer of 100 Ω is connected between the two ends

13) *loc. cit.*, (9).

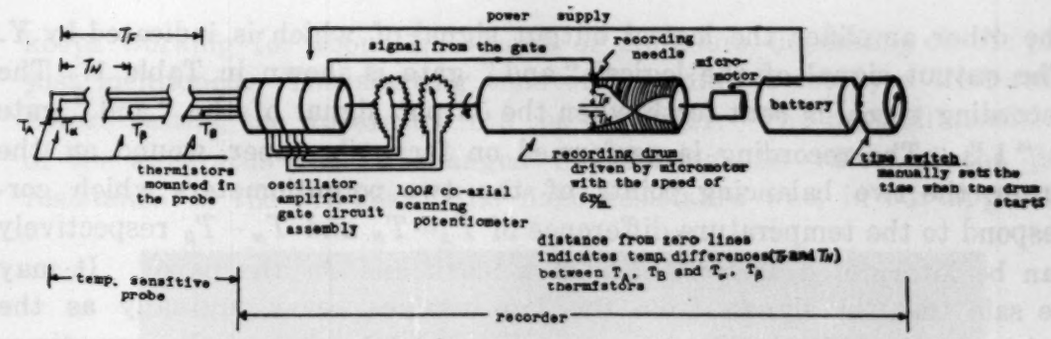

Fig. 5. Schematic diagram of the recorder of apparatus R. 1.

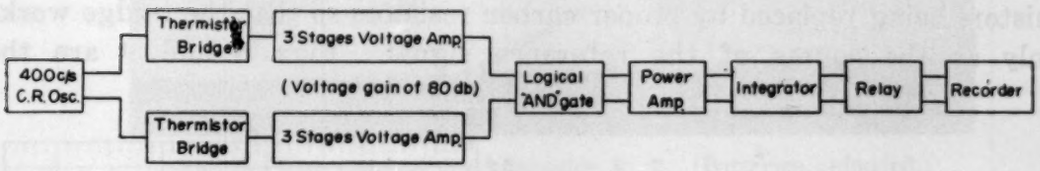

Fig. 6. Simplified block diagram of the recorder of apparatus R. 1.

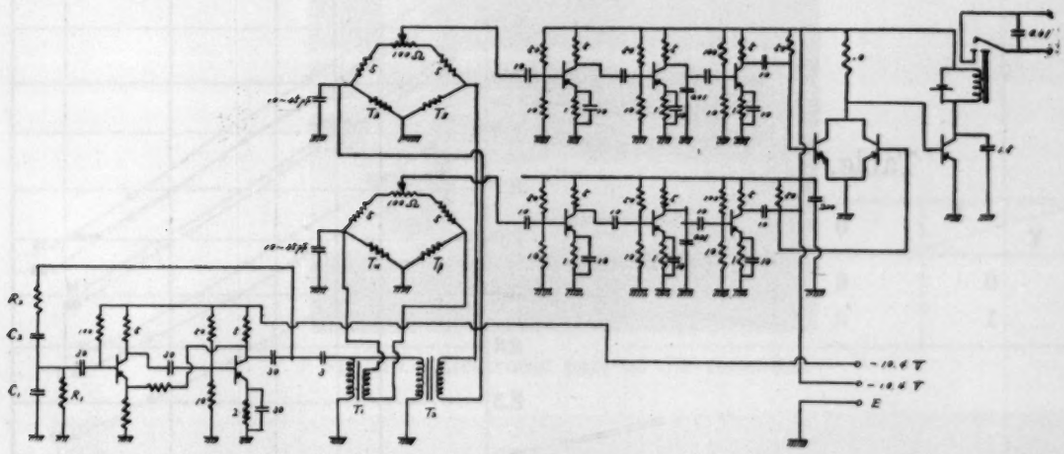

Fig. 7. Circuit diagram of the recorder of apparatus R. 1.

of the fixed arms of 5 kΩ (or 2.5 kΩ) of the bridge. This potentiometer rotates at the same rate of revolution as the recording drum. The unbalance output A.C. voltage from the two bridges are independently amplified through transitorized amplifiers with a voltage gain of 80 db. The phase angle of the output signal of the amplifier changes 180° when the potentiometer passes its balancing position, therefore as far as the phase angle is concerned the behaviour of the amplifier can be represented logically, namely "yes" or "no" or "1" or "0". The logical output signal X of the amplifier changes from "0" to "1" at the instance when the potentiometer passes through its balancing point. It is the same for

the other amplifier the logical output signal of which is indicated by Y. The output signal of the logical "and" gate is shown in Table 1. The recording signal is sent forth when the output signal of the "and" gate is "1". The recording is performed on facsimile paper wound on the drum, the two balancing points of the two potentiometers which correspond to the temperature difference of $T_A - T_B$ and $T_\alpha - T_\beta$ respectively can be interpreted as both ends of a black line on the paper. It may be said that the signals from the two bridges serve mutually as the reference signal in the "and" gate. For the 1.5 m long probe, sometimes only a pair of thermistors, T_A and T_B, are used, the other pair of thermistors being replaced by proper carbon resistors so that the bridge works only as the source of the reference signal. Figs. 8 and 9 are the

Table. 1.

Y \ X	0	1
0	0	0
1	0	1

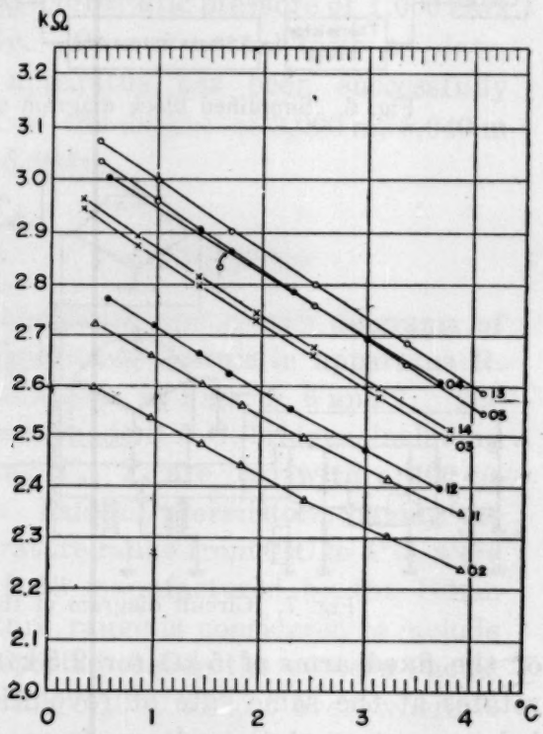

Fig. 8. Examples of the temperature-resistance characteristics of the thermistors used. Numbers attached to each curve are the thermistor numbers.

photographs of the instrument. The drum and two continuous potentiometers, driven by a micromotor, rotate once per 10 seconds and the pitch of the recording needle is either 0.5 mm or 0.25 mm for one revolution. The effective length of the drum being 20 cm, the apparatus

keeps working for about 1.25 hours or 2.5 hours, depending on the pitch just mentioned. The starting time of recording is set by a time-switch before setting the apparatus into the container. The over-all sensitivity of the apparatus can be changed by altering the value of the fixed resistance in the bridges. The fixed resistance was, in our apparatus,

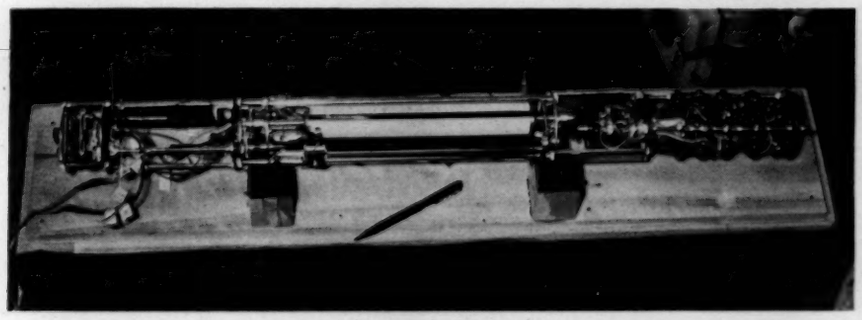

Fig. 9. The recorder for apparatus R. 1. (Batteries unlaoded.)

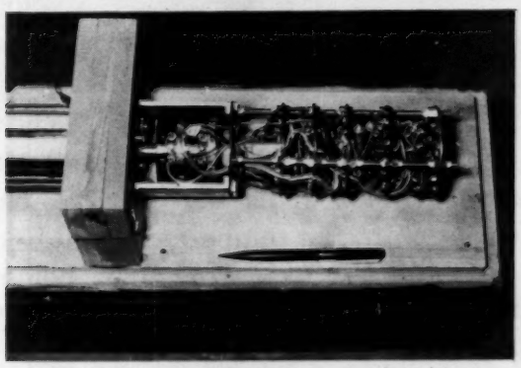

Fig. 10. Electronic part of the recorder.

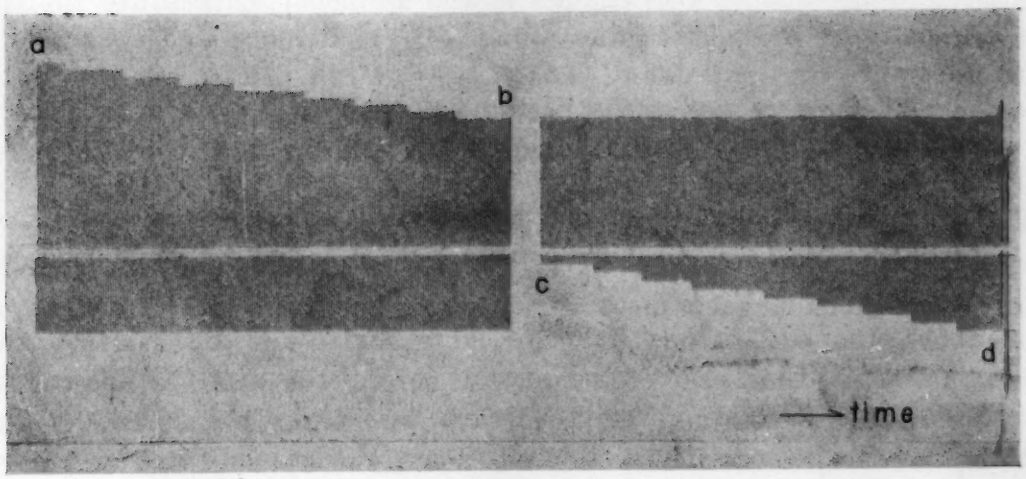

Fig. 11. Sensitivity calibration recording of the apparatus R. 1.

either 5 kΩ or 2.5 kΩ. Fig. 11 is an example of the records of calibration tests, obtained by inserting 3 kΩ carbon resistors in place of thermistors, and altering stepwise the resistance of a helical potentiometer connected as shown in Fig. 12. In Fig. 11, between a and b, the stepwise change was made in the bridge for T_A and T_B, while keeping the state of affairs in the bridge for T_α and T_β unchanged. Between c and d the stepwise change was made in the bridge for T_α and T_β, keeping the other bridge untouched. The step (~1.5 mm) in the record corresponds to the stepwise change of 2 Ω which is equivalent to the temperature difference of about 0.02°C for the thermistors used. The width of the recording paper being 93 mm, the maximum recordable temperature difference in this case is about 1.24°C. Fig. 13 is an example of the laboratory recording tests for the pairs of thermistors (08–18) and (09–17) when they were immersed into a water bath in which the temperature was controlled at *ca* 0.3°C. The envelopes T_H and T_F represent the time variation in the temperature differences in eash bridge, the asymptotic values indicated by dotted lines being the zero-lines.

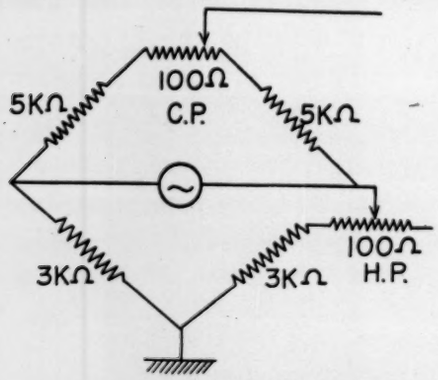

Fig. 12. Sensitivity calibration.
C. P.....continuous potentiometer
H. P.....helical potentiometer.

Owing to the fact that the resistance-temperature characteristics of thermistors forming a pair are not exactly identical, the position of the zero-line on the record depends on the ambient temperature. The shift of the zero-line due to 1°C change in the ambient temperature for the present pairs of thermistors was found to be equivalent to the temperature difference of the order of 0.01°C. As it can not be expected that the ambient temperature at the bottom of oceans will always be known, it would not be worthwhile to carry out the tedious work of predetermining the zero-line at various temperatures for each pair of thermistors. The precise position of the zero-line would be more conveniently determined in situ : it is planned that the zero-line will be easily determined on each measurement by keeping the whole apparatus just above the sea bottom for say 30 minutes and by starting the recording some time, say 10 minutes, before the probe is allowed to penetrate into the bottom. The vertical temperature gradient in the water near the bottom of the deep sea is extremely small, and as shown from the actual observation on the time constant of the probe, the

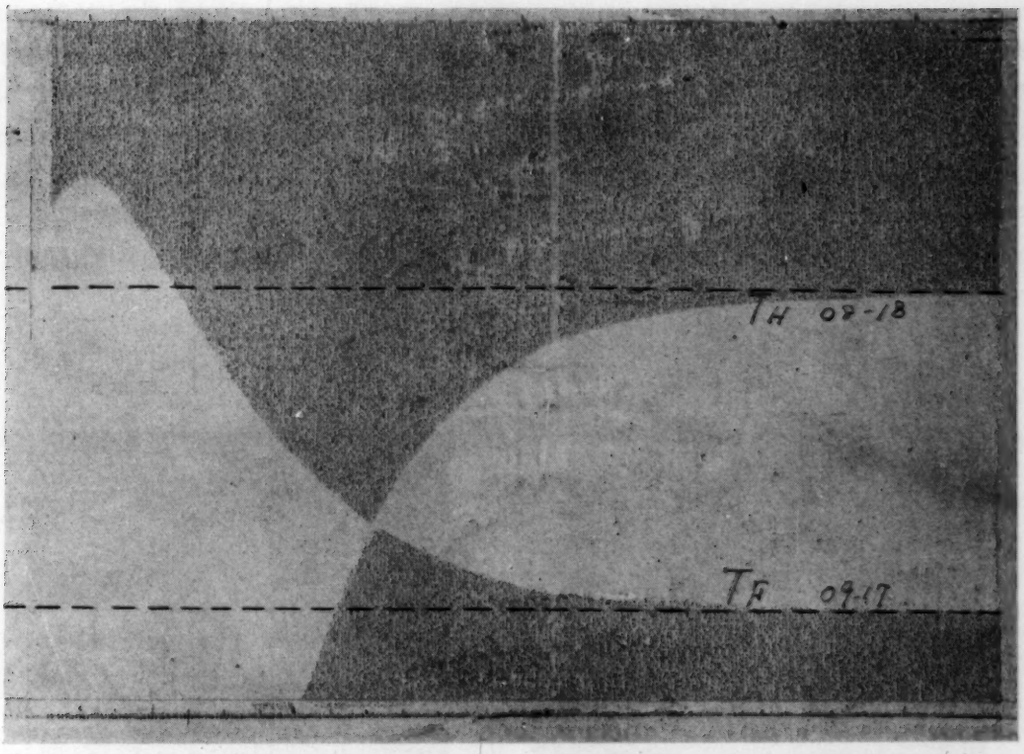

Fig. 13. Example of recording tests.

thermistors in the probe reach a nearly perfect thermal equiliblium with the water oustide in 30 minutes. Therefore the record obtained during the said period when the apparatus is just above the sea bottom will show the zero-line for that measurement. The continuous potentiometers and the drum are driven by a small D.C. motor. A set of batteries, i.e. a 10.4 volt mercury cell for the ampifier, and the oscillator and a 5.2 volt mercury cell for the micromotor and a 67.5 volt dry cell for the recorder are able to keep the apparatus working for two complete runs.

A flash bulb inclinometer as used in the equipment of the Scripps Institution of Oceanography[14] is attached to the recorder. Some preliminary tests in the Pacific proved that the apparatus works well in the sea bottom at depths of 5,040 m and 5,400 m.

5. Apparatus to be used on Board

When the depth is not great as in the continental shelf or lakes, it may be possible to sink the probe only and take the measurements

14) R. von. HERZEN, private communication

aboard by using an electric cable connecting the probe and the recorder. It will be useful especially when the ship does not have a powerful winch. A couple of handy apparatuses (named S. 1.) were made for the purpose of measuring heat flow at the sea bottom shallower than, say 1500 m. The probe shown in Fig. 14 (a)~(b) is made of a steel tube

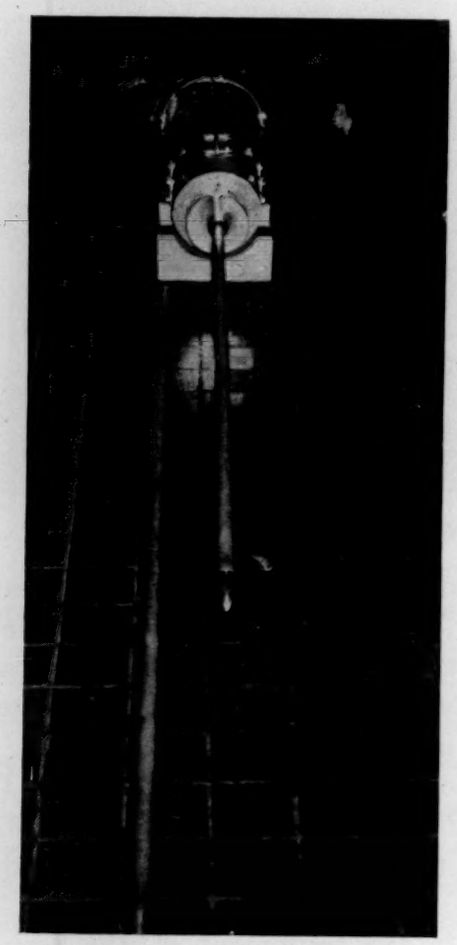

Fig. 14(a). The probe for the apparatus S. 1.

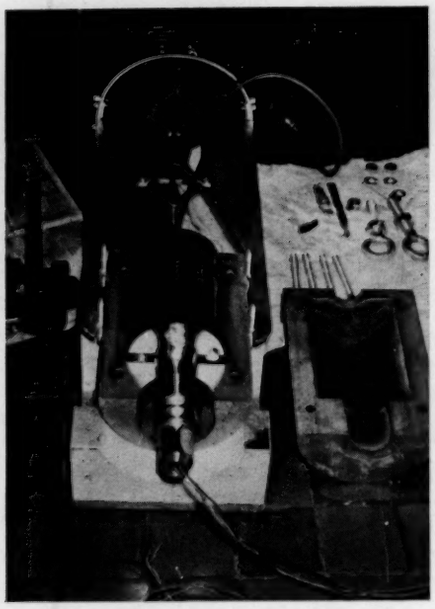

Fig. 14(b). The weight and the junction-container of the apparatus S. 1.

whose outer and inner diameters are 2.6 cm and 2.2 cm respectively. In order to facilitate the penetration of the probe a 25 kg weight made of steel was attached at an end of the probe. The connector between the thermistors and the cable is placed in a space made inside the weight and sealed by means of an O-ring. When necessary, additional weights with fins can be attached as observed in Fig. 14(b). The electrical circuit diagram of the handy thermogradmeter is shown in Fig. 15. In this

instrument, a helical potentiometer is used in the reference arms of the bridge. The temperature difference is read by the scale of the helical potentiometer which is manipulated to find the null position in the microammeter. Fig. 16 is the photograph of the instruments. Since 0.1 Ω can be read on the scale of the potentiometer, in the bridge used in the present case the unbalance resistance of 0.12 Ω of the thermistors can easily be detected : for the bridge as shown in Fig. 17, the relation

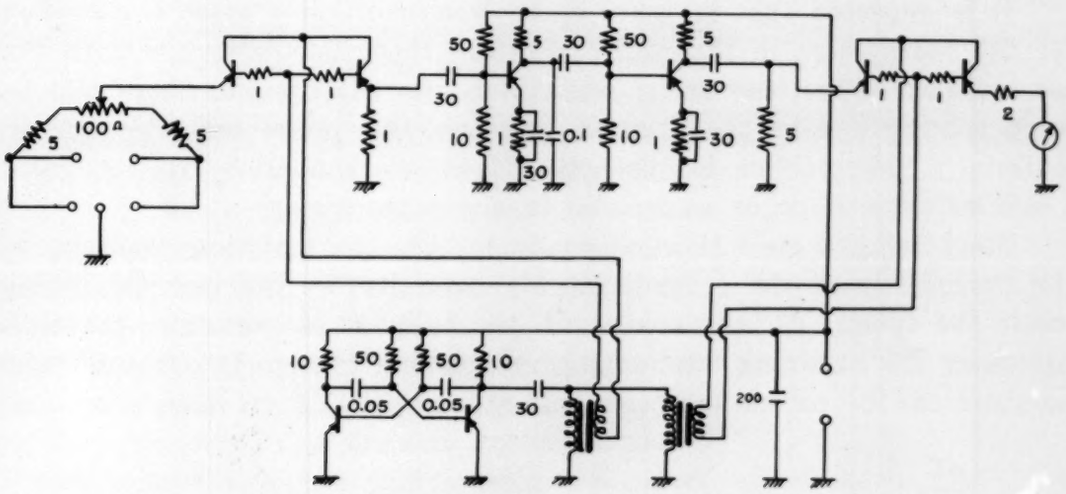

Fig. 15. Circuit diagram of the apparatus S. 1.

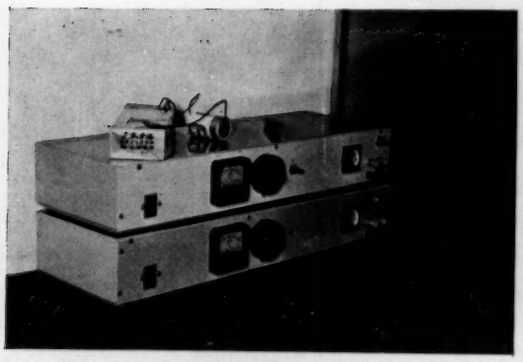

Fig. 16. Apparatus S. 1.

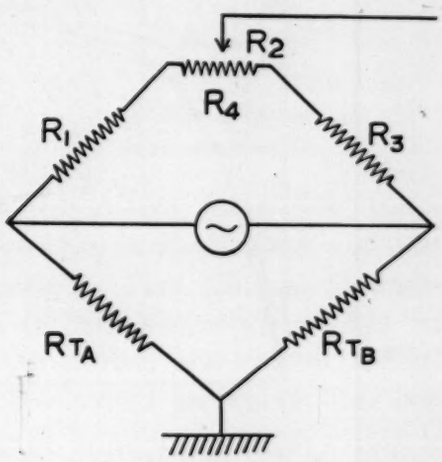

Fig. 17.

between the change in R_2, (ΔR_2), to nullify the unbalance caused by the change in, say, R_{T_B}, (ΔR_{T_B}), is given as

$$\Delta R_{T_B}=\frac{R_{T_A}+R_{T_B}}{R_1+(R_4-R_2-\Delta R_2)}\Delta R_2 .$$

For the present case, $R_{T_A} \fallingdotseq R_{T_B} \fallingdotseq 3\,\mathrm{k}\Omega$, $R_1 = R_3 = 5\,\mathrm{k}\Omega$, $R_4 = 100\,\Omega$

$$\therefore \Delta R_{T_B} \fallingdotseq 6/5\,\Delta R_2 .$$

This means that the sensitivity of the apparatus is of the order of 0.001°C, using the present thermistors.

6. Time Constants

It is expected that it takes some length of time after penetration for the thermistors in the probe to attain thermal equilibrium with the sea bottom. When the probe penetrates into the bottom, there will be some heating due to the friction between the probe and the bottom material. This problem has been thoroughly worked out by Bullard[15] for a similar type of probe as is used in our apparatus.

Steel being a good thermal conductor the thermal time-constant of the thermistors in the probe is largely controlled by the paraphin filling inside the tube. At the centre of the cylinder of paraphin, the time necessary for attaining 90% of a given sudden change in external temperature can be estimated[16] as 6 min (tube with 1.5 cm inner diameter)

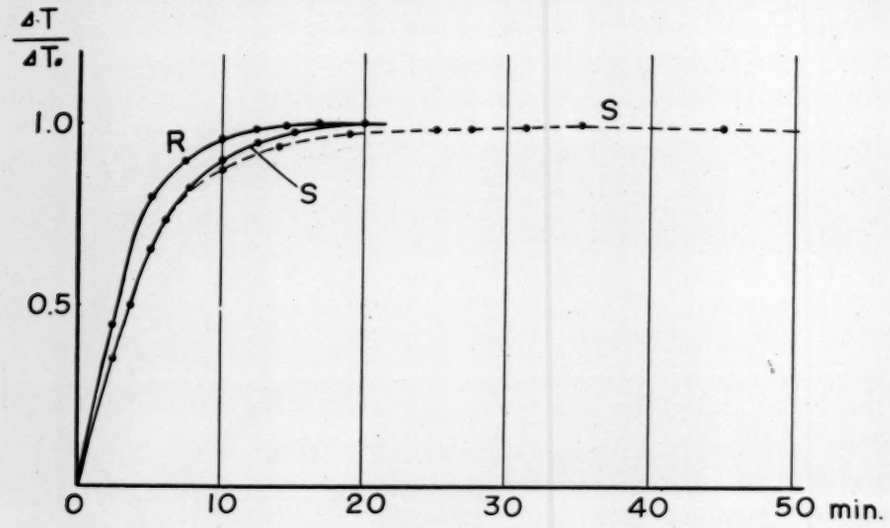

Fig. 18. Changes in the temperature of probes when the external temperature is suddenly changed by submersion into a water-bath (full lines), and by penetrating into the sea bottom (broken line).
R....probe for the apparatus R. 1.
S....probe for the apparatus R. 1.

15) *loc. cit.* (1).

16) H. S. CARSLAW and J. C. JAEGER, *Conduction of Heat in Solids, 2nd ed.*, (1959), 199, Oxford.

and 12 min (tube with 2.2 cm inner diameter). These values were found to be almost correct by experiment: in Fig. 18, the full curves show the process of attainment to thermal equilibrium with the surrounding water.

As described by Bullard, the attainment of thermal equilibrium in bottom material will be slower owing to the poorer diffusivity of the bottom material. This was found to be the case as the broken curve, taken when the probe was driven into the sea-bottom, shows. For these reasons, at least half an hour seems to be necessary for the probe to stay in the sea-bottom to give useful data.

In actual operation, it is frequently found difficult to keep the probe still in the bottom for such a long time, because of, for instance, the drift of the ship. To avoid this drawback, in the instrument used by the Lamont Geological Observatory, thermistors are sealed in a small probe, having a short time constant, attached to the core-sampler. The present authors also are experimenting with the said system. Some of the preliminary tests made are as follows. Outside the core-sampler with a 2 inch diameter, 3 small probes, 5 mm and 8 mm in the inner and outer diameters, were attached as shown in Fig. 19. Each of the probes as well as the corer were equipped with an electric heater wound outside. After keeping the system in the sea-bottom for a long time, heating current was supplied to these heaters for a short time and the temperature change caused by it was measured. Figs. 20 and 21 summarize the results. The time variations in the temperature due to heating by the heaters attached to the small probes are shown in Fig. 20. This shows that the time-constant of the small probes in the sea bottom is very short: the disturbance decays more than 90% within a few minutes. The effect of heating by a heater wound on the corer varies much more slowly as shown in Fig. 21. Fig. 21 also assures that keeping the probe 10 cm away from the corer, the heating disturbance from the corer is not practically perceptible at least until one hour later. From these observations, it is concluded that using probes such as No. 3 in Fig. 19, the time required for measurement will be greatly lessened.

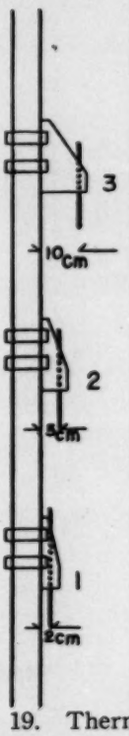

Fig. 19. Thermistor probes attached to the core-sampler.

In our apparatus No. 2 (R. 2), which is now under construction, we adopted this system.

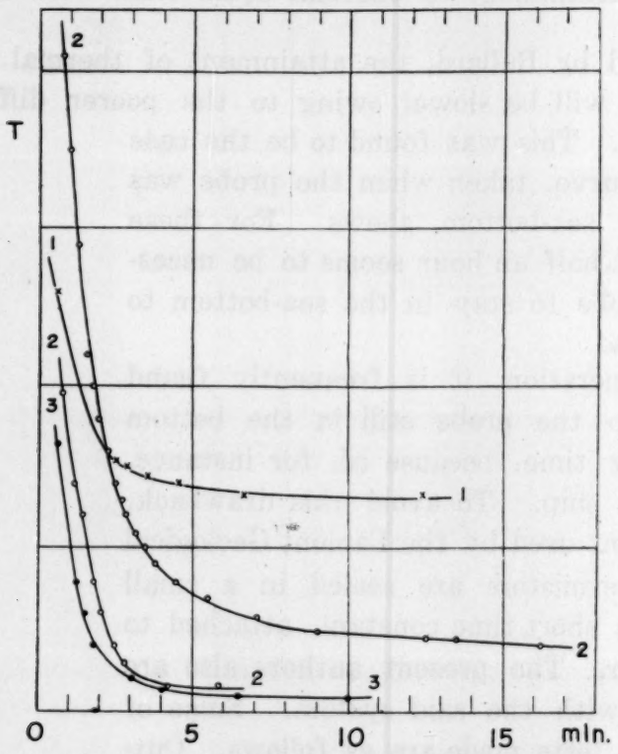

Fig. 20. Temperature variations with time after instantaneous heating by a heater attached to the probes.

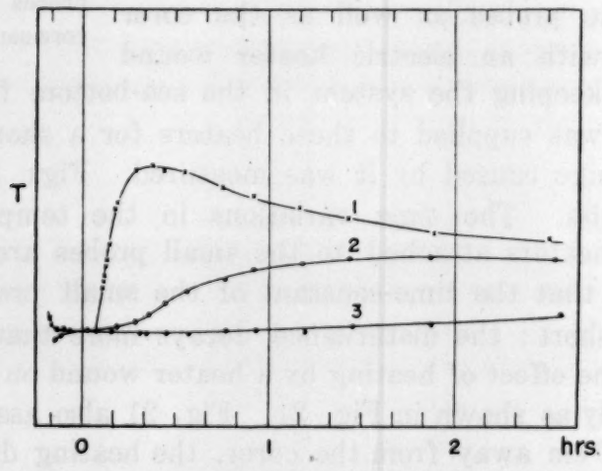

Fig. 21. Temperature variations with time after 5 minute heating by a heater attached to the core-sampler.

7. Concluding Remarks

The work of determining the terrestrial heat flow through the ocean floor has only been set about recently in Japan. So far, we have only built the apparatus for this purpose, and the actual measurements will be taken in the forthcoming years. The authors thank Drs. T. Rikitake, and N. Nasu, Tokyo University and Dr. K. Terada, Japan Meteorological Agency, for their encouragement and supervision. In designing the apparatus, kind advice was given to the authors from colleagues of the institutes having experience in this work. In particular, the authors wish to acknowledge the information given by Sir Edward Bullard, Department of Geodesy and Geophysics, University of Cambridge, Dr. R. von Herzen, Scripps Institution of Oceanography, University of California, and Drs. M. Langseth, and S. Gerard, Lamont Geological Observatory, Columbia University. Thanks are also due to the staff of the Sokkisha Company, Tokyo and the Rigosha Company, Tokyo for their wholehearted cooperation in the construction of the apparatus. Kind assistance rendered by the crew of the m.s. Ryofu Maru throughout the sea work is also gratefully acknowledged.

The present work has been supported by the Special Fund for the Promotin of Scientific Research of the Science and Technics Agency and the Scientific Research Fund of the Ministry of Education.

---

6. 地球熱学 (第7報) 海底地温勾配測定装置

地震研究所 上田誠也
地震研究所 友田好文
東京大学大学院地球物理学専門課程 宝来帰一
東京大学大学院地球物理学専門課程 金森博雄
気象庁 淵秀隆

日本列島をとりかこむ海域において地殻熱流量の実測を行なう目的のため，船より吊り下げ海底地層に貫入せしめて，海底での地温勾配を測定記録する装置を試作した．サーミスタを用いた交流ブリッヂ法を用い，0°～2°C 程度の温度差が，0.001°C の精度で自動記録されるもので，その概要は本文第5図の通りである．全装置は耐圧容器に収められる．浅海測定用には，測定器を船上に留め感熱部のみを海底に突差す方式を採用した．太平洋上での試験結果はおおむね良好で，今後は実測を行なう予定である．なお，本研究は，科学技術庁特別調整費，文部省科学研究費によつて行なわれた．

BULLETIN OF THE EARTHQUAKE
RESEARCH INSTITUTE
Vol. 39 (1961), pp. 133-248

7. *A Study of the Textural Characteristics of Pyroclastic Flow Deposits in Japan.*

By Isamu MURAI,

Earthquake Research Institute.

(Read Dec. 20, 1960.—Received April 30, 1961.)

Contents

Abstract 134
Introduction 136
Acknowledgments 140
Terminology 141
Classification of pyroclastic flows 143
Materials for the study 147
Size characteristics of pyroclastic flow deposits 158
  General statement 158
  Methods of mechanical analyses 159
  Parameters of particle size distribution 185
  Summary of results 190
    1) Lack of sorting 191
    2) Homogeneity 199
    3) Median diameters 200
    4) Shape of particle size distribution 203
    5) Subdivisions of pyroclastic flow deposits based upon size characteristics 211
    6) Comparison of the size characteristics of dry mud-flow deposits and auto-brecciated lava flows 213
Roundness of particles 214
Types of vesicular shards and pumice 220
Constituent characteristics 223
Bulk density of essential fragments 228
Succession of eruptive events 230
Chemical properties of pyroclastic flow deposits 232
Discussions on the mode of origin and mechanism of pyroclastic flows 238
  Gas-emission process 238
  Dual character of pyroclastic flows 242
  Sorting agency 244

Intermediate cases between pyroclastic flows and dry mud-flows 246
Concluding remarks 247

Abstract

Phenomena of pyroclastic flows (nuées ardentes or glowing avalanches in a broad sense) involve all kinds of flows of incandescent fragmental materials of juvenile origin, graduating from the Pelean type eruptions attending protrusion of domes to eruptions that produce vast ash-flow sheets. Textural and constituent characteristics vary widely in accordance with differences in the types of pyroclastic flows. It is possible to consider that the nature and mode of origin of pyroclastic flows are precisely reflected in these characteristics of the deposits. The writer tried a quantitative study of these characteristics of pyroclastic flow deposits in Japan. His study was carried out on samples collected from non-welded deposits or non-welded parts of welded deposits. 192 samples of pyroclastic flow deposits and 35 samples of pyroclastic fall deposits were collected from various volcanic regions in Japan, and mechanical analyses of these samples were performed. Among these samples, 59 samples of pyroclastic flow deposits were selected as representative of every unit of flows. Moreover, 5 samples of pyroclastic fall deposits which were caused by preceding eruptions immediately before the discharge of pyroclastic flows were selected to compare their characteristics with those of pyroclastic flows. On these samples, measurements of the roundness of constituent particles, the bulk density of essential fragments, the relative abundance of a peculiar type of glass shards and pumice or scoria crowded with fine tubular vesicles, and of the relative proportion of each element of the constituents were carried out. Besides these, 15 samples of dry mud-flow deposits and 5 samples of auto-brecciated lava flows were collected, and their size characteristics were analysed in order to compare them with those of pyroclastic flow deposits.

The most distinct features of pyroclastic flow deposits are the poorly sorted size characteristics. Data of mechanical analyses of every kind of pyroclastic flow deposits usually show a chaotic mingling of particles graduating from large blocks to fine dust, contrasting strikingly with the well-sorted size characteristics of pyroclastic fall deposits. The shape of the particle size distribution curves of every kind of pyroclastic flow deposit shows a close resemblance, each with the other. Each curve has tailingout parts both in coarser and finer fractions, a gentle mode in medium fractions, and a sub-mode, conspicuous or faint, in coarser fractions. Such size characteristics are

always found in all deposits of pyroclastic flows. There exists, however, considerable room for variation within the framework of size distribution curves. Pyroclastic flows are grouped into several subdivisions based upon the differences in the mode of origin and mechanism of emplacement as well as the differences in size characteristics and other textural characteristics of their deposits as follows: (1) nuée ardente of Pelée type and Sakurajima type, (2) intermediate type pyroclastic flow, (3) St. Vincent ash-flow, (4) Krakatoa type ash-flow (fine-grained and medium-grained), (5) Valley of Ten Thousand Smokes type ash-flow (or fissure eruption type ash-flow).

The size characteristics of dry mud-flow deposits and auto-brecciated lava flows are similar to those of pyroclastic flow deposits, but usually more poorly sorted and of coarser grain. Their size distribution curves tend to conform to Rosin's law of crushing. On the contrary, those of pyroclastic flow deposits show some disparities from Rosin's law, indicating the efficiency of sorting at the time of eruption and during flowage. It is possible to consider that sorting in a vertically rising column of ash or during the flowage of expanding cloud, as well as explosive disintegration and attrition or collision on the way of the ascent of frothing magma and during flowage, control the size characteristics of pyroclastic flow deposits. Although particles of all sizes are transported *en masse* in a state of turbulent flow as indicated by the distinct ill-sorted features of the deposits, the sorting agency has some effects upon their size characteristics.

Judging from the results of measurements of the roundness of particles and types of pumice and glass shards, together with the results of inspections of other features of pyroclastic flow deposits, it is clarified that in eruptions of the intermediate type pyroclastic flows and nuées ardentes, most of the vesiculation takes place during flowage, while in eruptions of the Krakatoa type ash-flows, it occurs within the vent, conduit or chamber, and in eruptions of the St. Vincent type ash-flows, vesiculation begins partly within the vent and occurs mostly at the time of discharge. In general, discharge of pyroclastic flows follows preliminary explosions. It is inferred that eruptions of pyroclastic flows take place after the removal of a confining load at the top of the vent by preliminary explosions.

It is possible to consider that magmas which produce pyroclastic flow eruptions have a relatively large amount of volatiles, and differences in the gas-emission process in the erupting magmas cause various types of pyroclastic flows. Rock types of the deposits seem to belong to the hypersthenic rock series which is produced by the contamination of the original magma and granitic substances. Perhaps such contamination may cause concentration of volatiles in magmas which is inferred to be responsible for the eruptions of pyroclastic flows.

Introduction

A characteristic eruption took place at Mt. Pelée on Martinique which is one of the Windward Islands of the West Indies on May 8th, 1902. A dark eruption-cloud was discharged laterally from the flank of the dome rising in the pre-existing summit crater, rushing down *en masse* along the mountain-slope of the volcano at a surprisingly high speed. St. Pierre, situated on the southwest foot of the volcano, was wiped away by this devastating hot cloud. The eruptive activity continued for the following several months, and similar peculiar eruptions occurred repeatedly. This type of eruption had not been recognized by any geologist until that time. The seething hot cloud cosisting of clastic materials and gases did not rise vertically into the air, but was swept down along the mountain-side. Lacroix (1903) introduced "nuée ardente" as a geological term for these disastrous eruptions on May 8th, 1902 and for the subsequent eruptions at Mt. Pelée[1].

Another similar peculiar eruption took place on May 7th, 1902 at the Soufrière on St. Vincent which also lies within the Windward Islands. The eruption occurred through an open crater on the summit, and a column of ash and steam rose to an enormous height. During the early climactic phase of the eruption, incandescent avalanches rose from the crater and poured over the mountain-slope. These avalanches also came to bear the same name "nuées ardentes". The characteristics of these two types of eruptions occurring almost at the same time in the Windward Islands were described in detail in the comprehensive reports assembled by Lacroix (1904, 1908) and Anderson and Flett (1903)[2]. Since then, phenomena of nuées ardentes have attracted the attention of many geologists and volcanologists. Detailed studies on eruptions of nuées ardentes occurring in this century, as well as those on pyroclastic deposits which were considered to be the products of nuées ardentes, have been induced by the two well-known papers. The two eruptions that occurred in the Windward Islands in 1902 have

1) Alfred LACROIX, "L'eruption de la montagne Pelée en janvier 1903," *Acad. Sci., (Paris), Comptes rendus*, **136** (1903), 442-445.

2) Alfred LACROIX, "La Montagne Pelée et ses éruptions," *Paris, Masson et Cie*, (1904), 662.

Alfred Lacroix, "La Montagne Pelée apres ses éruptions," Acid. Sci., Paris, (1908), 74-93.

Tempest ANDERSON and J. S. FLETT, "Report on the eruption of the Soufrière in St. Vincent in 1902, and on a visit to Montagne Pelée in Martinique, Pt. I," *Philos. Trans. Royal Soc. London, ser. A*, **200** (1903), 353-553.

been considered as the classic examples of nuées ardentes or glowing avalanches.

In 1929–1932, similar eruptions took place at Mt. Pelée. Perret (1935), who witnessed more than 100 nuées ardentes from Pelée, discussed the nature of these eruptions in detail[3]. It became clear that similar eruptions had occurred repeatedly since the historic ages at the Merapi Volcano in Central Java. In 1930–1935, violent nuées ardentes occurred at the Merapi Volcano, which were reported in detail by Stehn (1936) and Neumann van Padang (1933)[4]. Van Bemmelen (1949) summarized the nuée ardente phenomenon on the basis of his observations in Indonesia, principally at Merapi[5]. Nuées ardentes occurred at Mt. Lamington in New Guinea in 1951–1952, which were reported by Fisher (1945) and Taylor (1954 and 1956)[6]. Macdonald and Alcaraz (1956) described nuées ardentes that took place at the Hibok-Hibok Volcano in the Philippines in 1948–1953[7]. Thus the data of nuées ardentes phenomena have been augmented by many accounts of these eruptions.

Besides, many examples of nuées ardentes products have been recognized through detailed studies on pyroclastic deposits in every volcanic region in the world. Now, it is well known that nuées ardentes or glowing avalanches have been discharged throughout the geologic column as far distant as the pre-Cambrian. Deposits of nuées ardentes are distributed widely along orogenic belts in the world. Fenner (1920, 1923, 1937 and 1950) studied the origin of the tuff deposits emplaced in the Valley of Ten Thousand Smokes, Katmai, at the time of the 1912 erup-

---

3) F. A. PERRET, "The eruption of Mt. Pelée 1929-1932," *Carnegie Inst. Washington, Pub.* No. 457 (1935), 125.

4) M. NEUMANN van PADANG, "De Uitbarsting van den Merapi (Midden Java) in de jaren 1930-1931," *Vulkan. en Seismol. Mededeel*, No. 12 (1933), Batavia, 135.

C. E. STEHN, "Beobachtungen an Glutwolken wahrend der erhohted Tatigkeit des Vulkans Merapi in Mittel-Java in den Jahren 1933-1935," *Handel. v/h 7 de Ned.-Indie Natuurwet Congres, Batavia*, (1936), 647-656.

5) R. W. van BEMMELEN, "Geology of Indonesia, v. 1A, General geology of Indonesia and adjacent archipelagoes," *The Hague, Government Printing Office*, (1949), 732.

6) N. H. FISHER, "Report of the subcommittee on volcanology 1951," *Bull. Volcanol., ser., 2*, **15** (1954), 71-80.

G. A. TAYLOR, "Volcanological observations Mount Lamington, 29th May 1952," *Bull. Volcanol., ser. 2*, **15** (1954), 81-97.

G. A. TAYLOR, "An outline of Mount Lamington eruption phenomena," *8th Pacific Sci. Cong., Philippines 1953*, **2** (1956), 83-88.

7) G. A. MACDONALD and A. ALCARAZ, "Nuées ardentes of the 1948-1953 eruption of Hibok-Hibok," *Bull, volcanol., ser. 2*, **18** (1956), 169-178.

tion. He wrote a number of papers in which he set out volcanological evidences and inferred from these the nature and mechanism of incandescent tuff-flows[8]. Moore (1934) described the recent pumice deposits of the Crater Lake region and discussed their origin. He concluded that one of them, named the "Older Pumice", was apparently different in origin from pumice deposits of the normal air-fall type, being regarded as a product of nuée ardente, judging from the size characteristics, distribution and other sedimentary features[9]. Marshall (1932, 1935 and 1953) discussed the origin of rhyolite tuff deposits named "ignimbrite", distributed in an extensive sheet-like form in the Taupo-Rotorua region, New Zealand. He assumed that ignimbrites were formed by nuée ardente type flows which were erupted as a highly mobile emulsion of incandescent ash, gas and other pyroclastic material[10]. Williams (1941) discussed the mechanism of the formation of calderas, and pointed out the fact that calderas of the "Krakatau type" were formed by collapse following the eruption of a tremendous amount of pumice, usually in the form of nuées ardentes[11]. Recently, Hay (1959) studied the deposits of glowing avalanches discharged from the Soufrière of St. Vincent on May 7th, 1902, discussing the mechanism of avalanches produced from a vertically rising column of ash and steam[12].

In Japan, deposits of nuées ardentes have been reported from several volcanic regions. In 1929, a great eruption took place on the

8) C. N. FENNER, "The Katmai region, Alaska, and the great eruption of 1912," *Jour. Geol.*, **28** (1920), 569–606.

C. N. FENNER, "The origin and mode of emplacement of the great tuff deposits in the Valley of Ten Thousand Smokes," *Natl. Geog. Soc. Contributed Tech. Papers, Katmai Ser.*, No. 1, (1923), 74.

C. N. FENNER, "Tuffs and other volcanic deposits of Katmai and Yellowstone Park," *Trans. Am. Geophys. Union, 18th Ann. Mtg., pt. 1*, (1937), 236–239.

C. N. FENNER, "The chemical kinetics of the Katmai eruption," *Am. Jour. Sci.*, **248** (1950), 593–627, 697–725.

9) B. N. MOORE, "Deposits of possible nuée ardente origin in the Crater Lake region, Oregon," *Jour. Geol.*, **42** (1934), 358–375.

10) Patrick Marshall, "Notes on some volcanic rocks of the North Island of New Zeland," *New Zealand Jour. Sci. and Tech.*, **13** (1932), 198–200.

Patrick MARSHALL, "Acid rocks of Taupo-Rotorua volcanic district," *Trans. Royal Soc. New Zealand*, **64** (1935), 323–366.

Patrick MARSHALL, "Ignimbrites," *7th Pacific Soc. Cong., New Zealand 1949*, **2** (1953), 407–411.

11) Howel WILLIAMS, "Calderas and their origin," *Bull. Dept. Geol. Sci., Univ. Calif.*, **25** (1941), 239–346.

12) Richard L. HAY, "Formation of the crystal-rich glowing avalanche deposits of St. Vincent, B.W.I.," *Jour. Geol.*, **67** (1959), 540–562.

Komagatake Volcano in southern Hokkaido. During the paroxysmal phase of the eruption, a large quantity of pumice blocks and ash materials effused from the crater and descended down the mountain-slope in a state of pumice-flow. Detailed studies on the mechanism of the eruption as well as on the nature of the deposits of pumice-flow were carried out by many geologists and volcanologists[13]. Kuno (1941) pointed out the fact that the sedimentary features and the size characteristics of the pumice-flow deposits are quite different from those of the normal projected air-fall pumice deposits[14]. Kuno (1953) indicated that most Japanese calderas belong to the "Krakatau type calderas" of Williams, being surrounded by extensive areas of unstratified pumice-flow deposits or welded tuffs[15]. Investigations of pyroclastic deposits resulting from eruptions of nuées ardentes in Japan have been advanced by Matsumoto, Kuno, Ishikawa, Yagi, Taneda, Minato, Yamasaki, Aramaki, Katsui, et al.[16] Taneda (1954 and 1957) and Taneda, Miyachi and Nishihara (1957) studied the "Shirasu" deposits in southern Kyushu, concluding that they might be regarded as nuées ardentes products showing size characteristics similar to those of the "Older Pumice" of the Crater Lake

13) Hiromichi TSUYA, etc. 7, "The eruption of Komagatake, Hokkaido, in 1929," *Bull. Earthq. Res. Inst., Tokyo Univ.*, **8** (1930), 237-319.

Shukusuke KOZU, "The great activity of Komagatake in 1929," *Min. Petr. Mitt.*, **45** (1934), 133-174.

14) Hisashi KUNO, "Characteristics of deposits formed by pumice flows and those by ejected pumice," *Bull. Earthq. Res. Inst., Tokyo Univ.*, **19** (1941), 144-149.

15) Hisashi KUNO, "Formation of calderas and magmatic evolution," *Trans. Am. Geoph. Union*, **34** (1953), 267-280.

16) Tadaiti MATUMOTO, "The four gigantic caldera volcanoes of Kyushu," *Japanese Jour. Geol. Geogr.*, **19** (1943), Special number, 57.

Tadaiti MATUMOTO, Toshio ISHIKAWA, and Masao MINATO, "Some problems of welded-lava and welded-tuff related with the sunken calderas in Japan," *8th Pacific Sci. Cong., Philippines 1953, Proc.*, **2** (1956), 130-138.

Toshio ISHIKAWA, Masao MINATO, Hisashi KUNO, Tadaichi MATSUMOTO, and Kenzo YAGI, "Welded tuffs and deposits of pumice flow and nuée ardente in Japan," *Intern. Geol. Cong.* (1956).

Masao YAMASAKI, "The volcanic activity in the later stages of the development of Nantai, Nikko," *Bull. Volcanol. Soc. Jap., 2nd Ser.* **2** (1957), 63-76. (Japanese with English abstract.)

Shigeo ARAMAKI, "The 1783 activity of Asama Volcano, Pt. I," *Jap. Jour. Geol. Geogr.*, **27** (1956), 189-229.

Shigeo ARAMAKI, "The 1783 activity of Asama Volcano, Pt. II," *Jap. Jour. Geol. Geogr.*, **28** (1957), 11-33.

Yoshio KATSUI, "Geology and petrology of the Volcano Mashû Hokkaido, Japan," *Jour. Geol. Soc. Jap.*, **61** (1955), 481-495. (Japanese with English abstract.)

region[17].

The study of nuées ardentes or glowing avalanches and their deposits is still in its infancy, althrough major progress is being made as mentioned. The outline of nuées ardentes eruptions has already been drawn through such researches mentioned above. A great number of problems about the origin and mechanism of these phenomena, however, are still left unsolved, and every argument is more or less inferential. A lot of detailed study on nuée ardente deposits, as well as the augmenting of data of actual observations of future eruptions of nuées ardentes, is needed. Complete solutions of many unsolved problems will come about only through careful progressive research. It has been noticed by some volcanologists that the mode and mechanism of nuées ardentes are related to the viscosity and gas content of erupting magmas and the condition of gas-emission. Aramaki (1957) pointed out that there exists a certain relationship between the mode of emplacement and the nature of nuée ardente deposits. This fact may suggest the course of the future studies. Quantitative study on the texture, structure and constituent of nuée ardente deposits, together with analytical study on the chemical and mineralogical composition and petrological features of the deposits, is necessary. It can be expected that analytical methods used in sedimentary petrology may be effective in solving problems on the phenomenon of nuée ardente. The writer is proceeding systematically with his quantitative study on the textural and constituent characteristics of pyroclastic flow deposits distributed in every volcanic region in Japan, to obtain some useful data for deciphering the mode of origin and mechanism of pyroclastic flows or nuées ardentes. Part of his work has already been published in several preliminary reports[18].

17) Sadakatu TANEDA, "Geological and petrological studies on the 'Shirasu' in south Kyushu, Japan, Part I, Preliminary note," *Kyushu Univ. Fac. Sci. Mem., ser. D. Geology*, **4** (1954), 167-177.

Sadakatu TANEDA, "Geological and petrological studies of the 'Shirasu' in south Kyushu, Japan, Part II, Preliminary note," *Kyushu Univ. Fac. Sci. Mem. ser. D, Geology*, **7** (1957), 91-105.

Sadakatu TANEDA, Sadanori MIYACHI, and Moto-o NISHIHARA "Geological and petrological studies of the 'Shirasu' in south Kyushu, Japan, Part III, The 'Shirasu' in the Tsuruda-Hiwaki-Koriyama area, north of Kagoshima City," *Kyushu Univ. Fac. Sci. Mem., ser. D, Geology*, **6** (1957), 107-127.

18) Hiromichi TSUYA, Isamu MURAI, and Yoshichi HOSOYA, "Size characteristics of the pumice deposits distributed in the vicinity of Komoro on the southwest foot of Asama Volcano," *Bull. Earthq. Res. Inst., Tokyo Univ.*, **36** (1958), 413-431. (Japanese with English abstract.)

Isamu MURAI and Hiromichi TSUYA, "Size characteristics of the 'Shirasu' deposit distributed in the southern part of Kyushu Island," *Bull. Earthq. Res. Inst., Tokyo Univ.*, **37** (1959), 637-647. (Japanese with English abstract.)

Isamu MURAI, "On the mud-flows of the 1926 eruption of Volcano Tokachi-daké, Central Hokkaido, Japan," *Bull. Earthq. Res. Inst., Tokyo Univ.*, **38** (1960), 55-70.

Acknowledgements

The writer wishes to express his sincere thanks to Prof. Hiromichi Tsuya of the Earthquake Research Institute, University of Tokyo, for introducing him to this study as well as for constant guidance in the course of the work. His grateful thanks are also due to Prof. Takao Sakamoto and Prof. Hisashi Kuno of the Faculty of Science of the the same University, for invaluable criticism and advice. Special thanks due to Prof. Seitaro Tsuboi of the same University for his critical reviewing of the manuscript. He greatly appreciates the valuable advice by Mr. Shigeo Aramaki and Ph. D. Takayasu Uchio of the same University. He is indebted to Mr. Masao Yamasaki, assistant professor of Kanazawa University, for kindly supplying unpublished data. He is also indebted to Mr. Yoshichi Hosoya of the Komoro Branch of the Earthquake Research Institute for his great help in carrying out laboratory work as well as in the preparation of the figures included in this paper.

Terminology

Nuée ardente: As already mentioned, Lacroix (1903) introduced this word as a geological term for the peculiar eruptions of Mt. Pelée in 1902–1903. Since then, this term has been adopted for all eruptions of similar types. The eruptions of the Soufrière, Katmai, Merapi, etc. were described in the same terminology "nuée ardente". Furthermore, "nuée ardente" has been adopted to designate eruptions which are considered to have been responsible for extensive tuff deposits or welded tuffs. Thus, the usage of the term "nuée ardente" has become ambiguous. It has been used for all kinds of eruptions which produced laterally moving masses of incandescent fragmentary materials of juvenile origin and gases. There exist wide variations of the mode and magnitude of eruptions and the nature of discharged materials among the eruptions termed nuées ardentes. Consequently, some confusion frequently exists in the accounts of these phenomena. In order to eliminate such ambiguity in the terminology, the usage of the term "nuée ardente" must be confined to eruptions of the Pelée type and their confederates. Aramaki (1957) used the term "pyroclastic flow" as a synonym of

Isamu MURAI, "Pyroclastic deposits distributed on the east foot of Volcano Myoko," *Bull. Earthq. Res. Inst.*, **38** *Tokyo Univ.*, (1960), 307-315.

Isamu MURAI, "Pumice-flow deposits of Komagatake Volcano, Southern Hokkaido," *Bull. Earthq. Res. Inst., Tokyo Univ.*, **38** (1960), 451-466.

"nuée ardente" or "glowing avalanche" in the broad sense. This term was already used by Gilbert (1938) and Williams (1941)[19]. The writer adopts this term in the following sections of this paper.

Ash-flow: The nomenclature of deposits emplaced by pyroclastic flows may be very controversial. A great number of terms, i.e. incandescent tuff flow, volcanic sand flow, pumice flow, scoria flow, block and ash flow, hot ash flow, ignimbrite, tuff lava, mud lava, welded tuff, etc., have been used to designate these deposits. It is generally considered that the most distinct features of these deposits are the non-sorted size characteristics, the constituent particles of which range in all sizes from huge blocks to fine dust. Most of the pyroclastic flow deposits, welded ones and their non-welded equivalents, contain a large quantity of fine materials and fall into the category of ash, consisting of a large percentage of particles of ash size (4 to 1/4 mm in diameter) and fine ash size (less than 1/4 mm in diameter), referring to the Wentworth and Williams' size scale (1932)[20]. Smith (1960) defined the term "ash flow deposits" as those consisting of 50 per cent or more in weight of ash and fine ash exclusive of foreign inclusions[21]. This term includes almost all of the pyroclastic flow deposits, although some consist mainly of particles larger than ash and will not conform to the arbitrary 50 per cent minimum for particles of juvenile origin less than 4 mm in diameter. The writer adopts the term "ash-flow" in his scheme of the classification of pyroclastic flows to designate the eruptions of pyroclastic flows which produce fine-grained pumiceous pyroclastic deposits. The term "ash-flow deposit" may be used as a substitute for many terms such as tuff flow, pumice flow, welded tuff, etc.

Mud-flow: Lack of sorting has been considered as a characteristic feature and a good criterion for recognition of pyroclastic flow deposits. It is generally believed that such size characteristics may be the result of deposition from a turbulent flow or an avalanche. A similar non-sorted feature is also recognized in mud-flow deposits. These two types of deposits are sometimes confused with each other because of their similarity in appearance. The usage of the term "mud-flow" is quite ambiguous. Volcanic mud-flows include all kinds of phenomena which

19) C. M. GIBERT, "Welded tuff in Eastern California," *Bull. Geol. Soc. Am.*, **49** (1938), 1829-1862.
Howel WILLIAMS, *op. cit.* (1941).

20) C. K. WENTWORTH and Howel WILLIAMS, "The classification and terminology of the pyroclastic rocks," *Bull. Natl. Research Council*, **89** (1932), 19-53.

21) Robert L. SMITH, "Ash flows," *Bull. Geol. Soc. Am.*, **71** (1960) 795-842.

originate as the result of eruptions through crater lakes (e.g. the 1919 eruption of the Klut Volcano in Java), causing the melting of ice and snow (e.g. the 1877 eruption of the Cotopaxi Volcano in Ecudor), and eruptions following or accompanied by heavy rains. They also include those which are caused not by eruptions, but by the collapse of the dam of a crater lake, by heavy rains falling on unconsolidated ejecta and by the rapid melting of ice and snow[22]. Further, the term "mud-flow" has been used for avalanches of disintegrated materials caused by the collapse of a part of a volcanic cone destroyed by a violent explosion. For example, those of the 1888 eruption of the Bantai Volcano were described as mud-flows. Flows of essential fragments and water caused by the entering of pyroclastic flows into streams are also classified as mud-flows. The word "lahar" is used as a synonym of volcanic mud-flow. This word comes from an Indonesian word for volcanic materials transported by water. Van Bemmelen (1949) defined this term as "a mudflow, containing debris and angular blocks of chiefly volcanic origin. . . ." As mentioned here, the term "mud-flow" has been used in the broad sense. Furthermore, some pyroclastic flow deposits have been confusedly given the same term occasionally. In order to eliminate such ambiguity of this term, a proper classification of mud-flows may be neccessary. In this paper, however, the writer omits the argument on such classification and discusses only the deposits of avalanches caused by the collapse of part of the volcanic cone destroyed by a violent explosion, descending down the mountain-slope by graviational force without the agency of water, for the purpose of comparing their size characteristics with those of pyroclastic flow deposits. In the following sections in this paper he uses the term "dry mud-flow" for such a tpye of flow of disintegrated materials.

Classification of Pyroclastic Flows

Since 1902 many examples of pyroclastic flows have been witnessed, and a large number of pyroclastic flow deposits have been recognized through the whole geologic column in the volcanic regions of the world. Some discussions and inferences on the origin and mechanism of pyroclastic flows have been presented, based upon results from actual investigations of the eruptions as well as studies of the discharged

22) C. A. Anderson, "The Tuscan formation of northern California," *Bull. Dept. Geol. Sci., Univ. Calif.*, **23** (1933), 215-276.

materials. Present concepts of the mode of eruption of pyroclastic flows depend almost entirely on the well-known published accounts of the 1902 eruptions of Mt. Pelée and the Soufrière and the eruption in 1912 in the Valley of Ten Thousand Smokes. These accounts have been augmented by several detailed observations of the later eruptions of pyroclastic flows which occurred on Mt. Pelée, Merapi, Mt. Lamington, Hibok-Hibok, etc. Now it is clarified that the phenomena of pyroclastic flows involve all kinds of flows of high-temperature essential fragmentary materials, graduating from the Pelean type eruptions emanating from the side of a dome to eruptions that produce vast ash-flow sheets. Among such various kinds of pyroclastic flows, there exist wide variations in the mode of eruption and nature of the discharged materials. Various classifications of pyroclastic flows have been proposed by many geologists and volcanologists. Lacroix (1930), Escher (1933), Neumann van Padang (1933), Fenner (1937), Cotton (1944), van Bemmelen (1949), MacGregor (1952 and 1955), Williams (1957) and Aramaki (1957) tried to analyze the mechanism of pyroclastic flows and proposed various schemes on the classification of this phenomenon[23].

Among these, Lacroix's classification is the most fundamental one, in which he established four subdivisions of pyroclastic flows or nuées ardentes in the broad sense. Lacroix carefully investigated the peculiar eruptions of Mt. Pelée in 1902–1903, which he named "nuées ardentes peléennes". These eruptions took place during the slow protrusion of viscous lava, forming a steep-sided dome. He distinguished two kinds

23) Alfred LACROIX, "Remarques sur les matériaux de projection des volcans et sur la genèse des roches pyroclastiques qu'ils constituent," *Centenaire Soc. Geol. France, Livre Jubliaire 1830-1930*, **2** (1930), 431-472.

B. G. ESCHER, "On a classification of central eruptions according to gas pressure of the magma and viscosity of the lava," *Leidsche Geol. Mededeel.*, **6** (1933), 45-49.

M. NEUMANN van PADANG, *op, cit.*, (1933).

C. N. FENNER, *op. cit.*, (1937).

C. A. COTTON, "Volcanoes as landscape forms," *Christchurch and London, Whitcomb and Tombs*, (1944 and 1952), 416.

R. W. van BEMMELEN, *op cit.*, (1949).

A. G. MACGREGOR, "Eruptive mechanisms—Mt. Pelée, the Soufrière of St. Vincent (West Indies) and the Valley of Ten Thousand Smokes (Alaska)," *Bull. Volcanol., ser. 2*, **12** (1952), 49-74.

A. G. MACGREGOR, "Classification of nuée ardente eruptions," *Bull. Volcanol., ser. 2*, **16** (1955), 7-10.

Howel WILLIAMS, "Glowing avalanche deposits of the Sudbury basin," *Ontario Dept. Mines 65th Ann. Rept.*, **65** (1957), 57-89.

Shigeo ARAMAKI, *op. cit.*, (1957).

of nuées ardentes at Mt. Pelée. One was initiated by the lateral explosive propulsion of the materials of a lava dome due to violent explosion through the flank of the dome. He termed this type "nuée ardente Peléenne d'explosion dirigée". The other originated through the collapse of part of the dome with a mild lateral explosion or without attendant explosions, which Lacroix termed "nuée ardente peléenne d'avalenche". The former is the most destructive type, such as the eruption that swept down from Mt. Pelée on May 8th, 1902. The latter is commonly recognized on the Merapi Volcano, and Escher called it the Merapi type. The pyroclastic flows at the Soufrière of St. Vincent differed from those of Mt. Pelée in being initiated by a vertical explosive eruption through an open crater. Lacroix termed this type "nuée ardente d'explosions vulcaniennes", and Escher called this "Glutwolken of the St. Vincent type". The last of Lacroix's subdivision is "nuée ardente du Massif du Katmai", named as it was first recognized from Fenner's study of the deposits emplaced in the Valley of Ten Thousand Smokes in the Katmai Region, Alaska, during the eruptions of 1912. Fenner (1937) termed this type a "Katmaian eruption". (See Table 1.)

Table 1. Classifications of pyroclastic flows.

Lacroix (1930)	Escher (1933) Fenner (1937)	Williams (1957)	Aramaki (1957)
Nuée ardente peléenne d'explosion dirigée	Pelée type	Pelean type	Nuée ardente in the strict sence
Nuée ardente peléenne d' avalanche	Merapi type		Intermediate type
Nuée ardente d'explosion vulcanienne	St. Vincent type	Vertical explosion type (Krakatoan type)	Pumice flow
Nuée ardente du Massif du Katmai	Katmaian type	Fissure eruption type (Valley of Ten Thousand Smokes type)	

MacGregor (1952 and 1955) proposed a detailed classification which was based upon the mode of initiation, source, specific type of eruption and magma. Williams (1957) distinguished three principal types of pyroclastic flows or glowing avalanches, namely, those attendant on the rise of Pelean domes, those formed by vertical explosions from craters and those produced by the discharge of effervescing magma from swarms of vertical fissures.

Most of the classifications of pyroclastic flows are based upon results

of direct observations on the mode of eruptions on the spot, although there are few examples of occurrences of pyroclastic flows ever witnessed. MacGregor (1952) stated that "the classification of nuées ardentes and tuff-flows should not be used as a kind of substitute for lithological classification of volcanic debris". Barksdale (1951), MacGregor (1952) and Neumann van Padang (1933) mentioned that deposits having lithologically similar features may be formed by different eruptive mechanisms. On the other hand, Williams (1957) discussed in detail the characteristics of deposits of the three principal types of pyroclastic flows. His precise accounts suggest the existence of some relationship between the types of pyroclastic flows and the textural and constituent characteristics of the deposits. Aramaki (1957) stated that there exists a certain relationship between the mode of emplacement and the nature of the deposits. He proposed a new classification of pyroclastic flows, mainly from the result of his study on the pyroclastic flow deposits discharged during the 1783 eruption of Mt. Asama.

There may be no marked discrepancy between Aramaki's classification based essentially upon the viscosity of essential fragmentary materials in the deposits and the others based mainly upon the mode and nature of eruptions. It may be wrong to discuss the nature and mechanism of eruptions of pyroclastic flows without investigating the characteristics of their deposits. For convenience in proceeding with his study, which is set out from quantitative inspections of the textural characteristics of pyroclastic flow deposits, the writer tries to draw a scheme of classification of pyroclastic flows by amending the previous ones. (See Table 2.) The classification is established on the basis of the nature of the representative eruptions of pyroclastic flows actually investigated by

Table 2. Proposed scheme of classification of pyroclastic flows.

Classification of pyroclastic flows		Pepresentatives
Nuée ardente	Pelée type (Merapi type)	Pelée (1902-03, 1929-32), Merapi (1930-31), Hibok-Hibok (1948-53), Lamington (1951-52).
	Sakurajima type	Sakurajima (1914, 1939), Asama-Kambara Nuée Ardente (1783).
Intermediate type		Tokachidake (1926), Asama-Agatsuma Pyroclastic Flow (1783).
Ash-flow	St. Vincent type	St. Vincent (1902), Komagatake (1929).
	Krakatoa type	Krakatoa (1883).
	V. T. T. S. type	Valley of Ten Thousand Smokes (1912).

geologists, as well as on the basis of the nature of their deposits, althouth there are rather few representatives. Detailed discussions on the nature of each type of pyroclastic flow and the characteristics of the deposit are presented in the later chapters. There are a large number of examples of pyroclastic flow deposits produced by pre-historic eruptions, and it is possible to deal with their characteristics consistenly in the framework of this classification. The writer classifies three subdivisions of pyroclastic flows, which generally correspond to three types of pyroclastic flows in Aramaki's classification (1957). The writers distinguishes two types of nuées ardentes; one takes place during the protrusion of viscous lava as a steep-sided dome, and the other is generated by the discharge of magma from a crater. Intermediate type pyroclastic flow shows intermediate nature between nuée ardente and ash-flow. The term "intermediate type" was proposed by Aramaki (1957), and the writer adopts this term in his classification. The writer adopts the term "ash-flow" to designate the pyroclastic flow which produces fine-grained pumiceous deposits. He distinguishes three types of ash-flows; one is produced by the vertical explosion through an open crater, being attendant on the rising of a lofty ash column, as explained by Hay (1959); the second one is caused also by the vertial explosion through a crater, but the magnitude of the eruption is by far greater in comparison with the former type, causing the collapse of a volcanic cone to form a characteristic depression, as stated by Williams (1941); and the last one is generated by the discharge of acidic magma through fissures.

Materials for the Study

The writer visited almost all the Japanese volcanoes where pyroclastic flow deposits, discharged mainly in the Holocene, have been recognized. He investigated the features of these deposits on the spot, and collected materials in order to examine their textural and constituent characteristics. Besides, he studied several examples of pyroclastic fall deposits, dry mud-flow deposits and auto-brecciated lava flows to compare their characteristics with those of pyroclastic flow deposits. The volcanoes visited by the writer shown in Fig. 1. There are a few other volcanoes having deposits of pyroclastic flows or mud-flows where he could not visit. He will investigate these volcanoes in the near future. The names of the volcanoes and brief descriptions of the pyroclastic flow deposits investigated by the writer are listed in Table 3. Localities

Table 3. List of the pyroclastic flows and their preceding falls in Japan which the writer studied.

Name of volume	Symbol	Remark	Rock type	SiO_2%	Volume	Welding	Sp. no.	Type of pyroclastic flow
Kutcharo	Kc	u	V	71.58(2)	80–100 km³	−	1,2,5,6,7,10	K
		m	V			−	3,4,8,9	K(f)
		l	V			+		K(f)
Mashu	Ms		V	65.53	5	−	1,2,3	K
Akan	Ak	u	V	65.87	60	−	1,2	K(f)
		l	V			+		K(f)
Akan (Meakandake)	Ak-cc		V		1	−	3,4	I
Daisetsuzan	D		VI			+	1,2	S
	D-fa		VI			−	3,4	
Tokachi Welded Tuff	TkW		XVI	71.57	60	+	1	K(f) or V
Tokachidake	Tk	1926-s	V	53.93	0.0035	−	5,6,7,8	I
		1926-p	V		0.0175	−	1,2,3,4	I
Shikotsu	S	u	VI	69.05	90–100	−	1∼11	K
		l	VI			+		K
	S-fa		VI	72.41	25	−	12	
Kuttara	Kt	u	V	64.27(4)	10	−	1,2	S
		l	V			+		
Toya	Ty	u	V		40	−	1,5,6,7,9	K
		l	V			−	2,3,4,8	K
	Ty-fa		V			−	11,12	
	Ty-o		V			−	10	S
Komagatake	Km	1929	V	59.15	0.15	−	1,2,3,4,5,6	S
	Km-fa	1929-fa	V		0.4	−	11	
	Km-o-K	Kurumizaka-fl	V		0.4	−	8	S
	Km-o-H	H.-shaped-cr.-fl	V		2.5	−	7,9,10	S
Towada	Tw		V	69.53(3)	50	−	1 19	K
	Tw-fa		V			−	23,24	
	Tw-o		V	60.44		−	20,21,22	S*
Osoreyama	Os		V			−	1	S*
Hakkodasan	Hd		V	68.51		+	1	K
Tazawa Welded Tuff	Tz		VI	74.16(2)	150	+	1	K or V
Onikobe	On		V			+∼−	1,2,3	K
Hijiori	Hj		VII		1.4	−	1,2	S
Numajiri Welded Tuff	Nm		V		1.15	+	1	I
Takaharayama	Th		V			−	1	K(f) or V

Table 3. (Continued)

Name of volume	Symbol	Rock type	SiO_2%	Volume	Remark	Welding	Sp. no.	Type of pyroclastic flow
Nantaisan	Nn-p	VI	62.86(2)	0.8 km³		+~−	2,3,4,5,6	S
	Nn-p-fa	VI		0.6		−		
	Nn-s		64.43	0.14		+~−	1	S
	Nn-s-fa			2.5		−	7	
Harunasan	Hr-u	VI		0.1		−	4	S
	Hr-u-fa	VI		0.6		−	5	
	Hr-l	VI		0.5		−	1,2,3	S*
Kusatsu-Shiranesan	KS	V		3	main part	+	1	S
		V			l	−	2,3,4	S*
Myoko	My	V	63.51	1.2		−	1~11	N-P
Asamayama	Am-up	V		1.0		−	17~23	S
	Am-up-fa	V				−	39	
	Am-lp	V	66.71	3·3		−	1~16	S
	Am-S	V		0.015	Shiraito-fl	−	35	I
	Am-O	V		0.6	Oiwake-fl	+~−	24~30	I
	Am-K	V		0.01~0.001	Kambara-na	−	34	N-S
	Am-A	V	60.8	0.1	Agatsuma-fl	+	31,32,33	I
	Am-1958	V				−	36,37,38	S
Hakone	Hn	V	60.87(2)	15	s	−	8,9,10	K
		V			p	−	1~7	K
Hakone Central Cone	Hn-cc	V				−	11,12,13	I
Ko-Fuji	KF	V				−	1~10	I
Aso	As	VI	62.88(4)	180	u	−	1,2	K
Aira	Ai	VI	74.53		u	−	5	K
		VI		150	m	−	1,2,6,7,11~13	K
		VI			l (or Ata-fl)	−	8,9,10	K(f)

Rock types were determined by Kuno's classification (1950) based upon mafic mineral assemblage. fl:pyroclastic flow, fa: pyroclastic fall, na:nuée ardente, s:scoria, p:pumice, o:pyroclastic flow of older stage, u:upper part, m:middle part, l:lower part, N-P:nuée ardente of Pelée type, N-S:nuée ardente of Sakurajima type, I:intermediate type pyroclastic flow, S:St. Vincent type ash-flow, S*:variety of St. Vincent type ash-flow having an intermediate nature between ash-flow and dry mud-flow, K:Krakatoa type ash-flow, f:fine-grained, V:V.T.T.S. type ash-flow. Values of SiO_2% attended by parenthese, figures in which are the numbers of data, are average values.

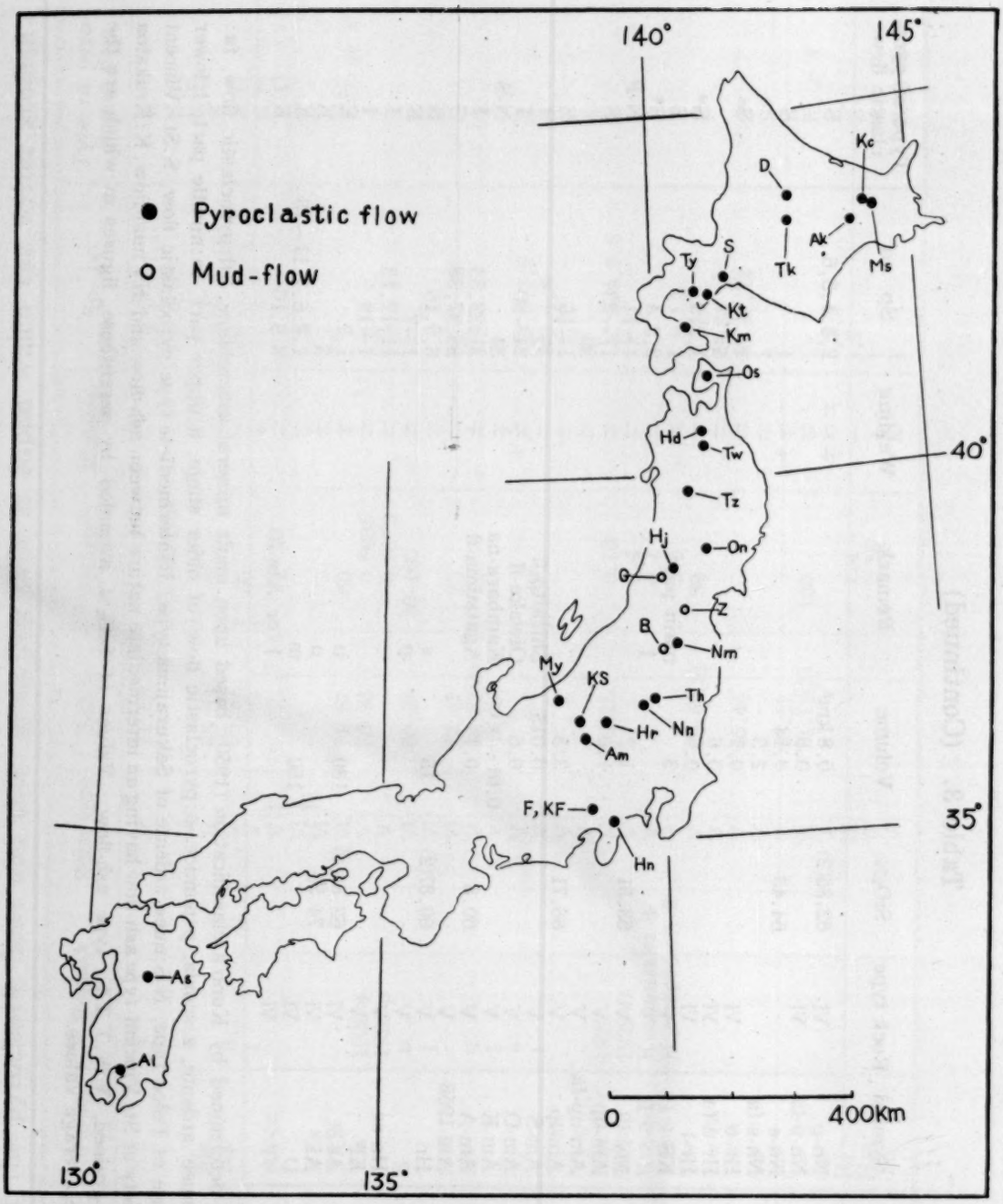

Fig. 1. Distribution map of the volcanoes, having deposits of pyroclastic flows and mud-flows, from which the samples were collected.

from which the materials were collected are shown in Figs. 2a–2k and Table 17. As shown in Table 3, the writer obtained many examples of pyroclastic flow deposits produced by the St. Vincent type and the Krakatoa type ash-flows. Almost entirety of the ash-flow deposits of

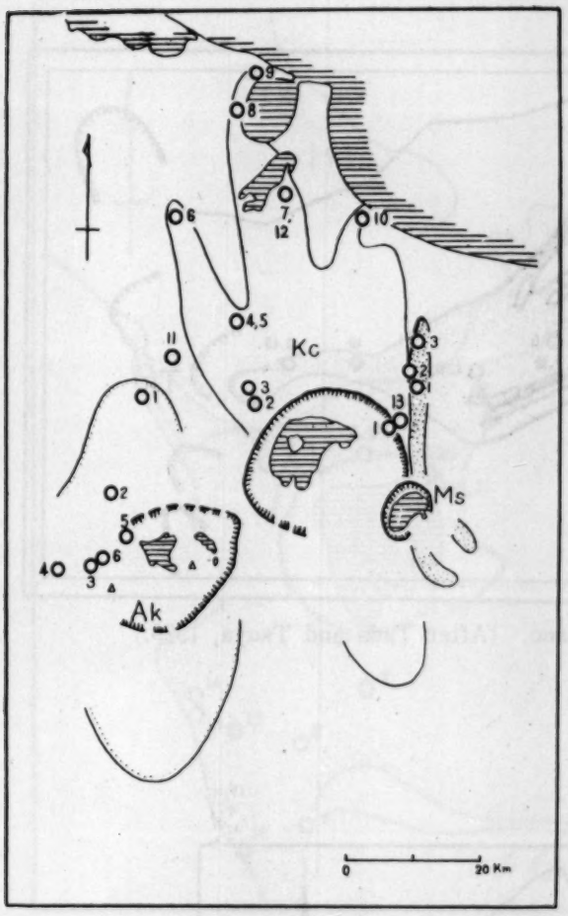

Fig. 2. Map showing the general distribution of pyroclastic flow deposits and the localities of samples collected for mechanical analyses.

Fig. 2a. The Kutcharo, Masyu and Akan Volcanoes.

Fig. 2b. The Shikotsu, Kuttara and Toya Volcanoes.

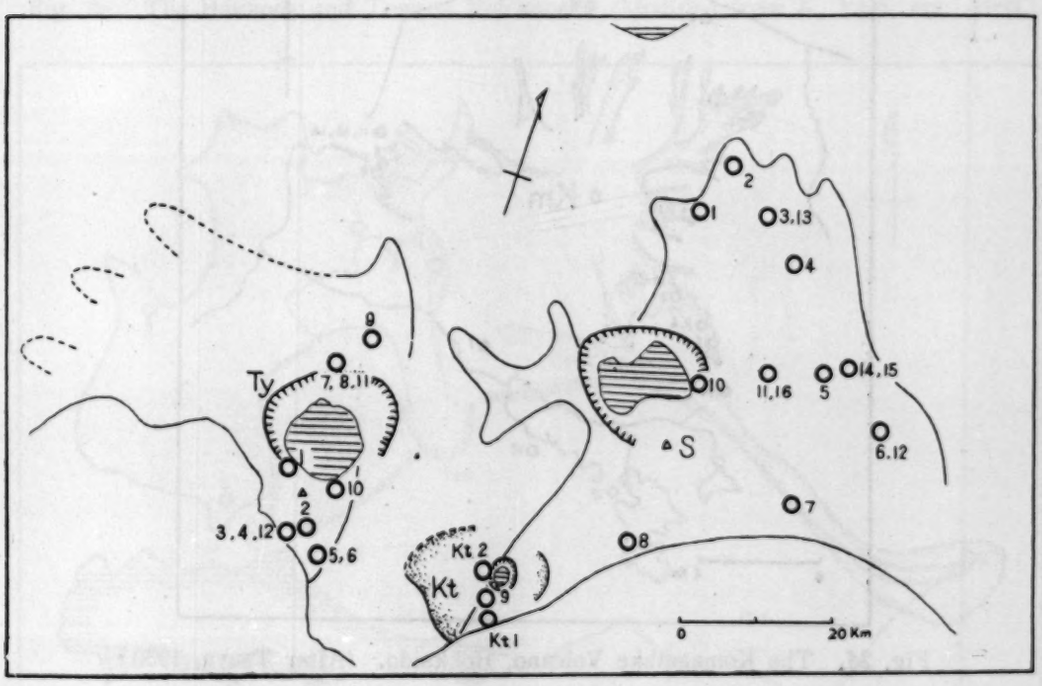

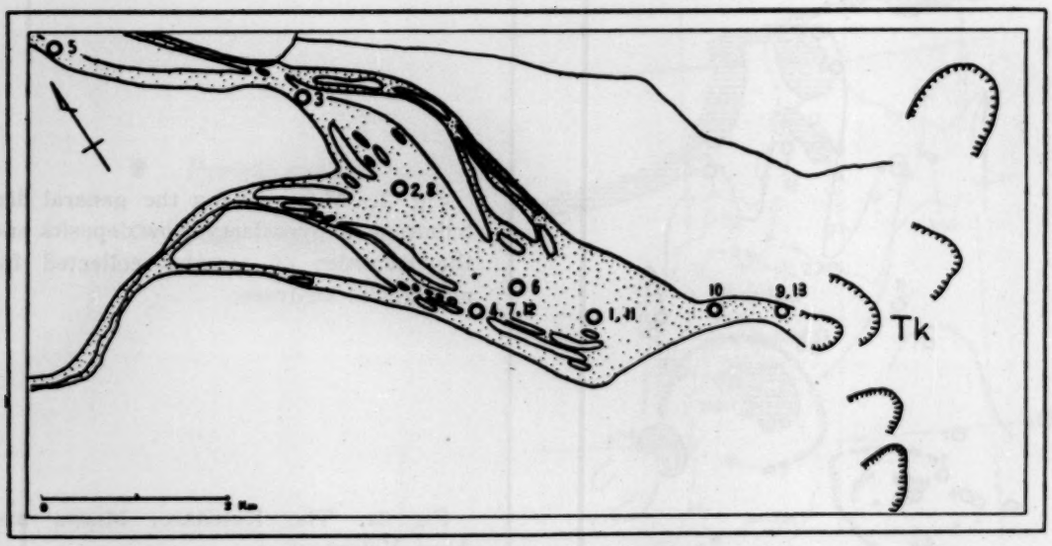

Fig. 2c. The Tokachidake Volcano. (After Tada and Tsuya, 1929.)

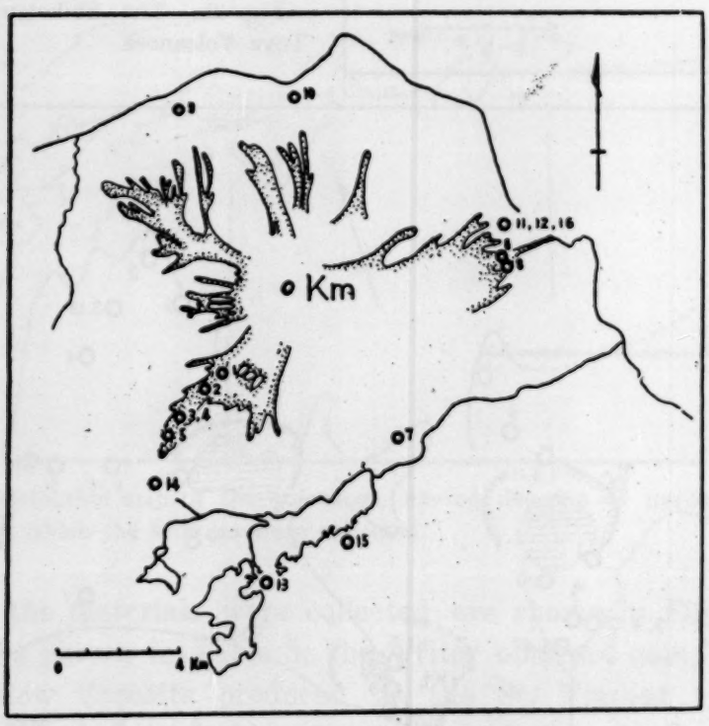

Fig. 2d. The Komagatake Volcano, Hokkaido. (After Tsuya, 1930)

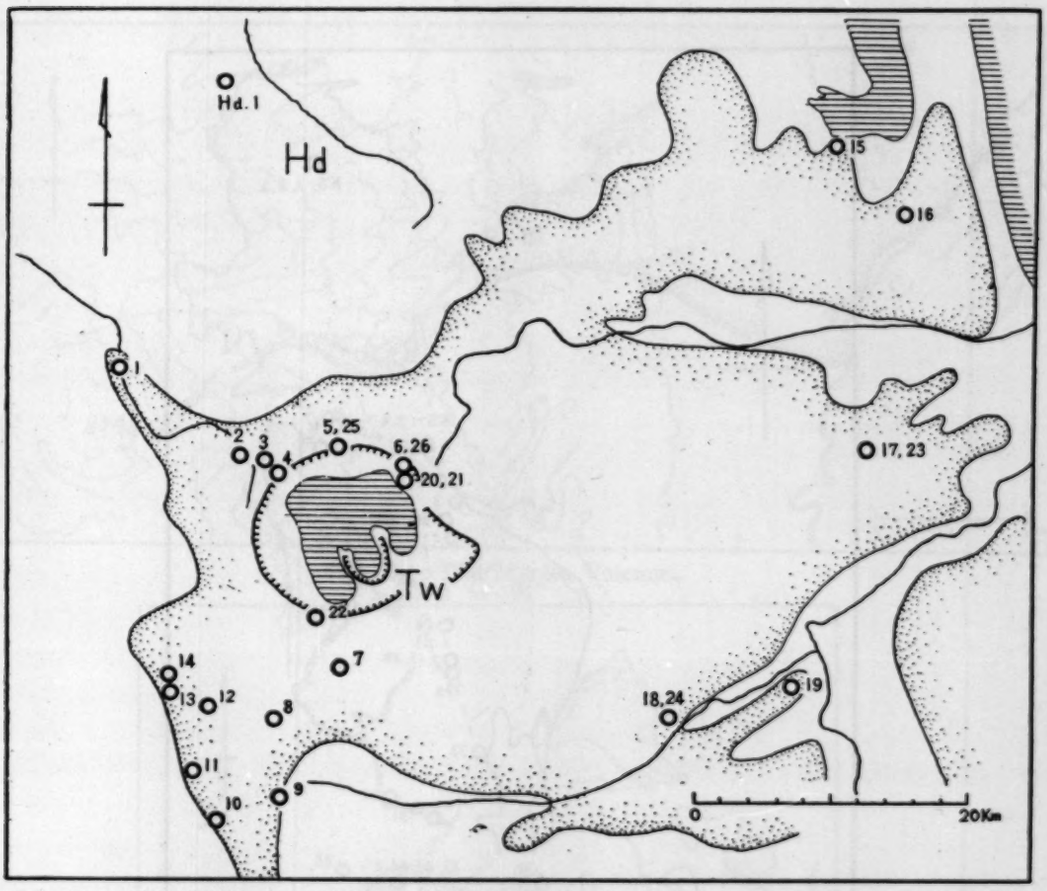

Fig. 2e. The Hakkoda and Towada Volcanoes. (Modified from K. Yagi, etc., 1960.)

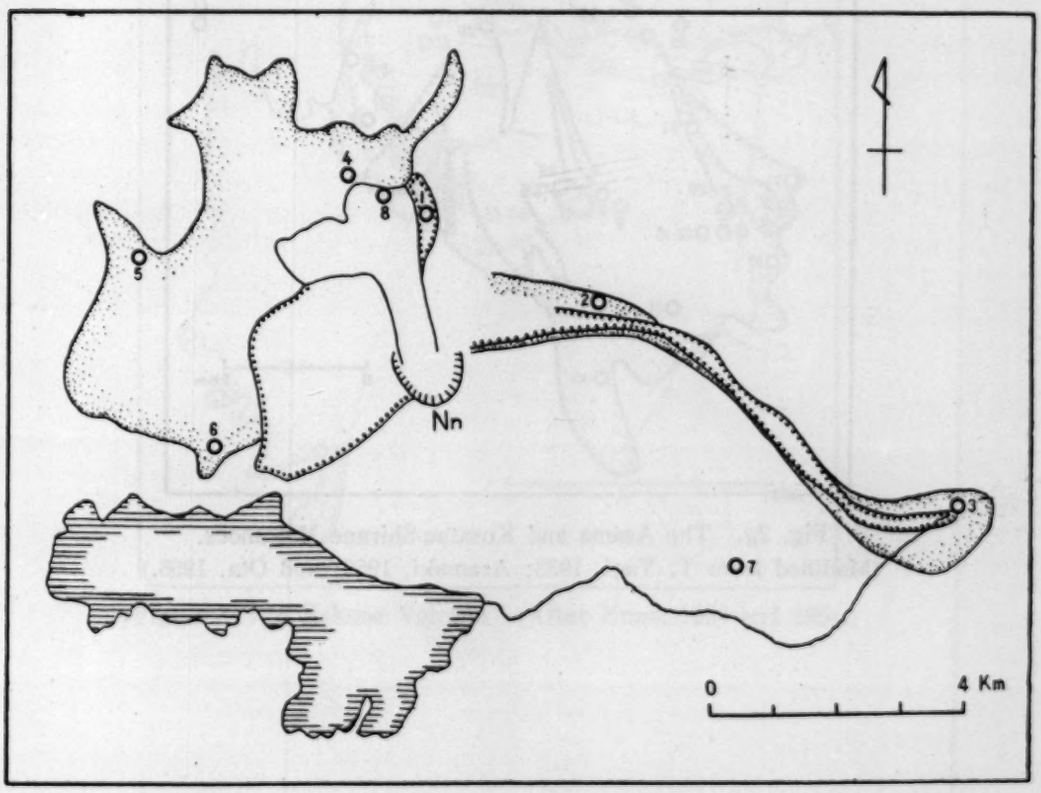

Fig. 2f. The Nantai Volcano, Nikko. (Modified from Yamasaki, 1957 and 1958.)

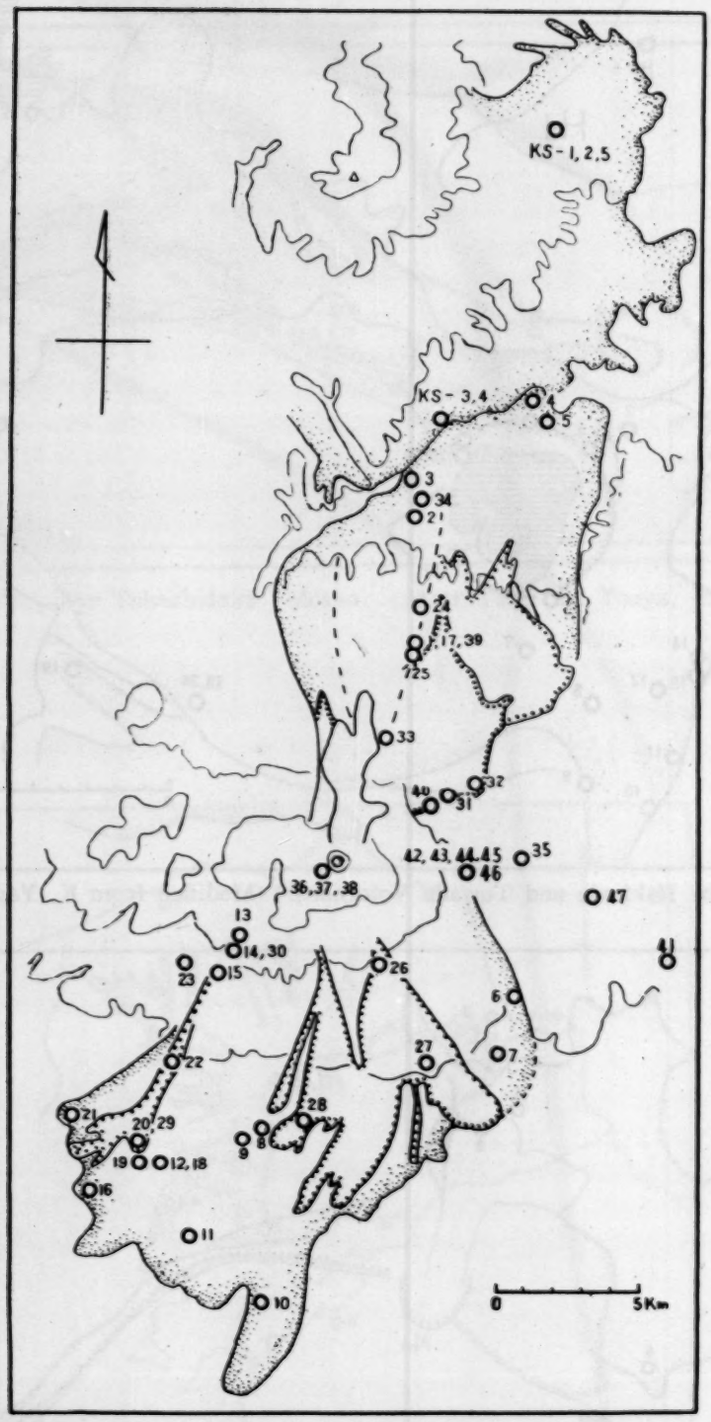

Fig. 2g. The Asama and Kusatsu-Shirane Volcanoes.
(Modified from T. Yagi, 1933; Aramaki, 1956; and Ota, 1956.)

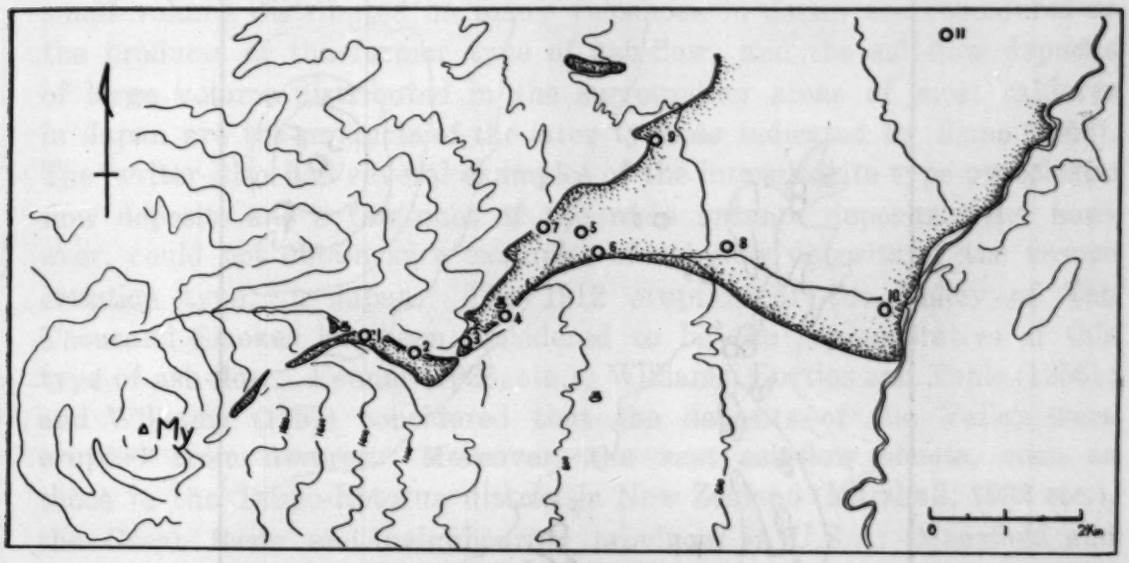

Fig. 2h. The Myoko Volcano.

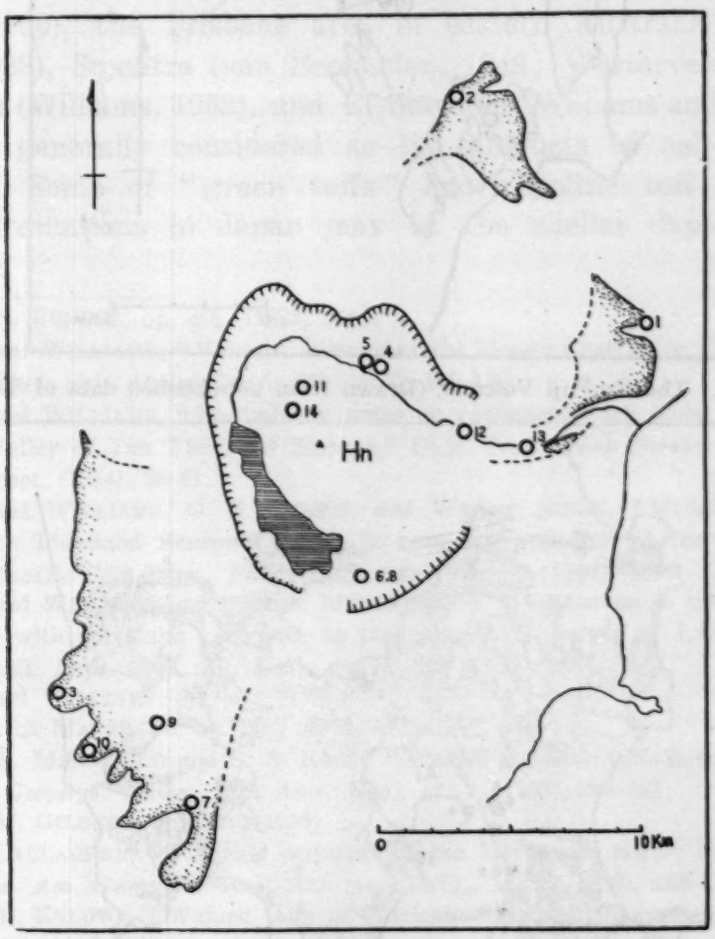

Fig. 2i. The Hakone Volcano. (After Kuno, 1950 and 1954.)

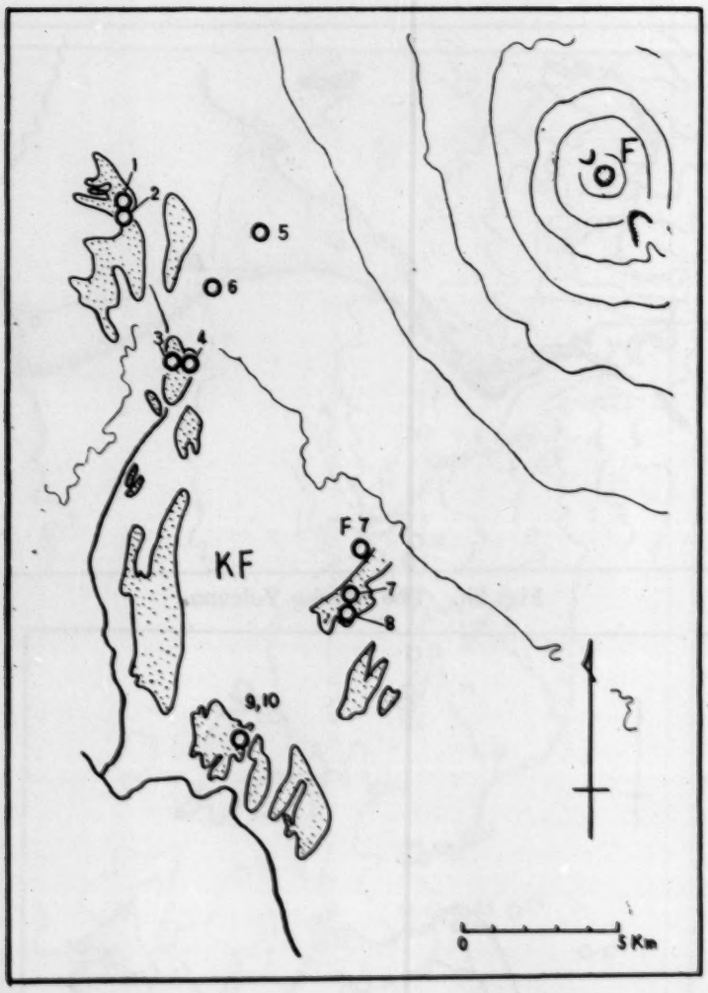

Fig. 2j. The Ko-Fuji Volcano. (Drawn from unpublished data of Tsuya.)

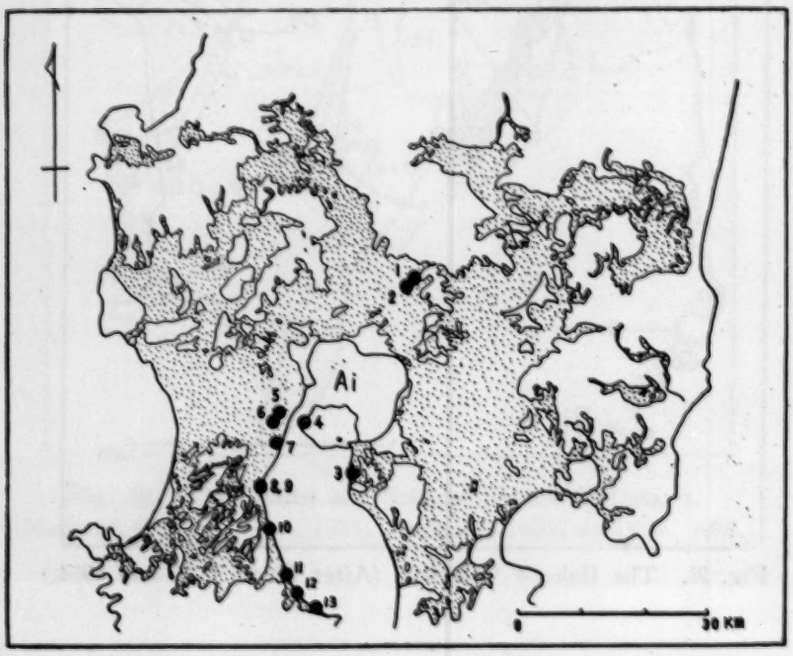

Fig. 2k. The Aira Volcano. (After Matsumoto.)

small volume distributed on many volcanoes in Japan are considered as the products of the former type of ash-flow, and the ash-flow deposits of large volume distributed in the surrounding areas of most calderas in Japan are the products of the later type as indicated by Kuno (1953). The writer also had several examples of the intermediate type pyroclastic flow deposits and a few ones of the nuée ardente deposits. He, however, could not obtain sure examples of ash-flow deposits of the fissure eruption type, in Japan. The 1912 eruption of the Valley of Ten Thousand Smokes has been considered to be the representative of this type of ash-flow. Fenner (1923, etc.); Williams, Curties and Tuhle (1956); and Williams (1957) considered that the deposits of the Valley were erupted from fissures. Moreover, the vast ash-flow sheets, such as those in the Taupo-Rotorua district in New Zealand (Marshall, 1932 etc.), the Great Basin and neighbouring provinces in U.S.A. (Mansfield and Ross, 1935; Gilbert, 1938; Callaghan, 1939; Enlows, 1955; Sabins, 1957; Mackin, 1960), the Brisbane area in eastern Australia (Richards and Bryan, 1933), Sumatra (van Bemmelen, 1949; Westerveld, 1942, etc.), Costa Rica (Williams, 1952), and El Salvador (Williams and Meyer-Abich, 1955), are generally considered as the products of ash-flows through fissures.[24] Some of "green tuffs" and rhyolitic tuff sheets in the Tertiary formations in Japan may be the similar deposits, the witer consideres.

---

24) C. N. FENNER, *op. cit.*, (1923, etc.).

Howel WILLIAMS, "Volcanic history of the Meseta Central Occidental, Costa Rica," *Bull. Dept. Geol. Sci., Univ. Calif.*, **29** (1952), 145-180.

Howel WILLIAMS, "Preliminary notes on geological work done on Mount Katmai and in the Valley of Ten Thousand Smokes," *U. S. Natl. Park Service Interim Rept. on Katmai Project*, (1954), 55-61.

Howel WILLIAMS, G. H. CURTIS, and Werner JUHLE, "Mount Katmai and the Valley of Ten Thousand Smokes, Alaska (a new interpretation of the great eruptions of 1912)," *8th Pacific Sci. Cong., Philippines 1953 Proc.*, **2** (1956), 129.

Howel WILLIAMS and Helmut MEYER-ABICH, "Volcanism in the southern part of El Salvador—with particular reference to the collapse of basins of Lake Coatepeque and Ilopango," *Bull. Dept. Geol. Sci. Univ. Calif.*, **32** (1955), 1-64.

Howel WILLIAMS, *op. cit.*, (1957).

Patrick MARSHALL, *op. cit.*, (1932, etc.).

G. R. MANSFIELD and C. S. ROSS., "Welded rhyolitic tuffs in southeastern Idaho," *Trans. Am. Geophys. Union, 16th Ann. Mtg., pt. 1*, (1935), 308-321.

C. M. GILBERT, *op. cit.*, (1938).

E. CALLAGHAN, "Volcanic sequence in the Marysvale region in southwest-central Utah," *Trans. Am. Geopys. Union, 20th Ann. Mtg., pt. 3*, (1939), 428-452.

H. E. ENLOWS, "Welded tuffs of Chiricahua National Monument," *Bull. Geol. Soc. Am.*, **66** (1955), 1215-1246.

Size Characteristics of Pyroclastic Flow Deposits.

General Statement

It is generally believed that the most distinct features of pyroclastic flow deposits are non-stratification and non-sorting (or ill-sorting) as can be seen at any outcrops of the deposits. There is no grading of any kind in the deposits, and fragments range in size from large blocks sometimes exceeding scores of meters in diameter to minute vesicular dust. This contrasts strikingly with the well-sorted features of air fall pyroclastic deposits. The difference may be clarified in diagrams of particle size distributions drawn from the results of mechanical analyses. In the case of pyroclastic flow, it is considered that large blocks, smaller fragments and fine dust travel *en masse* for long distances from the source in a state of turbulent flow. Such motion of the pyroclastic flow may give rise to the characteristic ill-sorted features of the deposits. On the contrary, in the case of pyroclastic fall, ejecta hurled up high into the air are transported by the atmospheric current under the agency of an eolian differentiation, the larger and the denser fragments falling first and closest to the vent while the smaller and the more vesicular fragments fall farther from the vent. Consequently, deposits of pyroclastic falls are well sorted and show distinct lateral and vertical regular grading in texture and composition.

Deposits of dry mud-flows exhibit distinct features of unstratification and ill-sorting, similar to those of pyroclastic flow deposits, although

---

Floyd F. SABINS JR., "Geology of the Cochise Head and western part of the Vanar Quadrangles, Arizona," *Bull. Geol. Soc. Am.*, **68** (1957), 1315-1342.

J. Hoover MACKIN, "Structural significance of Tertiary volcanic rocks in southwestern Utah," *Am. Jour. Sci.*, **258** (1960), 81-131.

H. C. RICHARDS and W. H. BRYAN, "The problem of the Brisbane tuff," *Pr. Roy. Soc. Queensland*, **45** (1933), 50-61.

R. W. van BEMMELEN, *op. cit.*, (1949).

J. WESTERVELD, "Welded rhyolitic tuffs or 'ignimbrites' in the Pasoemah region, West Palembang, South Sumatra," *Leidsche Geol. mededeel.*, **13** (1942), 202-217.

J. WESTERVELD, "On the origin of the acid volcanic rocks around Lake Toba, North Sumatra," *Verh. Kon. Ned. Akad. van Wetensch., Afd. Natuurk., Tweede Sectie*, **43** (1947), 1-51.

J. WESTERVELD, "Quaternary volcanism on Sumatra," *Bull. Geol. Soc. Am.*, **63** (1952), 561-594.

J. WESTERVELD, "Eruptions of acid pumice tuffs and related phenomena along the great Sumatran fault-trough system," *7th Pacific Sci. Cong., New Zealand 1949, Proc.*, **2** (1953), 411-438.

there exists a pronounced difference in composition between these two types of deposits. This indicates the fact that the mode of emplacement and mechanism of flowage may be similar in both cases. Auto-brecciated parts of lava flows also show similar features to those of pyroclastic flow deposits.

Data on the size characteristics of various kinds of pyroclastic flow deposits suggest that there is considerable room for variation within the framework of size distribution curves. This may be clearly indicated in diagrams of size distribution curves and in diagrams of parameters of size distributions. The variations among size distribution curves represent the difference in the proportion of coarse to fine materials and in the degree of sorting, and originally may result from the difference in the mode of origin and mechanism of pyroclastic flow eruption. Accordingly, detailed studies on many examples of the deposits should yield some useful data for deciphering the origin and mechanism of this phenomenon.

Methods of Mechanical Analyses

The writer collected samples, each about 1 to 4 kg in weight, for analyses of textural characteristics of the deposits. As the methods of mechanical analyses have already been explained in detail by the writer

Table 4. Results of mechanical analyses of pyroclastic flow deposis deposits. The result of the analysis of a given sample is noted in the column beneath its sample with weight per cent of each fraction.

ϕ	Kc 1	2	3	4	5	6	7	8	9	10
～−6	0.2	2.2			0.4	0.3	0.4			
−6～−5	1.0	4.6	0.3		0.8	1.1	1.4		0.1	0.2
−5～−4	1.6	6.2	0.9	0.4	2.1	1.9	2.5	0.1	0.1	1.1
−4～−3	5.2	6.7	1.3	0.5	4.0	3.1	2.9	0.3	0.2	2.4
−3～−2	6.3	7.5	2.2	1.1	5.0	4.4	3.6	0.7	0.6	2.6
−2～−1	7.0	7.6	3.4	2.4	5.5	4.6	4.2	0.8	1.0	4.6
−1～−0	15.6	11.8	12.3	7.3	11.9	9.1	9.1	3.4	3.3	9.7
0～ 1	14.6	15.2	19.4	14.5	17.1	17.6	16.6	8.7	9.3	17.7
1～ 2	10.3	10.0	13.0	13.7	12.2	14.4	14.0	10.3	13.1	13.5
2～ 3	6.9	8.5	11.0	14.3	10.7	15.1	14.9	18.0	18.0	12.4
3～ 4	6.0	6.0	12.9	15.1	10.6	14.6	14.0	21.0	23.6	14.5
4～ 5	4.6	4.9	8.8	12.8	7.7	9.3	8.7	16.1	13.7	9.8
5～ 6	6.5	4.0	5.5	7.3	4.3	3.5	4.0	9.7	6.2	4.5
6～ 7	7.3	2.4	5.3	4.4	3.9	0.7	2.2	6.4	2.6	2.6
7～ 8	4.4	1.4	2.5	2.5	2.5	0.1	0.9	2.8	2.8	1.3
8～ 9	1.2	0.8	0.7	0.9	0.9	0.1	0.2	1.0	2.8	0.8
9～	1.3	0.2	0.5	2.8	0.4	0.1	0.4	0.7	2.6	2.3

Table 4. (Continued)

ϕ	Ms 1	2	3	Ak 1	2	3	4	D 1	2
~−8								2.5	
−8~−7			0.2					3.7	
−7~−6		0.5	0.2			1.7		4.4	1.6
−6~−5		1.8	1.6	0.1		2.1	3.5	4.0	4.4
−5~−4	1.3	3.3	2.5	1.1		2.5	8.7	4.1	5.7
−4~−3	5.4	4.2	3.8	2.6	2.3	3.8	9.5	4.6	5.6
−3~−2	8.1	4.7	4.6	3.9	3.7	5.2	9.7	5.1	5.9
−2~−1	10.9	5.5	4.8	5.2	5.5	5.9	6.8	4.9	4.8
−1~−0	14.9	11.2	8.4	10.9	7.3	7.1	12.0	11.1	10.9
0~ 1	15.7	15.0	13.5	19.0	16.9	19.6	16.5	19.2	19.6
1~ 2	12.0	11.8	10.2	14.8	14.5	21.6	11.9	12.6	13.8
2~ 3	9.2	11.7	11.4	12.3	13.5	15.8	7.1	7.3	8.8
3~ 4	7.3	10.9	11.5	14.3	14.0	9.7	4.6	4.8	5.7
4~ 5	5.5	7.4	8.3	9.7	10.0	3.6	3.5	3.7	4.0
5~ 6	3.5	5.7	6.5	2.9	5.5	0.6	2.5	2.8	3.0
6~ 7	1.9	3.0	5.0	1.5	3.2	0.3	1.8	2.5	2.8
7~ 8	2.0	2.1	3.5	0.7	1.9	0.3	1.1	1.5	1.6
8~ 9	2.1	0.8	1.9	0.5	0.5	0.1	0.7	0.6	0.5
9~	0.2	0.4	2.1	0.5	1.2	0.1	0.1	0.6	1.3

ϕ	TkW 1	Tk 1	2	3	4	5	6	7	8
~−9				1.3					1.2
−9~−8		1.2	2.0	1.4		1.0	0.8		5.5
−8~−7		5.2	1.7	1.9		2.0	2.9	4.0	5.8
−7~−6		5.4	2.1	2.2		3.3	4.3	5.3	5.1
−6~−5		3.4	7.2	3.2		4.6	4.7	3.4	3.5
−5~−4	0.2	4.1	11.5	6.1		5.8	3.8	2.0	4.2
−4~−3	2.5	4.1	10.1	8.2		6.1	6.2	4.0	5.0
−3~−2	3.0	6.0	8.2	7.9	1.2	8.1	7.3	6.0	5.4
−2~−1	3.1	7.4	7.0	7.1	1.5	8.4	6.3	6.5	6.2
−1~ 0	11.3	10.5	9.2	10.2	3.5	10.0	10.6	8.8	9.1
0~ 1	15.5	17.9	15.7	17.0	10.4	14.2	16.6	17.0	14.3
1~ 2	15.0	16.8	12.0	14.8	15.3	12.3	15.0	15.7	12.7
2~ 3	16.7	10.2	7.5	9.5	18.3	8.9	9.5	12.4	8.8
3~ 4	15.5	4.2	2.8	4.5	18.9	6.0	6.1	7.2	5.9
4~ 5	9.0	1.0	1.3	1.9	15.9	3.8	2.9	3.8	3.8
5~ 6	3.4	0.7	0.5	0.7	5.4	1.9	1.3	1.2	1.6
6~ 7	1.9	0.7	0.4	1.4	3.3	1.4	1.2	1.2	0.7
7~ 8	1.0	0.5	0.5	0.4	2.4	0.8	0.3	0.6	0.8
8~ 9	0.6	0.3	0.2	0.2	2.1	1.3	0.1	0.7	0.2
9~	1.3	0.2	0.1	0.1	1.8	0.2	0.1	0.2	0.2

Table 4. (Continued)

ϕ	S 1	2	3	4	5	6	7	8	9	10	11
~−6						0.2					0.4
−6~−5			0.3	0.3	1.4	0.5	0.5				0.7
−5~−4	0.7	0.8	1.0	0.9	3.6	1.5	4.5	2.2	1.5	3.1	1.1
−4~−3	1.7	2.2	3.7	2.4	5.2	2.9	6.0	7.5	2.6	4.8	2.0
−3~−2	3.4	3.8	6.0	5.1	6.6	4.5	7.8	9.0	4.0	6.3	3.1
−2~−1	5.9	5.7	7.7	7.0	6.5	5.4	7.6	10.0	4.7	7.0	4.8
−1~ 0	7.8	7.9	9.4	8.4	8.5	6.8	7.5	12.5	5.3	9.5	8.1
0~ 1	12.7	11.9	11.1	11.9	10.7	9.2	9.9	11.7	9.7	11.6	14.8
1~ 2	12.5	12.0	11.9	13.0	12.0	12.0	10.3	9.5	12.3	12.3	14.7
2~ 3	15.6	13.9	13.2	14.8	11.3	16.2	10.2	9.4	15.9	13.0	12.0
3~ 4	14.3	15.6	13.0	13.7	11.2	14.8	9.8	8.5	17.1	10.9	9.8
4~ 5	10.8	11.4	8.7	8.6	8.8	10.4	8.3	7.0	12.7	7.5	8.5
5~ 6	6.6	5.8	5.0	6.1	5.4	6.8	7.2	4.4	5.5	4.2	7.0
6~ 7	3.4	3.3	3.3	3.1	3.8	3.2	4.7	3.0	4.4	2.5	5.3
7~ 8	2.1	2.4	1.4	1.9	1.9	2.6	2.9	1.6	2.5	2.2	3.1
8~ 9	0.4	1.5	0.8	0.6	1.0	0.6	1.8	1.3	0.6	1.7	1.6
9~	2.1	1.8	3.5	2.2	2.0	2.4	1.0	2.4	1.2	3.4	3.0

ϕ	Kt 1	2	Ty 1	2	3	4	5	6	7	8	9	10
~−6		0.6									0.7	
−6~−5	1.7	1.2									2.3	
−5~−4	4.8	4.5	0.3	0.3		0.4	2.2	5.2	2.9		3.5	2.5
−4~−3	5.2	7.4	2.8	2.7		2.5	8.1	7.6	7.8		1.8	5.8
−3~−2	5.5	6.7	3.9	4.6	1.7	5.0	10.5	9.2	11.0	0.3	3.6	7.4
−2~−1	4.8	5.6	9.2	6.4	5.2	7.9	11.4	10.8	12.1	1.7	6.2	8.0
−1~ 0	8.0	8.3	14.2	8.7	8.9	8.8	11.7	11.9	15.4	3.9	14.2	18.9
0~ 1	24.3	16.7	17.3	12.0	11.7	11.4	10.8	10.3	13.9	8.1	20.3	20.3
1~ 2	18.9	23.6	13.3	11.9	13.2	9.8	7.7	7.3	8.7	12.9	15.9	10.9
2~ 3	8.5	8.6	12.5	13.0	16.6	11.2	6.1	6.7	6.6	17.6	11.1	8.4
3~ 4	4.2	5.1	11.8	15.1	17.0	13.0	8.8	7.3	5.5	20.8	7.2	6.6
4~ 5	3.1	3.3	7.0	10.6	11.4	11.5	8.0	7.0	4.4	16.4	4.7	3.5
5~ 6	3.3	2.3	2.6	5.8	6.0	6.8	4.9	6.0	3.6	7.4	1.8	2.4
6~ 7	3.0	1.7	1.7	3.9	3.3	5.1	3.6	4.4	2.4	4.0	1.5	2.3
7~ 8	2.4	1.3	0.4	2.0	2.3	2.9	2.9	2.9	1.4	3.1	1.5	1.3
8~ 9	0.9	0.8	0.6	1.1	0.7	1.3	0.8	1.3	1.8	2.3	1.7	0.6
9~	1.4	2.3	2.4	1.9	2.0	2.4	2.0	1.1	2.2	1.5	2.0	1.1

Table 4. (Continued)

ϕ	Km 1	2	3	4	5	6	7	8	9	10
~−8	2.0	1.2				1.5				
−8~−7	2.8	1.8		1.6	1.6	6.8		1.4	1·4	
−7~−6	3.1	3.0	0.4	3.2	4.1	8.1	1.8	2.4	3.5	3.2
−6~−5	3.5	3.6	2.9	6.7	8.1	7.9	3.9	3.9	4.6	4.8
−5~−4	4.4	4.7	7.5	12.8	9.2	8.6	5.6	7.6	5.7	6.8
−4~−3	7.2	6.7	6.8	7.4	6.2	6.8	6.5	8.2	5.2	6.4
−3~−2	6.1	5.8	5.6	3.5	4.5	3.9	5.5	6.1	4.6	4.0
−2~−1	3.1	3.5	3.8	3.8	3.3	2.7	4.7	4.0	5.0	3.1
−1~ 0	12.3	11.5	9.8	9.5	8.7	8.3	12.2	11.8	15.6	9.0
0~ 1	26.0	26.7	27.8	22.3	22.3	19.0	27.6	22.2	23.9	25.0
1~ 2	13.0	13.8	15.7	12.3	13.9	10.9	16.3	14.5	12.9	14.0
2~ 3	5.0	5.5	6.1	4.8	5.3	4.2	5.9	5.7	6.8	6.3
3~ 4	2.1	2.7	2.8	1.8	2.4	2.4	1.3	2.5	3.3	2.7
4~ 5	1.7	1.9	1.9	1.5	1.7	1.3	1.4	1.9	3.1	1.8
5~ 6	2.3	1.9	1.7	2.3	2.8	1.3	1.2	2.0	2.2	4.1
6~ 7	2.5	2.8	3.5	3.5	2.8	3.0	2.2	2.8	1.5	4.6
7~ 8	2.2	2.0	2.4	1.7	1.9	2.6	2.2	1.7	0.5	2.2
8~ 9	0.3	0.7	1.1	1.0	0.8	0.6	0.5	1.0	0.1	1.1
9~	0.2	0.2	0.2	0.3	0.4	0.1	1.5	0.3	0.2	0.9

ϕ	Tw 1	2	3	4	5	6	7	8	9	10	11	12
~−7									0.7			0.2
−7~−6									1.1			0.6
−6~−5	0.7		3.1			1.2			2.3	0.3	0.3	1.7
−5~−4	3.2	0.9	5.2	1.3	1.2	2.0			4.3	2.0	1.1	3.7
−4~−3	6.9	1.9	6.3	2.4	5.5	2.6	1.0	1.6	9.6	3.6	1.9	6.0
−3~−2	9.8	3.2	6.8	3.3	8.4	4.5	1.3	3.3	11.3	5.1	2.5	7.1
−2~−1	11.1	6.0	9.3	3.5	8.3	8.3	3.9	4.7	9.8	5.7	4.7	7.4
−1~ 0	12.7	10.8	11.6	6.6	8.5	9.9	8.4	6.3	9.6	7.2	6.9	9.9
0~ 1	17.9	12.2	13.9	14.1	11.8	12.5	14.3	11.1	14.9	13.8	11.9	15.2
1~ 2	12.7	14.5	10·2	17.0	10.9	10.3	14.3	12.3	12.1	13.5	10.9	11.8
2~ 3	8.3	11.7	7.2	13.2	8.2	7.1	12.1	9.9	6.3	8.8	9.6	7.7
3~ 4	6.5	9.5	6.6	9.9	8.4	6.8	11.4	9.4	4.1	8.0	11.5	6.0
4~ 5	4.7	8.3	6.1	5.9	8.6	8.3	10.0	9.1	3.7	7.4	11.5	5.5
5~ 6	2.5	6.7	5.0	5.8	7.4	8.8	8.5	9.9	3.0	8.2	9.5	4.9
6~ 7	1.3	6.1	3.9	6.4	5.6	7.5	6.9	9.1	2.8	7.5	7.5	4.3
7~ 8	0.5	4.4	3.0	4.4	3.3	5.4	4.0	6.9	2.1	4.8	4.7	3.5
8~ 9	0.4	1.6	0.9	1.8	1.6	1.8	1.7	3.1	0.5	1.3	2.3	1.8
9~	0.8	2.2	0.9	4.8	2.3	3.0	2.2	3.3	1.8	2.8	3.2	2.7

Table 4. (Continued)

ϕ	Tw 13	14	15	16	17	18	19	20	21	22	Os 1	Hd 1
~−8	0.7											
−8~−7	1.4				0.1	0.3		0.7	0.8			1.1
−7~−6	2.9	0.3			0.2	0.7		1.5	1.4			1.9
−6~−5	4.3	3.2	0.1		2.0	1.9	0.5	5.5	1.8		0.3	1.7
−5~−4	6.4	7.0	4.6	0.1	5.0	3.6	2.5	11.8	2.1	6.4	1.7	1.4
−4~−3	7.8	9.8	8.0	1.1	7.1	5.7	3.9	14.1	2.7	10.4	3.7	0.7
−3~−2	8.8	10.5	10.0	2.6	7.8	6.4	4.3	14.4	4.0	10.9	4.8	1.3
−2~−1	9.5	9.9	9.5	4.1	9.1	7.1	5.0	11.3	7.6	9.0	7.2	1.9
−1~ 0	9.4	10.0	10.8	9.4	8.7	9.1	5.3	9.5	11.3	10.4	9.4	9.7
0~ 1	12.1	12.7	8.7	14.4	12.8	14.5	9.5	8.8	15.4	12.5	14.0	21.4
1~ 2	11.7	12.1	6.8	12.3	15.5	13.5	12.5	6.9	15.6	8.7	15.6	12.4
2~ 3	6.3	6.2	6.0	11.3	9.5	7.9	9.3	4.8	12.8	7.4	13.3	7.2
3~ 4	3.9	3.3	6.5	11.7	5.2	5.9	9.2	3.1	9.5	6.6	10.9	6.1
4~ 5	3.0	1.9	6.7	10.7	4.2	6.0	10.5	2.8	6.2	6.2	7.1	6.0
5~ 6	3.1	4.0	6.0	8.1	3.5	5.2	9.7	1.7	3.5	5.2	4.0	5.5
6~ 7	4.0	3.6	4.6	6.2	3.6	4.8	8.3	0.9	2.2	3.7	3.4	4.7
7~ 8	2.4	2.4	4.0	3.9	3.0	3.6	5.8	0.9	1.1	1.6	2.4	4.4
8~ 9	1.0	0.6	2.3	2.0	1.7	2.3	1.8	0.4	0.6	0.8	0.9	3.7
9~	1.3	2.5	5.4	2.1	1.0	1.5	1.9	0.9	1.4	0.2	1.3	8.9

ϕ	Tz 1	On 1	2	3	Hj 1	2	Nm 1	Nn 1	2	3	4	5	6
~−9							1.0						
−9~−8							2.0						
−8~−7							3.0	1.3	0.3	2.0		2.0	1.7
−7~−6							4.2	5.7	3.9	3.8	0.8	3.2	6.0
−6~−5	1.3	1.3	4.2	1.2		0.5	5.0	13.5	8.1	6.5	1.5	4.8	8.1
−5~−4	1.1	2.2	6.4	2.1	1.7	3.3	5.4	12.6	9.7	7.9	1.0	4.2	8.2
−4~−3	1.6	4.8	5.1	2.5	5.7	7.0	4.5	8.4	13.5	6.9	1.1	3.0	7.2
−3~−2	1.0	6.7	3.5	2.9	7.7	7.9	4.2	5.8	12.4	5.9	1.4	2.1	5.8
−2~−1	2.3	6.1	2.8	3.5	7.8	7.6	4.7	5.7	9.4	4.3	3.0	1.4	5.5
−1~ 0	16.5	6.4	4.2	11.2	12.2	8.9	14.5	7.3	9.0	11.3	19.0	7.5	7.9
0~ 1	20.9	18.7	5.6	16.6	22.8	17.8	18.7	5.0	8.9	18.5	23.5	15.8	13.2
1~ 2	13.3	18.9	7.6	10.4	19.1	15.3	10.9	4.5	7.3	11.2	13.3	12.7	10.2
2~ 3	10.0	10.8	10.9	8.3	12.3	11.7	6.0	5.0	6.2	5.9	7.7	8.9	7.9
3~ 4	8.7	6.6	16.2	8.1	5.9	7.2	4.6	5.6	5.6	3.5	7.1	8.1	6.3
4~ 5	7.1	4.8	12.2	6.4	2.1	3.5	4.5	4.7	3.5	2.8	8.2	8.1	4.2
5~ 6	5.5	4.3	9.6	4.0	0.8	2.8	3.7	3.6	0.9	3.3	7.0	7.0	3.2
6~ 7	3.6	2.9	6.5	3.8	0.7	2.9	1.9	3.0	0.9	3.1	3.6	5.8	2.4
7~ 8	2.5	2.3	2.8	4.2	0.3	1.8	0.5	2.2	0.2	1.8	1.1	3.4	1.2
8~ 9	1.6	1.0	1.0	4.6	0.3	1.0	0.2	1.5	0.1	0.5	0.6	1.6	0.4
9~	3.0	2.2	1.4	10.2	0.6	0.8	0.5	4.6	0.1	0.8	0.1	0.4	0.6

Table 4. (Continued)

ϕ	Th 1	Hr 1	2	3	4	KS 1	2	3	4
~−7			0.7						
−7~−6		2.7	2.3						2.2
−6~−5	0.1	5.5	4.8		0.9	2.6	0.7	8.5	3.1
−5~−4	0.2	7.3	8.4		4.2	6.1	4.6	7.5	4.2
−4~−3	1.4	9.2	11.8		6.3	7.3	6.7	5.9	4.5
−3~−2	3.1	10.6	11.0		6.9	4.0	7.1	4.7	4.3
−2~−1	3.5	10.0	8.6	0.5	5.9	1.1	8.1	3.7	4.4
−1~ 0	5.1	10.7	9.4	1.2	9.4	4.9	10.5	11.1	10.5
0~ 1	15.9	13.9	14.6	4.5	16.9	14.7	16.5	18.0	17.6
1~ 2	16.7	12.1	12.7	11.1	17.9	15.8	15.5	13.8	15.7
2~ 3	15.7	7.7	7.0	14.0	12.1	12.0	11.5	9.0	11.2
3~ 4	16.5	4.5	3.8	17.2	7.3	9.0	8.1	6.0	6.5
4~ 5	8.8	2.2	2.0	16.8	4.0	6.4	4.3	3.8	3.6
5~ 6	3.6	1.6	0.9	11.0	2.5	4.3	2.2	2.7	0.8
6~ 7	2.4	0.8	0.7	7.8	2.5	3.7	2.1	2.3	1.8
7~ 8	2.5	0.4	0.8	5.7	1.5	3.5	1.3	1.8	0.6
8~ 9	1.5	0.1	0.3	3.4	0.7	1.9	0.3	0.4	0.9
9~	3.0	0.7	0.2	6.8	1.0	2.7	0.5	0.8	8.1

ϕ	My 1	2	3	4	5	6	7	8	9	10	11
~−10	1.1		1.0								
−10~− 9	2.2	1.5	2.2		0.6					1.7	
−9~− 8	2.6	2.5	3.9	2.0	1.8		2.0	0.8		2.3	
−8~− 7	2.8	3.2	2.7	3.0	2.9	1.8	3.0	2.5	1.5	3.1	3.5
−7~− 6	4.2	4.0	4.4	4.1	4.0	3.4	5.5	3.9	3.0	3.7	4.0
−6~− 5	5.3	6.2	6.3	4.2	6.5	3.6	7.1	5.0	4.1	3.7	4.5
−5~− 4	6.6	6.3	8.1	4.8	8.5	3.9	6.3	5.1	4.6	4.0	5.5
−4~− 3	4.8	5.2	7.4	4.9	8.0	6.0	4.2	4.7	5.9	3.3	6.0
−3~− 2	2.9	4.8	6.7	5.0	6.0	10.0	3.9	4.5	6.9	4.1	6.5
−2~− 1	4.4	5.1	7.0	5.8	5.5	10.1	4.7	4.9	7.0	5.1	6.7
−1~ 0	9.6	7.8	8.8	8.6	6.4	9.1	8.0	8.8	10.5	9.2	10.2
0~ 1	13.5	12.6	9.8	12.0	11.8	13.1	12.9	12.5	13.5	13.7	12.1
1~ 2	12.8	11.5	8.7	12.9	11.2	11.0	12.6	10.8	13.0	13.4	12.2
2~ 3	10.0	9.5	7.0	11.9	5.5	9.5	10.0	9.3	10.4	10.0	10.9
3~ 4	6.9	7.4	5.3	9.3	7.3	6.9	7.9	7.9	8.2	8.4	7.2
4~ 5	4.5	5.4	4.4	6.8	5.0	5.2	5.2	6.8	5.4	6.5	4.9
5~ 6	2.1	3.2	2.6	2.8	2.2	2.7	2.6	5.3	2.5	3.3	1.8
6~ 7	1.7	2.1	0.8	0.7	1.4	1.6	1.9	3.4	1.3	2.0	1.4
7~ 8	1.0	0.9	0.7	0.5	0.4	0.9	1.1	1.1	1.2	1.1	1.0
8~ 9	0.6	0.3	0.9	0.6	0.4	1.0	0.8	0.8	0.7	0.6	0.9
9~	0.4	0.5	0.3	0.1	0.6	0.2	0.3	1.9	0.3	0.8	0.7

Table 4. (Continued)

ϕ	Am	1	2	3	4	5	6	7	8	9	10	11	12	13
~−7											0.3			
−7~−6			0.8				1.6		0.7	0.2	1.0			
−6~−5		1.5	2.0	1.5	0.5		2.6	1.5	2.3	1.8	1.4	1.0	0.4	
−5~−4		3.0	3.3	5.8	2.2	0.1	2.9	4.6	3.5	4.0	2.6	1.7	1.9	0.1
−4~−3		4.3	4.1	7.9	4.4	1.6	5.4	5.9	5.3	5.1	5.2	3.4	1.4	0.7
−3~−2		4.4	5.0	7.2	5.6	0.5	6.8	6.7	6.4	6.2	7.5	4.3	3.6	1.5
−2~−1		5.6	5.8	6.1	6.1	1.3	7.2	5.5	7.2	6.4	8.0	4.8	5.1	2.1
−1~ 0		11.9	13.3	9.1	9.8	11.7	13.8	15.8	9.8	11.2	12.1	11.8	9.8	7.3
0~ 1		23.0	21.4	18.4	18.9	19.8	21.2	22.0	21.3	19.8	18.1	19.6	20.3	19.9
1~ 2		14.0	14.3	14.4	13.3	15.6	14.6	12.4	14.9	15.8	13.4	14.8	16.5	22.7
2~ 3		9.4	9.3	9.6	10.3	11.8	8.7	7.9	8.9	11.0	8.2	10.3	12.1	19.9
3~ 4		9.0	7.8	6.9	9.6	13.2	6.0	5.6	5.0	7.2	5.7	7.1	10.5	13.6
4~ 5		7.2	5.7	5.4	7.6	12.2	3.6	4.2	4.7	3.5	5.6	6.2	7.7	7.4
5~ 6		2.5	2.9	3.4	4.8	6.2	1.9	2.1	4.0	2.3	5.1	5.4	4.2	2.3
6~ 7		2.0	1.8	2.1	3.2	3.3	1.5	1.9	3.0	2.5	3.1	4.0	2.6	1.0
7~ 8		1.0	1.3	1.5	2.0	1.9	0.6	1.1	1.7	1.8	1.3	2.8	1.6	0.7
8~ 9		0.2	0.7	0.4	0.8	0.5	0.3	0.5	0.4	0.8	0.7	1.5	1.0	0.5
9~		1.0	0.5	0.3	0.9	0.3	0.3	2.3	0.9	0.4	0.7	1.3	1.3	0.3

ϕ	Am	14	15	16	17	18	19	20	21	22	23	24	25	26
~−9														0.3
−9~−8														2.0
−8~−7					0.5		0.2		0.3	0.8		0.6		3.1
−7~−6		0.2			2.3	2.3	2.3	2.2	1.9	1.3		1.2	5.5	4.8
−6~−5		1.1			4.7	4.7	3.5	6.6	4.5	1.9		3.4	9.5	6.6
−5~−4		2.0	0.5		6.3	5.5	4.1	7.5	5.5	2.2	2.7	4.2	12.8	8.0
−4~−3		2.2	3.3		6.5	5.6	4.8	7.0	6.0	2.7	5.1	7.3	9.9	7.9
−3~−2		2.8	2.8		6.5	5.1	4.8	6.7	6.3	3.5	6.5	8.1	8.1	7.3
−2~−1		3.9	5.7	0.1	7.8	4.7	4.6	6.0	6.0	6.8	6.7	8.0	6.2	6.4
−1~ 0		11.3	11.9	0.2	11.6	10.7	11.3	11.2	12.5	15.5	12.7	9.5	7.9	8.4
0~ 1		22.8	21.8	4.4	18.4	15.6	18.0	17.9	18.8	22.4	21.5	16.4	11.9	12.2
1~ 2		19.3	17.5	13.2	11.4	13.2	14.4	12.9	12.7	15.9	19.8	14.0	9.9	10.4
2~ 3		11.9	12.5	19.5	7.5	10.0	9.7	8.5	8.2	10.1	13.3	10.9	7.0	8.1
3~ 4		6.3	8.4	19.2	4.6	6.9	5.5	4.5	4.5	5.2	6.1	6.7	4.5	5.2
4~ 5		4.2	5.1	12.0	3.9	4.3	4.6	2.3	2.8	3.0	2.2	4.4	2.5	3.8
5~ 6		3.3	3.3	9.2	2.9	3.1	4.2	1.9	2.6	2.5	0.9	2.3	1.5	2.3
6~ 7		1.4	2.2	7.4	2.7	3.6	3.5	1.7	2.4	2.3	0.9	1.7	1.1	1.6
7~ 8		1.7	1.9	5.6	1.0	2.7	2.4	1.4	3.0	1.6	0.7	0.5	0.9	0.8
8~ 9		1.7	2.0	3.3	1.0	1.2	1.2	0.6	1.0	1.1	0.2	0.5	0.5	0.5
9~		1.9	1.1	5.9	0.4	0.8	0.9	1.1	1.0	1.2	0.7	0.3	0.3	0.3

Table 4. (Continued)

ϕ	Am	27	28	29	30	31	32	33	34	35	36	37	38
~−9				0.3				3.7					
−9~−8		2.3	4.3	0.5		1.5		3.1					
−8~−7		6.5	6.7	2.2		3.5	4.2	2.2					
−7~−6		11.0	8.2	4.1		5.0	5.8	1.2					
−6~−5		13.2	8.8	6.6		5.8	6.2	1.6	6.7	10.7			
−5~−4		10.5	8.2	7.5		5.7	6.1	2.7	7.1	8.8			2.5
−4~−3		6.5	7.0	7.5		4.6	5.6	4.3	6.9	6.8		2.4	7.9
−3~−2		5.7	6.0	6.1	0.7	4.2	5.5	5.4	5.5	5.1	1.8	6.9	10.3
−2~−1		4.6	5.1	5.2	1.2	4.0	5.9	5.8	4.8	3.9	7.2	9.2	11.7
−1~ 0		5.8	6.4	8.5	2.4	7.9	8.7	11.0	12.1	11.2	10.8	9.5	13.1
0~ 1		11.2	11.7	14.8	10.2	17.8	15.0	19.7	20.5	20.3	18.3	16.0	17.6
1~ 2		9.0	10.6	14.2	17.8	13.2	10.8	16.4	12.1	12.9	19.1	19.0	15.9
2~ 3		6.2	7.4	10.7	23.4	7.9	6.9	9.6	7.1	8.0	17.8	16.6	10.1
3~ 4		3.7	4.6	5.8	21.2	5.3	5.9	7.1	5.0	5.9	11.7	9.9	5.1
4~ 5		2.1	2.2	2.8	13.0	4.6	5.4	4.4	4.3	3.7	7.2	5.0	2.3
5~ 6		0.9	1.2	1.0	7.6	3.6	4.4	1.1	3.4	1.6	4.1	1.8	1.2
6~ 7		0.5	0.9	1.2	2.0	2.7	2.4	0.3	2.7	0.7	0.7	1.4	0.8
7~ 8		0.1	0.5	0.5	0.2	2.0	0.9	0.2	1.2	0.2	0.7	1.1	0.7
8~ 9		0.1	0.1	0.2	0.2	0.5	0.2	0.1	0.3	0.1	0.3	0.7	0.4
9~		0.1	0.1	0.3	0.1	0.2	0.1	0.1	0.3	0.1	0.3	0.5	0.4

ϕ	Hn	1	2	3	4	5	6	7	8	9	10	11	12	13
~−9												5.1	2.0	
−9~−8												6.6	8.5	3.3
−8~−7		0.3										8.7	6.3	3.3
−7~−6		0.8	0.2				0.1	0.4	3.8		0.4	7.3	5.0	4.0
−6~−5		2.1	0.5	0.4		0.1	1.4	1.6	6.0	1.0	4.1	5.0	6.9	4.8
−5~−4		4.6	1.5	1.2		0.3	3.4	6.8	6.7	3.3	5.9	4.8	8.8	5.6
−4~−3		5.5	4.0	2.6	4.1	2.1	7.1	8.0	7.5	7.2	9.5	6.3	5.9	6.0
−3~−2		6.7	6.1	5.1	8.9	7.1	9.3	9.0	8.3	10.1	10.6	7.2	5.9	6.7
−2~−1		7.2	8.7	13.4	12.5	11.2	10.0	9.5	8.4	10.9	11.3	9.3	10.7	9.5
−1~ 0		11.8	12.0	21.4	15.0	15.4	10.6	13.4	8.2	13.7	11.3	13.5	10.2	16.0
0~ 1		20.0	20.7	23.4	15.2	21.3	17.3	19.0	14.3	15.5	10.6	10.8	9.1	11.9
1~ 2		13.7	16.1	17.7	11.8	17.0	12.5	13.5	10.6	12.0	8.4	6.4	6.9	10.2
2~ 3		8.5	10.2	6.9	9.5	11.5	7.5	6.7	6.6	9.6	6.2	3.8	5.3	7.4
3~ 4		4.8	6.2	2.4	7.8	5.1	6.1	2.7	4.0	7.4	3.7	2.3	3.8	4.9
4~ 5		3.8	3.6	1.2	3.8	2.5	3.8	1.5	2.9	4.3	4.7	1.4	2.0	3.0
5~ 6		2.6	2.7	0.8	3.7	0.8	2.9	1.5	3.4	2.1	3.2	0.3	0.6	1.4
6~ 7		3.2	3.4	1.4	2.7	1.5	2.9	1.9	3.7	1.3	2.9	0.3	0.5	1.0
7~ 8		2.2	1.7	0.4	2.1	1.7	1.8	2.3	2.3	1.0	2.1	0.4	0.5	0.6
8~ 9		0.6	0.2	0.4	1.5	1.3	0.8	0.4	0.8	0.3	1.4	0.3	0.3	0.3
9~		1.6	2.2	2.3	1.4	1.1	2.5	1.8	2.5	0.3	3.7	0.2	0.8	0.1

Table 4. (Continued)

ϕ	KF 1	2	3	4	5	6	7	8	9	10	As 1	2
~−9	1.3		1.0									
−9~−8	4.3	1.8	1.8									
−8~−7	6.4	6.4	3.9	1.7	2.0	1.8	1.4	1.2		0.7		
−7~−6	7.4	8.1	6.5	4.5	3.2	7.2	5.8	6.0	2.1	5.5		0.3
−6~−5	7.3	8.7	8.6	7.1	6.0	9.5	7.6	8.9	7.1	12.3		0.5
−5~−4	7.0	8.2	11.2	9.0	8.8	9.8	9.5	11.2	10.2	17.3		0.9
−4~−3	6.9	6.8	10.9	11.0	11.6	8.5	8.0	10.5	9.9	11.9	0.8	1.3
−3~−2	6.5	5.2	8.4	9.7	10.5	8.0	6.8	8.4	8.6	8.3	1.7	1.2
−2~−1	5.3	6.6	6.0	7.3	8.9	7.4	5.9	7.0	9.1	6.6	2.1	1.6
−1~ 0	6.7	6.4	7.0	8.6	8.3	7.5	7.1	9.6	9.6	6.3	4.4	2.2
0~ 1	9.7	8.4	9.0	9.3	9.5	9.0	9.0	9.4	13.0	8.8	7.8	6.1
1~ 2	8.0	8.8	8.3	9.0	9.0	8.0	8.2	6.9	12.8	8.4	10.0	9.1
2~ 3	6.9	11.3	6.2	7.2	8.1	7.0	7.0	5.6	8.8	5.8	11.2	14.3
3~ 4	4.7	7.1	4.5	5.6	5.9	6.0	6.0	4.6	4.9	3.4	13.3	18.1
4~ 5	3.8	2.7	3.1	3.6	4.0	4.3	5.3	4.0	1.7	1.7	15.5	14.3
5~ 6	2.9	1.3	1.7	2.3	1.9	2.3	3.6	2.2	0.4	1.0	11.4	12.5
6~ 7	2.0	1.1	0.5	1.5	0.9	1.4	2.9	1.5	0.4	0.4	8.6	7.1
7~ 8	1.2	0.4	0.4	0.6	0.6	0.7	2.0	0.7	0.3	0.2	5.8	2.7
8~ 9	0.7	0.3	0.3	0.4	0.4	0.7	1.1	0.4	0.3	0.2	1.5	1.1
9~	1.0	0.4	0.7	1.6	0.4	1.3	2.8	1.9	0.8	1.2	5.9	6.7

ϕ	Ai 1	2	3	4	5	6	7	8	9	10	11	12	13
~−8	1.1												
−8~−7	0.9												0.9
−7~−6	1.2		1.1			1.1	0.4		0.2		0.3		0.4
−6~−5	0.9	2.0	2.4		1.2	2.4	2.4		1.5		1.8	2.0	1.5
−5~−4	1.2	6.0	5.2	1.5	1.4	5.8	6.7		4.8	1.0	2.2	5.4	3.7
−4~−3	2.7	6.5	11.9	1.6	1.5	5.4	5.7		8.2	1.0	2.7	2.9	4.3
−3~−2	5.0	7.2	12.3	1.1	1.2	4.5	4.6	1.0	9.3	1.3	3.3	3.1	3.9
−2~−1	5.1	8.2	11.9	1.7	5.2	5.8	5.2	1.7	7.0	2.4	4.3	2.9	3.3
−1~ 0	8.2	7.1	13.0	2.8	14.0	10.1	8.9	4.2	2.1	5.9	9.3	7.1	7.7
0~ 1	13.0	13.3	15.3	6.5	17.8	13.2	13.4	14.1	8.7	13.8	15.5	12.6	14.8
1~ 2	15.7	12.9	12.9	9.8	14.3	13.7	14.0	18.8	13.5	18.9	17.6	16.3	15.1
2~ 3	13.8	11.8	6.1	11.8	12.6	12.4	12.5	17.1	12.9	19.9	17.7	15.7	14.7
3~ 4	11.9	10.0	2.2	16.8	10.6	10.3	10.6	12.3	11.2	15.8	12.5	13.6	12.4
4~ 5	7.2	4.9	1.0	16.3	7.3	5.3	7.3	7.9	6.8	8.6	5.7	8.9	7.3
5~ 6	4.8	2.5	1.0	11.1	4.4	3.0	2.9	5.5	3.2	4.3	2.1	4.1	2.8
6~ 7	1.6	1.7	0.5	6.9	3.7	2.6	2.3	4.1	2.5	2.5	2.3	2.7	2.1
7~ 8	0.3	1.4	0.4	3.6	1.6	0.5	1.1	3.3	2.9	1.1	1.0	0.9	0.8
8~ 9	0.3	0.3	0.2	2.0	0.2	0.9	0.5	1.7	1.3	0.3	0.7	0.9	0.1
9~	5.1	4.2	2.6	6.5	3.0	3.0	1.5	8.3	3.9	3.2	1.0	0.9	4.2

Table 5. Results of mechanical analyses of pyroclastic fall deposits.

ϕ	Kc 11	12	13	Ms 4	Ak 5	D 3	4	S 12	13	14	15	16
− 6~−5.5				—								
−5.5~− 5				4.8			2.6					
− 5~−4.5			5.0	7.0								
−4.5~− 4			7.2	7.7		2.9	12.0	—		—	13.5	1.7
− 4~−3.5			7.7	7.8				1.8		2.5	12.2	4.6
−3.5~− 3			8.6	8.5		6.4	7.6	4.5		6.3	11.2	6.0
− 3~−2.5			10.3	8.5			10.0	10.0		11.4	12.1	10.1
−2.5~− 2	1.2		10.9	8.1		5.9	10.0	12.7		13.6	9.8	11.2
− 2~−1.5			9.7	6.9		10.8	8.9	13.9		12.5	6.4	11.9
−1.5~− 1	4.1		8.4	5.9		14.2	6.7	12.7	0.8	10.7	6.5	10.2
− 5~−0.5			6.8	4.9		11.6	4.9	11.7		12.0	4.4	10.3
−0.5~ 0	9.2	0.2	5.8	5.0		8.2	11.8	8.7	1.7	12.2	3.2	9.3
0~ 0.5	12.5	1.2	5.5	7.2	0.3	9.2	12.5	7.5	9.1	9.5	5.1	8.2
0.5~ 1	17.5		3.2	7.0		14.0		6.5		5.0	8.1	6.5
1~ 1.5	18.8	8.9	3.0	5.7	0.6	7.3	5.9	4.5	8.9	1.5	4.3	3.2
1.5~ 2	13.4			3.2		3.7		2.5	13.0	1.1	2.4	1.9
2~ 2.5	11.5	10.4	2.1	1.3	21.6	2.1	2.2	1.0	14.5	0.6	0.4	1.0
2.5~ 3		15.6							16.5			
3~ 3.5	4.1	19.9	1.9	0.2	24.0	1.4	1.7	0.5	15.7	0.4	0.2	0.8
3.5~ 4		15.1							8.8			
4~ 4.5	2.4	9.9	1.0	0.1	16.0	1.0	1.0	0.5	5.1	0.4	0.1	1.1
4.5~ 5		5.3										
5~ 6	1.8	4.7	2.9	0.2	13.3	0.8	0.7	1.0	1.2	0.3	0.1	2.0
6~ 7	1.3	3.1			11.7		0.7		1.0			
7~ 8	1.0	1.9			8.0		0.4		0.7			
8~ 9	0.7	0.7			3.7		0.2		1.1			
9~	0.5	3.1			0.8		0.2		1.9			

ϕ	Ty 11	12	Km 11	12	Tw 23	24	25	26	Nn 7	Hr 5	KS 5
− 6~−5.5			15.0	—	2.7	—		2.7		—	
−5.5~− 5			22.4	24.5		5.6				7.8	
− 5~−4.5			24.8	19.7	9.4	33.9		10.0	—	17.4	
−4.5~− 4			21.6	15.0		16.5	2.7		12.4	17.3	
− 4~−3.5					6.2	11.7		6.7	17.4	13.3	
−3.5~− 3	3.0	4.0	10.1	18.0	8.4	8.6	9.3	8.2	19.7	12.4	1.8
− 3~−2.5					9.0		7.9	8.4	15.7	9.1	
−2.5~− 2	9.5	10.5	1.8	8.4	8.6	11.5	10.4	9.4	10.5	6.2	7.7
− 2~−1.5	7.5				7.4		12.4	9.1	6.5		6.2
−1.5~− 1	8.2	13.5	1.0	5.7	6.8	5.7	12.4	9.5	5.0	7.5	8.1
− 1~−0.5	9.5	7.0			6.8		11.8	8.7			11.7
−0.5~ 0	10.0	7.4	1.0	4.3	7.4	2.8	10.8	8.2	7.1	3.6	16.3
0~ 0.5	18.8	13.9			7.8		11.2	8.9			26.8
0.5~ 1	24.0	21.2	1.0	2.7	6.2	1.9	6.7	5.9	3.0	2.7	14.4
1~ 1.5	7.9	12.3	0.5	1.1	5.3	0.6	3.6	3.2	0.9	1.4	5.0
1.5~ 2		5.5									
2~ 3	1.0	2.4	0.3	0.2	2.0	0.4	0.6	0.5	0.6	0.4	0.8
3~ 4	0.3	0.9	0.2	0.2	1.3	0.3	0.3	0.3	0.4	0.3	0.6
4~ 5	0.2	0.8	0.2	0.2	1.3	0.2	0.2	0.2	0.4	0.2	0.3
5~	0.1	0.4			3.4	0.3	0.1	0.1	0.4	0.4	0.3

Table 5. (Continued)

ϕ	Am 39	40	41	46	47	KF 11	F 1	2	3	4	5	6
− 6~−5.5	2.3	—										
−5.5~− 5	19.0	4.5										
− 5~−4.5	19.2	11.3				—	—	—				
−4.5~− 4	17.9	12.7				1.2	5.2	2.5				
− 4~−3.5	8.6	14.6	14.3			3.8	9.5	6.3	2.2	1.9		1.5
−3.5~− 3	4.3	16.4				13.5	23.8	7.7		14.1		23.8
− 3~−2.5	5.4	11.2	23.8	20.0		20.8	27.2	10.8	12.3	14.7	9.6	21.9
−2.5~− 2		4.9				22.2	15.1	11.1		16.1		16.6
− 2~−1.5	2.5	4.2	17.9	18.4		13.6	6.7	9.2	12.0	16.5	7.6	11.9
−1.5~− 1				18.5		7.2	3.6	7.8	13.8	16.4	10.8	7.7
− 1~−0.5	2.7	2.1	15.4	18.4		3.7	3.5	12.6	17.7	10.1	15.0	8.5
−0.5~ 0				13.2		2.3			18.0	6.1	21.5	
0~ 0.5	4.1	2.1	12.6	5.0	—	2.7	2.1	9.7	15.0	3.9	22.7	4.9
0.5~ 1				1.5	3.0				5.8		9.9	
1~ 1.5	4.2	2.3	1.6	3.5	5.7	1.3	1.5	6.8	2.8	0.1	2.6	2.2
1.5~ 2					15.5							
2~ 2.5	3.7	3.1	0.3	1.1	30.8	1.7	0.9	4.9	0.2	0.03	0.2	0.8
2.5~ 3					21.8							
3~ 3.5	3.0	3.8	1.3	0.3	10.0	1.9	0.5	3.3	0.1	0.04	0.05	0.1
3.5~ 4					4.4							
4~ 5	1.9	3.1	1.6	0.1	4.5	2.2	0.3	1.6	0.07	0.02	0.03	0.05
5~ 6	1.2	3.7	4.9		4.3	1.9	0.1	1.7	0.03	0.01	0.02	0.05
6~ 7			3.4			0.9		1.5				
7~ 8			1.5			0.5		1.5				
8~ 9			1.3			0.4		0.4				
9~			0.1			0.2		0.6				

in another paper, full description of them is omitted here. Mechanical analyses were carried out through several steps in order to obtain accurate results of thorough analyses of every size fraction. Each sample was divided into three parts, one was reserved for preservation, another was prepared for analyses of the coarse fractions, and the rest was used for analyses of the fine and medium fractions. The analyses were carried out by means of the decantation, sieving and pipette methods in sequence. All results obtained through such steps of laboratory work were corrected for the coarser fractions by referring to photographs of the outcrops from which the samples were picked up. The resuls of mechanical analyses of the pyroclastic flow deposits are shown in Table 4, where each figure listed in the column represents the weight per cent of each fraction sized out by mechanical analyses. Figs. 3a–3k show cumulative curves of particle size distribution of the pyroclastic flow deposits. The results of mechanical analyses of the pyroclastic fall deposits are shown in Table 5 and Fig. 4. The results of mechanical analyses of the dry mud-flow deposits and the auto-brecciated lava flows are shown in Table 6 and Figs. 5a and 5b. The diameters of particles ξ in millimeters are replaced here by ϕ as expressed in the equations $\xi=(1/2)^{\phi}$ or $\phi=-\log_2 \xi$, for convenience.

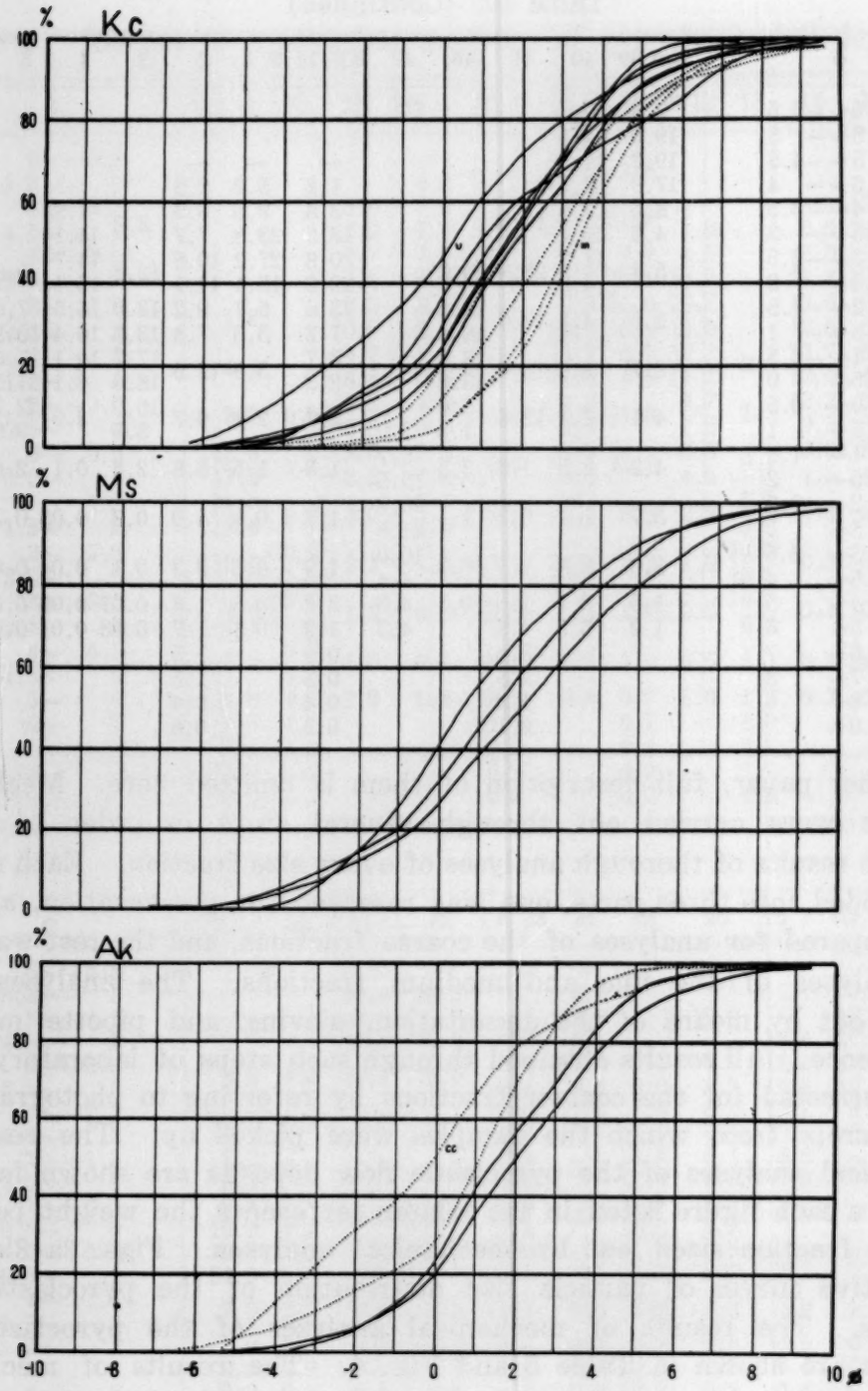

Fig. 3. Cumulative curves of the particle size distribution of pyroclastic flow deposits.

Fig. 3a. Upper: the Kutcharo Volcano, middle: the Mashu Volcano, lower: the Akan Volcano.

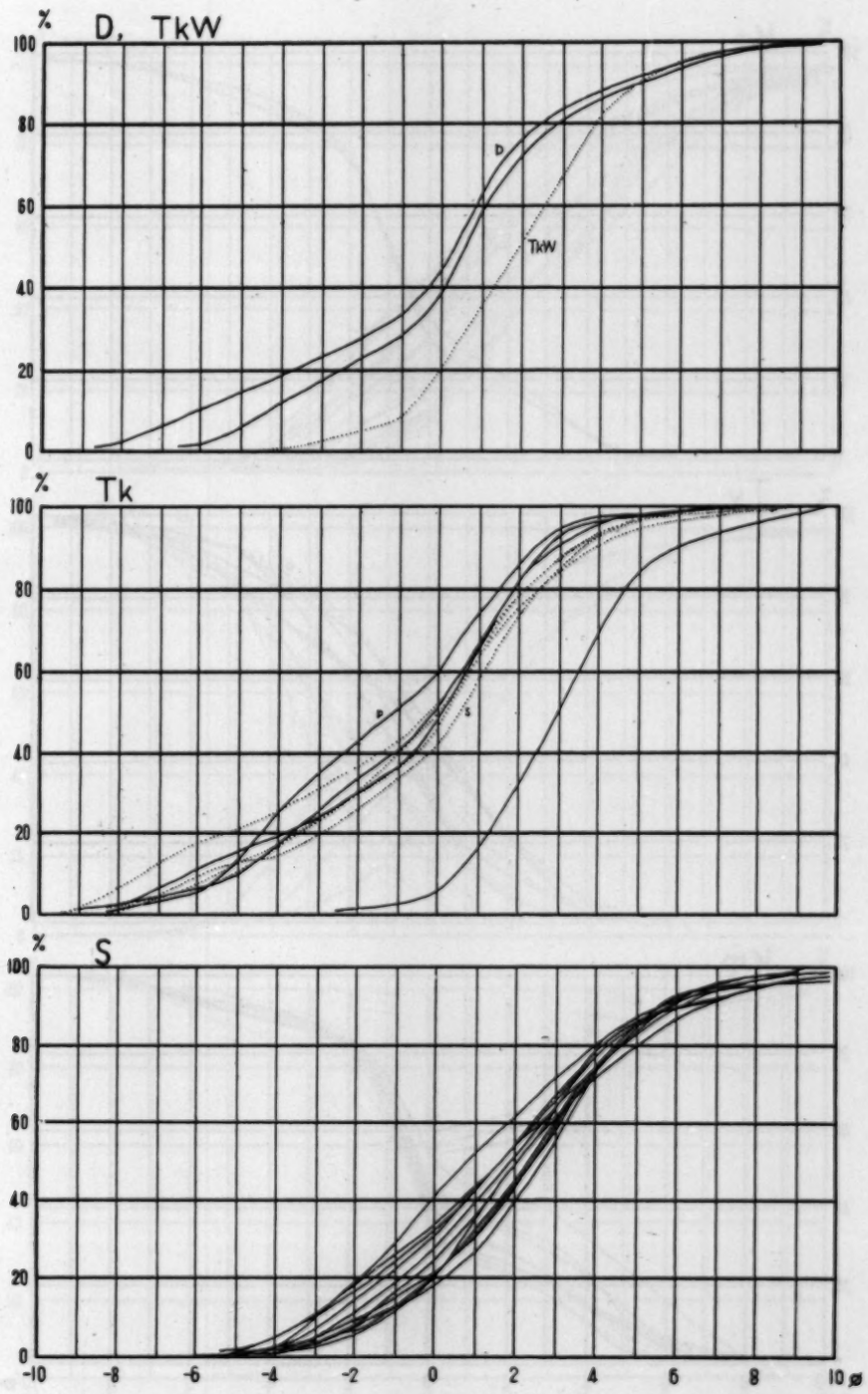

Fig. 3b. Upper: the Daisetsu Volcano and the Tokachi Welded Tuff, middle: the Tokachidake Volcano, lower: the Shikotsu Volcano.

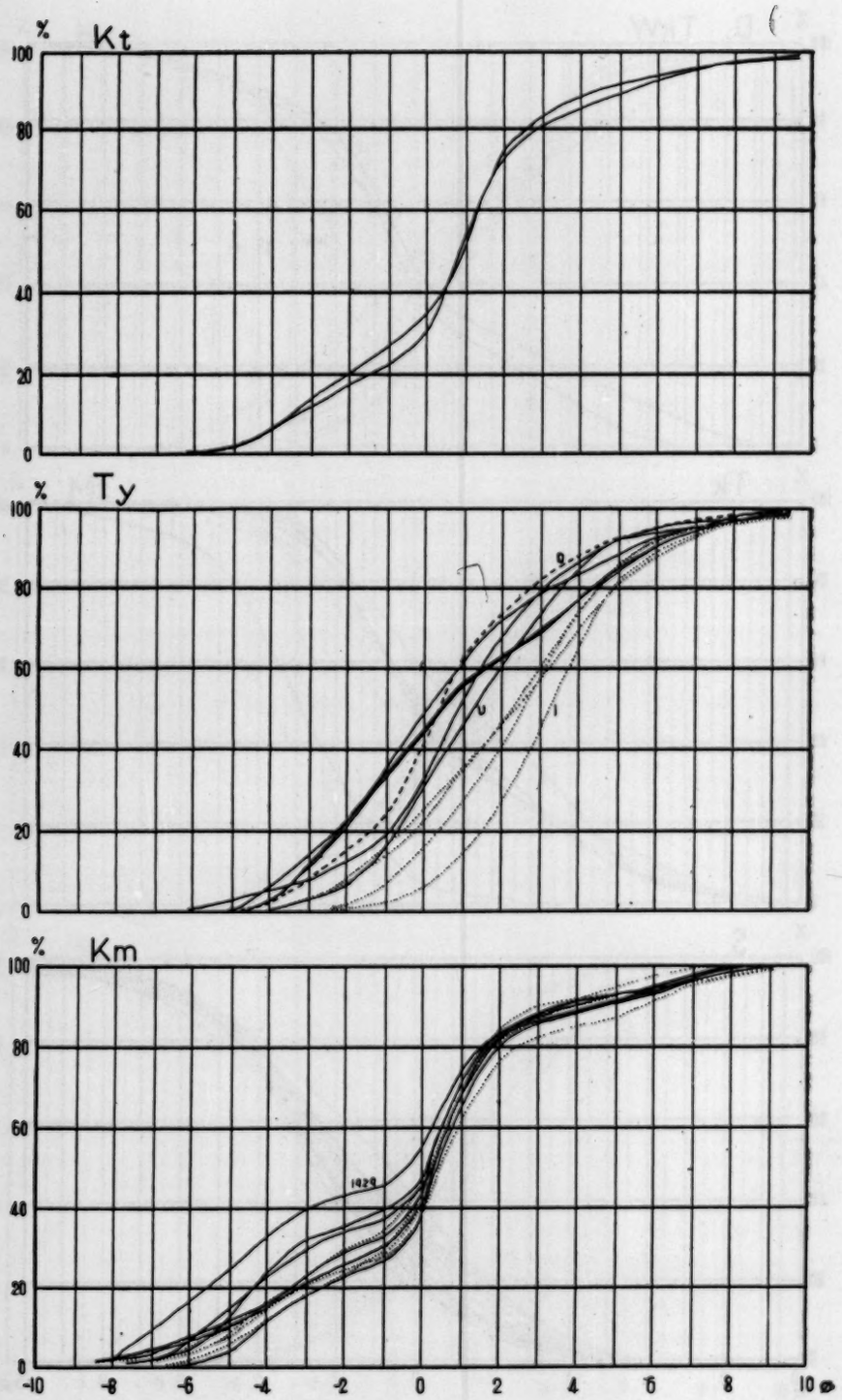

Fig. 3c. Upper: the Kuttara Volcano, middle: the Toya Volcano, lowere: the Komagatake Volcano.

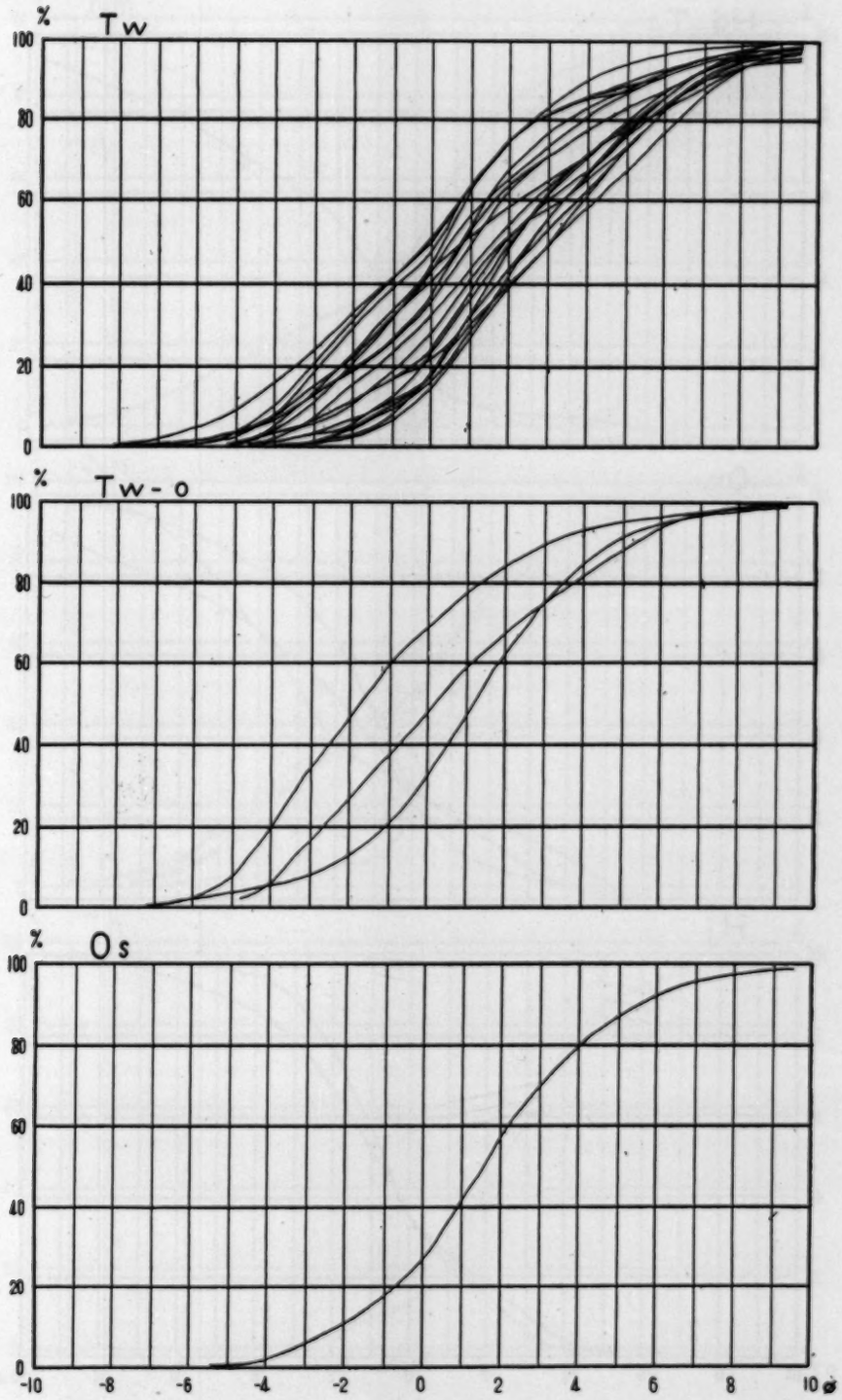

Fig. 3d. Upper: the Younger Ash-flow of the first stage of the Towada Volcano, middle: the Older Ash-flow of the first stage of the Towada Volcano, lower: the Osoreyama Volcano.

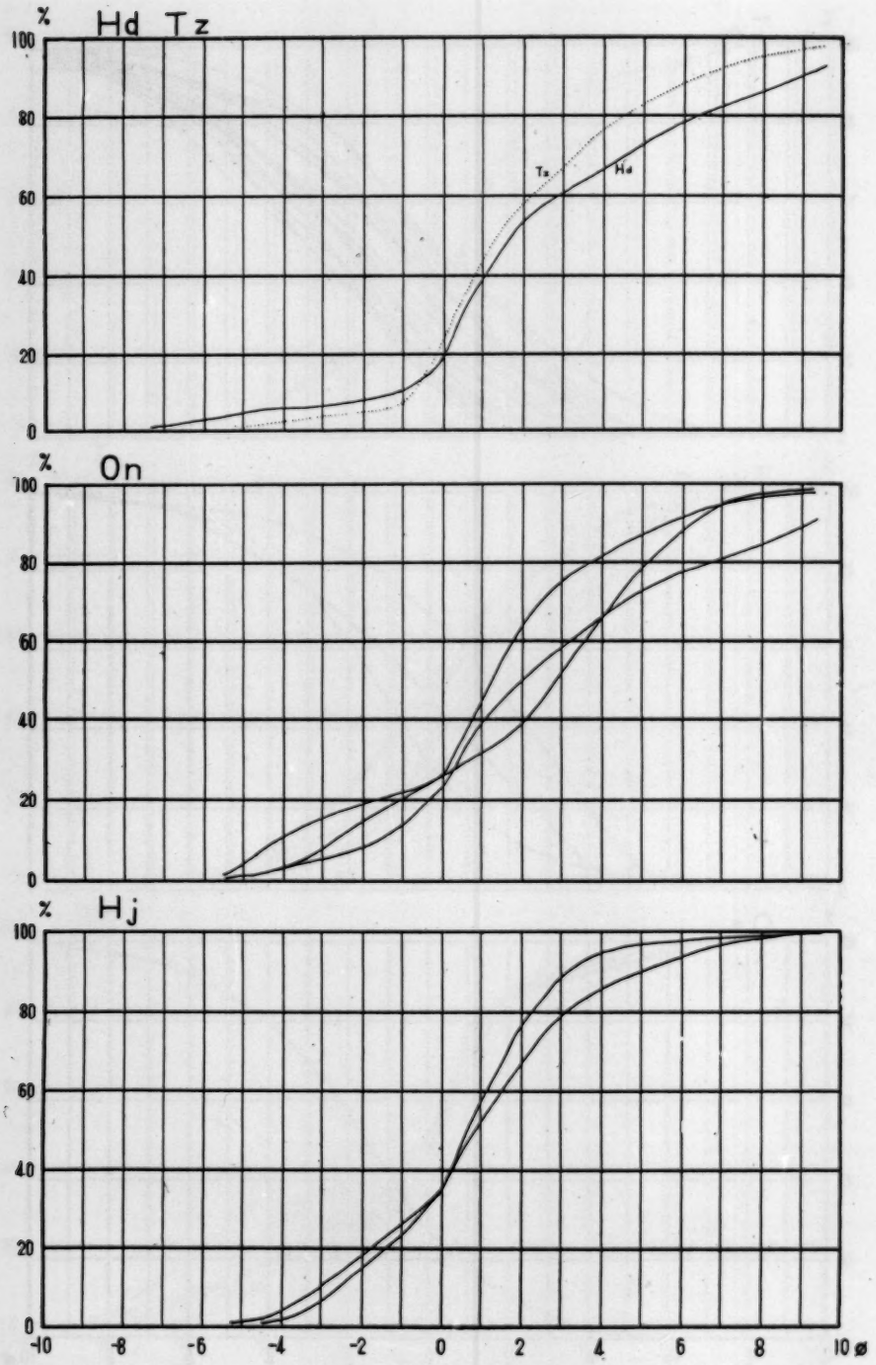

Fig. 3e. Upper: the Hakkoda and Tazawa Welded Tuffs, middle: the Onikobe Volcano, lower: the Hijiori Ash-flow.

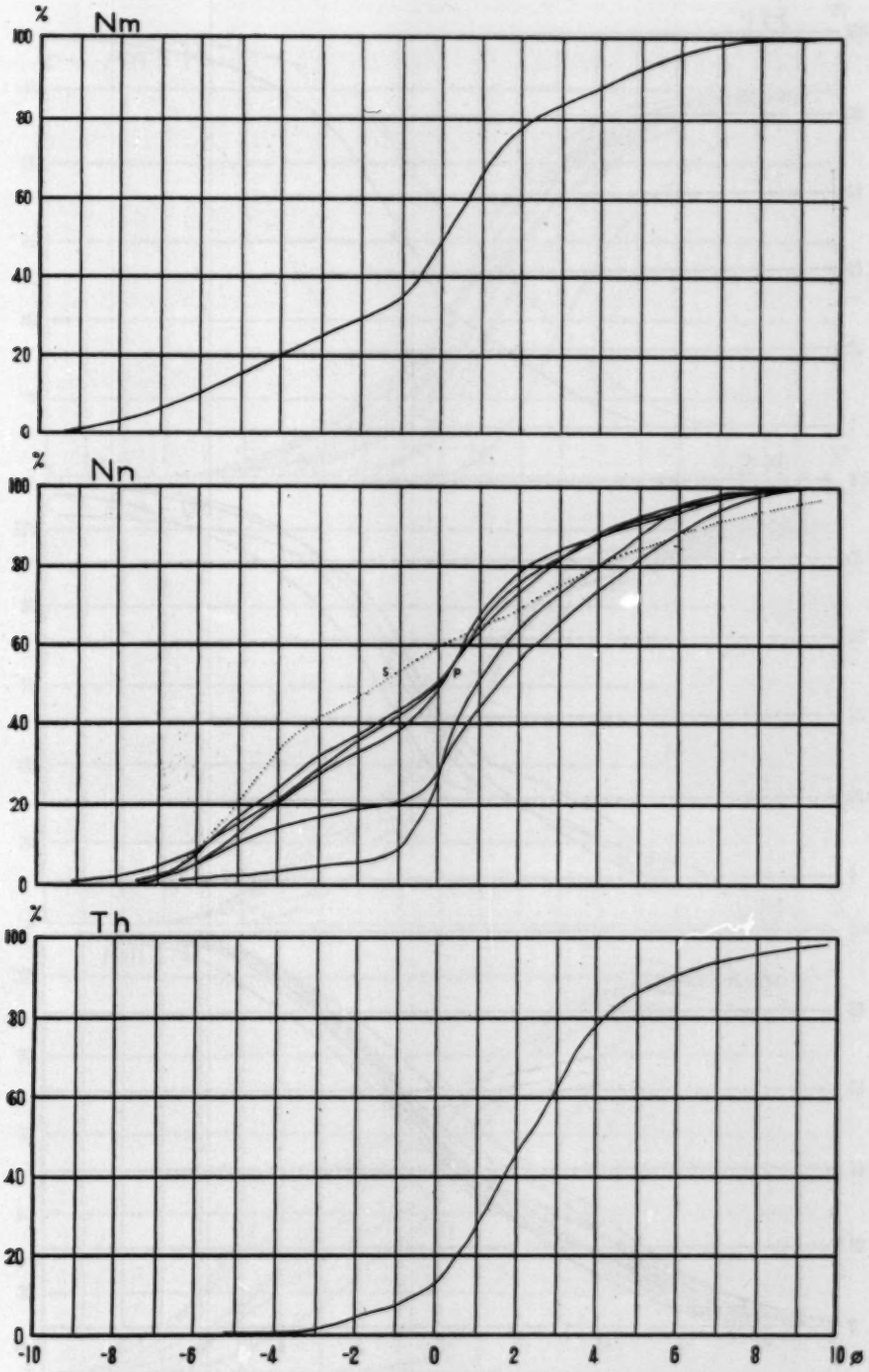

Fig. 3f. Upper: the Numajiri Welded Tuff, middle: the Nantai Volcano, lower: the Takahara Volcano.

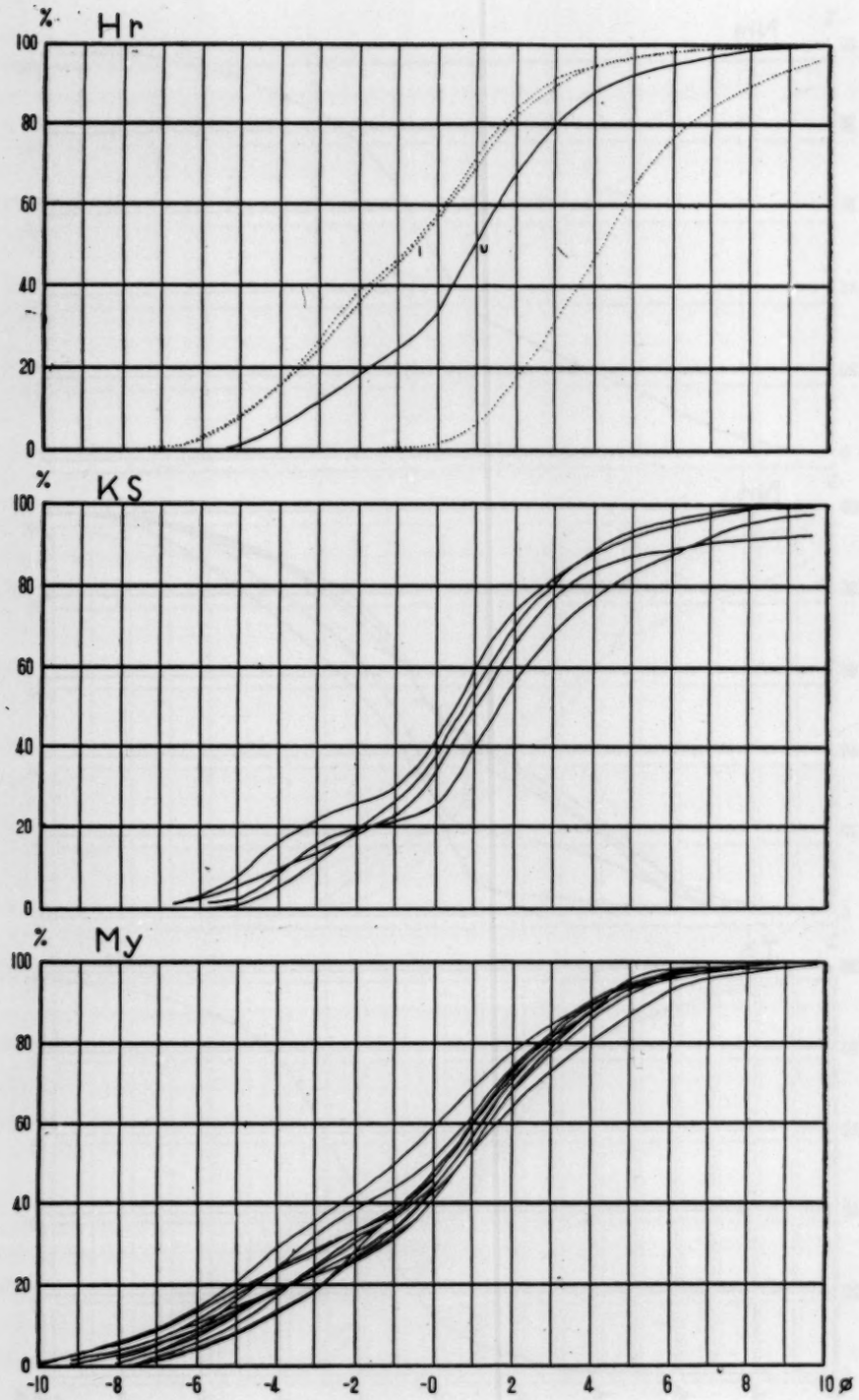

Fig. 3g. Upper: the Haruna Volcano, middle: the Kusatsu-Shirane Volcano, lower: the Myoko Volcano.

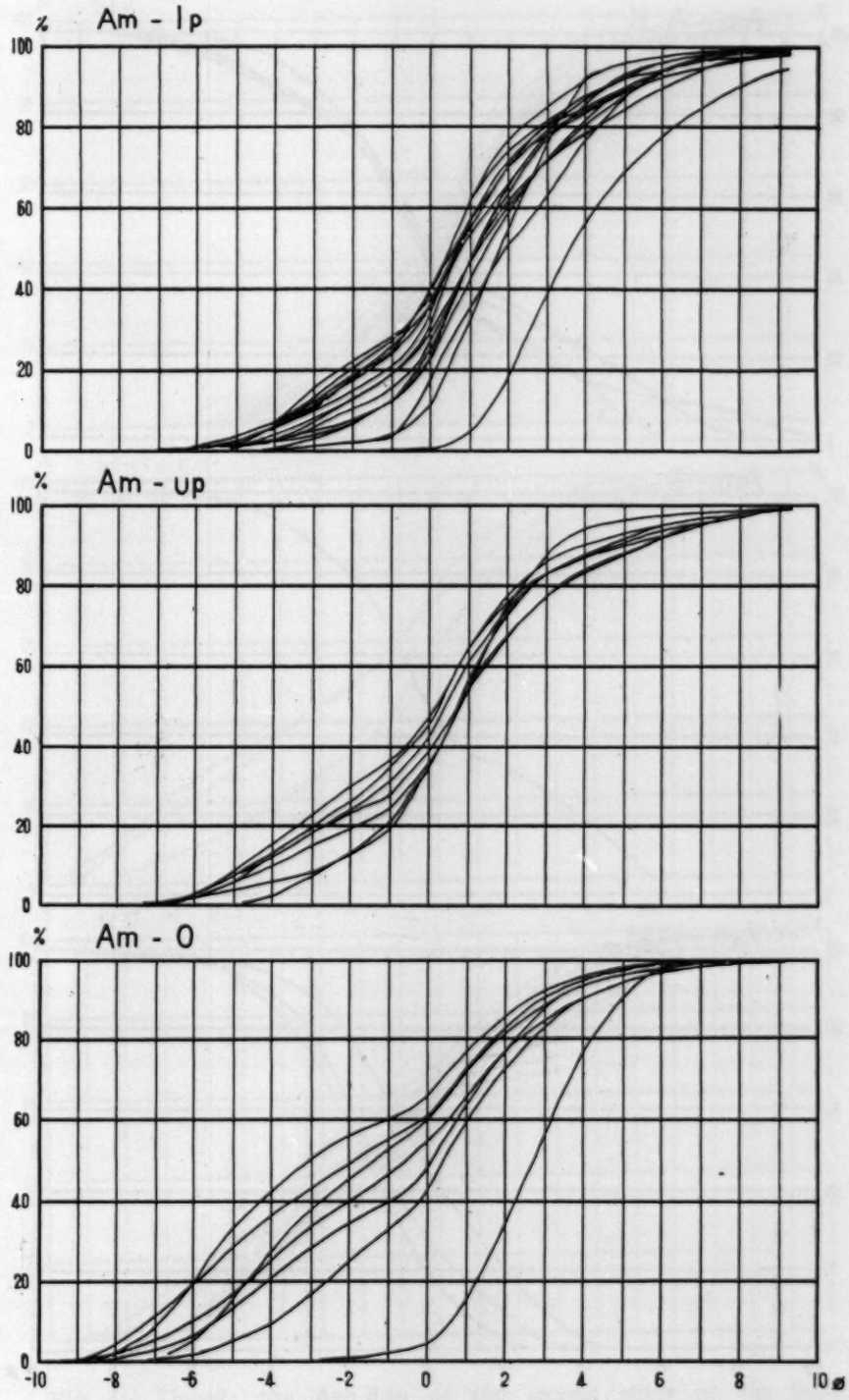

Fig. 3h. Pyroclastic flows of the Asama Volcano. Upper: the Lower Ash-flow, middle: the Upper Ash-flow, lower: the Oiwake Pyroclastic Flow.

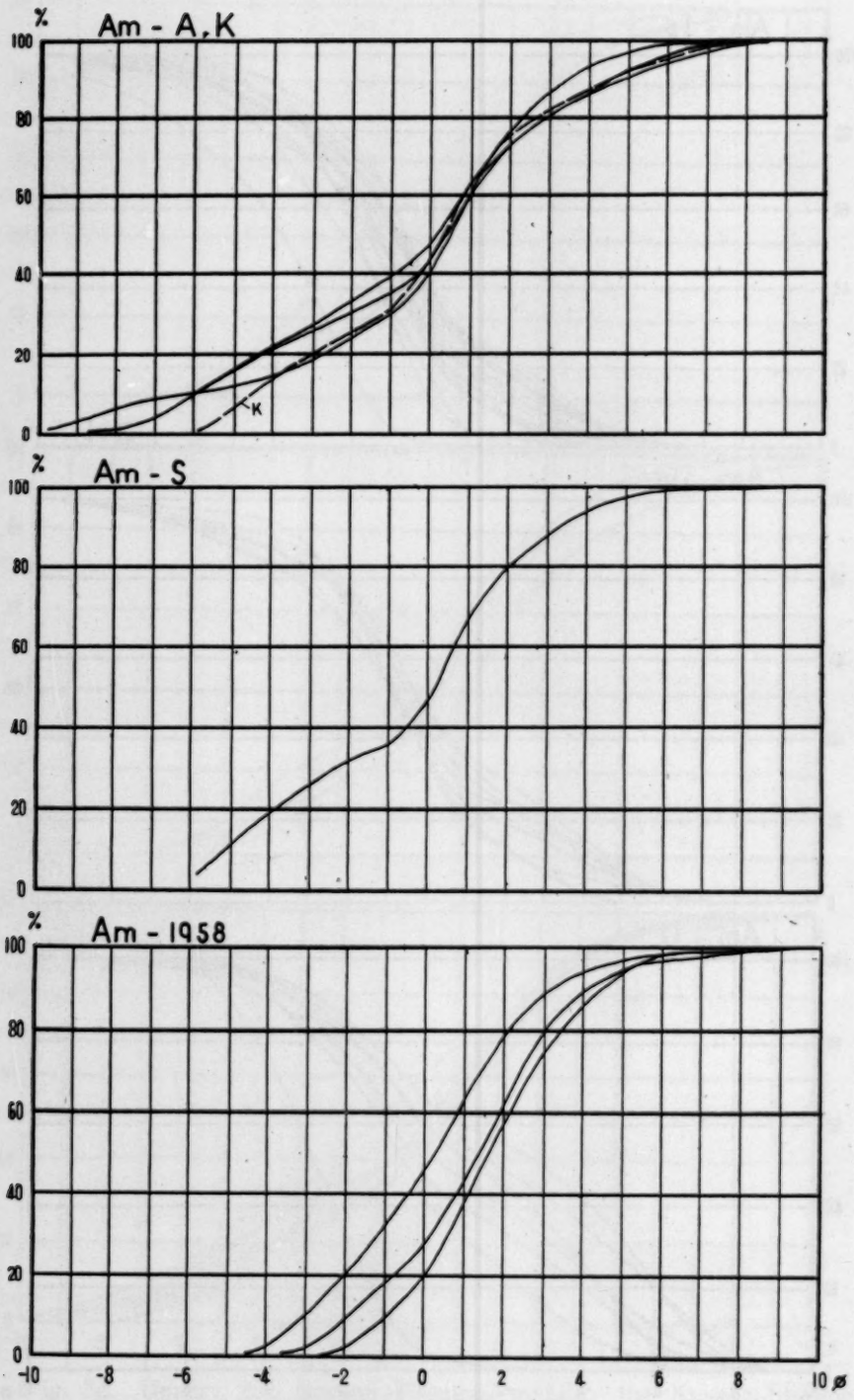

Fig. 3i. Pyroclastic flows of the Asama Volcano. Upper: the Agatsuma Pyroclastic Flow of the 1783 eruption, middle: the Shiraito Pyroclastic Flow, lower: the Ash-flow of the 1958 eruption.

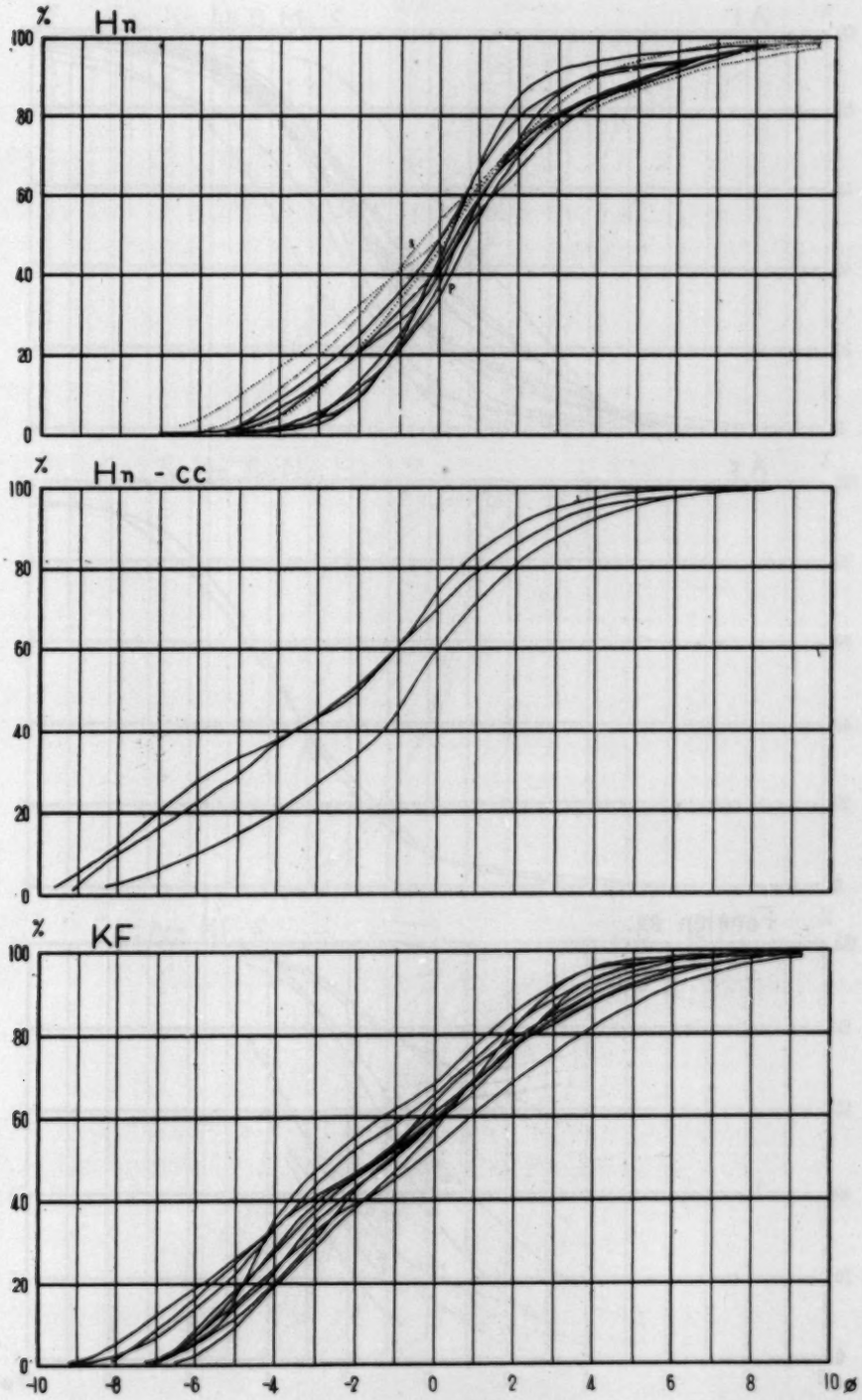

Fig. 3j. Upper: the Ash-flow of the second stage of the Hakone Volcano, middle: the Central Cone Pyroclastic Flow of the Hakone Volcano, lower: the Lower and Upper Pyroclastic Flows of the Ko-Fuji Volcano.

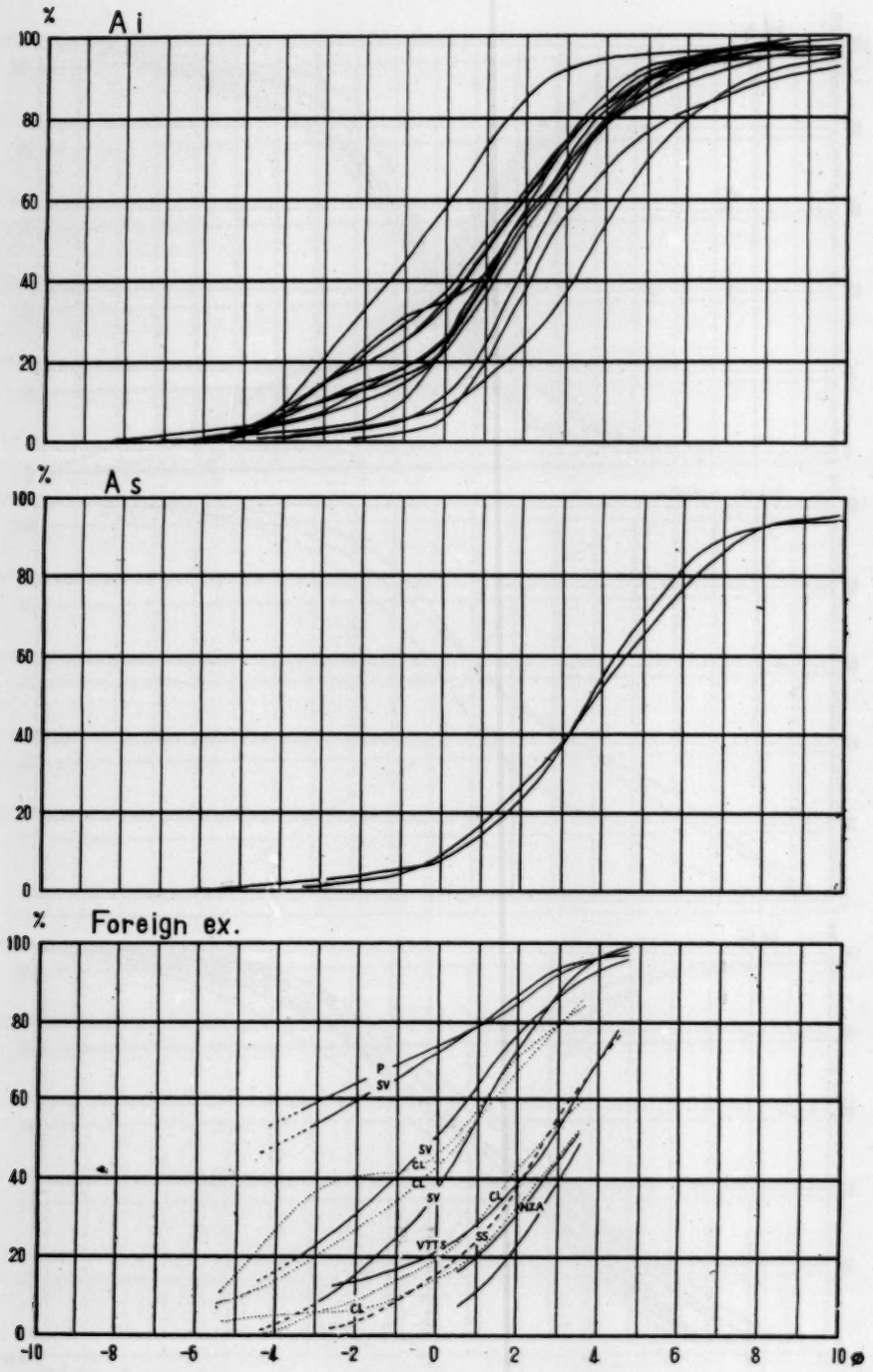

Fig. 3k. Upper: the Aira Volcano, middle: the Aso Volcano, lower: foreign examples of pyroclastic flows.

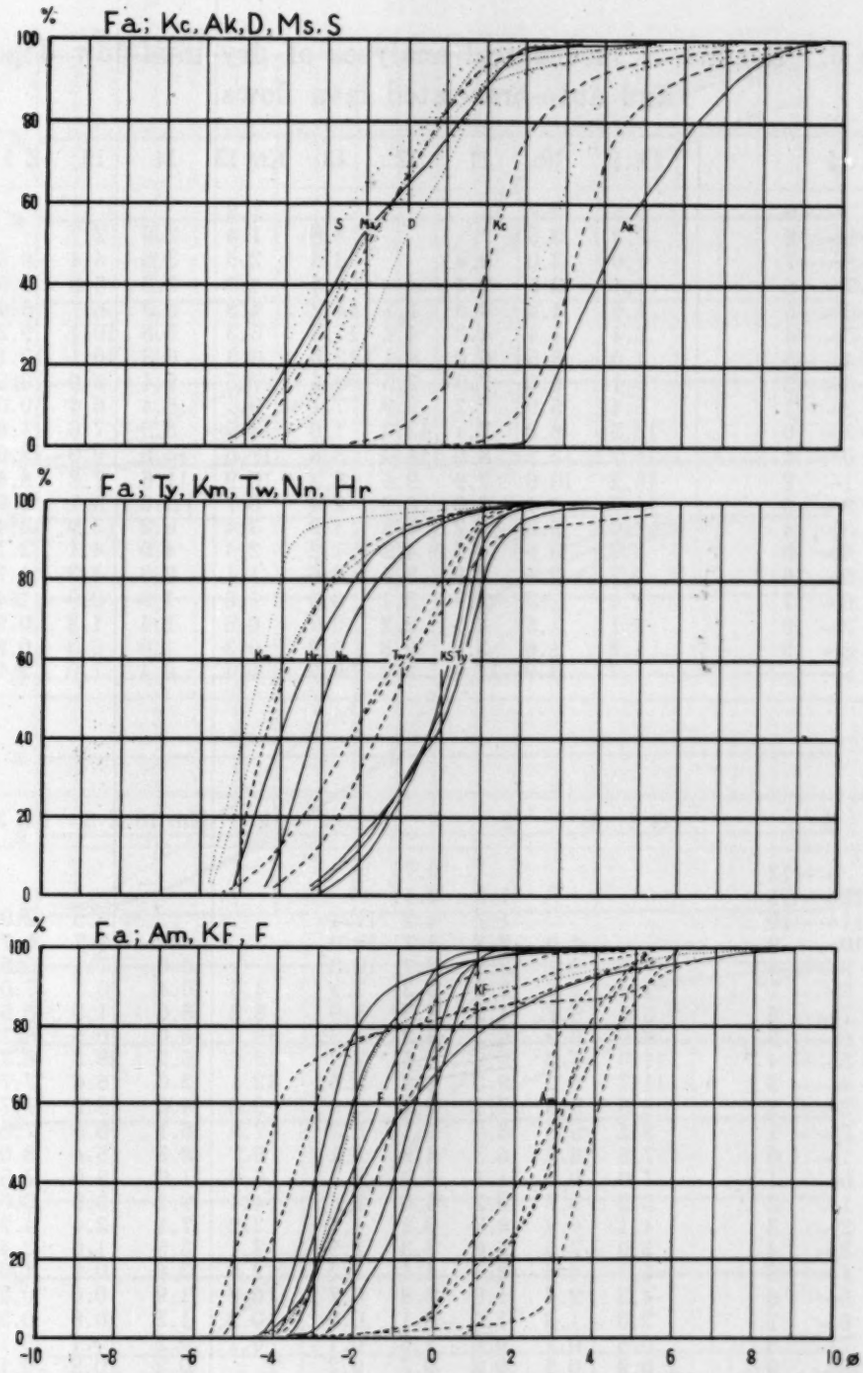

Fig. 4 Cumulative curves of the particle size distribution of pyroclastic fall deposits

Table 6. Results of mechanical analyses of dry mud-flow deposits and auto-brecciated lava flows.

ϕ	Tk 9	10	11	12	13	Km 13	14	15	Z 1	2
~−9	3.5	3.7				1.2				
−9~−8	2.2	3.5			3.8	1.4	2.0	2.7		
−8~−7	1.0	3.0	0.8		3.6	2.6	3.6	4.4	0.6	
−7~−6	1.1	3.5	2.4		8.4	4.0	3.8	5.3	2.5	1.8
−6~−5	1.0	4.4	4.8	1.1	14.2	4.8	5.3	6.7	6.4	9.2
−5~−4	2.4	4.4	4.0	4.7	17.8	5.3	5.8	10.1	9.2	9.6
−4~−3	4.0	5.5	6.0	8.1	12.0	6.3	6.3	10.1	10.1	10.4
−3~−2	5.1	6.0	7.9	9.5	8.4	7.5	6.4	8.0	10.2	9.4
−2~−1	6.4	5.9	7.2	9.9	7.1	9.1	6.4	6.4	10.0	8.2
−1~ 0	12.5	8.3	7.1	13.3	7.6	13.5	8.5	7.6	11.8	7.9
0~ 1	15 2	12.2	8.0	14.0	5.8	17.6	13.6	9.0	13.0	7.2
1~ 2	15.2	10.0	7.9	9.6	3.2	10.9	11.6	7.8	8.4	5.1
2~ 3	11.7	8.4	6.9	6.9	2.4	6.7	9.0	5.1	5.5	4.1
3~ 4	7.0	5.8	6.2	5.3	1.9	3.4	6.2	3.9	3.4	3.7
4~ 5	3.0	3.6	4.5	4.2	1.2	2.4	4.5	4.1	2.1	3.9
5~ 6	1.7	2.9	3.9	3.4	0.6	1.1	2.3	3.3	1.7	4.0
6~ 7	1.4	1.9	3.7	3.1	0.8	1.0	1.9	2.9	1.4	4.5
7~ 8	2.1	1.5	4.1	2.2	0.7	0.5	1.4	1.3	0.9	4.5
8~ 9	1.8	1.6	3.5	0.8	0.2	0.3	1.0	0.3	0.8	2.5
9~	1.7	3.9	11.1	3.9	0.3	0.4	0.4	1.0	2.0	4.0

ϕ	G 1	B 1	2	3	Hn 14	Ak 6	Km 16	Z 3	Nn 8	F 7
~−12				0.7						
−12~−11			1.0	3.1						
−11~−10			1.7	4.2	11.4			2.5	2.0	
−10~− 9		1.0	2.3	6.7	18.0			1.7	5.7	
− 9~− 8		3.4	2.3	8.7	10.8		8.0	1.1	6.8	2.4
− 8~− 7	1.6	4.6	2.7	8.3	7.9	4.3	10.4	0.7	7.0	5.2
− 7~− 6	5.8	6.7	4.2	7.3	5.9	8.2	8.0	1.3	8.5	7.1
− 6~− 5	8.6	6.9	6.3	5.3	6.3	13.5	6.0	10.5	8.7	9.9
− 5~− 4	11.0	7.2	9.2	4.6	7.2	18.6	5.2	28.3	8.3	11.2
− 4~− 3	11.7	6.0	9.0	5.2	5.8	12.1	3.6	16.4	7.7	14.3
− 3~− 2	9.6	5.5	7.1	5.2	5.4	9.6	4.0	9.9	7.7	15.6
− 2~− 1	8.2	5.5	6.0	5.1	5.3	7.5	6.1	6.5	7.8	10.0
− 1~ 0	7.5	6.2	6.3	4.9	3.1	6.7	8.3	5.4	8.0	6.3
0~ 1	7.0	9.5	11.1	5.9	3.8	6.9	11.0	5.0	7.8	4.8
1~ 2	5.2	9.7	10.2	4.0	2.8	4.4	9.1	3.5	5.6	3.9
2~ 3	4.1	9.8	8.3	3.2	1.7	3.2	7.1	2.4	4.2	3.6
3~ 4	5.0	7.5	5.6	3.3	1.5	2.1	5.5	1.6	2.4	3.0
4~ 5	5.7	4.6	2.7	4.1	1.2	2.0	3.6	0.9	1.0	1.8
5~ 6	4.5	2.3	1.6	3.8	0.7	0.6	1.9	0.6	0.2	0.3
6~ 7	2.0	1.6	1.0	3.1	0.8	0.2	1.2	0.8	0.3	0.2
7~ 8	0.8	0.7	0.6	1.8	0.1	0.1	0.2	0.1	0.1	0.2
8~ 9	0.9	0.5	0.2	0.7	0.2		0.2	0.2	0.1	0.1
9~	0.8	0.8	0.6	1.2	0.1		0.6	0.6	0.1	0.1

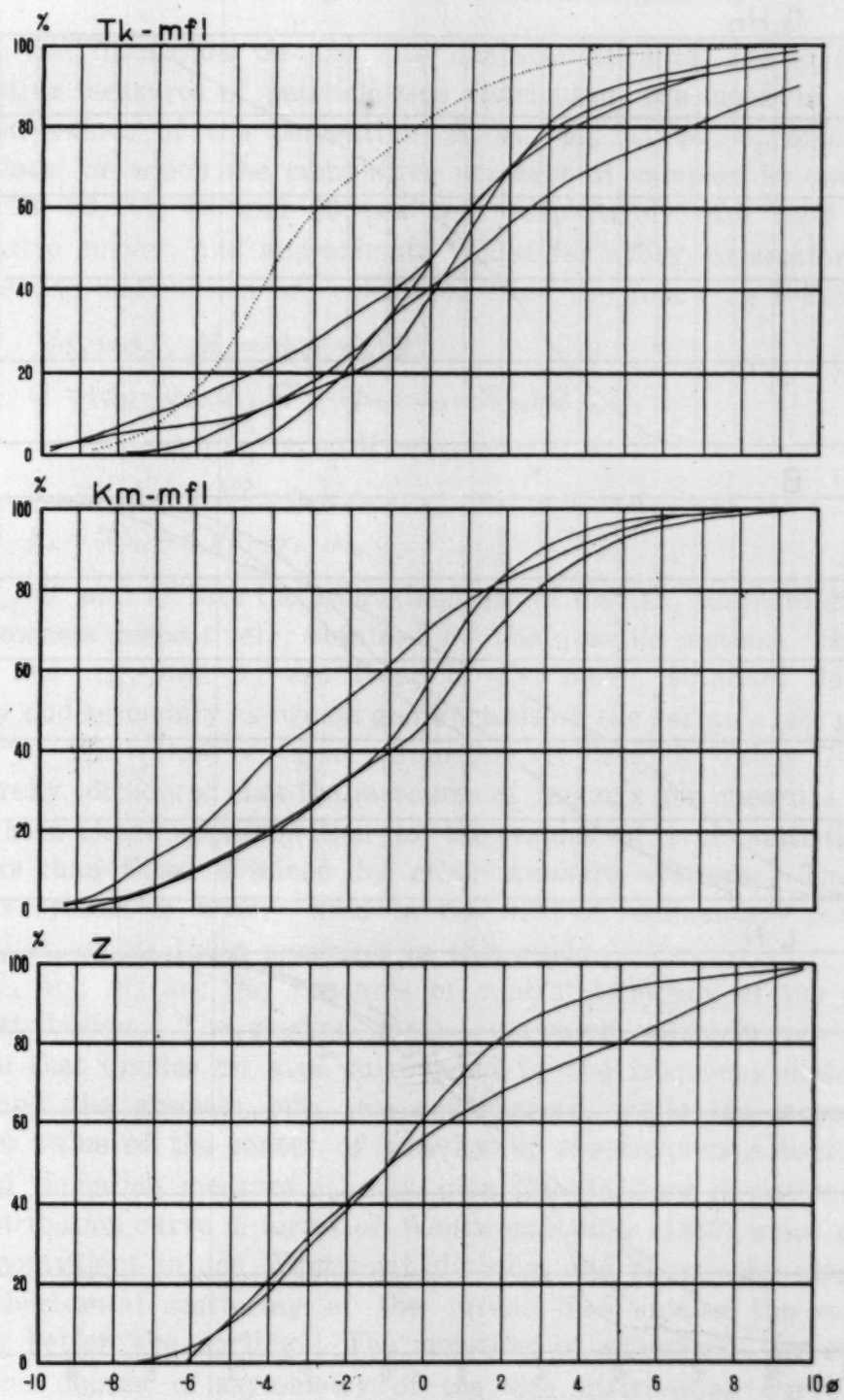

Fig. 5a. Cumulative curves of the particle size distribution of dry mud-flow deposits. Upper: the Tokachidake Volcano (solid line: May 24th, 1926, dotted line: Sept. 3rd, 1926), middle: the Komagatake Volcano, lower: the Zao Volcano.

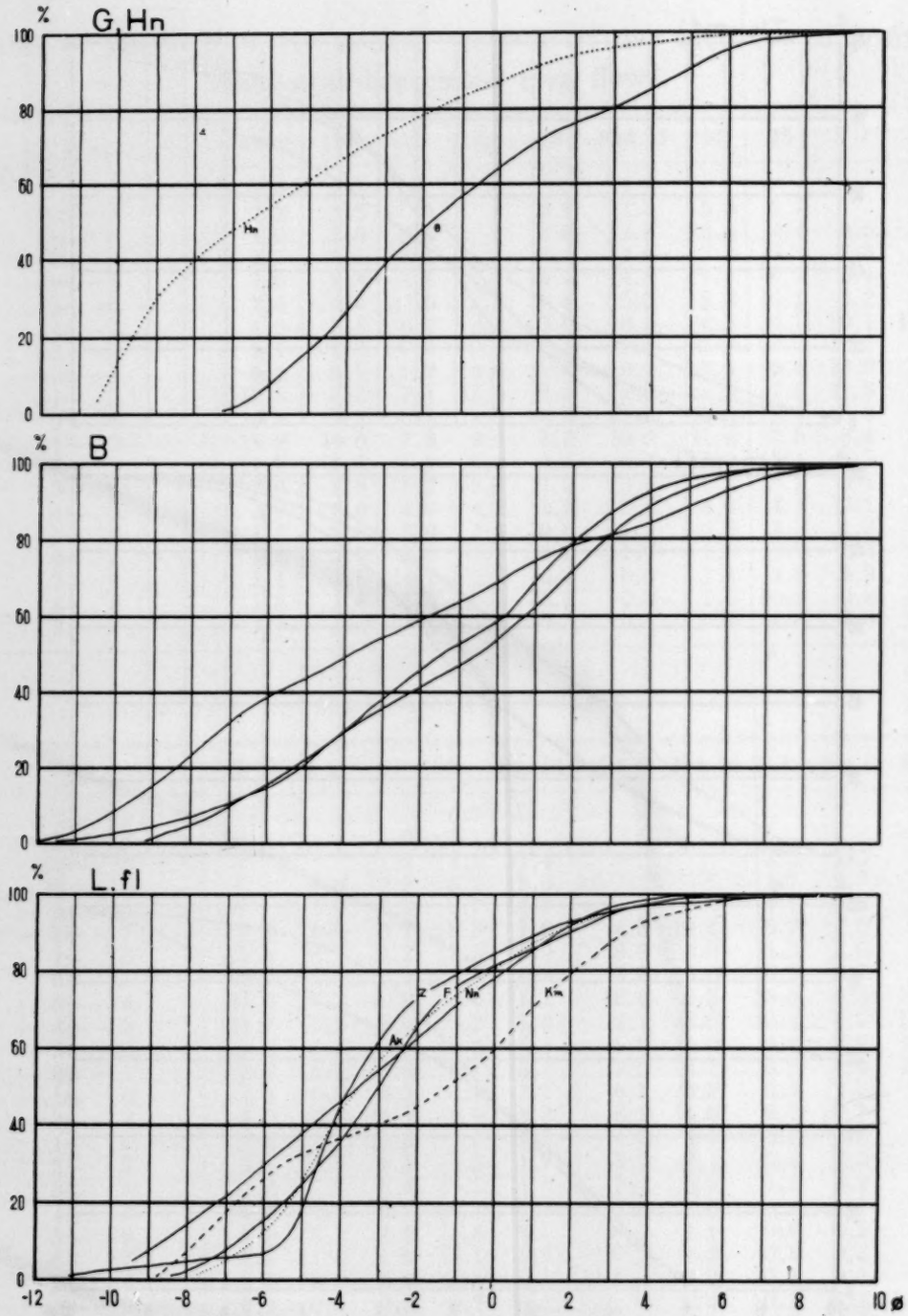

Fig. 5b. Cumulative curves of the particle size distribution of dry mud-flow deposits and auto-brecciated lava flows. Upper: mud-flows of the Gassan and Hakone Volcanoes, middle: the 1888 Mud-flow of the Bantai Volcano, lower: autobrecciated lava flows.

Parameters of Particle Size Distribution

In the discussion on the size characteristics of clastic deposits, descriptive measures of patrticle size distribution are used in general. The phi values of the percentiles, ϕ_5, ϕ_{16}, ϕ_{25}, ϕ_{50}, ϕ_{75}, ϕ_{84} and ϕ_{95}, the phi values for which the cumulative per cent of samples by weight is 5, 16, 25, 50, 75, 84 and 95 per cent respectively, are read on the cumulative curves, and approximate values for every parameter of the particle size distribution are calculated from the following relations.

$$Md_\phi = \phi_{50}\ ,\quad M_\phi = (\phi_{16}+\phi_{84})/2\ ,$$
$$Q' = (\phi_{75}-\phi_{25})/2\ ,\quad Q'' = (\phi_{75}+\phi_{25}-2\phi_{50})/Q'\ ,$$
$$\sigma_\phi = (\phi_{84}-\phi_{16})/2\ ,\quad \alpha_\phi = (M_\phi-\phi_{50})/\sigma_\phi\ ,$$
$$\alpha_{2\phi} = \{(\phi_5+\phi_{95})/2-\phi_{50}\}/\sigma_\phi\ ,$$
$$\beta_\phi = \{(\phi_{95}-\phi_5)/2-\sigma_\phi\}/\sigma_\phi\ .$$

M_ϕ, Q' and Q'' are the approximations of median, standard deviation and skewness respectively, obtained by the quartile method, while M_ϕ, σ_ϕ, α_ϕ and $\alpha_{2\phi}$, and β_ϕ are those of the mean, standard deviation, primary and secondary skewness and kurtosis of the Inman's phi measure system[25]. The values of these parameters are listed in Tables 7–12. It is generally considered that the measures of Inman's phi measure system represent a closer approximation to the values of true statistical parameters than those obtained by other measure systems. Therefore, Inman's system is widely used in the field of sedimentary petrology. The writer adopts these measures in this study.

Md_ϕ and M_ϕ are the measures of central tendency of the particle size distribution. The median is the diameter value in phi of the ordinate that divides an area surrounded by the frequency distribution curve and the abscissa into two equal areas, while the mean is the diameter value of the center of gravity of the frequency distribution. The phi deviation measure σ_ϕ may give the standard deviation of the size distribution curve in terms of Wentworth units (1922), since one phi unit is equivalent to one Wentworth division, and shows the magnitude of the horizontal scattering of the curve. The smaller the values of σ_ϕ, the better the sorting. The measures of skewness, α_ϕ and $\alpha_{2\phi}$, show the degree of asymmetry of the size distribution curve. In a symmetrical distribution the mean and the median coincide and the

25) D. L. INMAN, "Measures of describing the size distribution of sediments," *Jour. Sed. Petrol.*, **22** (1952), 125-145.

Table 7. Data of parameters of the particle size distribution of pyroclastic flow deposits.

Sp.	no.	Md_ϕ	Q'	Q''	M_ϕ	σ_ϕ	α_ϕ	$\alpha_{2\phi}$	β_ϕ	Remark
Kc	1	0.87	2.37	0.67	1.98	3.75	0.30	0.28	0.45	u
	2	0.19	2.31	−0.16	0.04	2.93	−0.05	0.04	0.93	u
	3	1.77	1.81	0.28	2.27	2.51	0.20	0.25	0.72	m
	4	2.72	1.76	−0.06	2.77	2.61	−0.13	0.10	0.76	m
	5	1.26	1.87	0.37	1.56	2.88	0.10	0.01	0.78	u
	6	1.52	1.59	0.15	1.45	2.39	−0.03	−0.33	0.75	u
	7	1.65	2.16	0.40	1.61	2.44	−0.02	−0.30	0.93	u
	8	3.37	1.32	−0.02	3.31	2.13	−0.03	0.04	0.64	m
	9	3.13	1.26	−0.05	3.11	2.00	−0.01	0.10	1.06	m
	10	1.85	1.75	0.14	2.06	2.43	0.09	0.12	0.90	u
Ms	1	0.56	1.89	0.29	0.99	2.86	0.15	0.42	0.74	
	2	1.32	1.97	0.13	1.36	3.06	0.01	−0.05	0.73	
	3	2.02	2.19	0.05	2.05	3.38	0.01	−0.03	0.70	
Ak	1	1.46	1.65	0.27	1.70	2.30	0.10	−0.08	0.71	
	2	1.98	1.72	0.09	2.11	2.48	0.05	0.05	0.76	
	3	1.09	1.33	−0.14	0.51	2.39	−0.25	−0.56	0.61	cc
	4	0.01	2.16	−0.49	−0.40	3.12	−0.13	0.10	0.76	cc
D	1	0.25	2.28	−0.56	−0.78	3.87	−0.27	−0.23	0.73	
	2	0.53	1.91	−0.23	0.09	3.35	−0.13	0.30	0.74	
TkW	1	1.97	1.57	−0.10	1.88	2.22	−0.04	−0.05	0.84	
Tk	1	0.16	2.13	−0.69	−1.36	3.51	−0.43	−0.59	0.55	p
	2	−0.98	2.48	−0.39	−1.51	3.23	−0.16	−0.16	0.47	p
	3	0.04	2.23	−0.66	−0.90	3.11	−0.30	−0.49	0.73	p
	4	2.98	1.39	0.00	2.98	2.03	0.00	0.32	0.93	p
	5	0.06	2.31	−0.38	−0.58	3.50	−0.18	−0.18	0.66	s
	6	0.21	2.24	−0.61	−0.80	3.30	−0.30	−0.43	0.64	s
	7	0.61	2.06	−0.50	−0.34	3.24	−0.30	−0.53	0.78	s
	8	−0.10	2.90	−0.73	−1.74	4.37	−0.37	−0.41	0.47	s
S	1	2.37	1.81	−0.16	2.22	2.64	−0.06	−0.02	0.72	
	2	2.44	1.86	−0.22	2.18	3.90	−0.07	0.00	0.24	
	3	1.93	2.05	−0.20	1.70	4.36	−0.05	0.06	0.19	
	4	2.07	1.84	−0.15	1.89	2.86	−0.06	0.02	0.67	
	5	1.63	2.29	−0.10	1.33	4.52	−0.07	0.03	0.22	
	6	2.48	1.86	−0.29	2.04	2.90	−0.15	0.15	0.75	
	7	1.60	2.66	−0.11	1.44	3.76	−0.04	−0.01	0.48	
	8	0.72	2.34	0.25	1.08	4.71	0.07	0.22	0.13	
	9	2.65	1.70	−0.26	2.23	3.61	−0.12	−0.17	0.33	
	10	1.64	2.11	−0.11	1.49	3.19	−0.05	0.19	0.82	
	11	2.03	2.04	0.34	2.58	2.98	0.18	0.17	0.77	
Kt	1	0.83	1.33	0.00	0.65	2.82	0.07	0.18	0.98	u
	2	0.96	1.60	−0.66	2.35	2.90	0.48	0.08	0.88	u
Ty	1	1.15	1.72	0.28	1.43	2.45	0.11	0.27	0.73	u
	2	2.27	1.93	−0.18	2.06	2.79	0.08	−0.01	0.51	l
	3	2.59	1.64	−0.22	2.43	2.41	−0.07	0.11	0.73	l
	4	2.43	2.19	−0.18	2.16	3.14	−0.09	0.03	0.59	l
	5	0.47	2.69	0.41	1.12	3.64	0.18	0.31	0.49	u
	6	0.37	2.74	0.42	1.10	3.85	0.19	0.28	0.46	u
	7	0.04	2.07	0.30	−0.02	3.08	−0.02	0.58	0.78	u
	8	3.27	1.35	−0.59	3.20	2.03	−0.04	0.22	0.89	l
	9	0.87	1.50	0.26	1.15	2.39	0.12	0.25	1.35	u
	10	0.27	1.50	0.48	0.64	2.61	0.14	0.39	0.84	o

Table 7. (Continued)

Sp.	no.	$Md\phi$	Q'	Q''	$M\phi$	$\sigma\phi$	$\alpha\phi$	$\alpha_{2}\phi$	$\beta\phi$	Remark
Km	1	0.20	1.97	−0.93	−0.97	3.00	−0.39	−0.21	1.17	1929
	2	0.29	1.86	−0.84	−0.77	3.00	−0.35	−0.10	1.10	1929
	3	0.47	1.55	−0.58	−0.36	2.88	−0.29	0.16	0.98	1929
	4	0.06	2.60	−1.07	−1.26	3.39	−0.39	0.33	0.53	1929
	5	0.17	2.55	−1.02	1.26	3.56	−0.40	−0.03	0.73	1929
	6	−0.30	3.02	−1.08	−2.06	3.99	−0.44	0.05	0.67	1929
	7	0.33	1.48	−0.62	−0.65	3.64	−0.37	−0.16	1.21	H.-shaped-cr.-fl
	8	0.20	2.11	−0.82	−0.83	3.09	−0.33	0.05	0.91	Kurumizaka-fl
	9	0.22	1.72	−0.58	−0.77	3.09	−0.32	−0.20	0.80	H.-shaped-cr.-fl
	10	0.50	1.94	−0.61	−0.23	3.60	−0.20	0.03	0.74	H.-shaped-cr.-fl
Tw	1	0.29	1.81	1.68	0.33	2.81	0.01	0.16	0.59	
	2	2.04	2.15	0.29	2.58	3.18	0.18	0.22	0.57	
	3	0.53	2.37	0.24	0.91	3.71	−0.10	0.17	0.56	
	4	2.13	1.99	0.48	2.53	2.63	0.15	0.38	1.18	
	5	1.56	2.63	0.19	1.83	3.71	0.07	0.17	0.46	
	6	1.84	2.77	0.40	2.46	3.74	0.17	0.13	0.50	
	7	2.57	2.05	0.21	2.97	2.87	0.14	0.21	0.56	
	8	3.08	2.45	0.16	3.36	3.35	0.08	0.03	0.54	
	9	0.10	2.15	−0.30	0.14	3.31	0.01	0.29	0.73	
	10	1.89	2.32	0.70	2.47	3.60	0.16	0.10	0.52	
	11	3.02	2.29	−0.09	3.01	3.18	−0.05	−0.02	0.63	
	12	0.88	2.40	0.25	1.41	3.87	0.14	0.24	0.57	
	13	0.11	2.41	−0.25	−1.70	3.80	−0.16	0.15	0.71	
	14	0.06	2.25	−0.21	0.10	3.50	0.05	0.36	0.70	
	15	0.75	3.19	0.42	1.70	4.36	0.22	0.42	0.51	
	16	2.53	2.12	0.10	2.87	2.93	0.12	0.18	0.61	
	17	0.82	3.14	−0.23	0.72	3.49	−0.03	0.17	0.67	
	18	1.07	2.39	0.20	1.25	3.82	0.05	0.14	0.57	
	19	2.68	2.41	0.13	2.58	3.61	−0.03	0.15	0.54	
	20	0.22	2.59	0.07	0.59	3.65	0.10	0.23	0.43	o
	21	−1.83	2.15	0.38	−1.17	3.09	0.21	0.52	0.50	o
	22	1.18	1.75	0.03	1.18	2.69	0.00	−0.13	0.96	o
Os	1	1.57	1.82	0.04	2.08	2.80	0.18	0.11	0.79	
Hd	1	0.66	2.60	0.57	3.50	3.69	0.77	0.74	1.06	
Tz	1	1.37	1.86	0.59	2.34	2.71	0.40	0.58	0.82	
On	1	1.18	1.59	0.17	1.20	3.05	0.07	0.20	0.76	
	2	2.97	2.44	−0.44	1.31	4.24	−0.39	−0.45	0.41	
	3	1.96	2.68	0.59	3.58	4.13	0.41	0.35	0.63	
Hj	1	0.66	1.31	−1.13	0.29	2.19	−0.17	−0.17	0.67	
	2	0.84	1.86	0.18	2.81	2.86	−0.10	0.18	0.83	
Nm	1	0.07	2.33	−0.66	−0.94	3.91	−0.26	−0.26	0.63	
Nn	1	−1.46	3.83	0.34	−0.32	5.02	0.23	0.54	0.47	s
	2	0.03	2.71	−0.66	−0.71	4.10	−0.18	−0.12	0.60	p
	3	0.10	2.48	−0.74	−0.29	3.74	−0.10	0.00	0.68	p
	4	0.93	1.63	1.00	2.03	2.55	0.43	0.33	0.69	p
	5	1.43	2.22	0.46	0.93	4.38	0.12	−0.20	0.51	p
	6	−0.05	3.01	−0.38	−0.82	4.16	−0.19	−0.05	0.47	p
Th	1	2.25	1.52	0.00	2.34	2.16	0.05	0.32	1.26	
Hr	1	−0.53	2.18	−0.24	−0.88	3.09	−0.11	−0.03	0.59	l
	2	−0.67	2.23	−0.29	−1.03	3.00	−0.11	−0.03	0.58	l
	3	4.10	1.65	0.15	4.44	2.54	0.13	0.53	0.81	l
	4	0.97	1.70	−0.21	0.52	2.86	−0.16	0.51	0.80	u

Table 7. (Continued)

Sp.	no.	Md_ϕ	Q'	Q''	M_ϕ	σ_ϕ	α_ϕ	$\alpha_{2\phi}$	β_ϕ	Remark
KS	1	1.58	1.89	0.22	1.01	4.01	−0.14	0.03	0.55	m
	2	0.73	1.84	0.14	0.44	2.86	−0.10	0.01	0.68	l
	3	0.22	2.27	−0.28	−0.38	3.63	−0.16	0.03	0.59	l
	4	0.96	1.70	0.09	0.71	3.26	−0.08	0.07	1.62	l
My	1	0.28	3.07	−0.76	−1.05	4.27	−0.31	−0.41	0.60	
	2	0.28	2.59	−0.36	−0.85	4.32	−0.26	−0.32	0.54	
	3	−0.98	3.03	−0.28	−1.39	4.24	−0.10	−0.16	0.59	
	4	0.63	2.61	−0.47	−0.43	3.96	−0.27	−0.42	0.51	
	5	−0.03	3.05	−0.56	−0.92	4.06	−0.22	−0.25	0.49	
	6	0.14	2.30	−0.15	−0.05	3.36	−0.06	−0.13	0.95	
	7	0.47	3.09	−0.74	−0.89	4.31	−0.32	−0.28	0.46	
	8	0.78	2.79	−0.21	−0.24	4.35	−0.12	−0.17	0.51	
	9	0.47	2.30	−0.27	−0.05	3.45	−0.15	−0.22	0.63	
	10	0.74	2.47	−0.39	−0.42	4.18	−0.28	−0.39	0.62	
	11	0.28	2.53	−0.42	−0.54	3.76	−0.22	−0.37	0.59	
Am	1	0.81	1.53	0.58	1.19	2.56	0.15	0.05	0.85	lp
	2	0.70	1.54	0.34	0.89	2.76	0.07	0.01	0.81	lp
	3	0.86	2.02	−0.26	0.33	3.23	0.11	0.00	0.57	lp
	4	1.17	1.84	0.42	1.48	2.92	0.10	0.13	0.74	lp
	5	1.96	1.24	1.47	2.33	2.30	0.16	0.33	0.53	lp
	6	0.40	1.58	−0.20	0.06	2.69	−0.13	−0.14	0.80	lp
	7	0.39	1.48	0.21	0.44	2.84	0.02	0.24	0.85	lp
	8	0.67	1.67	−0.07	0.70	3.00	0.01	0.11	0.79	lp
	9	0.74	1.62	0.02	0.56	2.74	−0.07	0.08	0.88	lp
	10	0.66	1.86	0.11	0.90	3.17	0.08	0.14	0.63	lp
	11	1.20	1.78	0.51	1.98	2.83	0.27	0.27	0.85	lp
	12	1.41	1.61	0.40	1.87	2.39	0.19	0.19	0.97	lp
	13	1.80	1.88	0.08	1.95	1.71	0.09	0.73	0.71	lp
	14	1.17	1.35	0.35	1.66	2.68	0.18	0.30	0.94	lp
	15	1.20	1.45	0.39	1.69	2.24	0.22	0.50	1.09	lp
	16	3.60	1.63	0.52	4.33	2.45	0.30	0.64	0.69	lp
	17	0.18	2.07	−0.36	−0.29	3.36	0.14	0.02	0.72	up
	18	0.70	2.17	−0.15	0.30	3.67	−0.12	0.01	0.68	up
	19	0.79	1.77	0.12	0.70	3.48	−0.03	0.01	0.75	up
	20	0.13	2.25	−0.58	−0.70	3.30	−0.25	0.02	0.72	up
	21	0.33	1.20	−0.28	−0.05	3.29	−0.11	0.16	0.87	up
	22	0.67	1.38	0.20	0.88	2.25	0.09	0.14	1.44	up
	23	0.75	1.26	−0.02	0.44	2.19	−0.14	−0.19	0.75	up
	24	0.52	2.07	−0.41	−0.01	3.06	−0.17	−0.15	0.66	Oiwake-fl
	25	−1.30	2.74	−0.13	−1.26	3.59	0.01	0.20	0.49	Oiwake-fl
	26	−0.48	2.87	−0.44	−1.17	3.94	−0.17	−0.12	0.57	Oiwake-fl
	27	−3.00	3.19	0.32	−2.31	4.03	0.17	0.26	0.39	Oiwake-fl
	28	−1.85	3.28	0.19	−2.05	4.30	−0.05	−0.02	0.87	Oiwake-fl
	29	0.10	2.66	−0.71	−1.06	3.62	−0.31	−0.33	0.47	Oiwake-fl
	30	2.77	1.13	−0.04	2.81	1.71	0.02	0.03	0.61	Oiwake-fl
	31	0.40	2.71	−0.68	−1.74	5.24	0.41	−0.16	0.25	Agatsuma-fl
	32	0.15	2.32	−0.29	−0.75	5.29	−0.26	−0.22	0.92	Agatsuma-fl
	33	0.46	1.89	−0.12	−0.45	3.15	0.00	−0.85	1.04	Agatsuma-fl
	34	0.30	2.07	−0.42	−0.26	3.46	−0.16	0.00	0.60	(Kambara-na)
	35	0.13	2.41	−0.80	−0.96	3.46	−0.32	−0.21	0.43	Shiraito-fl
	36	1.63	1.34	0.04	1.72	2.02	0.04	0.11	0.68	1958-XI-10-fl
	37	1.33	1.21	−0.20	1.05	2.33	−0.12	−0.01	0.66	1958-XI-10-fl
	38	0.26	1.66	−0.24	−0.01	3.45	−0.08	0.02	0.14	1958-XI-10-fl
Hn	1	0.52	1.76	−0.07	0.40	3.09	−0.02	0.20	0.84	p
	2	0.83	1.55	0.11	1.04	2.57	0.08	0.33	0.94	p
	3	0.24	1.12	0.02	0.24	1.69	0.00	0.44	1.08	p
	4	0.60	1.90	0.29	1.15	2.88	0.19	0.51	0.72	p

Table 7. (Continued)

Sp.	no.	Md_ϕ	Q'	Q''	M_ϕ	σ_ϕ	α_ϕ	$\alpha_{2\phi}$	β_ϕ	Remark
Hn	5	0.62	1.37	0.07	0.67	2.08	0.02	0.62	1.14	p
	6	0.46	1.98	−0.09	0.57	3.13	0.02	0.34	1.76	p
	7	0.07	1.78	−0.41	−0.38	2.71	−0.16	0.38	1.06	p
	8	0.10	2.50	−0.38	−0.10	3.97	−0.05	0.16	0.63	s
	9	0.21	1.90	0.01	0.27	2.81	0.02	0.13	0.41	s
	10	−0.28	2.98	0.20	0.44	3.81	0.19	0.48	0.70	s
	11	−2.12	3.25	−0.65	−3.28	4.22	−0.27	−0.20	0.43	cc
	12	−1.93	3.00	−0.38	−2.74	4.36	−0.19	−0.10	0.44	cc
	13	−0.53	2.34	−0.40	−1.29	3.59	−0.21	−0.27	0.65	cc
KF	1	−1.42	3.50	−0.18	−1.71	4.76	−0.06	0.24	0.48	
	2	−1.25	3.48	−0.16	−1.64	4.39	−0.09	0.06	0.36	
	3	−2.36	2.88	0.39	−1.70	3.93	0.17	0.24	0.52	
	4	−1.03	1.75	0.00	0.15	2.79	0.32	0.62	0.77	
	5	−1.11	0.95	0.35	−0.84	3.57	0.21	0.12	0.52	
	6	−1.33	3.07	0.02	−1.11	4.16	0.05	0.20	0.46	
	7	−0.24	3.36	−0.27	−0.30	4.57	−0.01	0.16	0.50	
	8	−1.47	2.79	0.04	−1.09	3.93	0.10	0.22	0.53	
	9	−0.67	2.42	−0.29	−1.09	3.24	−0.13	0.01	0.35	
	10	−2.73	2.66	0.56	−1.76	3.47	0.28	0.55	0.37	
As	1	3.92	1.93	−0.16	3.77	2.85	−0.03	0.23	0.91	
	2	3.68	1.59	0.11	3.70	2.48	−0.01	0.49	1.55	
Ai	1	1.67	1.79	−0.02	1.52	2.88	−0.05	0.29	1.30	m
	2	0.98	2.30	−0.24	0.55	3.32	−0.13	0.17	0.81	m
	3	−0.57	1.85	−0.23	−0.78	2.60	−0.08	−0.21	0.76	
	4	3.77	1.70	−0.08	3.72	2.62	−0.02	0.15	1.14	
	5	1.52	1.75	0.26	1.97	2.54	0.18	0.33	0.81	u
	6	1.13	2.02	−0.11	0.60	3.30	−0.16	−0.02	0.75	m
	7	1.20	2.04	−0.16	0.56	3.39	−0.19	−0.15	0.59	m
	8	2.57	1.72	0.44	3.50	2.82	0.33	0.89	0.92	l
	9	1.67	2.71	−0.60	0.85	3.73	−0.21	0.09	0.66	l
	10	2.29	1.32	0.15	2.37	2.04	0.04	0.25	0.98	l
	11	1.62	1.47	−0.11	1.44	2.19	−0.08	−0.22	1.23	m
	12	1.77	1.66	0.05	1.58	2.65	−0.07	−0.36	1.00	m
	13	1.63	1.70	0.00	1.27	2.87	−0.13	−0.09	1.00	m

value of α_ϕ is zero. On the other hand, in a skewed distribution, the mean departs from the median. If the size distribution is skewed towards smaller phi values (coarser diameters), the skewness measure α_ϕ is positive, and conversely α_ϕ is negative for the size distribution skewed towards higher phi values (finer diameters), and the larger the values the stronger the degree of asymmetry. The measure of primary skewness α_ϕ is related to the moment skewness α_3 of statistics by the approximate relationship, $\alpha_3=6\alpha_\phi$. The secondary skewness $\alpha_{2\phi}$ is another measure of the departure of the curve from normal distribution. It is most sensitive to skew properties within the tails of the size distribution of the deposit, and also serves as a check on the continuity of the skew properties of the size distribution. The measure of kurtosis β_ϕ is that of the degree of peakness. For a normal distribution β_ϕ has a values

Table 8. Ranges of parameter values in a single unit of pyroclastic flows.

Volc.	Md_ϕ	M_ϕ	σ_ϕ	α_ϕ	$\alpha_{2\phi}$	β_ϕ	
Kc	1.77~ 3.37	2.27~ 3.31	1.99~2.61	−0.13~ 0.20	0.04~ 0.25	0.64~1.06	m
Kc	0.19~ 1.85	0.04~ 2.06	2.38~3.75	−0.05~ 0.30	−0.33~ 0.28	0.45~0.74	u
Ms	0.56~ 2.02	0.99~ 2.05	2.86~3.38	0.01~ 0.15	−0.05~ 0.41	0.70~0.74	
Ak	1.46~ 1.98	1.70~ 2.11	2.30~2.48	0.05~ 0.10	−0.08~ 0.05	0.71~0.76	
Ak	0.01~ 1.09	−0.40~ 0.51	2.39~3.12	−0.25~−0.13	−0.56~ 0.10	0.61~0.76	cc
D	1.91~ 2.28	−0.78~ 0.09	3.35~3.87	−0.27~−0.13	−0.23~−0.30	0.73~0.74	
TkW	1.97	1.88	2.22	−0.04	−0.05	0.84	
Tk	−0.98~ 0.16	−1.51~−0.90	3.11~3.50	−0.43~−0.16	−0.59~ 0.16	0.47~0.73	p
Tk	−0.10~ 0.61	−1.74~−0.34	3.24~4.37	−0.37~−0.18	−0.53~ 0.18	0.47~0.78	s
S	0.72~ 2.46	1.08~ 2.58	2.64~4.71	−0.15~ 0.18	−0.17~ 0.22	0.13~0.77	
Kt	0.83~ 0.96	0.65~ 2.35	2.82~2.90	−0.07~ 0.48	0.08~ 0.18	0.88~0.98	
Ty	0.27	0.64	2.61	0.14	0.39	0.84	o
Ty	2.27~ 3.27	2.06~ 3.20	2.03~3.14	−0.09~ 0.08	−0.01~ 0.22	0.51~0.89	l
Ty	0.04~ 1.15	−0.02~ 1.15	2.39~3.85	−0.02~ 0.18	0.25~ 0.58	0.46~1.35	u
Km	−0.30~ 0.47	−2.06~−0.36	2.88~3.99	−0.44~−0.29	−0.21~ 0.33	0.53~1.17	
Km	0.20~ 0.50	−0.83~−0.23	3.06~3.64	−0.37~−0.20	−0.20~ 0.05	0.74~1.21	o
Tw	−1.83~ 1.18	−1.17~ 1.18	2.69~3.65	0.00~ 0.21	−0.13~ 0.52	0.43~0.96	o
Tw	−0.11~ 3.08	−1.70~ 3.36	2.63~4.36	−0.16~ 0.18	−0.16~ 0.22	0.46~1.18	
Os	1.57	2.08	2.80	0.18	0.11	0.79	
Hd	0.66	3.50	3.69	0.77	0.74	1.06	
Tz	1.37	2.34	2.71	0.40	0.58	0.82	
On	1.18~ 2.97	1.20~ 3.58	3.05~4.24	−0.39~ 0.41	−0.45~ 0.35	0.41~0.76	
Hj	0.66~ 0.84	0.29~ 0.56	2.19~2.81	−0.17~−0.10	−0.17~ 0.18	0.67~0.83	
Nm	0.07	−0.94	3.91	−0.26	−0.26	0.63	
Nn	−1.46	−0.32	5.02	0.23	0.54	0.47	s
Nn	−0.05~ 1.43	−0.82~ 2.03	2.55~4.38	−0.19~ 0.43	−0.20~ 0.33	0.47~0.69	p
Th	2.25	2.34	2.16	0.05	0.32	1.26	
Hr	−0.67 −0.53	−1.03~−0.88	3.00~3.09	−0.11	−0.03	0.58~0.59	l
Hr	0.92	0.52	2.86	−0.16	0.51	0.80	u
KS	0.22~ 1.58	−0.38~ 1.01	2.86~4.61	−0.14~−0.10	0.01~ 0.77	0.55~1.62	
My	−0.98~ 0.78	−1.05~ 0.24	3.36~4.35	−0.32~−0.06	−0.42~−0.13	0.46~0.95	
Am	0.39~ 1.96	0.33~ 2.33	1.71~3.17	−0.13~ 0.27	−0.14~ 0.73	0.53~1.09	l
Am	0.13~ 0.79	−0.70~ 0.88	2.19~3.67	−0.25~ 0.14	−0.19~ 0.16	0.68~1.44	u
Am	−3.00~ 0.52	−2.31~−0.01	3.06~4.30	−0.31~ 0.17	−0.33~ 0.26	0.39~0.87	O
Am	0.13	−0.96	3.46	−0.32	−0.21	0.43	S
Am	0.15~ 0.46	−1.74~−0.26	3.15~5.24	−0.26~ 0.41	−0.85~ 0.00	0.25~1.04	A
Am	0.26~ 1.63	−0.01~ 1.72	2.02~3.45	−0.12~ 0.04	−0.01~ 0.11	0.14~0.68	
Hn	0.07~ 0.83	−0.38~ 1.15	1.69~3.13	−0.16~ 0.19	0.20~ 0.62	0.72~1.76	p
Hn	−0.28~ 0.21	−0.10~ 0.44	2.81~3.97	−0.05~ 0.19	0.13~ 0.48	0.03~0.70	s
Hn	−2.12~−0.53	−3.28~−1.29	3.59~4.36	−0.27~−0.19	−0.27~−0.10	0.43~0.65	cc
KF	−2.73~−0.24	−1.76~ 0.15	2.79~4.76	−0.13~ 0.32	0.01~ 0.62	0.35~0.77	
As	3.68~ 3.92	3.70~ 3.77	2.48~2.85	−0.03~−0.01	0.23~ 0.49	0.91~1.55	
Ai	1.67~ 2.57	0.85~ 3.50	2.04~3.73	−0.21~ 0.33	0.09~ 0.89	0.66~0.98	l
Ai	1.13~ 1.77	0.55~ 1.97	2.19~3.39	−0.19~ 0.18	−0.36~ 0.33	0.59~1.30	m

of 0.65, and if the distribution is less peaked than normal, β_ϕ is greater than this value. Conversely, values of β_ϕ less than 0.65 indicate that the distribution is more peaked than normal.

Summary of Results

The results of mechanical analyses of the pyroclastic flow deposits are summarized as follows.

Table 9. Data of parameters of the particle size distribution of pyroclastic fall deposits

Sp.	no.	$Md\phi$	Q'	Q''	$M\phi$	$\sigma\phi$	$\alpha\phi$	$\alpha_2\phi$	$\beta\phi$	Remark
Kc	11	1.14	0.75	0.11	1.28	1.21	0.11	0.72	0.46	
	12	3.32	0.75	0.26	3.50	1.22	0.15	0.91	0.29	
	13	−1.98	1.36	0.24	−1.70	2.03	0.14	0.69	0.94	
Ms	4	−2.23	1.83	0.33	−1.81	2.41	0.15	0.17	0.35	
Ak	5	4.20	1.40	0.39	4.78	1.91	0.30	0.28	0.20	1959-X-3-fa
D	3	−1.08	1.06	0.20	−0.96	1.48	0.08	0.25	0.95	
	4	−2.06	1.71	0.46	−1.59	2.29	0.21	0.51	0.63	
S	12	−1.73	1.05	0.23	−1.49	1.54	0.16	0.36	0.54	
	13	2.57	0.82	−0.17	2.48	1.20	−0.08	0.40	1.22	
	14	−1.83	1.03	0.07	−1.75	1.43	0.07	0.22	0.45	
	15	−2.94	1.44	0.54	−2.22	2.18	0.33	0.41	0.27	
	16	−1.78	1.18	0.13	−1.64	1.68	0.09	0.43	0.81	
Ty	11	0.10	0.92	−0.80	−0.47	1.29	−0.44	−0.64	0.55	
	12	0.32	1.08	−0.87	−0.33	1.54	−0.42	−0.33	0.56	
Km	11	−4.73	0.53	−0.10	−4.73	0.73	0.00	0.89	1.23	1929-fa
	12	−4.32	0.87	0.59	−3.70	1.47	0.42	1.12	0.85	
Tw	23	−1.61	1.61	0.02	−1.45	2.22	0.07	0.53	0.89	
	24	−4.21	0.86	0.67	−3.65	1.25	0.45	1.15	0.80	
	25	−1.19	1.05	0.02	−1.22	1.51	−0.02	0.10	0.54	
	26	−1.74	1.40	−0.05	−1.78	1.96	−0.20	−0.09	0.44	
Nn	7	−2.98	0.80	0.38	−2.61	1.28	0.30	0.74	0.69	
Hr	5	−3.70	0.95	0.25	−3.37	1.42	0.24	0.87	0.83	u-fa
KS	5	−0.05	0.69	−0.57	−0.44	1.04	−0.42	−0.63	0.78	
Am	39	−4.25	1.27	0.96	−2.31	2.86	0.68	1.12	0.54	
	40	−3.29	1.03	0.39	−1.75	2.75	0.56	1.13	0.74	
	41	−1.34	1.38	0.25	−0.96	1.96	0.19	1.40	1.49	1783-fa
	42	−3.15	1.18	0.30	−2.80	2.02	0.17	0.25	0.48	1783-fa
	43	−2.73	1.41	0.52	−2.19	1.92	0.28	0.28	0.43	1783-fa
	44	−2.99	0.85	0.41	−2.60	1.37	0.29	0.52	0.79	1783-fa
	45	−3.95	0.44	−0.05	−3.94	0.71	0.01	0.44	1.68	1783-fa
	46	−1.16	1.20	−1.03	−1.16	0.96	0.00	−0.08	1.33	1958-XI-10-fa
	47	2.42	0.47	0.28	2.58	0.73	0.21	0.79	1.43	1958-XI-11-fa
KF	11	−2.23	0.72	0.32	−1.79	1.29	0.34	2.13	2.11	
F	1	−2.80	0.50	0.28	−2.62	0.84	0.21	1.07	1.52	
	2	−1.35	1.63	0.49	−0.56	2.48	0.32	0.89	0.87	
	3	−0.73	0.77	−0.17	−0.85	1.13	−0.11	0.16	0.52	
	4	−1.89	0.76	−0.08	−1.91	1.09	−0.02	0.13	0.51	
	5	−0.32	0.66	−0.39	−0.58	1.00	−0.26	−0.48	0.59	
	6	−2.42	0.74	0.43	−2.07	1.14	0.32	0.89	0.76	

1) Lack of sorting: Size characteristics of the pyroclastic flow deposits are quite particular, and make a distinct contrast with those of the pyroclastic fall deposits. The lack of sorting or ill-sorting of the pyroclastic flow deposits has been emphasized as a characteristic feature and a criterion for the recognition of them, contrasting with the well-sorted character of the pyroclastic fall deposits. This is clearly indicated

Table 10. Data of parameters of the particle size distribution of foreign pyroclastic flow deposits.

Sp.	no.	$Md\phi$	Q'	Q''	$M\phi$	$\sigma\phi$	$\alpha\phi$	$\alpha_2\phi$	$\beta\phi$
SV	1	0.72	1.55	0.23	0.42	2.26	−0.14	−0.20	0.60
	2	−3.50	4.29	−0.19					
	3	−0.05	2.25	0.42	−0.62	3.25	−0.17	0.20	0.57
P	1	−4.75	4.74	0.92					
SS	1	2.65	1.74	0.13	2.74	2.67	0.03	0.00	0.64
CL	1	0.62	2.46	−0.39	−0.03	3.66	−0.18		
	2	0.38	3.31	−0.31	−0.67	4.24	−0.25		
	3	2.65	2.01	−0.01	2.04	3.04	−0.20		
	4	3.28	1.77	−0.17	2.98	2.57	−0.12		
NZA	1	3.50	1.15	−0.26	3.30	1.75	−0.11		
	2	3.25	1.58	−0.29	2.65	2.45	−0.25		
VTTS	1	2.80	1.90	−0.42	1.88	2.93	−0.32		

Table 11. Data of parameters of the particle size distribution of dry mud-flow deposits.

Sp.	no.	$Md\phi$	Q'	Q''	$M\phi$	$\sigma\phi$	$\alpha\phi$	$\alpha_2\phi$	$\beta\phi$	Remark
Tk	9	0.73	1.81	−0.14	0.25	3.07	−0.16	−0.17	1.56	1926-mfl
	10	0.16	3.01	−0.43	−0.80	4.66	−0.21	−0.07	0.82	1926-mfl
	11	1.23	3.72	0.20	2.20	5.43	0.18	0.27	0.54	1926-mfl
	12	0.20	2.24	0.19	0.76	3.07	0.18	0.54	0.96	1926-mfl
	13	−3.82	2.12	0.63	−2.92	3.56	0.31	0.54	0.79	1926-mfl
Km	13	−0.37	2.10	−0.06	−1.30	3.28	−0.30	−0.31	0.73	
	14	0.15	2.72	−0.05	−0.76	3.99	−0.23	−0.21	0.62	
	15	−1.53	3.96	0.09	−1.09	4.29	0.10	0.21	0.58	
Z	1	−0.90	2.23	−0.21	−1.01	3.28	0.37	0.34	0.78	Sukawa-mfl
	2	−0.80	3.57	0.45	0.72	5.15	−0.30	0.43	0.37	Sukawa-mfl
G	1	−1.80	2.95	0.39	−0.64	4.37	0.27	0.36	0.40	Sasagawa-mfl
B	1	−0.38	3.45	−0.47	−1.36	4.59	−0.21	−0.19	0.44	1888-mfl
	2	−1.33	3.02	−0.08	−1.54	4.07	−0.05	−0.21	0.67	1888-mfl
	3	−3.75	4.41	0.17	−2.62	6·22	0.18	0.27	0.38	1888-mfl
Hn	14	−6.68	3.29	0.44	−5.27	4.51	0.31	0.64	0.45	

Table 12. Data of parameters of the particle size distribution of auto-brecciated lava flows

Sp.	no.	$Md\phi$	Q'	Q''	$M\phi$	$\sigma\phi$	$\alpha\phi$	$\alpha_2\phi$	$\beta\phi$	Remark
Ak	5	−3.60	2.11	0.63	−2.60	3.04	0.33	0.54	0.21	cc-1 fl
Km	16	−1.14	3.84	−0.91	−2.34	4.94	−0.24	−0.13	0.31	
Z	3	−3.79	1.57	0.79	−2.57	2.52	0.46	0.45	1.21	Kanno-lfl
Nn	8	−3.60	3.08	−0.25	−3.53	4.26	0.02	0.06	0.44	Osawa-lfl
F	7	−3.01	1.93	0.61	−2.73	3.16	0.09	0.28	0.68	

in values of σ_ϕ, the parameter of standard deviation. Those of the pyroclastic flow deposits are generally larger than 2, while those of the

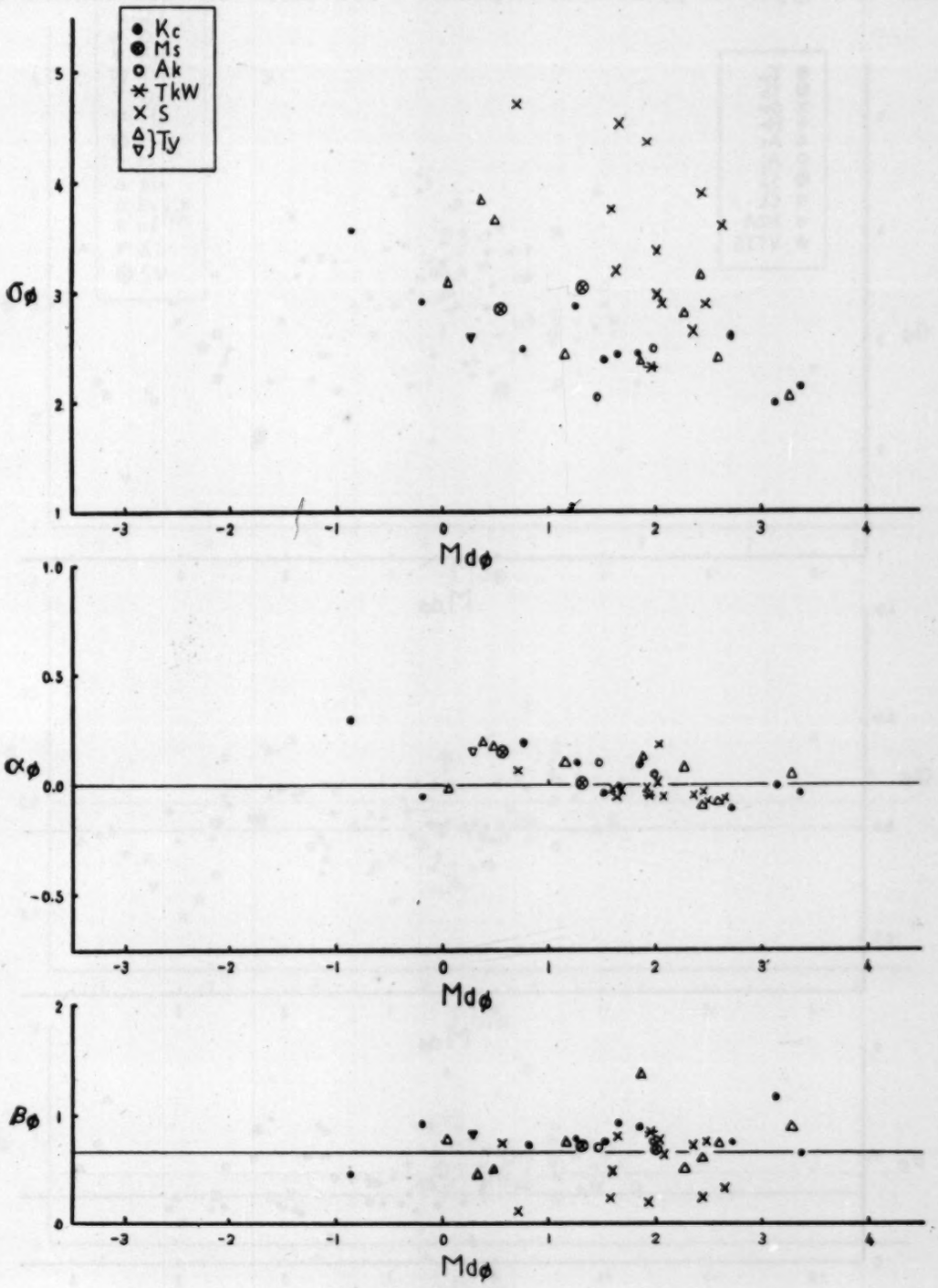

Fig. 6. Relation of values of $\sigma\phi$, $\alpha\phi$, and $\beta\phi$ to values of $Md\phi$.
Fig. 6a. The Krakatoa type ash-flows.

pyroclastic fall deposits are usually less than 2 (see Figs. 6a–6f).

The shape of the size distribution curve is quite different between these two types of pyroclastic deposits. The most distinct feature of

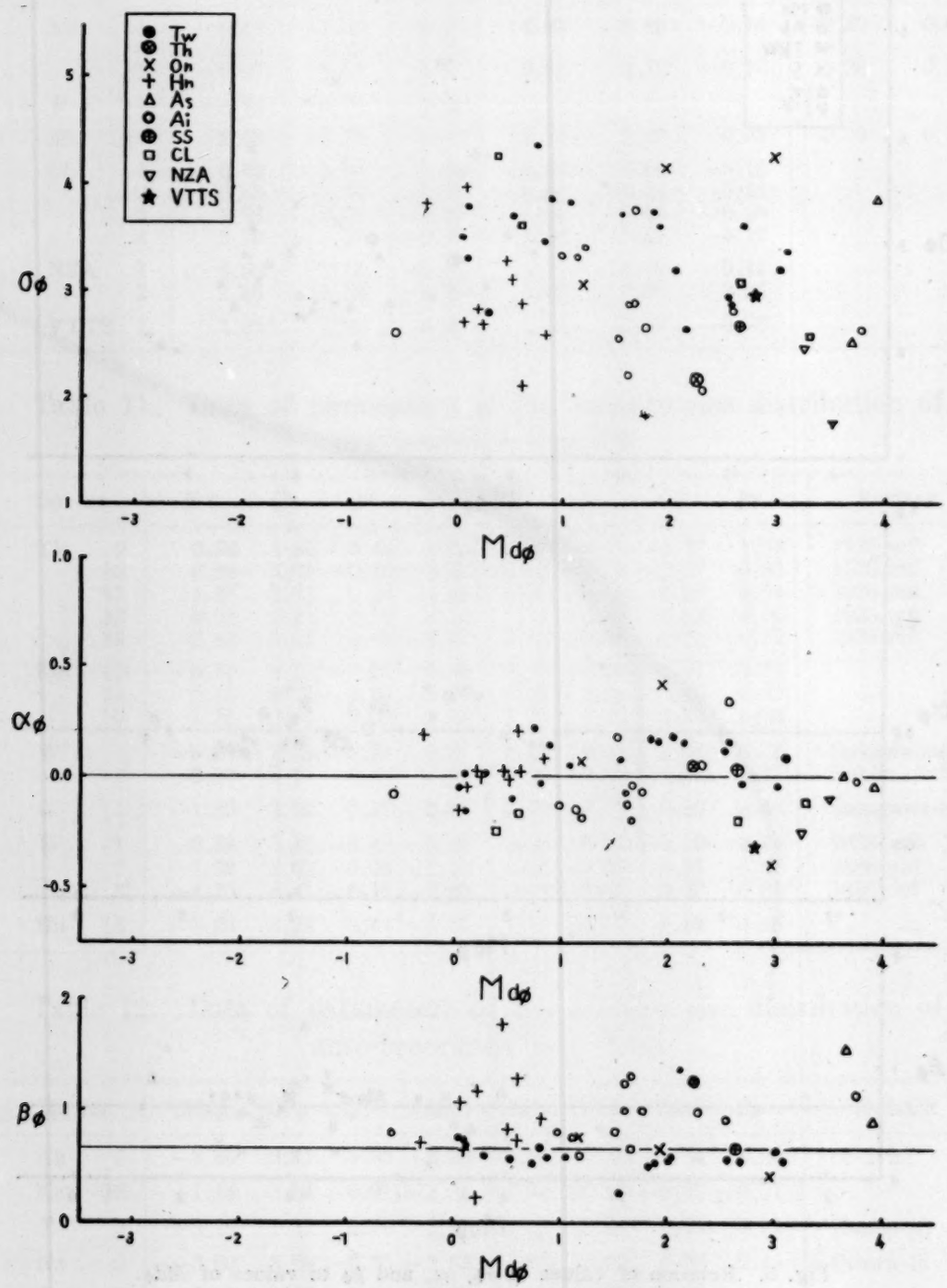

Fig. 6b. The Krakatoa type ash-flows.

the particle size distribution of the pyroclastic fall deposits is a pronounced modal peak and asymmetrical property skewed towards coarser

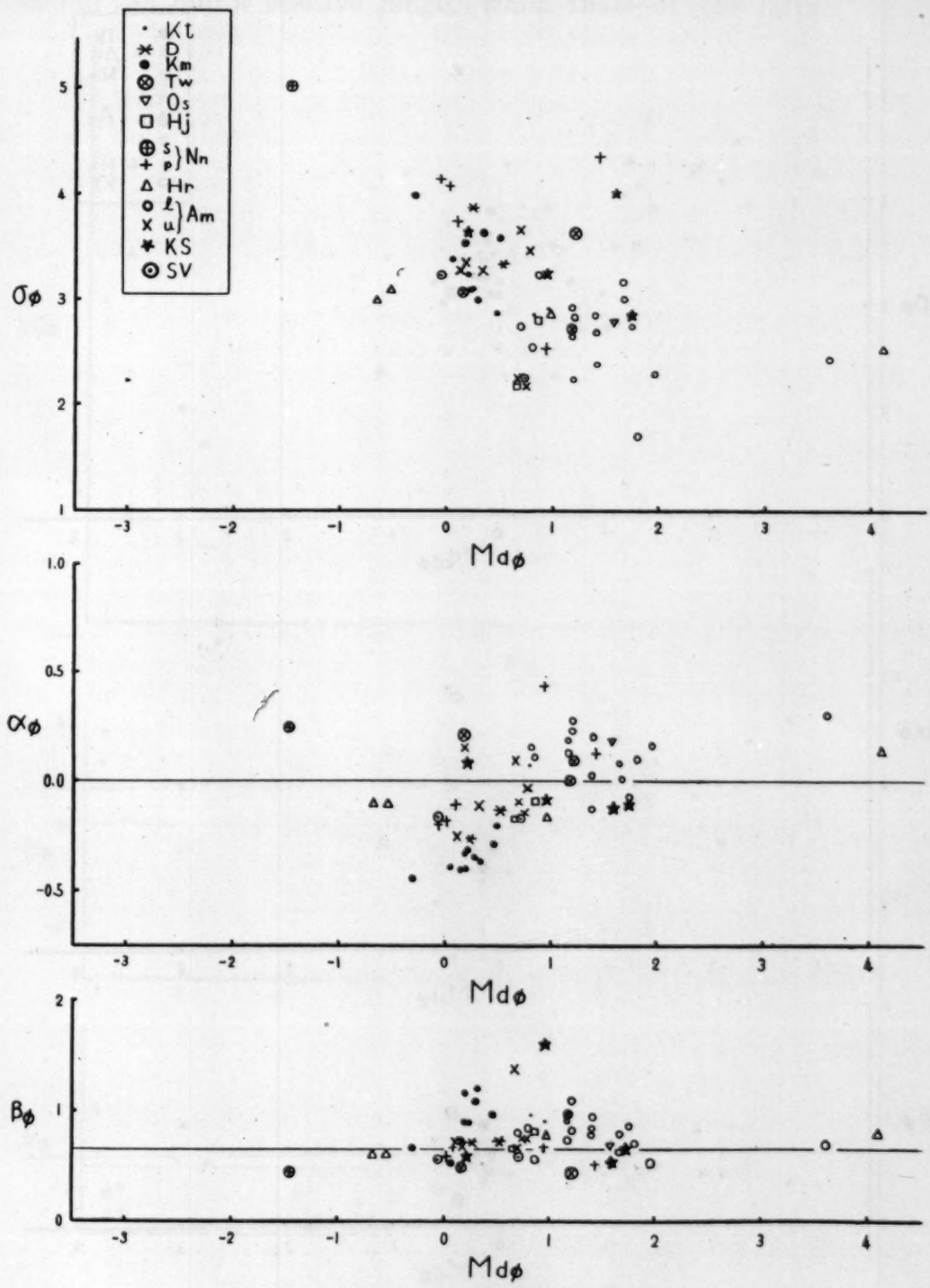

Fig. 6c. The St. Vincent type ash-flows.

diameters, being cut the tail in the coarser fractions, while the distribution curve of the pyroclastic flow deposits shows a gentle mode and

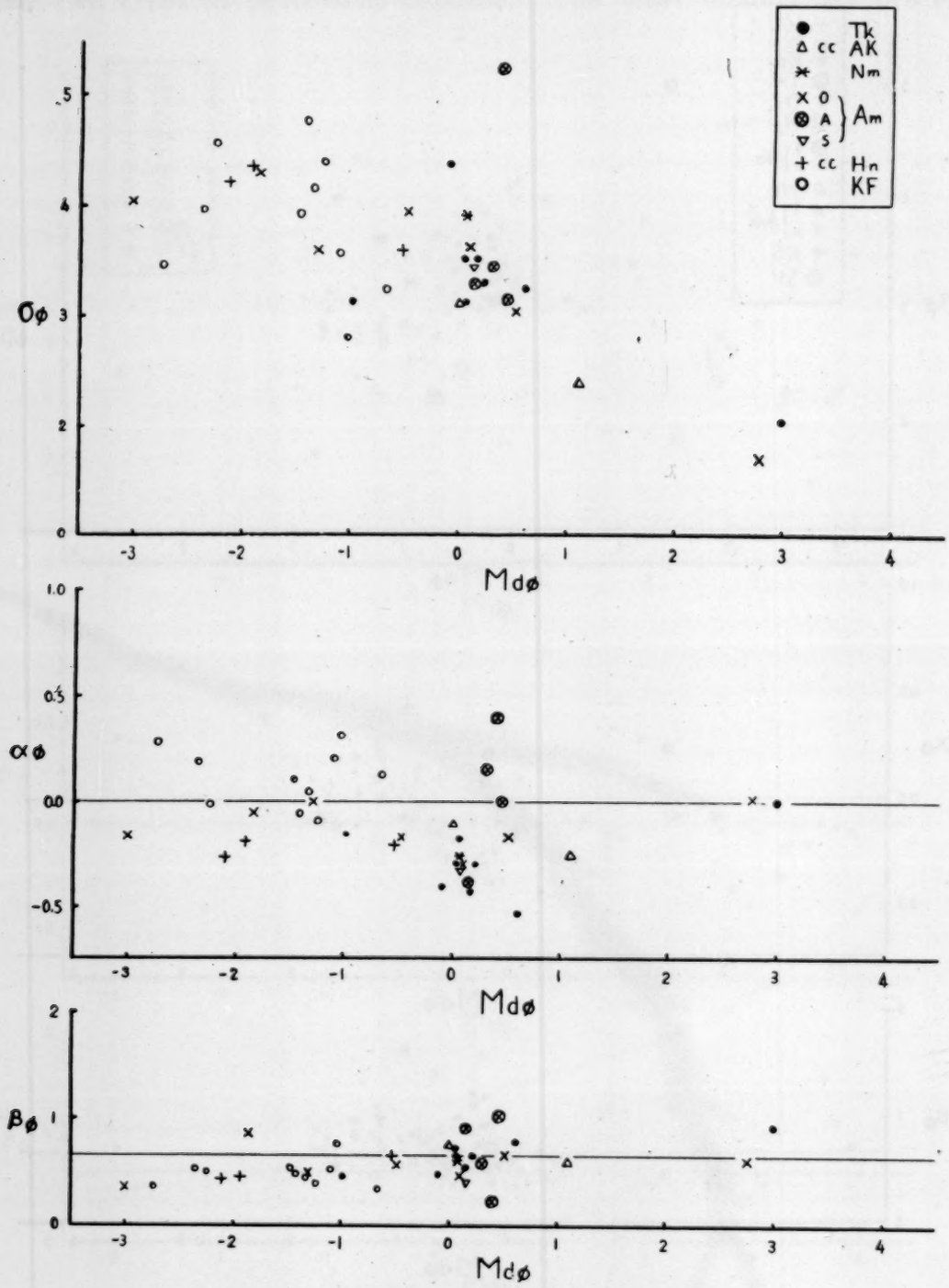

Fig. 6d. The Intermediate type pyroclastic flows.

marked tails at both ends of the curve. Consequently, the values of α_ϕ and $\alpha_{2\phi}$, the parameters of skewness, of the pyroclastic fall deposits tend to fall into a positive range, while those of the pyroclastic flow

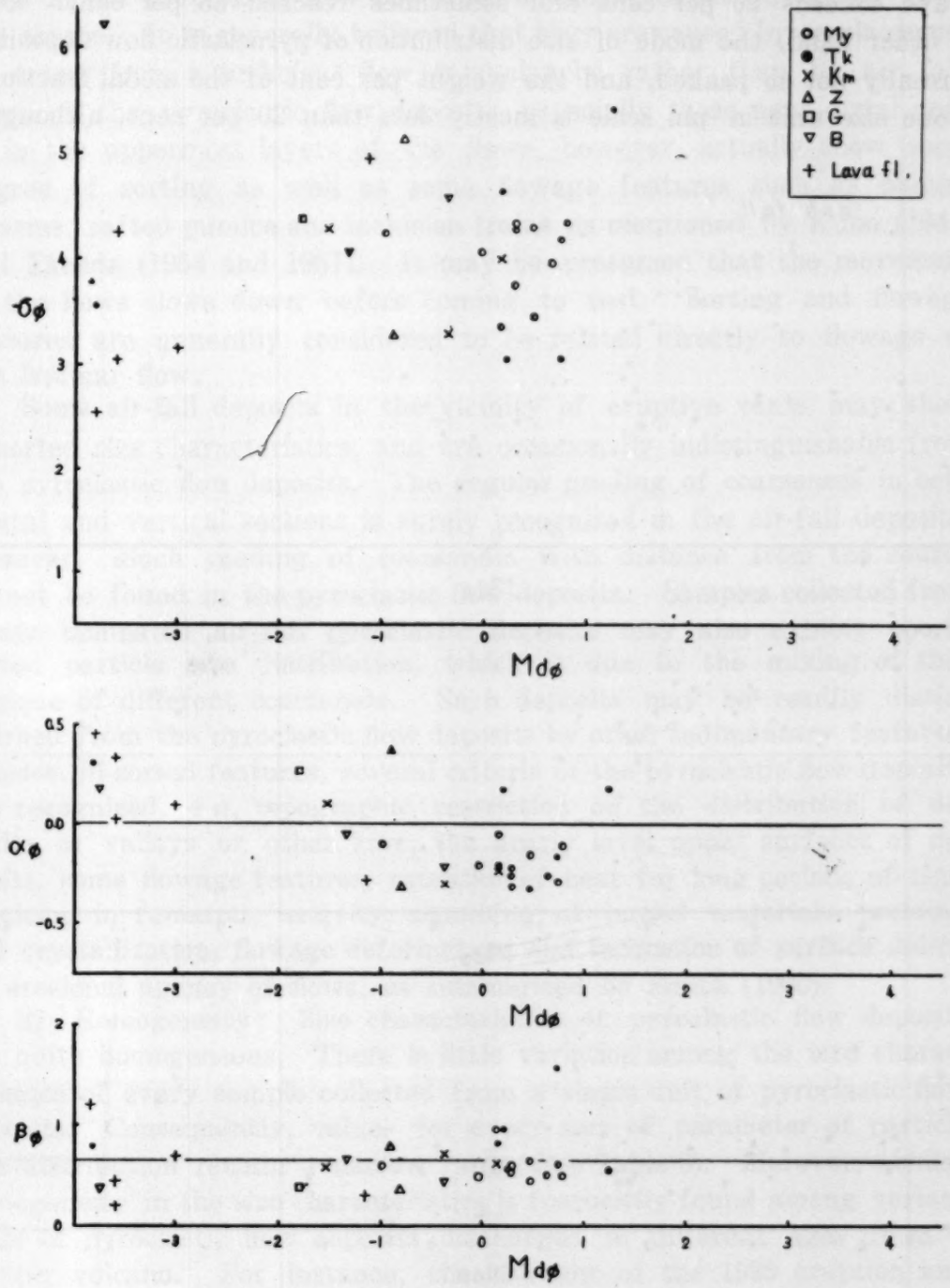

Fig. 6e. The nuées ardentes, dry mud-flows, and auto-brecciated lava flows.

deposits scatter in both possitive and negative ranges (see Figs. 6a–6f). The weight per cent of the modal fraction in histograms of the size distribution of the pyroclastic fall deposits in one size unit in phi scale always exceeds 20 per cent and sometimes reaches 35 per cent. On the other hand, the mode of size distribution of pyroclastic flow deposits is usually not so peaked, and the weight per cent of the modal fraction on one size unit in phi scale is mostly less than 20 per cent, although

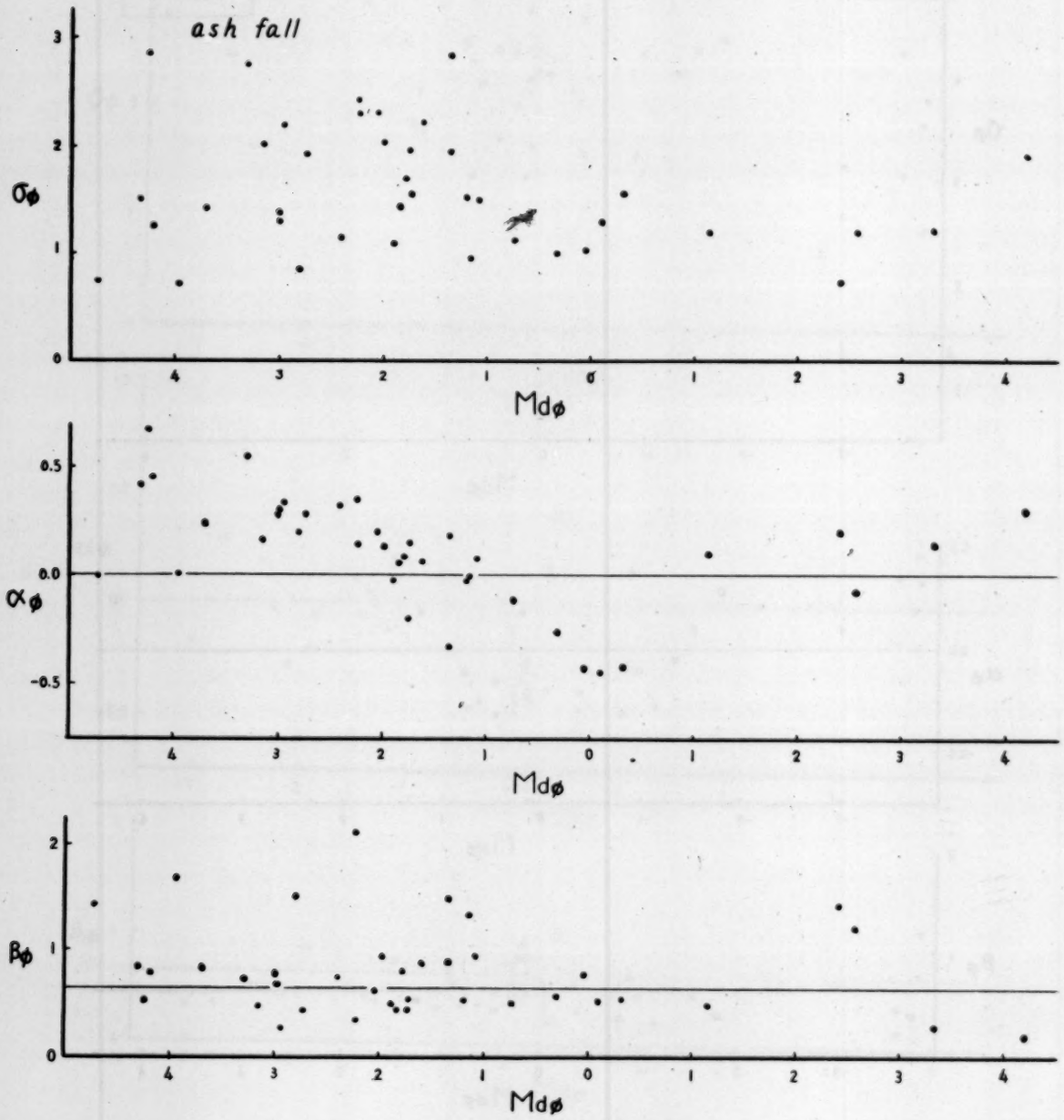

Fig. 6f. Pyroclastic falls.

there are a few exceptional cases having a mode that exceeds 20 per cent or 25 per cent (see Tables 4 and 5, and Figs. 11a–11c).

Ill-sorted size characteristics as mentioned here are always recognized in the pyroclastic flow deposits, whether closest to or far from the source. It is generally believed that they are caused by emplacement *en masse* from a turbulent flow or avalanche rather than by air fall. Most of the pyroclastic flow deposits, especially those near distal ends or in the uppermost layers of the flows, however, actually show some degree of sorting as well as some flowage features such as pumice swarms, rafted pumice and inclusion trains as mentioned by Kuno (1941) and Taneda (1954 and 1957). It may be presumed that the movement of the flows slows down before coming to rest. Sorting and flowage features are generally considered to be related directly to flowage of the laminar flow.

Some air-fall deposits in the vicinity of eruptive vents may show ill-sorted size characteristics, and are occasionally indistinguishable from the pyroclastic flow deposits. The regular grading of coarseness in both lateral and vertical sections is surely recognized in the air-fall deposits, however. Such grading of coarseness with distance from the source cannot be found in the pyroclastic flow deposits. Samples collected from thinly laminated air-fall pyroclastic deposits may also exhibit poorly sorted particle size distribution, which is due to the mixing of thin laminae of different coarseness. Such deposits may be readily distinguished from the pyroclastic flow deposits by other sedimentary features. Besides, ill-sorted features, several criteria of the pyroclastic flow deposits are recognized, e.g. topographic restriction on the distribution of deposits to valleys or other lows, the nearly level upper surfaces of deposits, some flowage features, retention of heat for long periods of time resulting in fumarolic activity, scorching of buried materials, welding and crystallization, flowage deformation, and incoration of surface debris by erosional agency of flows, as summarized by Smith (1960).

2) Homogeneity: Size characteristics of pyroclastic flow deposits are quite homogeneous. There is little variation among the size characteristics of every sample collected from a single unit of pyroclastic flow deposits. Consequently, values for every sort of parameter of particle size distribution remain a narrow range (see Table 8). Morever, similar homogeneity in the size characteristics is frequently found among various units of pyroclastic flow deposits discharged in different ages from a certain volcano. For instance, the ash-flow of the 1929 eruption and those of the previous eruptions of the Komagatake Volcano in Hokkaido

have the same size characteristics (see Fig. 3c). This indicates that similar eruptions of pyroclastic flows took place repeatedly on the Komagatake Volcano.

Homogeneity in size characteristics within a single unit of pyroclastic flow deposits always exists, irrespective of the magnitude of the unit. In ash-flow deposits of huge magnitude such as those surrounding the Krakatoa type calderas, usually comprising several units which represent various periods in eruptions separated by some time intervals, a tendency toward homogeneity in their size characteristics is found throughout the whole mass of the deposits. For example, in the ash-flow deposits of the Kutcharo, Toya, Towada, and Aira Volcanoes, such homogeneity in size characteristics is found (see Figs. 3a–u, 3c–m, 3d–u, and 3k–m). The deposits caused by repeated eruptions of pyroclastic flows of small magnitude, such as nuées ardentes of the Pelée type, usually consist of layers separated from each other by block accumulations, beds of ash, materials reworked by wind and water or minor erosional disconformities. In such deposits, homogeneity in size characteristics also exists. For example, every sample of the pyroclastic flow deposits of the Myoko Volcano shows the same size characteristics with each other (see Fig. 3g–l). Moreover, size characteristics of pyroclastic flow deposits in adjoining volcanoes exhibit some resemblance to each other. For example, among the deposits of ash-flows of the Asama, Haruna, Akagi and Nantai Volcanoes (see Figs. 3f–m, 3g–u, 3h–u and 3h–m), and between those of the Kutcharo and Akan Volcanoes, resemblance in size characteristics is found (see Figs. 3a–u and 3a–l).

3) Median diameters: Phi values of median diameters, Md_ϕ, vary within a wide range. Most of them, however, fall within a range of -2 to 4. This indicates that most of the pyroclastic flow deposits belong to the category of "ash flow deposits" defined by Smith (1960), which consist of 50 per cent or more in weight of ash and fine ash in terms of the Wentworth and Williams' size scale. Moreover, it may be possible to group Md_ϕ values in accordance with the subdivisions of types of pyroclastic flows. Md_ϕ values of the Krakatoa type ash-flow deposits, and perhaps those of the fissure eruption type ash-flow deposits, are generally within a range of 0 to 4 (see Figs. 6a and 6b), those of the St. Vincent type ash-flow deposits are within a range of 0 to 2 (see Fig. 6c), and those of the intermediate type pyroclastic flow deposits and the nuée ardente deposits are smaller than 1 (see Figs. 6d and 6e).

The regular variation of Md_ϕ values with distance from a source

can not be found. Values of Md_ϕ are almost constant throughout a single unit of pyroclastic flow deposits (see Figs. 7a, 7b and 7c). Whereas,

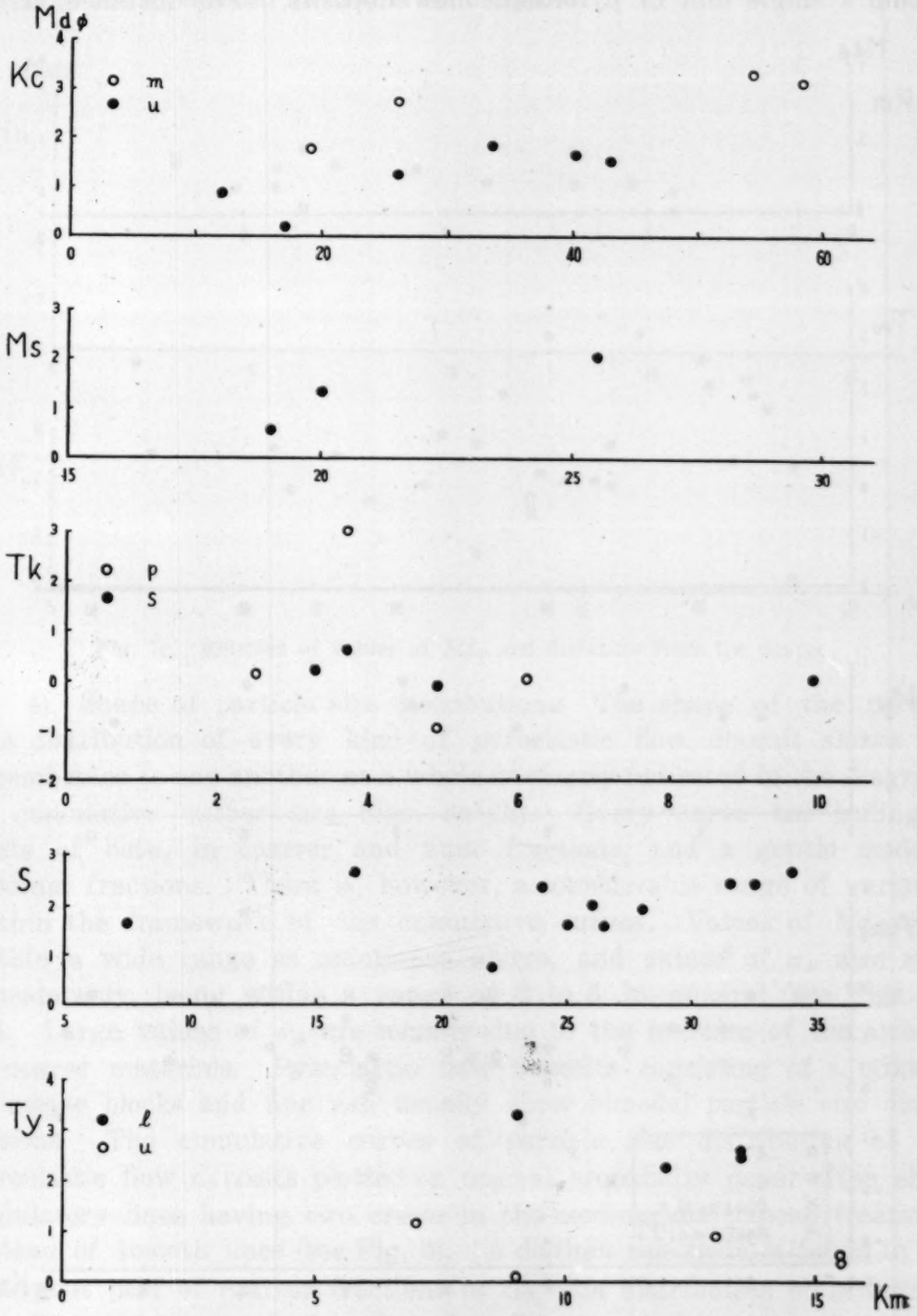

Fig. 7a. Relation of values of Md_ϕ and distances from the source.

other features, such as the roundness of particles and the proportions of lithic fragments or vesicular dust to the whole of the deposits, may vary within a single unit of pyroclastic flow deposits. For instance, it has

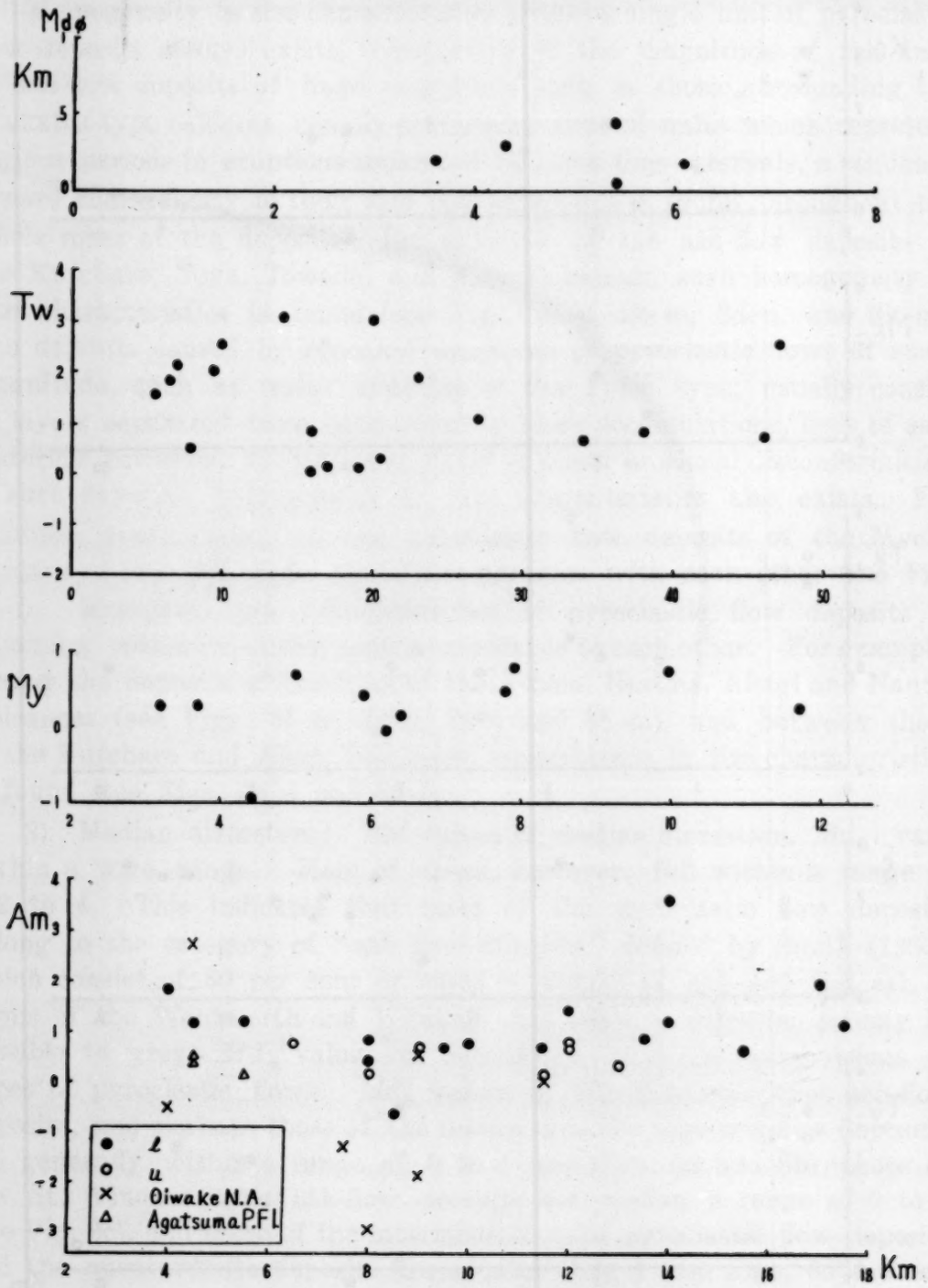

Fig. 7b. Relation of values of *Mdφ* and distances from the source.

been clarified that fine dust in the Pelean deposits tends to increase in amount away from the parent dome. Detailed discussions on these respects are presented in the later chapters.

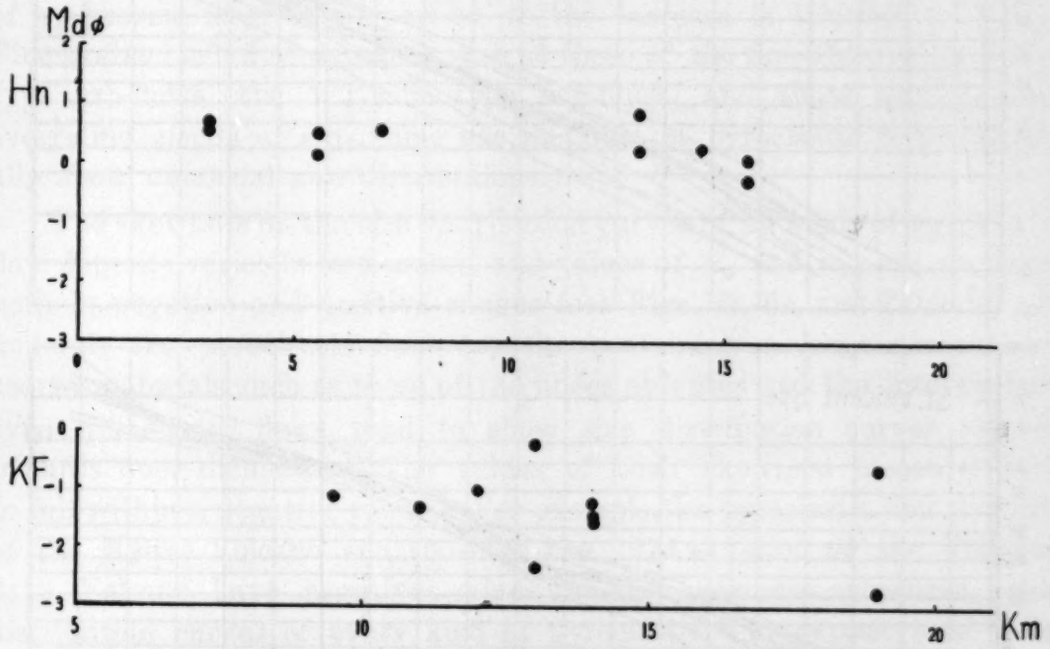

Fig. 7c. Relation of values of $Md\phi$ and distances from the source.

4) Shape of particle size distribution: The shape of the particle size distribution of every kind of pyroclastic flow deposit shows the resemblance to one another as a whole as clearly indicated in the diagrams of cumulative curves (see Figs. 3a–3k). Every curve has tailingout parts of both, in coarser and finer fractions, and a gentle mode in medium fractions. There is, however, a considerable range of variation within the framework of the cumulative curves. Values of Md_ϕ vary within a wide range as mentioned above, and values of σ_ϕ also vary considerably, being within a range of 2 to 5 in general (see Figs 6a–6e). Large values of σ_ϕ are usually due to the increase of the amount of coarse materials. Pyroclastic flow deposits consisting of a mixture of coarse blocks and fine ash usually show bimodal particle size distributions. The cumulative curves of particle size distribution of the pyroclastic flow deposits plotted on normal probability paper often show undulatory lines having two crests in the medium and coarse fractions, instead of smooth lines (see Fig. 8). A distinct sub-mode is found in the tailingout part of coarser fractions in the size distribution on histogram (see Figs. 11a–11c). Such a bimodal character is most conspicuous in

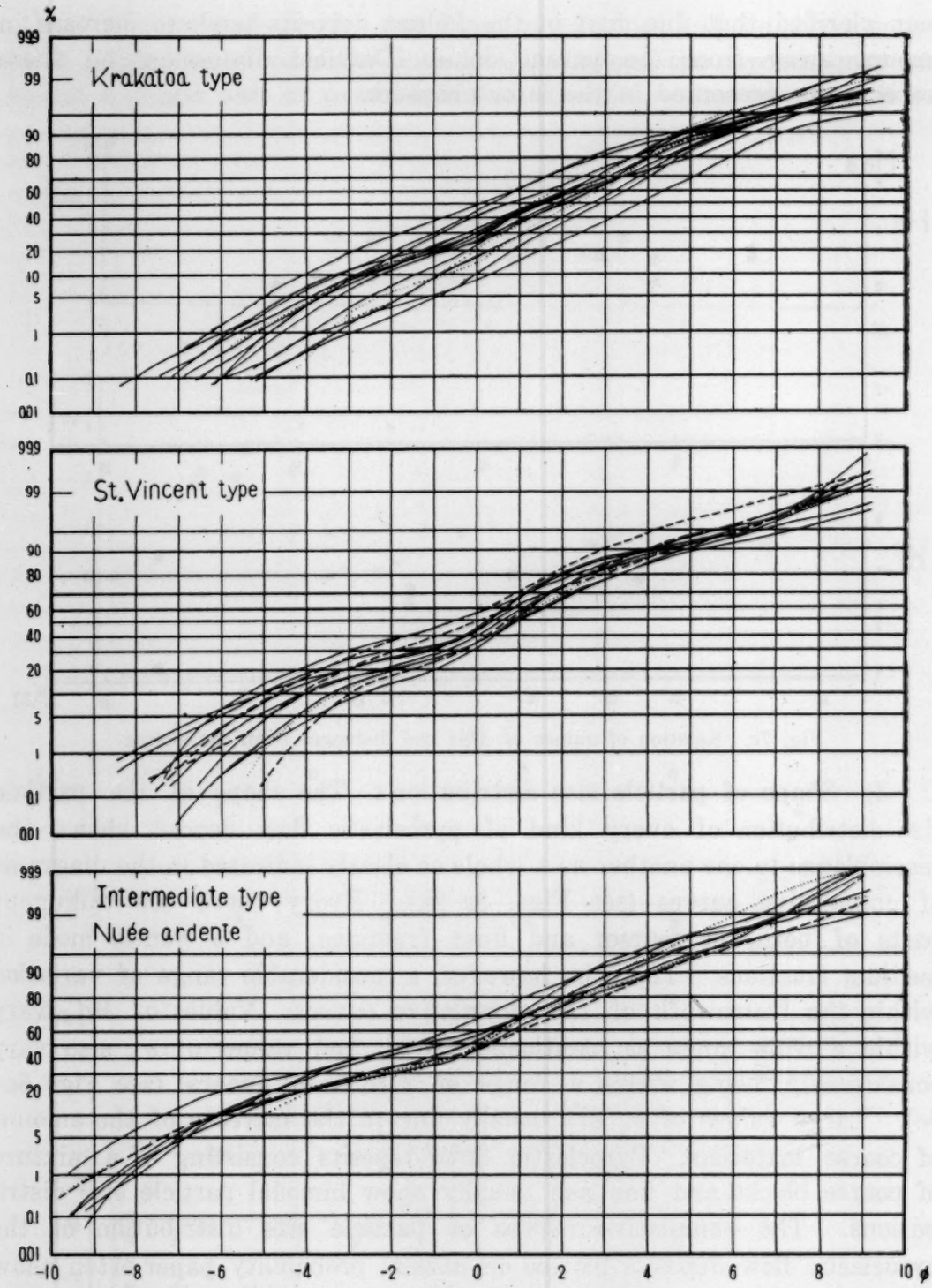

Fig. 8. Cumulative curves of the pyroclastic flow deposits plotted on normal probability paper. Solid lines are average curves of samples in a single unit of pyroclastic flow. Dotted lines are curves of one sample. Each curve represents one unit of flow. Broken lines in the middle figure represent the variety having an intermediate nature between the St. Vincent type ash-flows and dry mud-flows. A broken line in the lower figure is a curve of a nuée ardente.

the nuée ardente deposits and also in the intermediate type pyroclastic flow deposits. Moreover, a similar tendency towards bimodal size distribution is found in most deposits of the various types of pyroclastic flows, although the degree of the bimodal tendency may vary greatly. Values of σ_ϕ become large in proportion to the increase in bimodal tendency. Fine-grained ash-flow deposits, such as those of the fine-grained Krakatoa type ash-flows, the V.T.T.S. type ash-flows, and those settled from overriding clouds of expanding gas and dust of pyroclastic flows, generally show unimodal size distributions.

The skewness of the size distribution curves of all kinds of pyroclastic flow deposits varies in two senses, and values of α_ϕ and $\alpha_{2\phi}$ are scattered both in negative and positive ranges (see Figs. 6a–6e, and Table 8). In general, the pyroclastic flow deposits containing a large amounts of coarse materials such as those of the nuées ardentes and the intermediate type pyroclastic flows tend to show size distribution curves skewed towards finer diameters. The values of their skewness measures tend to fall within a negative range. For example,the pyroclastic flow deposits of the Myoko Volcano and those of the 1929 eruption of the Tokachidake Volcano have negative values for the skewness measures. Size distribution curves of every kind of pyroclastic flow deposit tend to be less peaked than the normal distribution curve. Values of β_ϕ in general tend to bear larger values than 0.65, although actually they scatter widely around the value 0.65 of normal (see Figs. 6a-e, and Table 8).

The main mode of medium fractions in size distribution curves of pyroclastic flow deposits is generally not peaked as sharply as that of air-fall deposits as already mentioned. The weight per cent of a modal fraction of one size unit in phi scale is usually less than 20 per cent (see Table 4). In some pyroclastic flow deposits, however, it attains to or exceedes 25 per cent. For example, in the ash-flow deposits of the Komagatake Volcano, it ranges from 19.0 to 27.8 per cent. In general, size distribution curves of the St. Vincent type ash-flow deposits exhibit such peaked main modes, in spite of their ill-sorting as indicated by large values of σ_ϕ. In the size distribution curves of the Krakatoa type ash-flow deposits, which show a general tendency toward a unimodal character, the mode is not peaked as sharply as in those of the St. Vincent type ash-flow deposits. The size distribution curves of the nuée ardente deposits and the intermediate type pyroclastic flow deposits show a dull main mode, contrasting with the peaked main mode of the St. Vincent type ash-flow deposits.

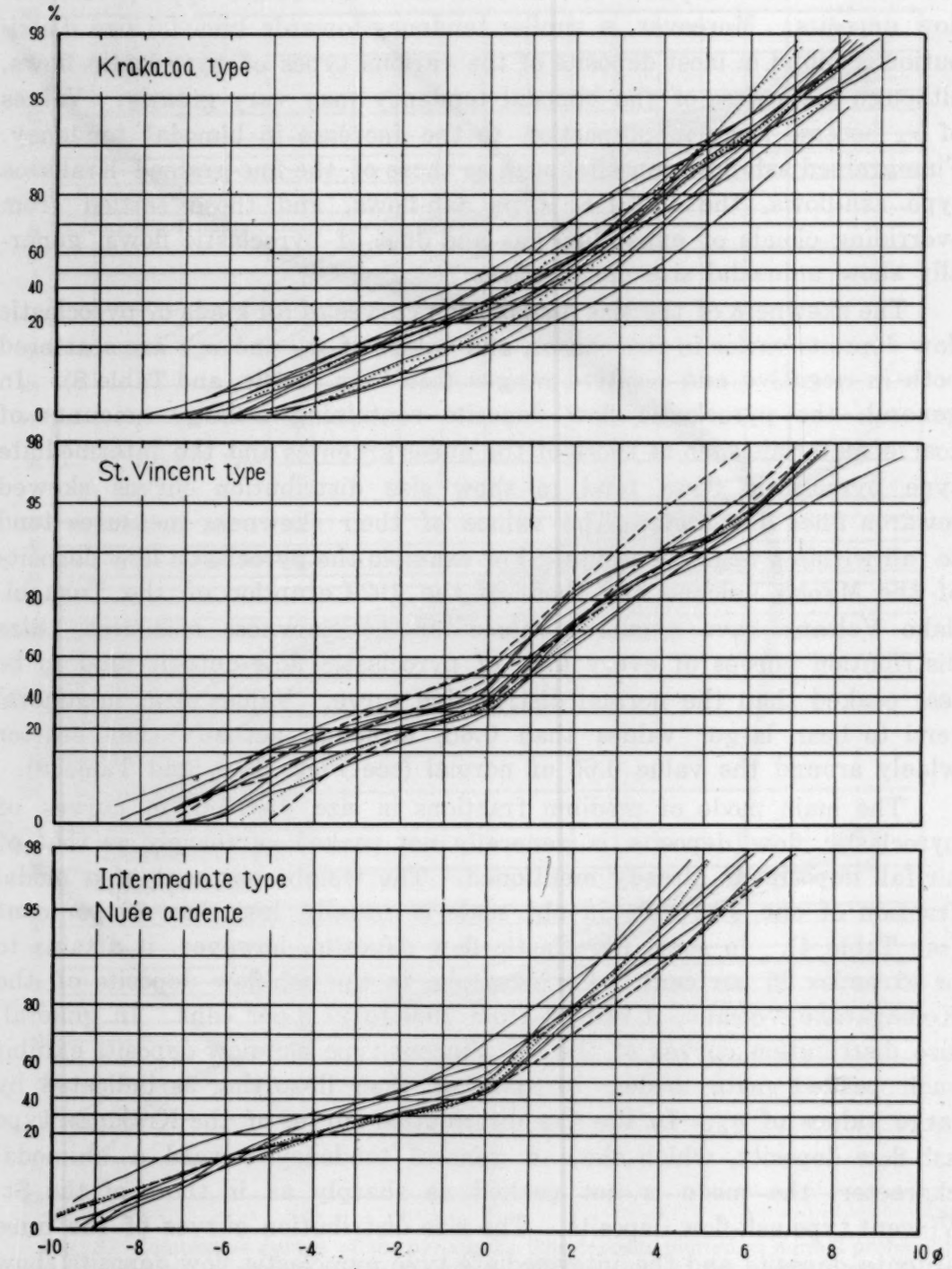

Fig. 9. Cumulative curves of the pyroclastic flow deposits plotted on Rosin law paper. The explanation of the curves is the same as in Fig. 8.

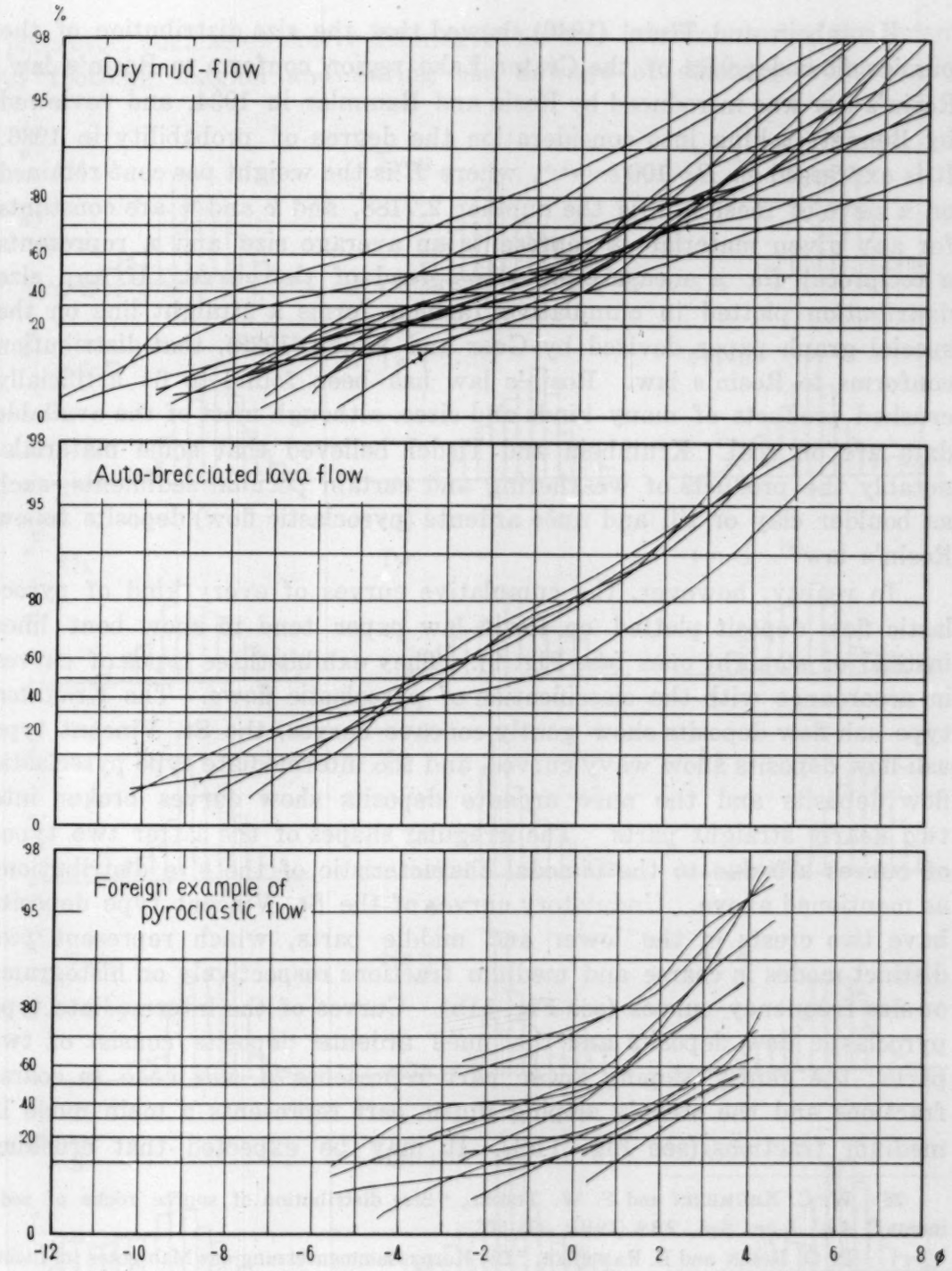

Fig. 10. Cumulative curves plotted on Rosin law paper. Upper: dry mud-flows, middle: auto-brecciated lava flows, lower: foreign examples of pyroclastic flows. Every line represents a curve of each individual sample.

Krumbein and Tisdel (1940) showed that the size distribution of the pumice flow deposits of the Crater Lake region conform to Rosin's law. Rosin's law was introduced by Rosin and Rammler in 1934, and reviewed by Bennett taking into consideration the degree of probability in 1936. It is expressed as $R=100\,e^{-(x/k)^n}$, where R is the weight per cent retained on a sieve of mesh x, e is the number 2.7188, and k and n are constants for any given material; k represents an average size and n represents a reciprocal for a measure of the spread of the curve. If any size distribution plotted in cumulative fashion forms a straight line on the special graph paper devised by Geer and Yancy (1938), that distribution conforms to Rosin's law. Rosin's law has been found to fit artificially crushed products of many kinds and sizes, although most of the available data are on coal. Krumbein and Tisdel believed that some materials, notably the products of weathering and certain peculiar sediments, such as boulder clay or till and nuée ardente (pyroclastic flow) deposits follow Rosin's law[26].

In reality, however, the cumulative curves of every kind of pyroclastic flow deposit plotted on Rosin law paper tend to show bent lines instead of straight ones (see Fig. 9). They exhibit three types of curves in accordance with the classification of pyroclastic flows. The Krakatoa type ash-flow deposits show gently concave curves, the St. Vincent type ash-flow deposits show wavy curves, and the intermediate type pyroclastic flow deposits and the nuée ardente deposits show curves broken into two nearly straight parts. The irregular shapes of the latter two types of curves are due to the bimodal characteristic of the size distributions as mentioned above. Undulatory curves of the St. Vincent type deposits have two crests in the lower and middle parts, which represent two distinct modes in coarse and medium fractions respectively on histograms or size frequency curves (see Fig. 11b). Curves of the intermediate type pyroclastic flow deposits and the nuée ardente deposits consist of two parts; the gently sloping lower part represents a sub-mode in coarse fractions and the steeply sloping upper part represents a main mode in medium fractions (see Fig. 11c). It may be expected that crushing

26) W. C. KRUMBEIN and F. W. TISDEL, "Size distribution of source rocks of sediments," *Am. Jour. Sci.*, **238** (1940), 296-305.

P. O. ROSIN and E. RAMMLER, "Die Kornzusammensetzung des Mahlgutes im Lichte der Wahrscheinlichkeitslehre," *Kolloid Zeits.*, **67** (1934), 16-26.

J. G. BENNETT, "Broken coal," *Jour. Inst. Fuel*, **10** (1936), 22-39.

M. R. GEER and H. F. YANCEY, "Expression and interpretation of the size composition of coal," *Am. Inst. Min. Met. Eng., Tech. Pub.*, **943** (1938).

processes, such as explosive disintegration and attrition during the ascent of frothing magma and during the flowage of discharged materials,

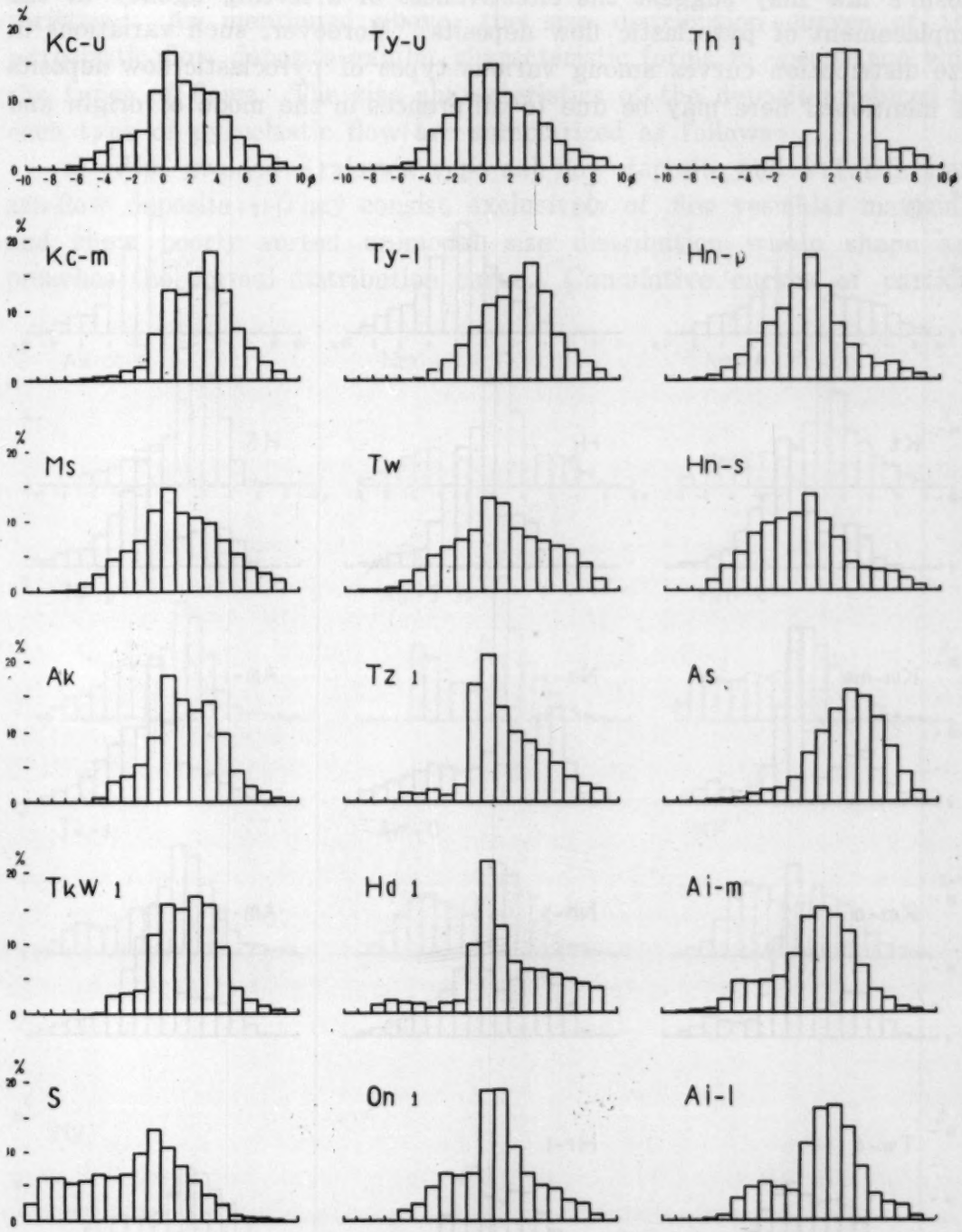

Fig. 11. Histograms of particle size distribution of the pyroclastic flow deposits. One which represents the individual result of only one sample is noted by its sample number. The others represent the average results of several samples.

Fig. 11a. Histograms of the Krakatoa type ash-flow deposits.

may produce size characteristics of pyroclastic flow deposits fitting to Rosin's law. Consequently, those size distributions uncompatible with Rosin's law may suggest the effectiveness of a sorting agency in the emplacement of pyroclastic flow deposits. Moreover, such variations in size distribution curves among various types of pyroclastic flow deposits as mentioned here may be due to differences in the mode of origin and

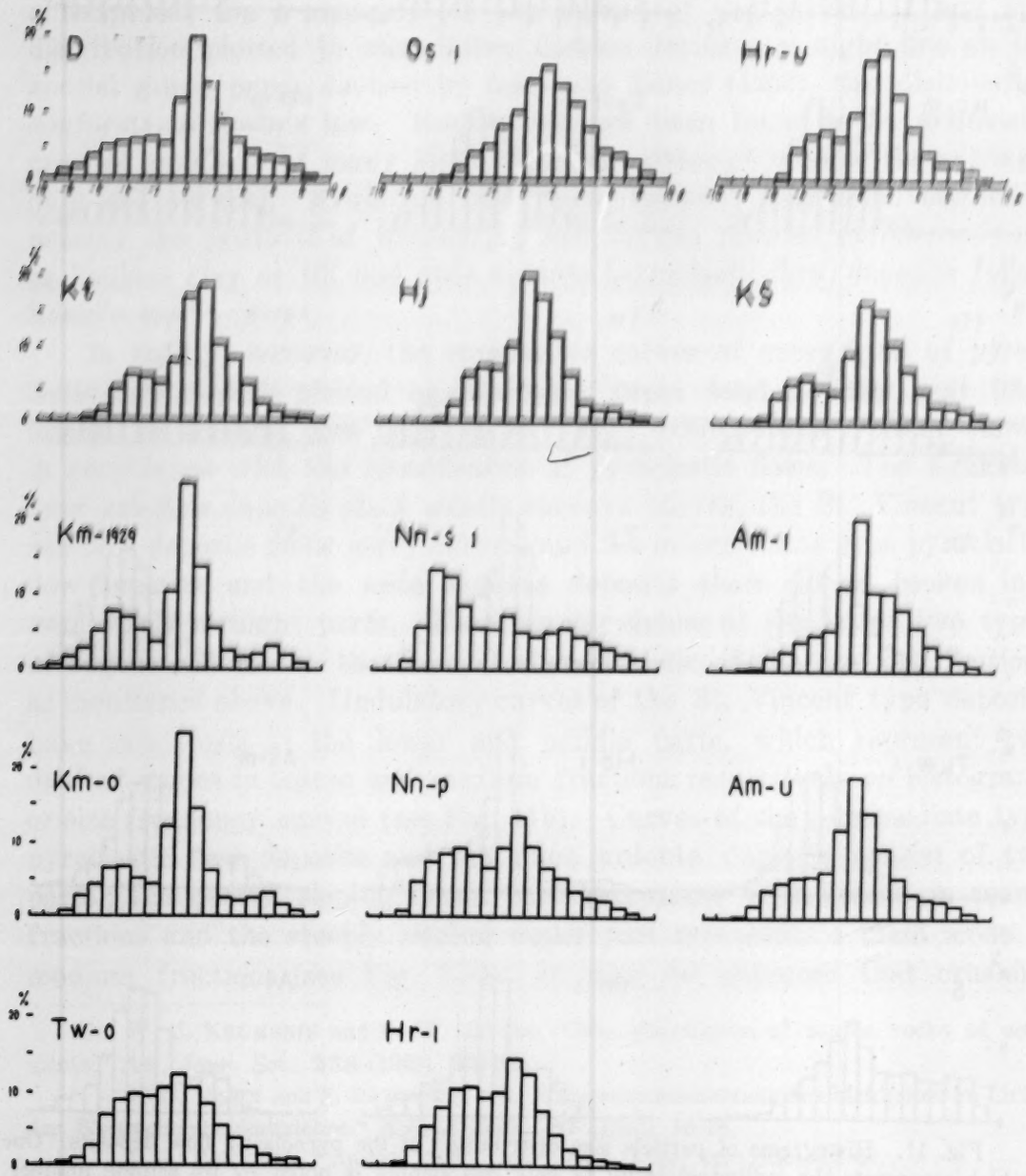

Fig. 11b. Histograms of the St. Vincent type ash-flow deposits and the deposits having an intermediate nature between pyroclastic flows and dry mud-flows.

mechanism of pyroclastic flows. Detailed discussions are presented in the later chapters.

5) Subdivisions of pyroclastic flow deposits based upon size characteristics: As mentioned above, the size distribution curves of the pyroclastic flow deposits exhibit characteristic forms in accordance with the types of flows. The size characteristics of the deposit produced by each type of pyroclastic flow are summarized as follows;

a) *Fine-grained Krakatoa type ash-flow deposits and V.T.T.S. type ash-flow deposits; They consist exclusively of fine vesicular materials and show poorly sorted unimodal size distribution whose shape approaches the normal distribution curve. Cumulative curves of particle*

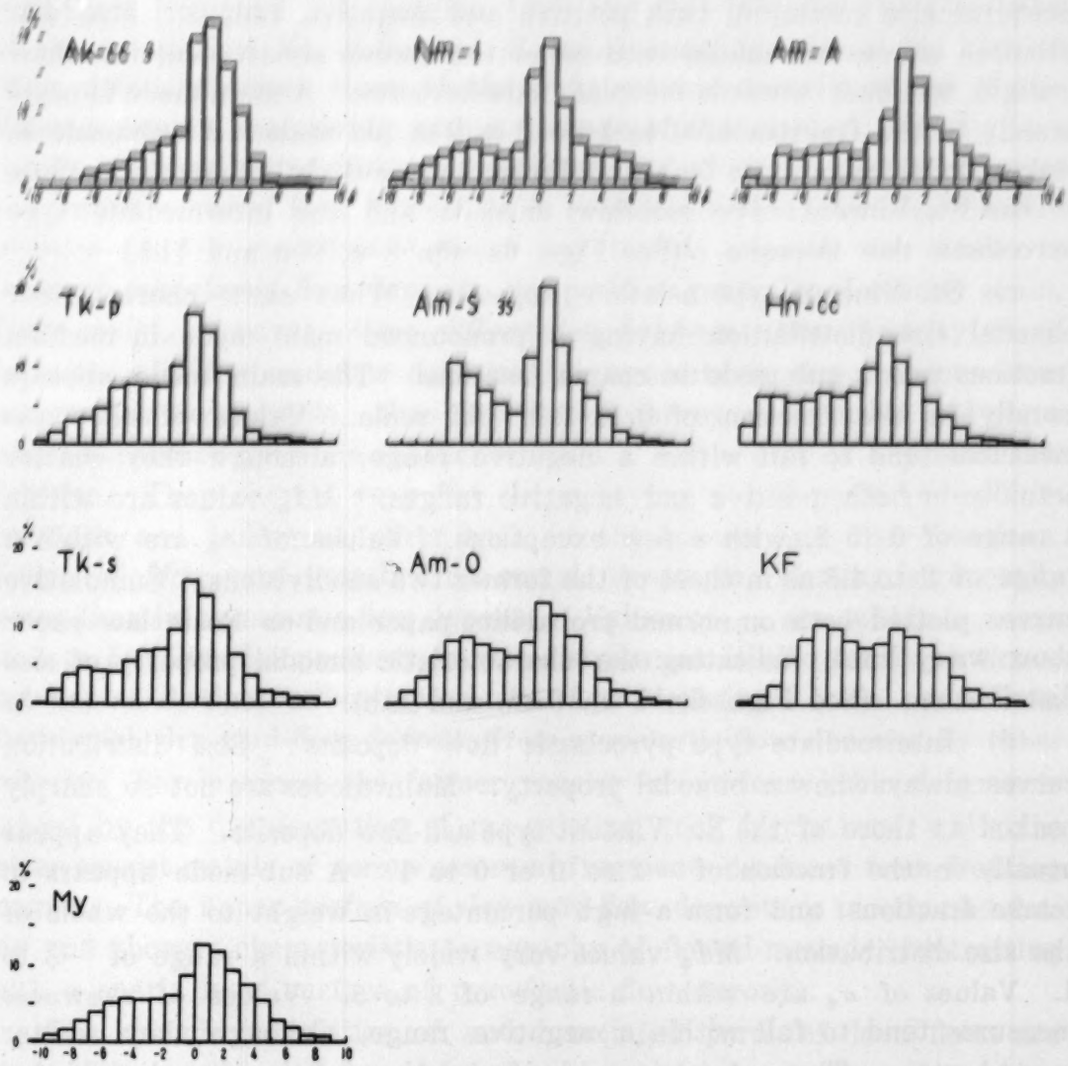

Fig. 11c. Histograms of the intermediate type pyroclastic flow deposits and the nuée ardente deposits.

size distribution plotted on normal probability paper form nearly straight lines (see Fig. 8-u). Cumulative curves plotted on Rosin law paper show gentle concave lines (see Fig. 9-u). A mode appears usually in the fraction of 1 to 2 or 2 to 3 in phi scale. Md_ϕ values are mostly within a range of 2 to 4. Values of skewness measures scatter in both positive and negative ranges. Values σ_ϕ are mostly within a range of 2 to 4.5. (See Figs. 6a, 6b and 11a.)

b) Medium-grained Krakatoa type ash-flow deposits: Md_ϕ values are usually larger than those of the former subdivision, being within a range of 0 to 2. Values of σ_ϕ are also mostly within a range of 2 to 4.5 as with those of the former subdivision. Values of skewness measures also scatter in both positive and negative ranges. Size distribution curves are similar to those of the former subdivision, but show a slight tendency towards bimodal characteristics. A main mode appears usually in the fraction of 0 to 1 or 1 to 2 in phi scale. A sub-mode in coarse fractions is quite feeble, differing in size distributions from those of the St. Vincent type ash-flow deposits and the intermediate type pyroclastic flow deposits. (See Figs. 6a, 6b, 8-u, 9-u and 11a.)

c) St. Vincent type ash-flow deposits: They show characteristic bimodal size distribution having a pronounced main mode in medium fractions and a sub-mode in coarse fractions. The main mode appears usually in the fraction of 0 to 1 in phi scale. Values of skewness measures tend to fall within a negative range, although they scatter actually in both positive and negative ranges. Md_ϕ values are within a range of 0 to 2, with a few exceptions. Values of σ_ϕ are within a range of 2 to 4.5 as in those of the former two subdivisions. Cumulative curves plotted both on normal probability paper and on Rosin law paper show wavy lines, indicating the characteristic bimodal property of size distribution. (See Figs. 6c, 8-m, 9-m, and 11b).

d) Intermediate type pyroclastic flow deposits: Size distribution curves always show a bimodal property. Main modes are not so sharply peaked as those of the St. Vincent type ash-flow deposits. They appear usually in the fraction of -1 to 0 or 0 to 1. A sub-mode appears in coarse fractions, and form a high percentage in weight to the whole of the size distribution. Md_ϕ values vary widely within a range of -3 to 1. Values of σ_ϕ are within a range of 3 to 5. Values of skewness measures tend to fall within a negative range, although they scatter around zero. There exists a minor variation in the size distribution curves among samples collected from a single unit of the flows, which

is due to the differences in the amount of coarse materials in the deposits. Cumulative curves plotted on normal probability paper show gently undulating lines. Those plotted on Rosin law paper show lines broken into two straight parts. (See Figs. 6d, 8-l, 9-l and 11c).

e) Nuée ardente deposits: The chaotic mingling of fragments of all sizes, graduating from large blocks to fine dust, is the most pronounced feature of the nuée ardente deposits. It is considered that they have similar size characteristics to those of the intermediate type pyroclastic flow deposits, although the writer could not obtain various examples of the nuée ardente deposits. The coarseness of the nuée ardente deposits may be remarkably large, and M_ϕ values may be sometimes less than -3, judging from the data on size characteristics of the deposits at Mt. Pelée and of the ancient deposits at St. Vincent (Hay, 1959), although those of the nuée ardente deposits of the Myoko Volcano remain exclusively within a range of 0 to 1.

6) Comparison of the size characteristics of dry mud-flow deposits and auto-brecciated lava flows: It is considered that the size characteristics of dry mud-flow deposits and laharic deposits are similar to those of pyroclastic flow deposits, but perhaps generally of coarser grain. There exist, however, some differences between these two types of deposits. In dry mud-flow deposits, homogeneity in size characteristics is rather unrecognizable. Size distribution curves are unstable and show large disparities with one another whithin a single unit of dry mud-flow deposits. They show a very flat shape having a dull mode in medium fractions and tailingout parts both in the coarser and finer fractions. Values of Md_ϕ vary greatly from sample to sample. Sorting is generally worse than in pyroclastic flow deposits. Values of σ_ϕ are within a range of 3 to 5. Bimodal property in size distribution is also found at times, but not as distinct as in pyroclastic flow deposits. It is possible to distinguish dry mud-flow deposits from pyroclastic flow deposits by other criteria. For instance, the former consist of various lithic fragments caused by the disintegration of pre-existing rock formations, while the latter consist mainly of porous essential fragments produced from frothing magma. The upper surface of dry mud-flow deposits is mostly undulating and shows a characteristic topography of flowed-mounds, contrasting with a nearly level surface of pyroclastic flow deposits.

The size characteristics of auto-brecciated parts of lava flows are also similar to those of pyroclastic flow deposits. In auto-brecciated lava flows, however, transition to solid parts of lava flows may be easily

discovered by a careful field survey. The homogeneity of size characteristics cannot be maintained even in a small portion of the bulk body. Size distribution curves are unstable and show large variations from sample to sample.

It may be possible to consider that both dry mud-flow deposits and auto-brecciated lava flows follow Rosin's law of crushing, for they are caused by the disintegration of solid or plastic materials. Their cumulative curves plotted on Rosin law paper appear to form roughly straight lines in general, although some of them tend to show irregular lines (see Fig. 10). Some dry mud-flow deposits show cumulative curves broken into two straight parts on Rosin law paper, suggesting some effectiveness in sorting during flowage. The writer considers that further detailed studies on the size characteristics of dry mud-flow deposits and auto-brecciated lava flows may reveal a closer conformity of their distribution curves to Rosin's law.

Roundness of Particles

It is well known that there is no regular variation in the coarseness of pyroclastic flow deposits with the distance from the source, as mentioned repeatedly. Some data, however, suggest an increase in the amount of fine vesicular materials in the deposits from the source to the distal ends of the flows. Some volcanologists have considered the agency of attrition during flowage to be responsible for the high proportion of fine ash in pyroclastic flow deposits. Williams (1957) stated that the size of pumice lumps bears no relation to the distance from the source although they are generally more rounded at the distal ends. The writer thinks that studies on the roundness of particles in pyroclastic flow deposits should supply important data in estimating the agency of attrition, which may take place on the way of ascent of effervescing magma, at the time of effusion, and during flowage of the flows. They offer some clues denoting the mechanism of the initiation and flowage of pyroclastic flows.

The writer conducted measurements of the roundness of particles on samples of pyroclastic flow deposits and also on those of preliminary pyroclastic falls which preceded the discharge of flows. The roundness of a particle is a measure of the curvature of the corners and edges expressed as a ratio to the average curvature of the particle as a whole. Actually it is more convenient to work with a two-dimensional figure rather than the three-dimensional object itself. In this case roundness is defined as the average radius of the curvature of the corners of a

particle image divided by the radius of the maximum inscribed circle drawn in a projection of the particle in a plane. Thus, roundness is expressed as $P=\sum(r_i/R)/N$, where r_i are the individual radii of the corners, N is the number of corners, and R is the radius of the maximum inscribed circle (Wadell, 1932)[27]. Wadell's method for measuring the roundness of a particle requires drawing an image of the particle at a standard magnification and determining the radii of the inscribed circle and of the edges and corners of the image, and from these data the value of roundness P is calculated. This method is fairly laborious and takes very much time. Therefore, the writer adopted Krumbein's rapid method (1941)[28]. The particle is compared with standard images of known roundness, redrawn from particles which were measured by Wadell's method. Scores or a hundred particles are measured, and the average value of roundness (PK) is calculated from these data. Statistical studies have shown that the average values (PK) agree well with Wadell's values (P). Particles are divided into size classes and the average roundness for each class size is determined separately. It has been already clarified that there is a marked correlation between the roundness and the particle size in natural clastic deposits, especially in those which have undergone considerable abrasion. The larger sizes of clastic materials are in general more rounded than the smaller grades[29]. Consequently, a comparison of roundness from sample to sample must be carried out in terms of a restricted range in size. The writer determined the average roundness in every kind of particle contained in pyroclastic flow deposits and preliminary air-fall deposits in the three size classes of 32–16 mm, 16–8 mm, and 8–4 mm in diameters. The values of average roundness (PK) are listed in Table 13 with the numbers of measured particles (N), the confidence ranges of average values with 95 per cent confidence coefficient (CR), and values of standard deviation (σ). Summary of the results are as follows:

1) It has been considered that particles in pyroclastic flow deposits,

27) Hakon WADELL, "Volume, shape, and roundness of rock particles," *Jour. Geol.*, **40** (1932), 443-451.

28) W. C. KRUMBEIN, "Measurement and geologic significance of shape, and roundness of sedimentary particles," *Jour. Sed. Petrol.*, **11** (1941), 64-72.

29) E. J. PETTIJOHN and A. C. LUNDHL, "Shape and roundness of Lake Erie beach sands," *Jour. Sed. Petrol.*, **13** (1943), 69-78.

R. D. RUSSELL and R. E. TAYLOR, "Roundness and shape of Mississippi River sands," *Jour. Geol.*, **45** (1937), 225-267.

Hakon WADELL, "Volume, shape and roundness of quartz particles," *Jour. Geol.*, **43** (1935), 250-280.

Table 13. Data on average values of roundness.

Sp.	no.		32−16mm				16−8mm				8−4mm			
			PK	CR	N	σ	PK	CR	N	σ	PK	CR	N	σ
Kc	2	p	0.419	±0.122	8	0.137	0.433	±0.026	36	0.075	0.445	±0.019	92	0.093
		l	0.325	0.152	4	0.083	0.344	0.018	18	0.102	0.363	0.018	89	0.095
Kc	5	p									0.502	0.004	65	0.018
		l									0.432	0.017	19	0.033
Kc	6	p	0.456	0.020	9	0.024	0.466	0.011	94	0.053	0.436	0.012	114	0.065
		l					0.375	0.152	4	0.083	0.424	0.023	34	0.064
Kc	9	p									0.487	0.016	43	0.051
Ms	2	p	0.383	0.079	6	0.069	0.341	0.015	70	0.064	0.328	0.012	106	0.064
		l					0.300	0.020	8	0.071	0.311	0.016	96	0.076
Ak	1	p	0.375	0.073	8	0.083	0.453	0.017	45	0.053	0.373	0.017	132	0.098
		l					0.367	0.143	6	0.125	0.410	0.019	100	0.093
Ak	3	p	0.400	0.065	4	0.035	0.377	0.027	30	0.072	0.368	0.020	65	0.081
		s					0.325	0.036	16	0.065	0.333	0.016	104	0.083
		l									0.348	0.023	46	0.077
Ak	4	p	0.440	0.068	5	0.048	0.378	0.048	9	0.058	0.377	0.015	99	0.076
		s	0.364	0.044	7	0.044	0.358	0.018	33	0.049	0.347	0.012	101	0.062
		l	0.288	0.027	8	0.086	0.302	0.017	42	0.060	0.322	0.027	54	0.098
D	4	p	0.423	0.038	11	0.054	0.400	0.022	39	0.068	0.397	0.023	59	0.086
		se									0.387	0.023	38	0.070
		l					0.400	0.066	6	0.058	0.372	0.018	58	0.069
TkW	1	p					0.390	0.023	49	0.079	0.387	0.017	133	0.096
		l									0.380	0.088	10	0.117
Tk	1	p	0.425	0.080	4	0.043	0.400	0.025	31	0.067	0.368	0.016	90	0.076
		se	0.417	0.043	6	0.036	0.400	0.038	9	0.046	0.360	0.020	72	0.084
		l					0.325	0.057	16	0.103	0.338	0.012	114	0.065
Tk	4	p									0.308	0.034	24	0.081
		se									0.300	0.051	14	0.085
		l									0.357	0.105	7	0.105
Tk	6	s					0.304	0.030	25	0.072	0.260	0.016	84	0.073
		ds	0.260	0.067	5	0.049	0.297	0.021	32	0.059	0.308	0.014	120	0.079
		l					0.311	0.063	10	0.083	0.335	0.013	126	0.074
S	1	p					0.485	0.013	24	0.097	0.428	0.011	104	0.056
		l									0.350	0.037	34	0.104
S	6	p	0.450	0.124	5	0.089	0.488	0.024	56	0.087	0.476	0.009	173	0.060
Kt	1	p	0.413	0.054	8	0.060	0.431	0.020	74	0.085	0.378	0.018	93	0.087
		l	0.320	0.104	5	0.075	0.314	0.017	44	0.092	0.336	0.018	67	0.073
Ty	7	p					0.406	0.020	33	0.055	0.370	0.013	138	0.078
		l					0.340	0.035	30	0.092	0.332	0.016	96	0.071
Ty	8	p									0.378	0.032	18	0.063
		l									0.330	0.048	10	0.203
Ty	10	p					0.356	0.039	18	0.076	0.384	0.012	111	0.064
		l					0.367	0.050	15	0.087	0.344	0.012	115	0.062
Km	3	p	0.421	0.037	28	0.098	0.398	0.030	44	0.099	0.403	0.024	71	0.100
		se					0.390	0.097	10	0.013	0.389	0.011	28	0.086
		l					0.383	0.123	6	0.107	0.323	0.033	35	0.099
Km	4	p	0.457	0.037	23	0.083	0.437	0.026	46	0.087	0.404	0.011	115	0.061
		se					0.433	0.086	6	0.075	0.405	0.047	21	0.100
		l									0.417	0.079	6	0.069
Km	7	p	0.421	0.037	24	0.085	0.434	0.019	59	0.074	0.402	0.016	93	0.095
		se	0.280	0.056	5	0.040	0.360	0.046	15	0.080	0.398	0.020	82	0.091
		l					0.343	0.105	7	0.105	0.379	0.020	56	0.077
Km	8	p	0.435	0.044	17	0.084	0.394	0.018	72	0.076	0.391	0.020	56	0.071
		se									0.367	0.041	24	0.094
		l									0.380	0.040	25	0.094
Tw	15	p	0.500	0.130	4	0.071	0.522	0.020	58	0.079	0.445	0.019	86	0.090
		l	0.329	0.070	7	0.070	0.381	0.034	36	0.100	0.360	0.061	82	0.087

Table 13. (Continued)

Sp. no.			32−26mm				16−8mm				8−4mm			
			PK	CR	N	σ	PK	CR	N	σ	PK	CR	N	σ
Tw	16	p					0.453	±0.018	18	0.034	0.438	±0.011	81	0.049
		l									0.350	0.033	23	0.077
Tw	17	p	0.456	±0.040	9	0.048	0.435	0.015	60	0.060	0.433	0.014	85	0.064
		l					0.330	0.083	10	0.110	0.394	0.017	70	0.074
Tw	21	p					0.408	0.025	26	0.062	0.399	0.014	94	0.068
		se					0.333	0.054	6	0.046	0.326	0.022	62	0.086
		l					0.380	0.080	10	0.105	0.373	0.024	49	0.083
Os	1	p					0.442	0.035	26	0.084	0.421	0.011	126	0.063
		l					0.384	0.037	19	0.074	0.398	0.023	80	0.102
Hj	2	p	0.441	0.047	11	0.067	0.453	0.017	44	0.057	0.443	0.014	87	0.064
		dp					0.408	0.107	6	0.093	0.402	0.024	42	0.076
		l					0.347	0.031	30	0.083	0.391	0.022	80	0.099
On	2	p	0.384	0.033	19	0.067	0.420	0.018	66	0.072	0.385	0.013	128	0.075
Nm	1	p	0.394	0.038	17	0.073	0.412	0.018	59	0.069	0.405	0.012	147	0.074
		se					0.360	0.111	5	0.080	0.360	0.055	15	0.095
		c					0.325	0.019	8	0.066	0.357	0.022	56	0.082
		l					0.317	0.079	6	0.069	0.335	0.026	34	0.072
Nn	1	p					0.422	0.045	23	0.102	0.398	0.026	61	0.100
		c									0.292	0.050	12	0.076
		l	0.333	0.077	9	0.094	0.377	0.035	26	0.085	0.384	0.019	75	0.083
Nn	6	p	0.429	0.029	21	0.063	0.379	0.020	53	0.071	0.348	0.013	103	0.065
		l									0.339	0.046	13	0.074
Th	1	p					0.426	0.035	23	0.079	0.400	0.018	120	0.099
		l									0.323	0.056	13	0.089
Hr	2	p	0.400	0.039	14	0.066	0.432	0.017	66	0.070	0.374	0.017	105	0.088
		c					0.358	0.046	19	0.094	0.358	0.016	89	0.075
		l	0.390	0.063	10	0.083	0.338	0.022	42	0.069	0.354	0.017	119	0.092
Hr	4	p	0.458	0.028	24	0.064	0.433	0.019	51	0.068	0.420	0.009	137	0.053
		l					0.300	0.088	5	0.063	0.342	0.011	150	0.070
KS	3	p									0.463	0.043	16	0.078
		l					0.309	0.036	22	0.079	0.321	0.013	116	0.073
My	1	p	0.322	0.064	9	0.079	0.330	0.031	20	0.064	0.340	0.017	81	0.075
		c	0.333	0.144	3	0.047	0.343	0.090	7	0.090	0.314	0.021	42	0.068
Am	1	p	0.416	0.029	19	0.059	0.404	0.023	50	0.080	0.374	0.017	97	0.082
		se									0.390	0.041	10	0.054
		l					0.346	0.040	13	0.063	0.351	0.016	89	0.077
Am	6	p	0.400	0.130	4	0.071	0.436	0.026	31	0.070	0.376	0.018	82	0.081
		l					0.282	0.033	17	0.062	0.333	0.020	60	0.077
Am	17	p	0.458	0.050	12	0.076	0.400	0.020	67	0.081	0.397	0.014	102	0.071
		se	0.368	0.014	8	0.047	0.372	0.044	18	0.087	0.346	0.016	93	0.077
		l					0.318	0.034	22	0.078	0.327	0.017	71	0.073
Am	20	p	0.415	0.054	13	0.086	0.422	0.015	85	0.068	0.378	0.016	100	0.078
		se									0.370	0.021	60	0.082
		l					0.378	0.045	23	0.102	0.357	0.019	72	0.080
Am	24	s	0.375	0.019	8	0.066	0.367	0.022	46	0.072	0.362	0.012	109	0.060
		l					0.300	0.019	46	0.063	0.320	0.013	115	0.070
Am	27	s	0.388	0.017	8	0.059	0.379	0.022	38	0.066	0.343	0.015	63	0.058
		ds					0.365	0.054	17	0.102	0.308	0.013	97	0.064
		l					0.300	0.054	9	0.067	0.346	0.017	68	0.072
Am	31	s	0.424	0.034	17	0.064	0.360	0.018	68	0.075	0.340	0.014	114	0.077
		ds	0.375	0.019	8	0.066	0.332	0.021	22	0.047	0.323	0.014	86	0.066
Am	35	ds	0.344	0.041	9	0.050	0.347	0.023	38	0.068	0.332	0.012	112	0.063
Hn	1	p	0.394	0.032	18	0.062	0.402	0.018	62	0.042	0.401	0.015	90	0.072
		l					0.315	0.025	26	0.060	0.375	0.018	76	0.080
Hn	8	p					0.411	0.059	9	0.074	0.378	0.019	45	0.063
		s	0.367	0.038	9	0.047	0.372	0.024	50	0.085	0.362	0.019	65	0.078

Table 13. (Continued)

Sp. no.			32–16mm				16–8mm				8–4mm			
			PK	CR	N	σ	PK	CR	N	σ	PK	CR	N	σ
Hn	8	l									0.326	±0.025	38	0.075
Hn	12	s					0.242	±0.050	12	0.076	0.252	0.029	23	0.065
		ds									0.309	0.017	53	0.062
		l									0.369	0.032	16	0.058
KF	1	ds					0.395	0.021	37	0.061	0.342	0.019	64	0.075
As	1	s									0.546	0.008	75	0.036
		l									0.470	0.056	5	0.040
Ai	1	p	0.533	±0.144	3	0.046	0.511	0.011	32	0.030	0.384	0.015	70	0.062
		l					0.325	0.080	4	0.043	0.338	0.032	29	0.081
Ai	4	p					0.492	0.012	6	0.019	0.506	0.008	50	0.029
Ai	10	p	0.483	0.017	3	0.024	0.514	0.022	11	0.031	0.515	0.008	60	0.031
		l									0.485	0.023	13	0.036
D	3	p	0.400	0.123	3	0.129	0.407	0.023	44	0.074	0.405	0.014	77	0.062
		l					0.376	0.021	49	0.072	0.406	0.016	48	0.056
S	12	p	0.300	0.094	6	0.082	0.364	0.021	68	0.081	0.343	0.012	168	0.078
		l									0.319	0.047	18	0.092
Ty	11	p					0.443	0.010	15	0.017	0.402	0.013	83	0.060
Km	11	p	0.384	0.019	64	0.075	0.342	0.017	71	0.073	0.333	0.018	88	0.086
Tw	23	p	0.362	0.019	46	0.064	0.370	0.013	86	0.082	0.386	0.073	162	0.083
		l					0.375	0.073	8	0.083	0.383	0.016	78	0.068
Nn	7	p	0.328	0.029	46	0.096	0.351	0.025	57	0.094	0.348	0.013	138	0.077
		l					0.262	0.021	21	0.044	0.263	0.012	136	0.072
Hr	5	p	0.404	0.014	10	0.049	0.378	0.014	78	0.063	0.367	0.015	125	0.084
		dp	0.370	0.048	10	0.064	0.370	0.033	23	0.074	0.373	0.019	71	0.080
		l	0.257	0.049	7	0.049	0.291	0.022	23	0.090	0.326	0.015	122	0.082
Am	39	p	0.328	0.015	54	0.056	0.322	0.016	83	0.071	0.229	0.013	93	0.061
		l									0.390	0.092	10	0.122

PK: value of average roundness, CR: confidence range with 95% confidence coefficient, N: number of measured particles, σ: standard deviation.

p: pumice, s: scoria, ds: dense scoria, se: basic segregation, l: lithic fragment.

especially at the distal ends of flows, may be rounded remarkably by attrition during flowage. Porous essential fragments in pyroclastic flow deposits, however, are actually not as remarkably rounded as have been expected in general. Values of the average roundness of porous essential particles in the ash-flow deposits are usually within a range of 0.3 to 0.5 on the size classes concerned with here, and belong to the roundness grade, "subrounded" defined by Russell and Taylor (1937)[30]. They are generally larger than values of solid lithic fragments in the same ash-flow deposits, but the difference between these two kinds of constituent particles is no more than about 0.1. No remarkable variation in roundness values with the distance from the source can be found, although data are insufficient for detailed discussion. These facts may

30) R. D. RUSSELL and R. E. TAYLOR, "Roundness and shape of sedimentary rock particles," *Rept. Comm. Sedimentation 1936-1937, Nat. Res. Council*, (1937), 225-267.

suggest that emitted gas may act as a lubricant during the flowage of ash-flows, reducing the effect of attrition. Particles may be transported in suspension in expanding gas. The rounding of particles due to attrition during flowage may proceed to some degree, but may be canceled with the reducing effect of breaking due to collision.

2) Eruptions of pyroclastic flow and pyroclastic fall often occur together in a single phase in eruption. Most of the Krakatoa type ash-flow deposits are underlain by deposits of preliminary pyroclastic falls. The discharge of St. Vincent type ash-flows usually succeeds the violent ejection of pumice and ash. Roundness values of particles in the preliminary air-fall deposits are generally smaller than those in the following pyroclastic flow deposits, but the difference between these two types of deposits is no more than about 0.1 in every case. This indicates that the rounding of particles due to attrition during the flowage of pyroclastic flows proceeds to a certain degree, but not as remarkably as has been generally considered. It may be possible to infer that particles of pyroclastic falls and also those of succeeding pyroclastic flows, especially ash-flows, may have been partly rounded on the way of ascent through the vent. Part of the ascending magma may have already been disintegrated into frothing clots of pumice within the vent, and some proportion of porous essential fragments may have already been rounded to some degree by attrition within the vent before the discharge from the crater-rim. This may be true especially in eruptions of the Krakatoa type, St. Vincent type, and V.T.T.S. type ash-flows.

3) In eruptions of the intermediate type pyroclastic flows and nuées ardentes, matters are somewhat different from in eruptions of the ash-flows. Porous essential fragments in their deposits are fairly angular, and the average values of roundness are mostly within a range of 0.25 to 0.4 in the three size classes concerned with here, which belong to the Russell and Taylor roundness grades of "subangular" and "subrounded". These values are relatively small in comparison with those of ash-flow deposits. Roundness values of lithic fragments in the same deposits are generally within the same range of 0.25 to 0.4 as are those of essential fragments. In some deposits, roundness values of porous essential fragments are conversely smaller than those of dense essential fragments, cognate lithic fragments and accessory and accidental lithic fragments. For example, in the pyroclastic flow deposits of the 1929 eruption of Tokachidake and of the central cone of the Hakone Volcano, the average roundness of porous essential fragments shows smaller values than those

of the other constituent fragments. This may indicate the auto-explosive property of pyroclastic flows during flowage, which has been discussed by many volcanologists (Fenner, 1923; Perret, 1935). It may be possible to infer that a greater part of ascending magma may have remained as effervescing melt at the crater-rim, and most of the gas-emission may have occurred after the flow had been initiated. Angular essential fragments characterized by a high degree of porosity may have been produced by explosive vesiculation during flowage.

Types of Vesicular Shards and Pumice

Essential fragments in pyroclastic flow deposits are typified by their high degree of vesiculation. It is considered that the movement of pyroclastic flows is controlled both by gravitational force and by the upward force of expanding gas. The unexpectedly high mobility of pyroclastic flows, especially over low gradients, as having been reported by many volcanologists, may be partly attributed to the lubricating action of expanding gas. Vesiculation of ascending magma may occur in several different ways. In some cases most vesiculation may take place during the flowage of pyroclastic flows, and in other case total vesiculation may occur before the discharge of magma from the crater-rim. The release of gas by vesiculation during flowage has been discussed by Fenner (1923, p. 74) and Perret (1935, p. 22–24) as a self-explosive or auto-explosive property. It may be possible to infer that such differences in the gas-emission process may be responsible for the existence of various types in the mode of eruption of pyroclastic flows and in the nature of discharged materials. In order to clear up fully the nature of the gas-emission process, quantitative studies on the types of glass shards and porous essential fragments in pyroclastic flow deposits should be most effective, together with studies on the roundness of constituent particles. They may offer important clues in deciphering the origin and mechanism of pyroclastic flows.

Some ash-flow deposits contain quantities of pumice crowded with stretched vesicles. It is considered that such pumice may have been formed by vesiculation within the vent, conduit, or magma chamber. On the way of the ascent of the magma, the shape of the vesicles in frothing clots of pumice may have been deformed into the characteristic fine tubular shape. The writer examined the rough proportion of such a type of pumice and of glass shards to the whole of the deposits, in

some samples of both pyroclastic flow and preceding fall deposits. The results are shown in Table 14, with figures of 5 to 0 in the order of

Table 14. Data on types of pumice and glass shards.

Kc-m	K	4	Km-1929	S	0	Hr-u-fa		1
Kc-u	K	3	Km-1929-fa		0	KS	S	0
Ms	K	3	Km-o	S	0	My	P-N	0
Ak	K	3	Tw-o	S*	0	Am-lp	S	1
Ak-cc	I	0	Tw	K	2	Am-up	S	1
D	S	1	Tw-fa		2	Am-up-fa		1
D-fa		1	Os	S*	0	Am-O	I	0
Tkw	K	2	On	K	3	Am-S	I	0
Tk-1926-p	I	0	Hj	S*	0	Am-A	I	0
Tk-1926-p	I	0	Nm	I	0	Hn-p	K	2
S	K	5	Nn-s	S	0	Hn-s	K	0
S-fa		5	Nn-p	S	1	Hn-cc	I	0
Kt	S	2	Nn-p-fa		0	KF	I	0
Ty-o	S	2	Th	K or V	3	As	K	4
Ty-l	K	4	Hr-l	S*	0	Ai-m	K	4
Ty-u	K	3	Hr-u	S	0	Ai-l	K	4

Figures represent the degree of abundance of pumice and glass shards crowded with fine tubular vesicles. K, etc. represent the types of pyroclastic flows.

abundance of such a type of pumice and shards.

Deposits of the Krakatoa type ash-flows, especially fine-grained deposits, are characterized by a large quantity of pumice and shards crowded with fine tubular vesicles. For example, the deposits of the lower layer of the ash-flows on the Toya, the middle layer of the ash-flows on the Kutcharo, the ash-flows on the Aso, and the ash-flows on the Aira Volcanoes contain abundant quantities of such a type of pumice and of shards. On the contrary, deposits of the intermediate type pyroclastic flows and the nuées ardentes are always lacking such essential fragments with stretched tubular vesicles. Almost the entirety of the essential fragments in these deposits shows irregular or spherical vesicles. Deposits of the St. Vincent type ash-flows have a paucity or lack of pumice and shards with stretched vesicles.

These facts may indicate the actual condition of the gas-emission process of pyroclastic flows. In eruptions of the nuées ardentes and intermediate type pyroclastic flows, most of the vesiculation may take place after the discharge of the flows. On the contrary, in eruptions of the Krakatoa type ash-flows and perhaps the V.T.T.S. type ash-

Table 15. Constituents of coarse fractions of lappili size in samples of pyroclastic flow deposits and preceding fall deposits.

Sp. no.		Remark	Type of fl.	p	s	de	se	l	c	etc
Kc	2	u	K	87.9				11.3		0.8
Kc	5	u	K	73.5				26.5		
Kc	6	u	K	83.3				13.5		3.2
Ms	2		K		49.7			50.3		
Ak	1		K	66.9				32.3		
Ak	3	cc	I	39.4	55.6			5.0		
Ak	4	cc	I	14.7	30.2			55.1		
D	2		S	83.1			5.0	11.9		
D	3	fa		87.8				12.2		
D	4	fa		91.2			2.4	6.4		
Tkw	1		K or V	94.4				5.6		
Tk	1	p	I	34.7	30.9			34.4		
Tk	4	p(f)	I	36.5	49.3			14.2		
Tk	6	s	I		25.3	53.9		20.8		
S	1	u	K	82.8				17.2		
S	6	u	K	97.4				2.6		
S	12	fa		97.9				2.1		
Kt	1	u	S	61.0				37.8		
Ty	3	l	K	35.0				59.6		
Ty	7	u	K	29.8				64.1		
Ty	8	l	K	38.3				61.7		
Ty	10	o	S	33.2				57.0		
Ty	11	fa		100.0						
Km	3	1929	S	90.0			4.5	5.5		
Km	4	1929	S	91.8			7.2	1.0		
Km	7	K-fl	S	79.4			13.4	7.2		
Km	8	H-fl	S	88.1			2.6	9.3		
Km	11	1929-fa		96.7			2.3	1.0		
Tw	6		K	72.6				27.4		
Tw	14		K	49.2				50.8		
Tw	15		K	24.6				75.4		
Tw	16		K	87.9				12.1		
Tw	17		K	69.3				30.7		
Tw	21	o	S*		5.0			93.7		1.3
Tw	23	fa		91.3				8.7		
Os	1		S*	28.2				71.8		
On	2		K	99.8				0.2		
Hj	2		S*	47.2			1.9	42.0	8.9	
Nm	1		I	77.6			2.9	11.2	8.3	
Nn	1	s	S		44.9			50.2	4.9	
Nn	3	p	S	70.6	(11.1)		10.2	8.1		
Nn	6	p	S	98.4				1.4		0.2
Nn	7	p-fa		73.2			11.8		15.0	
Th	1		K or V	93.0				7.0		
Hr	2	l	S*	40.0				46.3	12.8	
Hr	4	u	S	80.7				16.7		2.6
Hr	5	u-fa		85.7				14.3		
KS	3	l	S*	11.9				36.9	51.2	
My	1		N-P	75.1				1.8	33.2	
My	10		N-P	64.9				1.9	33.2	
Am	1	lp	S	72.8			5.3	21.9		
Am	6	lp	S	33.8			2.6	63.6		
Am	17	up	S	43.6			23.0	33.4		
Am	20	up	S	59.5			6.3	33.0		1.2
Am	24	O-fl	I		8.2	34.7		57.1		
Am	27	O-fl	I		69.7	16.0		14.3		
Am	31	A-fl	I		52.4	43.7		1.8		2.1

Table 15. (Continued)

Sp. no.		Remark	Type of fl.	p	s	de	se	l	c	etc
Am	34	K-na	N-S		72.3	25.3		0.3		2.1
Am	35	S-fl	I			96.4		3.6		
Am	36	up-fa		99.6				0.4		
Hn	1	p	K	48.2			3.7	48.1		
Hn	7	p	K	16.8	29.7		2.6	50.9		
Hn	8	s	K	10.6	84.0			5.4		
Hn	12	cc	I		63.5	27.6		8.9		
As	1		K		89.2			10.8		
Ai	1	m	K	69.7	89.2			30.3		
Ai	4		K	99.3				0.7		
Ai	10	l	K	88.1				11.9		

p: pumice, s: scoria, de: dense essential fragment, se: basic segregation, l: accessory and accidental lithic fragment, c: cognate lithic fragment.

flows, total vesiculation may occur before the discharge of the flows, although the release of gas may continue during flowage, partly caused by the rupture of vesicles that contain gas or by diffusion from pumice clots and shards. In eruptions of the St. Vincent type ash-flows, vesiculation may occur explosively at the time of effusion. Detailed discussions are presented in the later chapters.

Constituent Characteristics

Pyroclastic flow deposits consist of several different constituents; the materials in the coarser fractions consist dominantly of porous essential fragments and non-vesicular lithic fragments; the materials in the medium fractions consist of crystals, porous essential fragments, and lithic fragments in order of abundance; and the materials in the finer fractions consist mainly of crystals and vesicular glass shards. Their constituent features vary greatly perhaps according to the difference in the type of the pyroclastic flows. The chief differences among the deposits seem to be in the relative proportions of essential and accessory or accidental lithic fragments, and the relative proportions of crystals and vitreous materials. It may be possible to consider that the nature of each type of pyroclastic flow is precisely reflected in the constituent characteristics of the deposits. In general, the composition in the coarser fractions of pyroclastic flow deposits may supply some information about the conditions of the initiation of the flows. On the other hand, the composition in finer fractions may represent the effectiveness of the sorting agency. The writer measured the percentage weight of every element in the composition of coarser fractions of some samples of

pyroclastic flow deposits and their preceding air-fall deposits. Measurement was carried out mainly on the size fractions of lapilli, e.g. 32 mm to 4 mm in the diameter of the particles, for convenience. Results are listed in Table 15. They show clearly the different constituent characteristics of the deposits according to the difference in the type of the pyroclastic flows.

1) Nuée ardente deposits: As Williams (1957) stated, the Pelean deposits show the distinct textural characteristics of chaotic mingling of fragments of all sizes and various porosity. They contain both cognate lithic fragments torn from the already solidified crust of the dome and vesicular essential fragments derived from the interior of the dome. For example, the pyroclastic flow deposits of the Myoko Volcano show such features. Cognate lithic fragments tend to bear angular and faceted shapes and also tend to be dense and non-vesicular, while essential fragments tend to be more vesicular and even pumiceous. Breadcrust bombs or ovoid bombs are very rare. Accidental lithic fragments torn from the basement beneath the volcano are quite scarce and usually lacking. Accessory lithic fragments torn from rocks around the vent are found, although they amount to a very small percentage.

Judging from accounts of the nuée ardente deposits by many geologists, fragments in the Merapi type deposits are generally less vesicular, while those in the Pelée type deposits are generally more vesicular. In general the deposits of the former contain a small quantity of fine material, while those of the latter contain a large quantity of vesicular ash and dust, in general. Most of the essential fragments in these deposits tend to bear poorly rounded shapes which suggest the auto-explosive property of effused materials during flowage.

Deposits of the Sakurajima type nuée ardente contain huge essential blocks typified by the characteristic shape and internal structure of which make appearance very much like breadcrust bombs. It is clear that these blocks were popped by internal expansion during emplacement or even after settlement. For example, those of the Kambara Nuée Ardente of the Asama Volcano in 1783 and those of the 1939 nuée ardente of the Sakurajima Volcano show such features[31]. The deposits of the Kambara Nuée Ardente contain a small amount of fine material and show a rugged surface due to huge blocks exceeding sometimes

31) Shigeo ARAMAKI, *op. cit.*, (1956),
Hiromichi TSUYA and Takeshi MINAKAMI, "Minor activity of Volcano Sakurazima in October, 1939," *Bull. Earthq. Res. Inst., Tokyo Univ.*, **18** (1940), 318-339. (Japanese with English abstract.)

several meters in diameter. It showed strong erosive power to produce a deep ditch along its lower course on the gentle slope of the volcano. Consequently, the deposits in the distal ends contain a great quantity of surface debris. At the foot of the volcano, it entered flowed into for surface water and produced secondary hot mud-flows.

2) Intermediate type pyroclastic flow deposits: The composition of intermediate type pyroclastic flow deposits resembles that of the Sakurajima type nuée ardente deposits, although the former contain a larger amount of fine materials than the latter. The deposits also show the distinct textural characteristics of the chaotic mingling of fragments of all sizes and of varying porosity. Most of the large blocks found in them are characterized by fairly high degrees of porosity and show an appearance very like breadcrust bombs which indicate that they were derived from bits of plastic magma torn apart at the time of effusion. The degree of porosity of the essential fragments varies within a wide range. As already mentioned, well-vesiculated fragments show in general an angular shape, which indicates the auto-explosive property during flowage. Lithic fragments of both accessory and accidental origin are found in the deposits, although their quantity is very small. The deposits at the distal ends of the flows, however, sometimes contain an increasing amount of surface debris, indicating the erosive power during flowage. The weight of fine ash materials often amounts to 50 per cent or more of the deposits. They consist of phenocrystic mineral grains and their fragments and minute vesicular glass shards. The deposits are considerably indurated at times, contrasting with the nuée ardente deposits which tend generally to be poorly indurated or incoherent.

3) St. Vincent type ash-flow deposits: Deposits of the St. Vincent type ash-flows vary greatly in composition. This may depend partly upon the degree to which the erupting magma has crystallized immediately before discharge, and partly upon the condition of the initiation of the flows. The distinct feature of the concentration of crystals in medium fractions of the deposits is usually recognized. For instance, the ash-flow deposits of the 1902 eruption of the Soufrière on St. Vincent (Hay, 1959) and those of the 1929 eruption of the Komagatake Volcano show such features. It is considered that crystals may be concentrated by the sorting of both in the vertically rising ash column and in the descending cloud of flows, as explained in detail in the later chapter. Concentration of crystals is found distinctly in the lower parts of the deposits. Coarse fragments of pumice or scoria are also concentrated in the St. Vincent

type ash-flow deposits, especially in their upper and frontal parts, although the degree of concentration varies considerably from part to part within a single unit of the flows. Breadcrust bombs derived from plastic magma make up an insignificant or no fraction of the whole of the deposits. Accessory and accidental lithic fragments torn from the walls of the vent and from the basement are usually small and quite subordinate in amount. Lithic fragments tend to concentrate in the lower part of the deposits. Dark colored fragments of basic segration and banded pumice are usually found in the deposits, and sometimes occupy a fairly large percentage. The deposits are generally incoherent, although some are considerably indurated.

There is another type of pyroclastic flow deposits which have size characteristics similar to those of the St. Vincent type ash-flow deposits but which show dissimilar features in their constituent characteristics. They have intermediate characteristics between dry mud-flow deposits and pyroclastic flow deposits, being described sometimes as the products of mud-flows and sometimes as those of pyroclastic flows. Such deposits contain large quantities of lithic fragments of mostly accessory origin. They also contain considerable amounts of lithic fragments of cognate origin derived from a solidified body at the apex of the magma column. It is considered that they may have been originated from violent explosions attended by the discharge of juvenile materials. Perhaps part of a volcanic cone may have been destroyed by a destructive explosion, and the disintegrated materials flowed down *en masse* along the mountain-slope in company with a large amount of juvenile materials discharged simultaneously. For instance, the Lower Ash-flow of the Haruna Volcano and the Ash-flow of the Osoreyama Volcano may belong to such types of flows each having an intermediate nature between pyroclastic flows and dry mud-flows. The bottom layers of the St. Vincent type ash-flow deposits sometimes show such an intermediate nature. For example, the bottom layer of the Ash-flow of the Kusatsu-Shirane Volcano shows such a nature. In these intermediate cases the deposits near the source contain large amounts of lithic fragments sometimes surpassing the amounts of essential fragments, while those far from the source contain increasing amounts of essential fragments as well as decreasing amounts of lithic fragments. The concentration of crystals in medium fractions of the deposits is recognized, but generally not as conspicuous as in the deposits of the St. Vincent type ash-flows, and the degree varies greatly. Strictly speaking, the deposits having such an intermediate nature be-

tween pyroclastic flows and dry mud-flows as mentioned here must be distinguished clearly from the pure pyroclastic flow deposits. In reality, however, they often accompany deposits of the St. Vincent ash-flows, showing some resemblances between them in size characteristics and in the nature of the discharged juvenile materials, and it may be convenient to deal with them as a variety of the St. Vincent type ash-flows.

4) Krakatoa type ash-flow deposits: The composition of the Krakatoa type ash-flow deposits resembles that of the St. Vincent type ash-flow deposits, although the former usually contain a larger amount of vesicular dust than the latter. The concentration of crystals in medium fractions is also generally recognized, but not as distinct as in the St. Vincent type ash-flow deposits, and its degree varies widely. Essential fragments are characterized by an extremely high degree of porosity and finely stretched vesicles. Deposits of the Krakatoa type ash-flows contain lithic fragments, both accessory and accidental, in fairly abundant amounts. Accidental fragments are derived from the deeper walls of the conduit and the chamber. During the ascent of frothing magma a large quantity of lithic fragments may be brought to the surface. The abundance of lithic fragments, especially of accidental origin, in deposits of the Krakatoa type ash-flows contrast strikingly with the paucity of them in deposits of the St. Vincent type ash-flows. Intense vesiculation arising within the conduit or even in the chamber may be responsible for such an abundance of lithic fragments. The deposits contain a small amount of surface debris, suggesting the lack of erosive power during flowage. They exhibit strong welding at times.

5) Valley of Ten Thousand Smokes type ash-flow deposits: There is another type of ash-flow deposit produced by fissure eruptions. This was first recognized from the study of tuff deposits emplaced in the Valley of Ten Thousand Smokes. They often form extensive ash-sheets whose volume sometimes exceeds 1,000 km^3. Many examples of this type of ash-flow deposits have been discovered in many regions of the world. Few examples have been discovered in Japan, but other many ones will be recognized in detailed studies in the near future. Such deposits may show fine-grained size characteristics which may resemble those of the fine-grained Krakatoa type ash-flow deposits. They may contain less amounts of lithic fragments than the Krakatoa type deposits.

Bulk Density of Essential Fragments

The mode of eruption of pyroclastic flows may be closely related to the content of volatiles in the eruping magma, and the difference in the volatile content in magma may be reflected in the degree of vesiculation of essential fragments. Aramaki's classification of pyroclastic flows (1957) is based upon the viscosity of discharged materials, which is inferred from the nature of the deposits, especially from the porosity of essential fragments. Accurate measurement of the porosity, however, is actually quite difficult. Therefore, the writer caried out measuremets of the bulk density instead of the porosity. Measurements were carried out on the essential fragments larger in diameter than lapilli size. Although values of the bulk density of essential fragments in samples collected from a single unit of pyroclastic flow deposits vary within a wide range, they tend to concentrate around a certain central value. An average values computed from a large number of individual measurements may offer a certain significant value which represents the degree of vesiculation of the erupting magma. The average values of bulk density of essential fragments ($\bar{d}_B$) both in pyroclastic flow deposits and the preceding pyroclastic fall deposits are listed in Table 16.

In general, values of the Krakatoa type ash-flows are within a range of 0.5 to 0.7, those of the St. Vincent type ash-flows are within a range of 0.7 to 1.2, and those of the intermediate type pyroclastic flows and of the nuées ardentes are large than 1.2. In the deposits of the intermediate type pyroclastic flows, and of nuées ardentes, the individual value of bulk density of each sample in a single unit of flow varies more remarkably than in the deposits of the ash-flows.

Average values of the bulk density of ovoid bombs ejected in eruptions of the Strombolian type are generally within a range of 1.5 to 2.0. Those of pumice and breadcrust bombs ejected in explosive eruptions of the Vulcanian type are usually within a range of 0.8 to 1.5. Those of pumice fragments in the Krakatoa type ash-flow deposits are remarkably small, compared with these values. On the other hand, those of essential fragments in the St. Vincent type ash-flow deposits are of the same order as those of pumice in the Vulcanian eruptions.

As already mentioned, eruptions of pyroclastic flows usually follow preliminary eruptions of pyroclastic falls. An average value of the bulk density of essential fragments in the succeeding pyroclastic flow deposits tends to be larger than those in the preceding pyroclastic fall deposits,

although the data are insufficient to discuss in detail. This relation is recognized between the preliminary pyroclastic falls and the succeeding flows of the Daisetsu, Shikotsu (Katsui, 1959), Komagatake, Towada, Nantai, Haruna, and Asama Volcanoes. Perhaps a preceding explosive

Table 16. Average values of the bulk density of essential fragments of pyroclastic flows and preceding falls.

	$\bar{d}_B$	No. of loc.	No. of sp.		$\bar{d}_B$	No. of loc.	No. of sp.
Kc-m	0.57	2	7	Hj	1.17	1	10
Kc-u	0.55	6	49	Nm	1.03	1	12
Ms	0.46	3	17	Nn-s	1.29	1	6
Ak	0.56	2	20	Nn-p	0.99	5	49
Ak-cc-p	1.08	2	19	Nn-p-fa	0.65	1	8
Ak-cc-s	1.55	1	9	Th	0.45	1	14
D	0.97	2	15	Hr-l	1.12	1	11
D-fa	0.90	2	20	Hr-u	0.87	1	12
Tkw	0.65	1	5	Hr-u-fa	0.69	1	11
Tk-1926-p	1.27	3	31	KS	1.25	2	8
Tk-1926-s	1.73	4	38	My	2.04	11	10
S	0.54	10	58	Am-lp	0.68	13	117
S-fa	0.53	1	9	Am-up	0.83	7	57
Kt	0.75	2	15	Am-up-fa	0.71	1	8
Ty-l	0.78	3	11	Am-O	1.41	5	40
Ty-u	0.74	5	37	Am-S	2.24	1	11
Km-1929	0.94	6	64	Am-A	1.13	3	27
Km-1929-fa	0.84	1	13	Hn-p	0.64	4	43
Km-K	1.09	1	11	Hn-p	0.84	2	17
Km-H	1.05	3	24	Hn-cc	1.78	3	26
Tw-o	1.03	2	14	KF	2.18	10	122
Tw	0.50	20	151	As	0.74	2	11
Tw-fa	0.47	1	12	Ai-l	0.59	2	22
Os	0.83	1	4	Ai-m	0.59	6	61
On	0.52	2	17	Ai-u	0.47	1	4

eruption which produces violent pyroclastic falls may be caused by intense vesiculation of gas-rich magma in the uppermost level of the magma column, and the rather fluent discharge of magma having a decreasing content of gas in the lower level of the magma column succeeds, forming flows of frothing materials. Such a succession of eruptive events is discussed in the following chapter.

Succession of Eruptive Events

The eruption of pyroclastic fall, pyroclastic flow and effusion of lava often occur together in a single phase of volcanic activity. Among these events a certain order of succession may be maintained in almost every case as Yamasaki (1959) and Kennedy (1955) pointed out[32]. The eruption of pyroclastic flows usually follows the preliminary eruption of pyroclastic falls. In the 1883 eruption of the Krakatoa Volcano, a voluminous discharge of pumice and ash in the form of ash-flows followed the preliminary eruptions of pumice falls. The eruption of the ash-flows in the Crater Lake region succeeded the eruption of pumice falls (Williams, 1942). A similar succession has been recognized in many cases of Japanese ash-flow deposits. In the 1929 eruption of the Komagatake Volcano the discharge of ash-flows followed the early powerful explosion which caused heavy pumice falls (Tsuya, 1930; and Kozu, 1934). The ash-flows of the Mashu, Daisetsu, Shikotsu, Tarumai, Towada, Nantai, Haruna, Akagi, Asama, Hakone and Aira Volcanoes are underlain by preliminary pyroclastic falls. In the eruption of the Asama Volcano in 1783, a systematic succession of eruptions of pumice fall, scoria flow, intermediate type pyroclastic flow, nuée ardente and lava flow took place. Throughout the whole of the eruptive events in this 1783 activity, the chemical composition and petrological character of the effused materials showed no significant variation, while the gas content of magma which was inferred from the porosity of the discharged materials decreased gradually (Aramaki, 1956 and 1957). A similar systematic succession of pyroclastic fall, flow and effusion of lava has been recognized in the 1739 eruption of the Tarumai Volcano (Katsui, 1958) and in the prehistoric eruptions of the Nantai (Yamasaki, 1957) and Haruna Volcanoes.

In the prehistoric eruption of the Shikotsu Volcano, an explosive eruption of rhyolitic magma which caused heavy pumice falls occurred in the initiation of the culminant phase of the eruptive activity. Katsui (1959) considered that this eruption originated from the apex of the magma column which was rich in volatiles and alkalies, and then followed the discharge of a tremendous amount of dacitic magma in a state of

32) Masao YAMASAKI, "Role of water in volcanic eruption," *Bull. Volcanol. Soc. Jap., 2nd Series*, **3** (1959), 95-106. (Japanese with English abstract.)

G. C. KENNEDY, "Some aspects of the role of water in rock melts," *Crust of the earth, Geol. Soc. Am. Special Paper*, **68** (1955), 489-503.

ash-flow, which originated from the lower level of the magma column[33]. Such a change of the composition of the effused materials, from more silicic to less silicic, or from felsic to mafic, has been recognized in other eruptions. In the prehistoric eruption of the Mashu Volcano, a succession of felsic pumice fall, mafic pumice fall and flow has been recognized (Katsui, 1955). During the culminating eruptions of ash-flows from Mt. Mazama in the Crater Lake region, a transition from dacite pumice whose silica content ranges from 66.4 to 68.9 per cent to basic scoria whose silica content rang as from 53.9 to 56.9 per cent occurred suddenly without a detectable time break[34]. In the eruption of the ash-flows from the Hakone Volcano, a similar transition from pumice to scoria was also recognized. Some volcanologists consider that these facts may suggest a role of water in the magma, where the water tended to concentrate at the top of the magma column, bringing together alkalies and silica (Kennedy, 1955; and Katsui, 1960).

The systematic succession of the pyroclastic fall and flow and effusion of lava as mentioned here, may suggest the important role of volatiles in erupting magma as noticed by Yamasaki (1959) and Kennedy (1955). At the initiation of a single phase of volcanic activity, an explosive eruption occurs suddenly. An intense vesiculation of erupting magma hurls up ash and pumice high above the crater, causing pyroclastic falls. The magma represents the higher level of the magma column, in which the gas content may be greater than in the lower level. This high content of gas, as well as the heavy confining load of solidified crust at the apex of the column, may be attributed to the violent explosion in the initial stage of eruptive activity. The gas content of magma decreases with the preceding violent explosion. In the following stage, because of the decreasing content of gas as well as the removal of the confining load of solidified crust at the top of the vent, magma discharges without powerful explosion, and may form pyroclastic flows at times. The magma in this stage represents the lower level of the magma column, containing relatively lesser amount of gas than in the preceding stage. The eruption of pyroclastic flows

33) Yoshio KATSUI, "On the Shikotsu pumice-fall deposit," *Bull. Volcanol. Soc. Jap., 2nd Series*, **4** (1959), 33-48. (Japanese with English abstract.)

Yoshio KATSUI and Tsutomu MURASE, "Some considerations on the activity of the Shikotsu Volcano," *Jour. Geol. Soc. Jap.*, **66** (1960), 631-638. (Japanese with English abstract.)

34) Howel WILLIAMS, "The geology of Crater Lake National Park, Gregon, with a reconnaissance of the Cascade Range southward to Mount Shasta," *Carnegie Inst., Washington Pub.* **540** (1942), 162.

may be generated by a less intense vesiculation than the preceding pyroclastic fall eruption. In the later stage of eruptive activity, magma does not contain a large amount of gas. The gas content of magma becomes poor partly because of the escape of volatiles during the earlier stages, and a calm extrusion of lava may occur.

Chemical Properties of Pyroclastic Flow Deposits

There exist wide variations in the chemical properties among various types of pyroclastic flow deposits. The deposits contain almost all the rock types from basalts to rhyolites, although basalts are exceedingly rare. Many chemical analyses of rocks recognized to be of pyroclastic flow origin have been published. They record compositions ranging from basalts to rhyolites and trachytes, but in general, silicic rocks predominate. Values of the silica content vary widely, mostly falling within a range of 55 to 75 per cent. Those of the nuées ardentes, the intermediate type pyroclastic flows and the St. Vincent type ash-flows are relatively less silicic and range from 55 to 65 per cent, while those of the Krakatoa type ash-flows and the Valley of Ten Thousand Smokes type ash-flows are more silicic and range from 60 to 75 per cent or more. Color indices (the percentage of normative ferromagnesian minerals) usually take values less than 20. There are no notable differences in the chemical properties between pyroclastic flow deposits and normal lava flows. Essential fragments of pyroclastic flow deposits are typified by a high degree of porosity, and consist of phenocrystic mineral grains and vesiculated amorphous groundmass. Consequently it is impossible to determine whether they belong to the pigeonitic rock series or the hypersthenic rock series of Kuno (1950 and 1953) in almost every case.[35] Bulk chemical compositions of all types of pyroclastic flow deposits, however, tend to show the chemical properties of the hypersthenic rock series. The ratio of $(FeO+Fe_2O_3) : MgO : (Na_2O+K_2O)$ plotted on the triangular diagram tends to fall in the region of the hypersthenic rock series and also shows a trend of variation almost coinciding with that of Daly's averages of igneous rocks (1941), except for a very few cases (see Fig. 12). Variation diagrams of oxides plotted against solidification indices (S. I.) of Kuno (1954 and 1959) generally manifest the general features of rocks of the calc-alkali rock series and of the hyper-

35) Hisashi KUNO, "Petrology of Hakone volcano and adjacent areas, Japan," *Bull. Geol. Soc. Am.*, **61** (1950), 957–1020.
Hisashi KUNO, *op. cit.*, (1953).

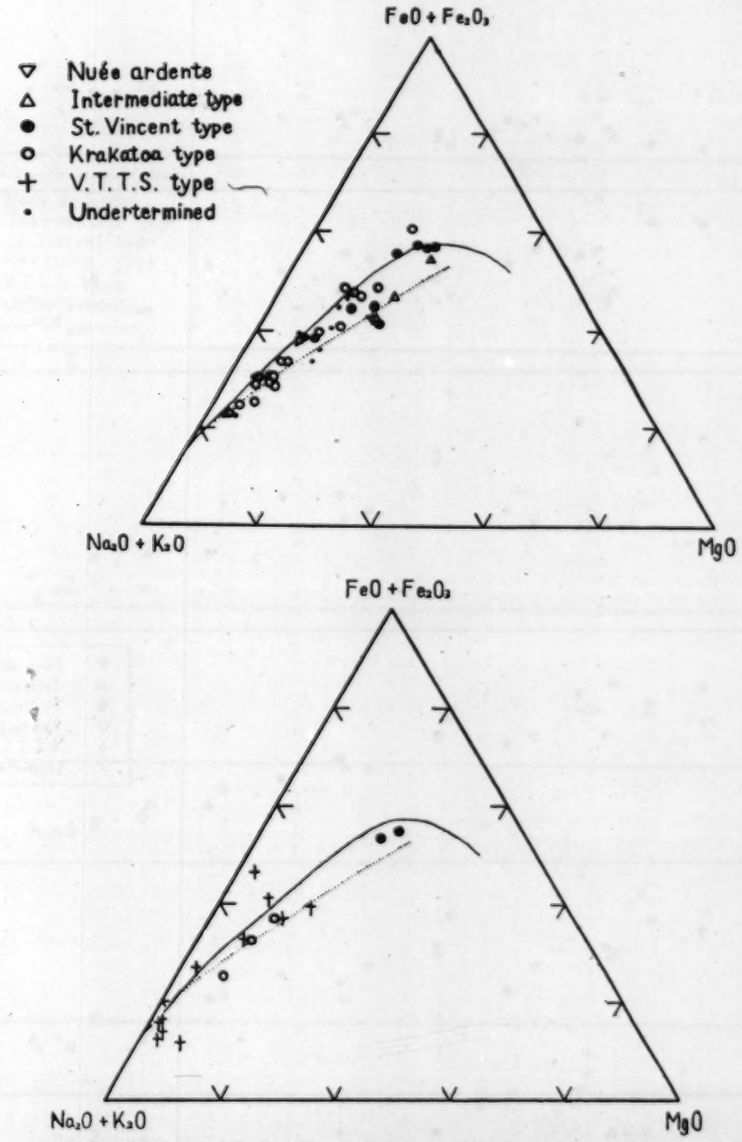

Fig. 12. MgO: $FeO+Fe_2O_3$: Na_2O+K_2O triangular diagram. Upper: Japanese examples, lower: foreign examples. The solid line is the border between the pigeonitic rock series and the hypersthenic rock series drawn by Kuno (1953). The dotted line represents the variation line of Daly's averages on volcanic rocks of the World (1941).

sthenic rock series (see Fig. 13). (S. I.) are values of $MgO\times 100/(MgO+FeO+Fe_2O_3+Na_2O+K_2O)$, which are adopted as measures of magmatic differentiation.[36] Every point on the diagram tends to center around a

36) Hisashi KUNO, "Volcanoes and volcanic rocks," *Iwanami and Co., Tokyo* (1954), 255. (Japanese)

Hisashi KUNO, "Origin of Cenozoic petrographic provinces of Japan and surrounding areas," *Bull. Volcanol., ser.* **ii**, **20** (1959), 37-76.

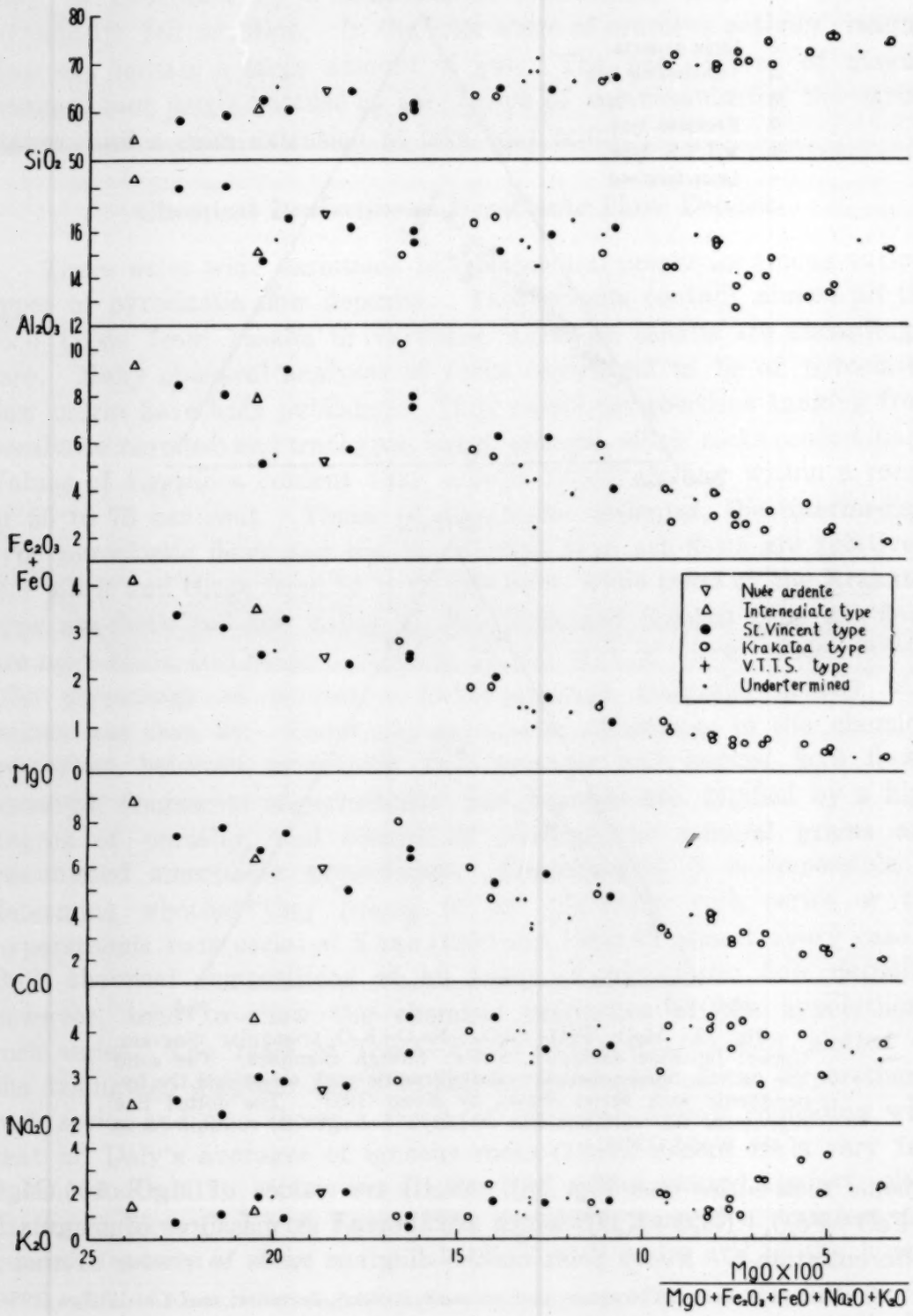

Fig. 13a. Variation diagrams of oxides, Japanese examples.

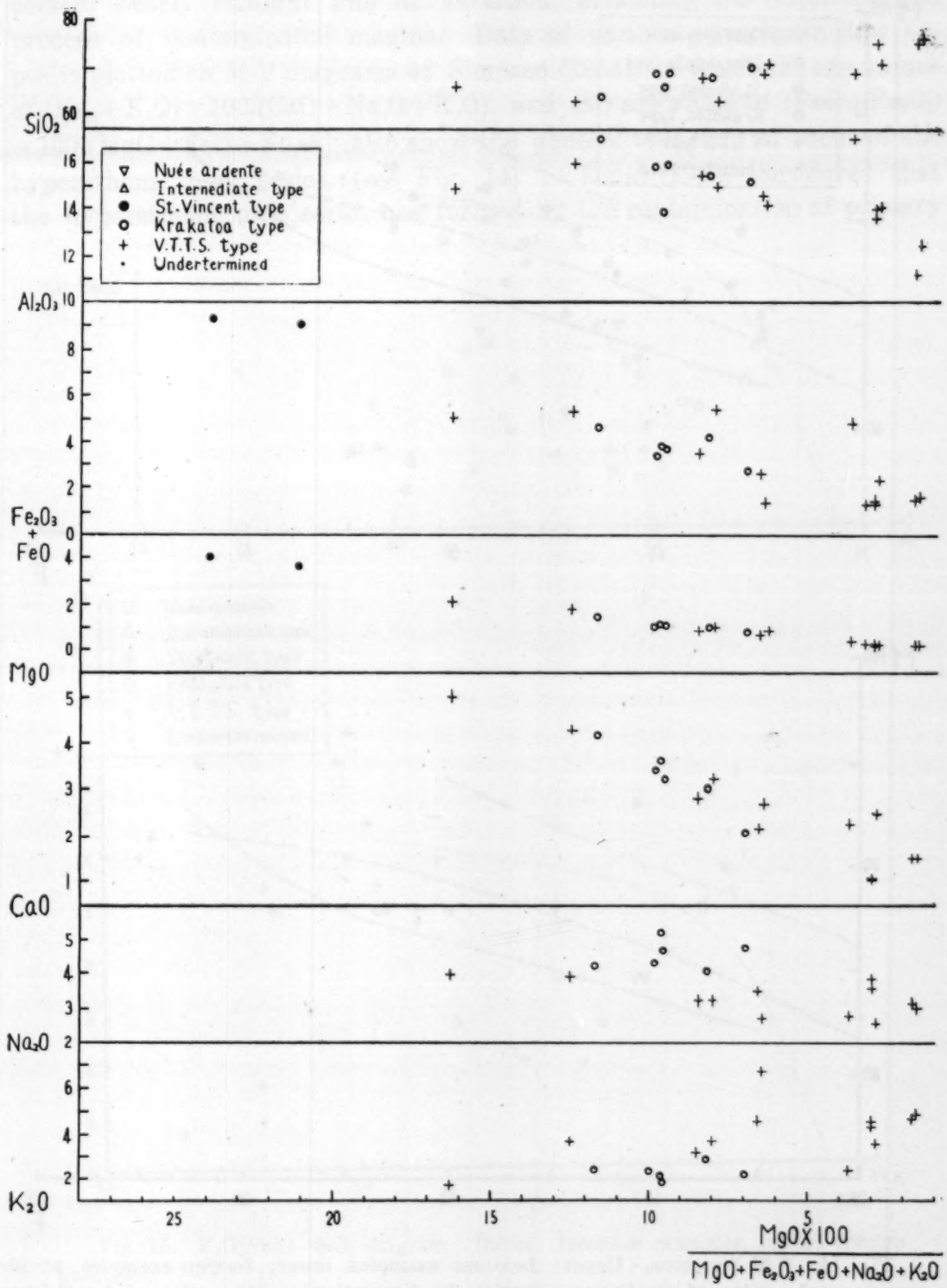

Fig. 13b. Variation diagrams of oxides, foreign examples.

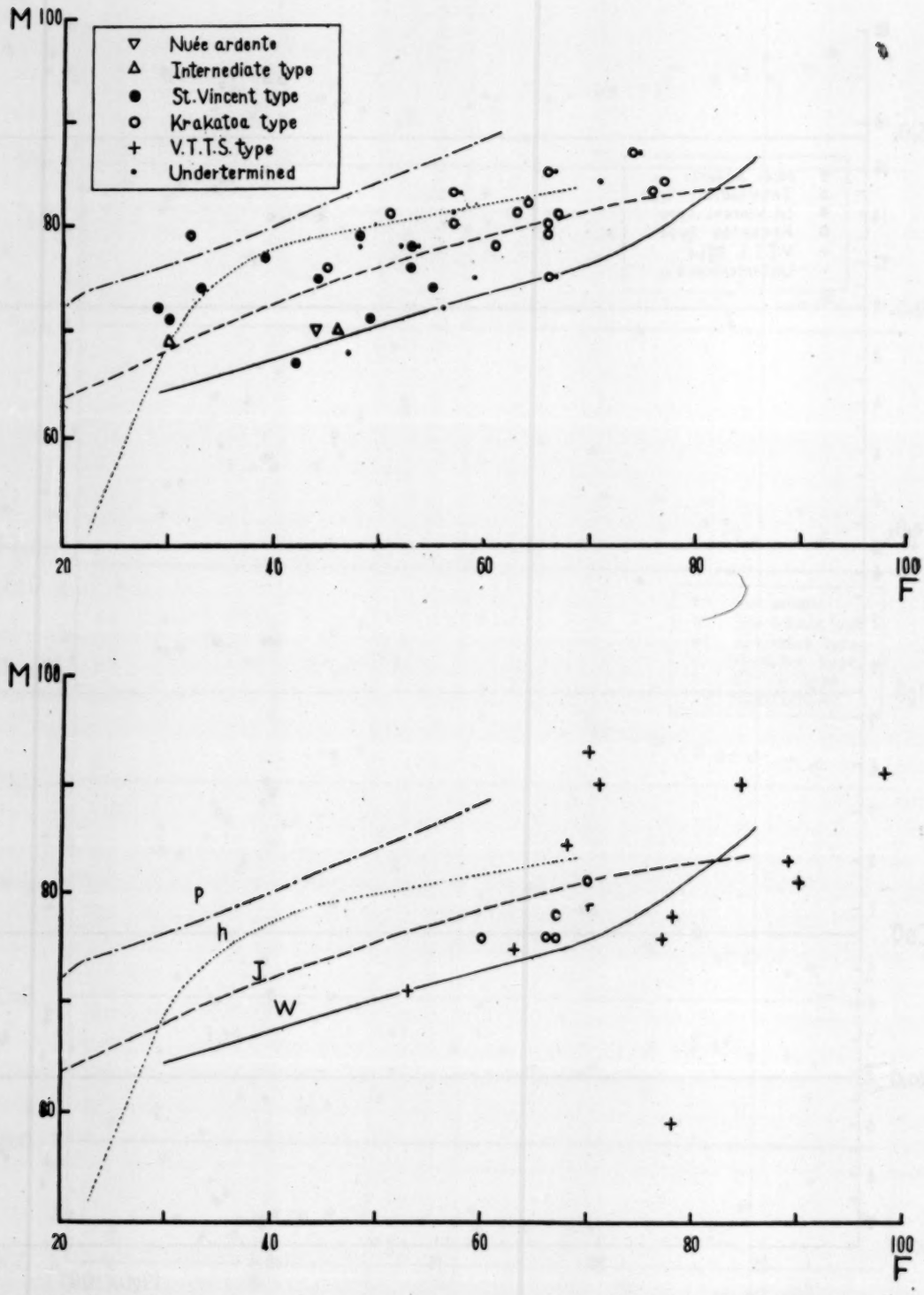

Fig. 14. F-M diagrams. Upper: Japanese examples, lower: foreign examples, p: pigeonitic rock series of Izu-Hakone district, h: hypersthenic rock series of Izu-Hakone district, J: the average of Japanese volcanic rocks (Iwasaki, 1948), W: average of volcanic rocks of the World (Daly, 1941).

certain nearly straight line of variation, indicating the differentiation process of contaminated magma. Data of various pyroclastic flow deposits plotted on M-F diagrams of Simpson (1954), in which (F) are values of $(Na_2+K_2O)\times 100/(CaO+Na_2O+K_2O)$, and (M) are value of $(FeO+Fe_2O_3)\times 100/(MgO+FeO+Fe_2O_3)$, also show the general tendency of rocks of the hypersthenic rock series. (see Fig. 14)[37]. Kuno (1950) considered that the hypersthenic rock series are formed by the contamination of primary

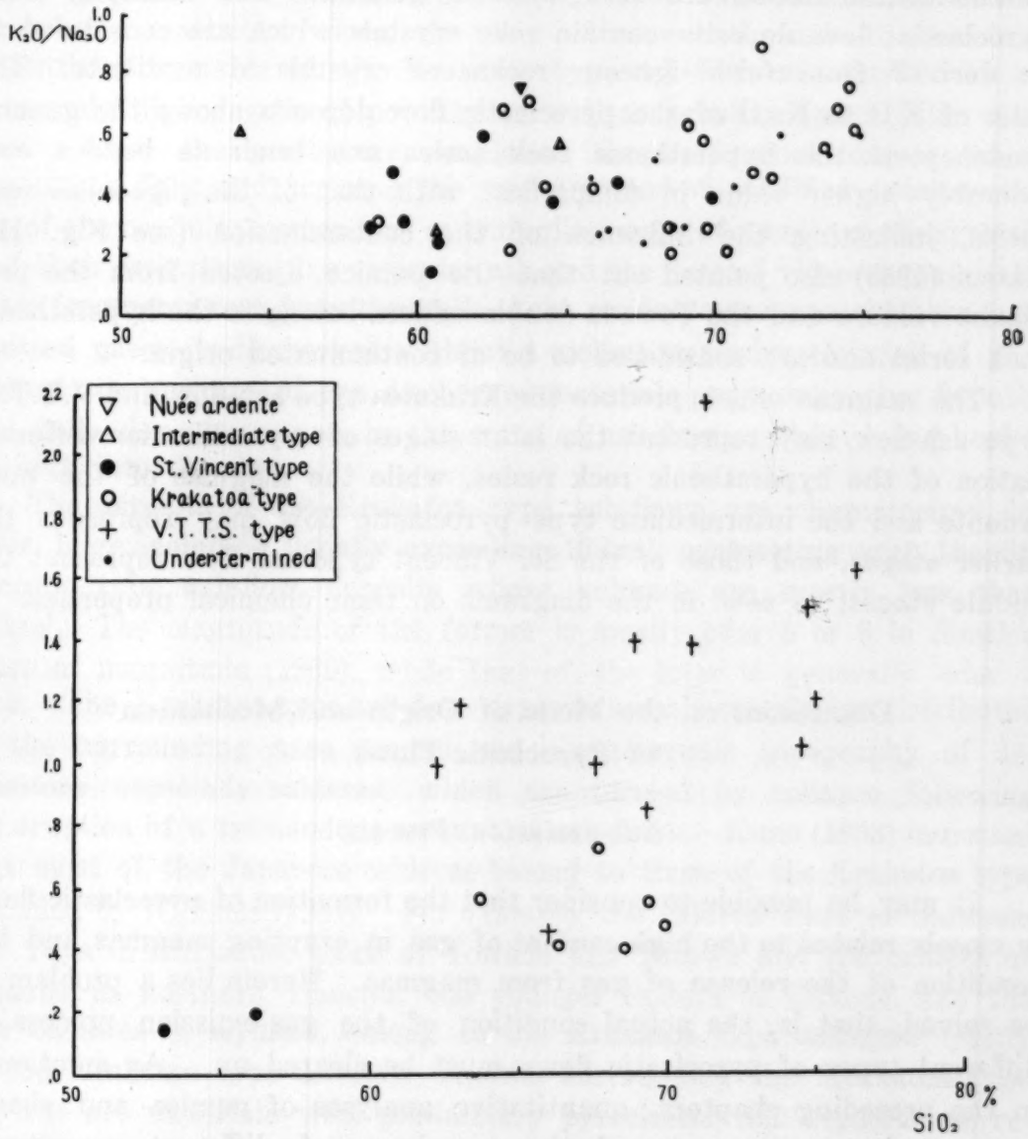

Fig. 15. K_2O/Na_2O-SiO_2 diagram. Upper: Japanese examples, lower: foreign examples.

37) E. S. SIMPSON, "On the graphic representation of differentiation trends in igneous rocks," *Geol. Mag.*, **91** (1954), 238-244.

magma with granitic materials. Volatiles dissolved in the primary magma may concentrate into the contaminated part and lower the temperature of crystallization, resulting in the growth of rhombic pyroxene in the groundmass. Magmas that cause the eruptions of pyroclastic flows may be formed by such contamination, which may be attributed to the high degree of concentration of volatiles in magmas. Chemical analyses of the deposits sometimes show a high content of $H_2O(+)$. Other proofs of the contamination are recognized in general. For example, some pyroclastic flow deposits contain relic crystals which are considered to be derived from felsic igneous rocks, or crystals of cordierite. The ratio of K_2O to Na_2O of the pyroclastic flow deposits shows the general tendency of the hypersthenic rock series and tends to bear a considerably higher value in comparison with that of the pigeonitic rock series, indicating the influence of the contamination (see Fig. 15). Katsui (1955) also pointed out that the pumice ejected from the pre-Mashu caldera and the Towada double caldera belong to the hypersthenic rock series and are considered to be of contaminated origin.

The magmas which produce the Krakatoa type ash-flow and V.T.T.S. type ash-flow may represent the later stages of crystallization differentiation of the hypersthenic rock resies, while the magmas of the nuée ardente and the intermediate type pyroclastic flow may represent the earlier stages, and those of the St. Vincent type ash-flow represent the middle stages, as seen in the diagrams on their chemical properties.

Discussions on the Mode of Origin and Mechanism of Pyroclastic Flows

Gas-emission Process

It may be possible to consider that the formation of pyroclastic flows is closely related to the high content of gas in erupting magmas and the condition of the release of gas from magmas. Herein lies a problem to be solved, that is, the actual condition of the gas-emission process in different types of pyroclastic flows must be cleared up. As mentioned in the preceding chapters, quantitative analyses of pumice and shards types and measurements of the roundness of different constituent particles in pyroclastic flow deposits may offer some important clues to help to solve this problem. Judging from the results of such examinations, together with the results of inspections of other characteristics

of the deposits, it may be possible to infer the actual condition of the gas-emission process in every type of pyroclastic flow as follows.

In eruptions of the Krakatoa type ash-flows, vesiculation commences within the conduit or even in the magma chamber, and most of the gas-emission takes place before the discharge of ash-flows. A large proportion of ascending magma may be disintegrated into frothing clots of pumice within the conduit, shattered to fine pieces and shards crowded with stretched fine tubular vesicles. Pumice clots are shattered and stretched by attrition along the way of ascent through the conduit. Essential fragments of the Krakatoa type ash-flows are typified by an extremely high degree of porosity as well as peculiar fine tubular vesicles. After the preliminary explosive eruption which causes heavy pyroclastic falls and removes the confining load of solidified crust at the top of the conduit, tremendous commingling mass of pumice clots, crystals and their fragments, fine vesicular ash and the dust of vitreous materials, lithic fragments torn from the walls of the conduit or magma chamber, and emitted gases, is discharged without a violent explosive emission of gas. Almost the entirety of the discharged materials pours out rather fluently and flows down *en masse* in the state of ash-flows without being hurled up high into the air.

The deposits of the Krakatoa type ash-flows are characterized by their huge volumes usually exceeding 10 km^3, contrasting with the St. Vincent type ash-flow deposits whose volumes are mostly less than 10 km^3. The magnitude of the former is mostly oder 5 or 6 in Smith's oders of magnitude (1960), while that of the later is generally oder 4 or 3. The Krakatoa type ash-flow deposits are almost always distributed in the surrounding area around the characteristic topography of depressions, especially calderas, which are formed by collapse following the eruption of a tremendous amount of ash-flows. Kuno (1953) indicated that most of the Japanese calderas belong to those of the Krakatoa type classified by Williams (1941). For example, the caldera lakes of Shikotsu and Toya in Hokkaido, those of Towada and Tazawa and the caldera of Onikobe in northern Honshu, the younger caldera of Hakone, and the four calderas in Kyushu, belong to the Krakatoa type calderas. Many of the Krakatoa type ash-flow deposits surrounding the Krakatoa type calderas are underlain with preliminary pyroclastic fall deposits as repeatedly mentioned. In every case, the volume of the ash-flow deposits is far larger than that of the preceding pyroclastic fall deposits. At the paroxysmal phase of the 1883 eruption of the Krakatoa Volcano, a tremendous volume of pumice and ash, amounting to more than 90 per

cent of all the effused materials of the 1883 eruption, was discharged in a short time, and fell virtually *en masse* as an avalanche and was accumulated close to the source as an unstratified pile up to 60 meters thick. Only the finer particles of vesicular fragments were thrown out high into the air, and drifted away for long distances (Williams, 1941). Perhaps, the mode of eruption in every case of Krakatoa type ash-flows may be similar to the paroxysmal phase of the 1883 eruption of the Krakatoa Volcano. Erupting magmas of the Krakatoa type ash-flows may have an extremely high content of volatile substances, judging from a distinct feature of fully-vesiculated essential fragments in the deposits. Such a high concentration of volatiles may be attributed to the eruptions of high magnitude which cause the effusion of a tremendous amount of ash-flows of the order of 5 or 6 (its volume is more than 10 km^3 or 100 km^3) and the following collapse of the apical part of the volcano.

It may be inferred that eruptions which produce the fine-grained Krakatoa type ash-flow deposits may somewhat resemble to those of the V.T.T.S. type ash-flows. Pyroclastic materials may effuse from fissures developed on the volcanic cone rather from a central crater, the writer considers.

In eruptions of the intermediate type pyroclastic flows and the Sakurajima type nuées ardentes, most of the vesiculation occurs after the discharge of the flows. Magmas ascend to the crater-rim in a state of effervescing melt. The intermediate type pyroclastic flows are generally formed without explosive eruption, and effervescing magmas discharge rather fluently over the crater-rim and rush down the mountain-slope. The rising of a lofty column of ash and steam which causes heavy pyroclastic fall, as in eruptions of the St. Vincent type ash-flows, may not occur in general. Almost the entirety of the discharged materials descend *en masse*, forming flows of frothing fragments.

In eruptions of the Pelée type nuées ardentes which are initiated by lateral propulsion due to powerful explosions, intense vesiculation occurs at the time of initiation and continues during flowage. On the other hand, in eruptions of the Merapi type nuées ardentes of Escher's classification (1933), initiated by feeble explosions or without explosion, the total vesiculation takes place during flowage. Such a process of gas-emission which occurs during flowage gives rise to the so-called "auto-explosive property" discussed by Perret (1935) and Fenner (1923).

In eruptions of the St. Vincent type ash-flows, matters are otherwise. Vesiculation begins partly within the vent, and occurs mostly at the time of the effusion of the magma. Gases are released explosively from

the erupting magma at the crater-rim. The erupting magma may no longer be an effervescing melt but have already been disintegrated into frothing clots of pumice and droplets of liquid at the time of effusion. The discharge of ash-flow follows the preliminary explosion. The gas content of the magma may be fairly high, but the initial velocity of the emitting gas at the crater-rim is lower than in the case of a major explosion of the Vulcanian type eruption, and in the preceding explosion. Most of the effused materials are ejected into the height in the ash column, and phenocrystic mineral grains and pumice blocks are sorted and concentrated in the slowly rising outer part of the ash column, and then form an ash-flow descending down the mountain-slope under the influence of graviational force (Hay, 1959). The release of gas may continue during flowage of the flows, although most of the vesiculation occurs before the discharge of the flows. Some vesiculation may continue even after the discharge of the flows. Gas may be also released by rupture of vesicles during flowage.

In eruptions of the Valley of Ten Thousand Smokes type ash-flows, the gas-emission process may be similar as in eruptions of the Krakatoa type ash-flows, although the writer has no available datum based upon sure examples.

There exist wide variations in the actual condition of the gas-emission process among different types of pyroclastic flow eruptions as explained here, and such variations may be due to the differences in the degrees of concentration of volatiles in the erupting magmas. Magmas which produce eruptions of the Krakatoa type ash-flows and the Valley of Ten Thousand Smokes type ash-flows are generally dacitic or rhyolitic, containing extremely high amounts of silica. Such magmas represent the later stages of crystallization differentiation and may contain high amounts of volatiles, and such a high concentration of volatiles may be attributed to the eruptions of high magnitude and the vesiculation of a tremendous mass of magma within the conduit or chamber. On the other hand, magmas which produce eruptions of the other types of pyroclastic flows of lower magnitude are generally less silicic and may contain lesser amounts of volatiles than the former two types of higher magnitude. Especially, magmas of the nuées ardentes and the intermediate type pyroclastic flows generally represent the earlier stages of crystallization differentiation and may contain the least amounts of volatiles, although they may show a considerably high content of volatiles in comparison with normal lava flows. The lesser concentration of volatiles in erupting magmas may be responsible for the delayed vesiculation that

takes place after the discharge of flows of these two types. Magmas which produce eruptions of the St. Vincent type ash-flows generally represent the middle stages of crystallization differentiation and may contain fairly large amounts of volatiles. Consequently, vesiculation takes place explosively, partly within the vent and mostly at the crater-rim, and the discharge of flows usually accompanies a violent effusion of the vertical column of ash and steam.

Dual Character of Pyroclastic Flows

Judging from descriptions of many observers on eruptions of pyroclastic flows, it appears that they consist of two parts, namely, a basal avalanche and an overriding spectacularly expanding cloud of gas and dust. Such a separation of the basal avalanche and the overriding cloud in pyroclastic flows may occur at any time, although a distinction between these two parts may not always be sharply drawn. This dual character of pyroclastic flows may be recognized most distinctly in eruptions of the nuées ardentes and the intermediate type pyroclastic flows in which most of the vesiculation takes place during flowage. During the eruption of May 8th, 1902, at Mt. Pelée, it was the overriding cloud that swept away St. Pierre. Deposits of ash and lapilli a few feet thick settled from the cloud. On the other hand, the basal avalanche from which the devastating cloud was derived flowed down in the confined area of the valley of the Rivière Blanche, on the south-west of the parent dome. Deposits characterized by the chaotic mingling of fragments of all sizes settled from the basal avalanche (Lacroix, 1904 and 1908). During the eruption of May 7th, 1902, at the Soufrière, a "great black cloud" descended from the crater, and the upper part of the cloud spread outward as a "hot blast" over the eastern and western slopes of the Soufrière, causing the death and devastation of the settlement, and deposited a few inches of ash. The lower, denser part of the cloud flowed down mostly in the valleys of the Rabaka and Wallibu Rivers on the east and west respectively. The deposits which settled from the lower avalanche are typical of this type of ash-flow scores or a hundred feet thick (Anderson and Flett, 1903).

It is possible to infer that the deposits which settled from the overriding cloud are very fine-grained and abundant in vesicular dust, showing a great disparity from those of the basal avalanche in size characteristics and constituents, judging from actual examples of these pyroclastic flow deposits. Such deposits which settled from the

Table 17. Localities of samples.

Sp. no.	Locality
Kc 1-13, Ms 1-4, Ak 1-6	See Fig. 2a.
D 1-4	Ôbako, Kamikawa-machi
TkW 1	Shimizuyama, Furano-machi
Tk 1-13	See Fig. 2c.
S 1-16, Kt 1-2, Ty 1-12	See Fig. 2b.
Km 1-16	See Fig. 2d.
Tw 1-26, Hd 1	See Fig. 2e.
Os 1	Futamata, Mutsu-machi
Tz 1	Funaba, Obonai-machi
On 1	Uehara, Narugo-machi
2	Haguro, Furukawa-shi
3	Tsuidate-machi
Z 1	Zaô hot spring, Yamagata-shi
2	Matsusan, Yamagatashi
4	Yamanokami, Yamagata-shi
Hj 1	Komatsukura, Ôkura-mura
2	Hikagekura, Ôkura-mura
G 1	Tôge, Haguro-machi
B 1	Goshiki-numa
2	South side of Hibara-ko
3	South side of Onogawa-ko
Nm 1	Nakanosawa, Inawashiro-machi
Nn 1-7	See Fig. 2f.
Th 1	Hariu, Yaita-machi
Hr 1	Ikaho hot spring
2-5	Kurosawa, Shibukawa-shi
KS 1-5, Am 1-47	See Fig. 2g.
My 1-11	See Fig. 2h.
Hn 1-14	See Fig. 2i.
KF 1-10	See Fig. 2j.
11	Hôei-zan
F 1-3	Subashiri-mura
4	Ôsaka, Gotenba-shi
5-6	Uchiyama, Yamakita-machi
As 1	Usuki-shi
2	Hitoyoshi-shi
Ai 1-13	See Fig. 2k.

overriding cloud are usually very thin, and easily worn away. Sometimes, however, deposits showing great disparities in their size

characteristics and constituents from those of the main deposits in a single unit of pyroclastic flow are found. They are distributed along the borders and distal ends of the flows, or form the uppermost layer of the deposits. For example, Sp. no. Tk 4 of the 1926 eruption of the Tokachidake Volcano, Sp. no. Hr 3 of the Lower Ash-flow of the Haruna Volcano, Sp. no. Am 16 of the Lower Ash-flow, and Sp. no. Am 30 of the Oiwake Pyroclastic Flow and Sp. no. Am 16 of the Lower Ash-flow of the Asama Volcano are deposits of more finely-grained and more abundant vesicular dust, compared with the bulk deposits of the flows. These deposits afford positive proof of the dual character of pyroclastic flows.

The dual character of pyroclastic flows is considered to be due to the release of gas during flowage. The conspicuous separation of cloud and avalanche may caused by delayed vesiculation and usually occurs in eruptions of the nuées ardentes and the intermediate type pyroclastic flows. It also occurs in eruptions of the St. Vincent type-flows, for the release of gas may continue after the discharge of the flows. In eruptions of the Krakatoa type ash-flows and the Valley of Ten Thousand Smokes type ash-flows, the dual character of the flows may be rather ambiguous, for most of the vesiculation may take place within the conduit.

Sorting Agency

As mentioned in the former chapter, particle size distribution curves of pyroclastic flow deposits do not in general conform to Rosin's law of crushing. This may indicate some efficiency in the sorting agency in the emplacement of deposits. The degree of disparity with Rosin's law is most remarkable in deposits of the St. Vincent type ash-flows. Cumulative curves of the St. Vincent type ash-flow deposits plotted on Rosin law paper show a distinct undulating shape which represents the pronounced bimodal property of size distribution. The deposits usually show a remarkable concentration of crystals in medium fractions as well as the concentration of pumice blocks in coarse fractions. Such size characteristics of the St. Vincent type ash-flow deposits which are different from those of the other types of pyroclastic flow deposits may be attributable to the strong efficacy of sorting in the vertically rising ash column as well as in the descending cloud of flows. Most of the deposits of the St. Vincent type ash-flows are underlain by preceding air-fall deposits, and their volumes are generally much less than those of the preceding air-fall deposits. The volume of the ash-fall is calculated as

0.35 km^3, while that of the ash-flow is 0.025 km^3, in the 1902 eruption of St. Vincent (Hay, 1959). In the 1929 eruption of the Komagatake Volcano, the volume of the air-fall is calculated as 0.4 km^3 or more, while that of the ash-flow is 0.15 km^3. This fact may suggest the subordinate origin of the St. Vincent type ash-flows from the vertically rising ash column.

In the eruptions of St. Vincent in 1902 and of the Komagatake Volcano in 1929, crystal-rich andesitic magma having a high content of gas was discharged through an open carter with relatively low initial velocity. At the time of discharge from the crater-rim, the magma was no longer an effervescing melt but had already disintegrated into frothing clots of pumice and droplets of liquid disrupted into crystals and finely comminuted shards of vesicular glass. Phenocrystic mineral grains and pumice blocks may have concentrated in the slowly rising outer part of the vertical ash column, settling within the turblent current of gas, while lighter shards of vesicular glass were born into the air in suspension. Consequently the dense outer part of the ash column tended to fall to the ground. When once the ash-flow began to descend, gas trapped in the vesicles of ash and pumice escaped and expanded in company with gas newly released by vesiculation from the liquid magma. Consequently the ash-flows were separated into two parts, and phenocrystic mineral grains and pumice blocks were concentrated in the basal avalanche and fine vitric ash was suspended in the overriding cloud. A concentration of crystals is usually found distinctly in the lower part of the deposits, which settled from the basal avalanche, while a concentration of pumice-blocks is seen in the upper part and especially in the front of the deposits. Fine-grained deposits rich in vesicular glass settled from the overriding cloud along the front and margin of the main deposits from the basal avalanche of the ash-flows.

The efficacy of sorting during the flowage of pyroclastic flows, which may cause the marked concentration of crystals in the deposits of their basal avalanches, is recognized in the intermediate type pyroclastic flows and the nuées ardentes. Cumulative curves of size distributions of their deposits, plotted on Rosin's law paper, show irregular lines broken in two nearly straight parts, as already explained. Such features indicate the fact that fine vesicular materials tend to be borne into the overriding cloud by the upward current of expanding gas emitted by auto-explosion during flowage of pyroclastic flows, being transported in suspension within the cloud. Fine materials are transported far from the source and settle beyond the margin and front of the main deposits from the

basal avalanche. In the eruptions of Mt. Pelée in 1902 and the Tokachidake Volcano in 1926, the deposition of fine materials from the overriding cloud was actually recognized. Such separation of the finer and coarser materials within the expanding cloud is explained in the preceding chapter as the dual character of pyroclastic flows.

In the deposits of the basal avalanche of the intermediate type pyroclastic flows, blocks of porous essential fragments tend to concentrate in the upper and frontal part of the deposits, as seen in the deposits of the St. Vincent type ash-flows. It is considered that at the time of settling the movement of flows slows down and the turbulence ceases gradually, changing into the laminar flow, especially in the lower layer of the basal avalanche. Porous blocks are tossed up with the turbulence and rafted on the upper surface of the basal avalanche, while medium particles consisting mainly of crystals settle down from the lower layer of the avalanche.

In the Krakatoa type ash-flows, and perhaps in the Valley of Ten Thousand Smokes type ash-flows, the efficacy of sorting is not as distinct as in the St. Vincent type ash-flows, as indicated by the size characteristics of their deposits. Size distribution curves plotted on Rosin law paper do not show such undulating lines as those of the St. Vincent type ash-flow deposits nor broken lines as with those of the intermediate type pyroclastic flow deposits and the nuée ardente deposits, but exhibit gentle concave lines, as mentioned in the former chapter. The concentration of crystals in medium fractions of the deposits is recognized, but generally not so conspiquous as in deposits of the St. Vincent type ash-flows, and its degree varies widely. The sorting agency in the vertically rising ash column may be not as effective as in the St. Vincent type ash-flows, and sorting in the descending cloud also may be not as effective as in the intermediate type pyroclastic flows and the nuées ardentes. Some effectiveness of sorting, however, may appear during the travelling of flows for long distances from the source. Deposits at the distal ends of flows usually contain large amounts of fine vesicular materials, suggesting such effectiveness of sorting during flowage.

Intermediate Cases between Pyroclastic Flows and Dry Mud-flows

There is a particular type of pyroclastic flow deposit having an intermediate nature between pyroclastic flow deposits and dry mud-flow deposits. They may have originated through violent explosions attended

by a discharge of juvenile materials, sometimes preceding the eruptions of the St. Vincent type ash-flows. Their size characteristics are roughly similar to those of the St. Vincent type ash-flow deposits, although there are small differences between the types of these two deposits. Their size distribution curves exhibit a bimodal character, but their main modes in medium fractions are usually not as pronounced as in the typical deposits of the St. Vincent type ash-flows. Cumulative curves plotted on Rosin law paper show lines similar to those of the St. Vincent type ash-flow deposits, but the remarkable convex crest in the middle part of the curves of the latter tends to disappear. Judging from such size characteristics the mode of initiation of the flows may be somewhat different from that of the typical St. Vincent type ash-flows. It may be able to be inferred that such pyroclastic flows were not attended by the violent emission of a lofty column of ash and steam. They may have been initiated by powerful explosions that caused the collapse of the apical part of the volcanic cone. Discharged materials derived from erupting magma flowed down *en masse*, accompanied by disintegrated rock fragments. Vesiculation may have taken place mostly at the time of explosion and continued during flowage. An expanding cloud of gas and dust may have risen from the flows. Such a mechanism of the flows may be rather similar to the intermediate type pyroclastic flows. The degree of vesiculation of the essential fragments, however, is of the same order as in the typical St. Vincent type ash-flows.

Concluding Remarks

Results of the study on the textural and constituent characteristics of different types of pyroclastic flow deposits are presented in this paper, with some discussions on the mode of origin and mechanism of pyroclastic flow eruptions. The study of the pyroclastic flows is still in a incipient stage, and a great deal of further study is needed. The writer classifies several subdivisions of pyroclastic flows on the basis of of the nature of the representative eruptions of pyroclastic flows actually investigated by geologists and volcanologists, as well as the nature of their deposits. Every discussion mainly centers on these representative eruptions and their deposits. He carried out the analytical investigations on many examples of the pyroclastic flow deposits produced by prehistorical eruptions, and obtained many consistent results sufficient to discuss on the formation and mechanism of pyroclastic flows. There are, however, rather few examples of occurrences of pyroclastic flows

ever investigated on the spot, and some arguments tend to be more or less inferential. Future studies that supply quantitative data to decipher unsolved problems of the phenomena of pyroclastic flows may eliminate the uncertainty of such inferential arguments. Among the main subdivisions classified by the writer, there are all transitions. Future studies may reveal the precise nature of such transitions. The writer could not obtain sure examples of the last subdivision of pyroclastic flows, namely, the Valley of Ten Thousand Smokes type ash-flow or fissure eruption type ash-flow, and the recognition and study of this type of deposit are necessary in the near future in Japan. He omitted in this paper detailed discussions on the origin of the magmas that produce eruption of pyroclastic flow. Herein lies a important problem to be solved, especially in the origin of the magma that produce vast ash-sheets of extremely high magnitude.

---

7. 火砕流堆積物の組織的性質

地震研究所 村 井 勇

概論 1902 年 Martinique 島の Mt. Pelée で烈しい噴火が起つた．側方向に噴出された物質が，ガスとともに一団となつて熱い黒雲を作り，山腹に沿つて非常な速度で流れ下つた．噴火はその後もつづき，同様な噴火が繰り返えされた．これらの噴火は，従来知られていなかつた型式のもので，これに対して，Lacroix は nuée ardente と命名した．同じ 1902 年，St. Vincent の Soufrière でも，同様な噴火が起つた．nuée ardente 噴火はこの二つの噴火によつて確認され，その研究が開始された．1929～1932 年にも Mt. Pelée は同様の噴火を行なつた．Merapi 火山 (1930～1935)，Mt. Lamington (1951～1952) や Hibok-Hibok 火山 (1948～1952) でも同様の噴火が起り，詳しく調査された．このようにして，nuée ardente 噴火は今世紀に入つて次々に確認され，その性質はしだいに明瞭になつてきた．一方，火山砕屑堆積物の研究から，nuée ardente の産物と認められるものが世界各地の火山地域で発見されるようになり，この型式の噴火が地域的にも時代的にもかなり普遍的に起つていることが明らかになつてきた．Fenner (1920, etc.) は Katmai 地域で起つた 1912 年の噴火による噴出物を詳細に調査し，Valley of Ten Thousand Smokes を埋めた火山灰が同様な噴火によるものであることを明らかにした．Moore (1934) は Crater Lake 地域に分布する軽石質堆積物の研究を行ない，“Older pumice” と呼んだ軽石層が，nuée ardente の産物であると結論した．Marshall (1935) は New-Zealand の Taupo-Rotorua 地方に分布する rhyolite tuff が同様に nuée ardente 噴火によるものであることを明らかにした．さらに，Williams (1941) は caldera の成因について詳しい検討を行ない，Krakatoa 火山の 1883 年の噴火のさいに大量の軽石が nuée ardente となつて噴出し，その結果，カルデラの陥没が起つたことを明らかにした．Katmai 地域，Crater Lake 地域や Krakatoa 火山で見られるこのような nuée ardente 起源の軽石質堆積物は，その後，世界各地の火山地帯で次々と発見されている．日本では，1929 年北海道駒ケ岳の噴火のさいに，軽石流の噴出が起つた．久野 (1941) はこの堆積物の特徴が一般の降下軽石堆積物と全く異な

ることを指摘した．さらに久野 (1954) は日本の数多くのカルデラが Williams の説と同様の機巧で生じたことを指摘した．日本の各地に分布する nuée ardente 起源の火山砕屑堆積物の確認と記載は多くの人々の手によつて進められている．

Nuée ardente 噴火の機巧とその原因については，実際の観察記録や堆積物の研究から，いくつかの推論が加えられている．しかし研究が進むにつれて，nuée ardente と呼んできた一連の噴火には，規模も型式も，噴出物の性質も著しく異なるものが含まれていることが明らかとなり，この現象の詳しい検討と解析とが必要になつてきた．Lacroix (1930), Escher (1933), Fenner (1937), MacGregor (1952, 1955), Williams (1957), 荒牧 (1957) らは，nuée ardente の機巧について解析を試み，その分類を行なつている．このようにして，nuée ardente の研究はすでに多くの成果をあげているが，しかしこの分野の研究をさらに前進させるためには，実際の噴火の観察記録をさらに充実させるとともに，噴出物の性質について綿密な定量的な調査を進めることが必要となつている．従来の研究により，nuée ardente 噴火の原因と機巧は，マグマの粘性，溶存ガス含量およびその放出の条件などに関係しており，その噴火型式と噴出物の組織的性質との間には密接な関係があるということが示唆されている．この事は研究の将来の方向を暗示するものといえる．すなわち，噴出物の化学組成，鉱物組成や岩石学的特徴の研究と並行して，その組織，構造，構成物質についての解析が必要と考えられる．従つて nuée ardente 起源の火山砕屑堆積物を sedimentary petrology の諸方法をもつて研究を進めれることは，多くの成果をもたらすものと期待できる．筆者はそのような観点から，日本の各火山に見られる nuée ardente 起源の火山砕屑堆積物について，その組織的諸性質と構成物質について定量的な調査を行なつて，nuée ardente 噴火の原因と機巧の解明に役立つような資料を見出そうと考えて研究を進めている．

用語 nuée ardente: この語は Lacroix が Pelée の噴火に対して用いたものである．しかしその後，Pelée の噴火と類似の性質を持つた噴火が次々に認められるようになり，そのいずれに対しても同一の語が適用され，その意味はきわめて広く解釈されるようになつた．こうした弊害を避けるためには，nuée ardente (熱雲) という語を，本来の Pelée 火山の噴火型式およびそれにきわめて近い型式のものに限つて用いるべきである．荒牧は広い意味の nuée ardente に代るものとして pyroclastic flow (火砕流) という語を提唱している．筆者もこれに従うことにする．

ash-flow: 火砕流堆積物の最も顕著な性質は，いろいろな粒径の粒子が雑然と混合していることである．しかし，大部分の堆積物は中位粒径が火山灰の粒径 (1/4～4 mm) 付近にあり，大きな比率で細粒物質が含まれている．これに対して，Smith (1960) は“ash flow deposit”(灰流堆積物) という語を提唱し，直径 4 mm 以下の粒子が 50% またはそれ以上の比率を占めるものと定義している．この語は従来用いられてきた tuff flow, volcanic sand flow, pumice flow, ignimbrite, welded tuff 等々の語のほとんど大部分のものを含めて用いることができる．筆者はこの語を，その火砕流の分類に採用している．

mud-flow: 火砕流堆積物と外見の非常によく似た堆積物に泥流堆積物がある．mud-flow (泥流) という語は一般には非常に広い意味で用いられている．実際に泥流堆積物と呼ばれているものを調査すると，いろいろな成因のものが含まれており，その意味はきわめてあいまいとなつている．ここでは筆者は，爆発によつて火山体が崩壊して発生した泥流堆積物のみを特に取りあげて，その組織的性質を論じたいと思う．このようなものをここでは dry mud-flow と呼ぶことにする．

火砕流の分類 火砕流にはいろいろの型式のものがあり，多くの人々によつてその分類が行なわれている．それらの分類のなかで最も基本的なものは Lacroix (1930) と Escher (1933) の分類である．Williams (1957) はさらに詳しい検討を加え，堆積物の特徴を詳述している．いずれも観察された実際の噴火についての研究の結果に基づいて分類が行なわれている．これらの分類に対し，荒牧の分類 (1956) はその基準が火砕流堆積物の性質に置かれている．この二つの分類法は出発点は異なるが，その内容は決して矛盾するものではない．火砕流の機巧は噴出物の性質と密接な関係があり，この両者を切離して考えることはできないからである．筆者は従来の分類に若干の手を加え，次のような scheme を作つてみた．この分類の基準は，実際の噴火の機巧及びその噴出物の性質に置かれている．(第 1 表および第 2 表参照)

熱雲	Pelée 型, (Merapi 型) 桜島型
中間型火砕流	
灰流	St. Vincent 型 Krakatoa 型 Valley of Ten Thousand Smokes 型

粒度組成 筆者の調査した火山は第1図および第3表に示す通りである．これ以外にも火砕流堆積物および泥流堆積物の例はいくつか知られているが，未だ調査の機会を得ていない．試料を採集して機械分析を行なつたが，その結果を総括して下に列記する．(第4, 5, 6, 7表および第3, 4, 5図参照)

1) 分級の悪さ．火砕流堆積物は分級が悪いことが特徴であり，この性質に基づいてこの種の堆積物の確認が行なわれている．標準偏差のパラメーターである $\sigma\phi$ は2～5の値をとり，一般の降下火砕堆積物がほとんど2以下の値をとるのと全く対称的である．mode の部分の占める比率が降下堆積物では ϕ scale の1区間について30% 以上になる場合が屢々であるが火砕流堆積物では25% 以上になることはほとんどなく，大部分の場合15～20% 程度である．火砕流堆積物では降下堆積物に見られるような火口からの距離に応じた粒度の変化は見られない．

2) 均質性．火砕流堆積物は単一の unit の中ではきわめて均質な性質を示し，試料間のばらつきは少ない．従つて粒度分布曲線はよくそろい，パラメーターの値は狭い範囲内に入る．また同一の火山から噴出した，時代を異にする火砕流堆積物は屢々ほとんど同様の粒度組成を示す．これは同一の火山では同様の火砕流噴火が屢々繰り返えされることを示している．大規模な火砕流では，かならずしも全体が同一時期に噴出したものではない場合が多いが，しかしそれらの全体を通じて粒度組成の特徴は同一の傾向を明瞭に示している．隣接する火山相互の間にも火砕流堆積物が類似の性質を示す傾向が認められることが多い．

3) 中位粒径 $Md\phi$ の値はかなり広い範囲にわたるが，大部分のものは ϕ: -2～4 の範囲に入る．すなわち大分部の火砕流堆積物は粒度組成からいえば Smith (1960) の定義による“ash flow deposit”に属する．火砕流堆積物の分類による各々の型では，$Md\phi$ の値が大体一定の範囲にある，すなわち，中間型火砕流および熱雲では $Md\phi > 1$, St. Vincent 型では，0～2, Krakatoa 型では0～4 である．

4) 粒度分布曲線の形．火砕流堆積物の粒度分布曲線の形はきわめて特徴的なものである．分級は悪く，分布曲線は粗粒部と細粒部に長く尾をひく．これは，降下堆積物の粒度分布曲線が粗粒部の尾が鋭く切られていることと全く対照的である．さらに細部について見れば，火砕流の型の相異に応じて，その堆積物の粒度分布曲線の型も変化している．$Md\phi$ の値は前記の通り広い範囲にわたつて変化する．歪度は正，負両方の場合があり，中間型火砕流では特に負の傾向が大きい．これは降下堆積物の場合正の傾向が大きいのと全く対照的である．尖度のパラメーターである $\beta\phi$ の値を見れば，0.65 (正規分布の場合) を中心にして上下に広く分布する．しかし一般には 0.65 より大きい値をとる傾向が見られる．粒度分布の型は unimodal と bimodal と両方の場合がある．Krakatoa 型灰流には中粒のものと細粒のものとあり，細粒のものはほとんど unimodal, 中粒のものは bimodal の傾向をわずかに示す．St. Vincent 型灰流は bimodal の傾向が著しく，かつ主 mode が卓越する傾向を示す．中間型火砕流および熱雲では bimodal の傾向が特に顕著となり，かつ分布曲線は変動が大きくなる．中粒部の主 mode はむしろ低くなり，全体として分級は非常に悪くなる．Krumbein と Tisdel (1940) によつて指摘されたような火砕流堆積物の粒度分布が Rosin の法則に適合するという事実は，一般には認められない．これは粒度分布の bimodal な性質からもただちに明らかなことである．Rosin の法則に従わないということは，分級作用がある程度有効に働らいていることを示すものと見られる．Rosin 紙に描かれた積算曲線は火砕流の各型にそれぞれ特徴的な形を示す．すなわち，Krakatoa 型灰流はなだらかな凹形，St. Vincent 型灰流は二つの山をもつ波形，中間型火砕流および熱雲は中央で折れた直線形を示す (第9図参照)．

5) 火砕流の各型の堆積物の粗度組成．火砕流の各型の堆積物にはそれぞれ特徴的な粒度組成が認められる．

細粒 Krakatoa 型灰流堆積物および V.T.T.S. 型灰流堆積物：細粒，unimodal，正規分布に近い型，分級は悪い．

中粒 Krakator 型灰流堆積物：中粒，unimodal であるが，かすかに bimodal の傾向を示す，中粒部の分級は，St. Vincent 型のようにはよくない．

Vt. Vincent 型灰流堆積物：中粒，bimodal，中粒部の分級はいちじるしくよく，卓越する主 mode を示す．しかし粗粒部に顕著な副 mode があり全体としては $\sigma\phi$ の値は大きくなる．

中間型火砕流堆積物および熱雲堆積物：粗粒ないし中粒，bimodal，粒度組成の変化は大きい，中粒部の主 mode は St. Vincent 型灰流のように顕著ではない．

6) dry mud-flow および自破砕熔岩流の粒度組成．火砕流堆積物，特に中間型火砕流および熱雲の堆積物は dry mud-flow の堆積物と粒度組成の点できわめてよく類似している．しかし dry mud-flow の堆積物の場合は均質性が乏しく，分布曲線の形の変化が著しく，分級はさらに一段と悪く，細粒部が特に多量となるなどの点で，火砕流堆積物と異なつている．構成物質についていえば，後者が本質破片を含まぬという点で全く異なつている．自破砕熔岩流も火砕流ときわめてよく似た粒度組成を示す．しかし，分布曲線の形の変化は非常に大きく，火砕流堆積物の場合のような均質性が認められない．恐らくこの二つのものの粒度組成は Rosin の法則に従う傾向があると考えられる(第 10 図参照)．

粒子の円磨度　火砕流堆積物を構成する粒子の roundness (円磨度)はその噴出および流動の状態を示す重要な要素と考えられる．筆者はその直径 32～4 mm の粒径のものについて Krumbein (1941) の方法で円磨度を測定した．また，火砕流の直前，あるいは同時に噴出した降下堆積物の試料を採集して，同様に構成粒子の円磨度を測定した(第 13 表参照)．その結果，次のような事実が知れた．

火砕流堆積物の構成粒子は普通に考えられていたように著しく円磨されてはいない．St. Vincent 型灰流と Krakatoa 型灰流では円磨度の値は 16～8 mm の粒子についていえば，一般に 0.3～0.5 の範囲の値を示す．孔隙率の大きい粒子ほど円磨度の値は大きくなる傾向を示すが，しかし石質破片と多孔質本質破片との間の円磨度の差は 0.1 程度にすぎない．同時，あるいは相次いで噴出した火砕流堆積物と降下堆積物とでは，後者の粒子の方が円磨度の値は小さい．しかしその差は 0.1 程度にすぎない．この事実は，粒子の円磨が火道の途中においてすでに始まつていることを示している．火砕流の流下中には，放出されたガスが滑剤として働らくために，粒子の円磨がその間に著しく進行することはないと考えられる．中間型火砕流と熱雲では，粒子はかなり角ばつており，16～8 mm の粒子については円磨度は 0.25～0.4 である．孔隙率の大きい軟かい粒子の方が，密度の大きい硬い粒子や石質破片より角ばつている場合が屢々あり，これは明らかに火砕流の流動中にガスの放出が続いて，多孔質本質破片の粒子が角ばることを示している．熱雲の流動の機巧については，“auto-explosion”の性質が多くの学者により重要視されているが，中間型火砕流についても同様と見られる．これに対し，灰流の場合は“auto-explosion”の性質がその流動の機巧の主要因をなしていると見ることはできない．

本質破片の形状　火砕流堆積物の本質破片は非常に多孔質であることが特徴である．岩漿からのガスの放出の条件が火砕流の形成と流動の機巧において重要な要因となつていると考えられるから．このガス放出の過程を知ることはきわめて重要であるが，それは本質破片の形状に明瞭に反映されている．特に注目すべき点は，長くひき伸ばされた気泡をもつた軽石質破片のあることと，その量である．このような粒子は細粒 Krakatoa 型灰流およびおそらく V.T.T.S. 型灰流に特に著しい．これに対して中間型火砕流および熱雲では気泡は不規則な形をしており，引き伸ばされたあとは見られない．St. Vincent 型灰流ではこの両者の中間の状態を示す．火砕流の各型の間に見られるこのような本質破片の形状の相異は，ガスの放出の過程の相異を明瞭に示すものである．(第 14 表参照)

構成物質　火砕流堆積物はいろいろな種類の粒子によつて構成されている．特に lapilli の粒径以上のものは多孔質の本質破片と各種の石質破片とによつて構成され，その構成の比率は火砕流の各型の特徴をよく表現してるい．これに対して ash の粒径の部分は主として結晶粒によつて構成されている．細粒の部分はガラス片および結晶片よりなる．Krakatoa 型灰流では類質および異質石質破片はかなり高い比率を示す．その岩石は基盤および火道の周囲の岩石と考えられるもので，流下の途中で火山体の表面より取り込まれた岩石はごく少ない．St. Vincent 型灰流では，類質および異質石質破片の比率は一般に低い．しかし，石質破片の比率の極度に高いものもあり，この場合，岩石

は火山を構成していた岩石から由来したと考えられ，また別に火道を埋めていたと見られる結晶度の高い同源石質破片が認められる場合が多い．このような型の灰流はむしろ dry mud-flow との中間の性質を持つたものであり，厳密には，St. Vincent 型灰流とは区別しなければならない．典型的な St. Vincent 型の灰流では石質破片の量は少なく，中粒部に結晶の著しい集中が認められる．すでに Hay (1959) が明らかにしているように，噴出のさいのガス圧力が低いことから，垂直方向の分級が噴火雲の柱中，特に外側の部分で起り，灰流の発生の原因となつたと考えられる．中間型火砕流では本質破片はかなり緻密なものから著しく多孔質なものまで見られるのが特徴である．火山弾の形状を示すものが普通に見られる．多孔質な破片は円磨度の値が非常に小さく，auto-explosion のあとを見せている．類質および異質石質破片は一般に少ない．しかし，流下のさいに火山体の表面より多量の岩片を取り込む場合がある．熱雲のうち Pelée 型の堆積物では円頂丘の皮殻を作つていたと見られる結晶質の同源石質破片が多孔質な本質破片とともに存在する．この同源石質破片は角ばり，多面形を呈する．類質または異質石質破片の量は非常に少ない．火山弾はほとんど見られない．桜島型熱雲では事情は少し異なつている．粗粒の岩塊はすべて本質岩塊で auto-explosion を示す著しく特徴的なパン皮状火山弾の形状を見せている．(第 15 表参照)

本質破片の見かけの比重　火砕流の噴出機巧を支配する最大の要因は magma 中の溶存ガスの量であり，それは本質破片の発泡状態，即ち孔隙率に反映されていると考えられる．本質破片の孔隙率を正確に測定することは非常に困難であるので，筆者は見かけの比重を測定して見た．その値は一般に変動が大きいが，試料数を十分大きくとれば，だいたい一定の平均値を求められる．この平均値について見ると，Krakatoa 型灰流では 0.5～0.7，St. Vincent 型灰流 (dry mud-flow との中間型も含めて) では 0.7～1.2，中間型火砕流では 1.2 以上となる．中間型火砕流では，特に各粒子についての変動が著しいのが特徴である．(第 16 表参照)

噴火の順序　火砕流の噴出に先行して爆発的な噴火が起り多量の軽石や火山灰を降らせることは屢々認められている．Kennedy (1955)，山崎 (1959)，勝井 (1960) によつて指摘されているように，一般に噴火の初期には magma 柱の上部のガスを多量に含んだ部分の噴出により爆発的噴火が起り，噴火の後期には次第に下部のガスに乏しい部分が上昇して，lava の流出に移行するという傾向が認められ，その推移の途中において火砕流の噴出が起ると考えられる．この間に岩漿の性質が silicic から mafic へと変化したことが確かめられた例も多い．このような事実は，火砕流の形成の主な要因が岩漿中のガスの量およびその放出の条件にあることを明瞭に物語つている．

化学組成　火砕流堆積物は岩石学的にも化学組成の上からも大きな範囲にわたつて変化を示している．玄武岩質の岩漿の噴火によつて生ずる火砕流はほとんど認められないが，安山岩，石英安山岩，流紋岩質の岩漿の噴火では屢々火砕流が認められる．SiO_2 含量は一般には，55% より 75% の範囲に入る．熱雲，中間型火砕流および St. Vincent 型灰流では SiO_2 % が 55～65% の範囲に入るものが多い．これに対して Krakatoa 型灰流では 65～75% の場合が多い．V.T.T.S. 型灰流では Krakatoa 型の場合とほぼ同程度であるが 75% を越えるものもある．火砕流堆積物中の本質破片はほとんどの場合，多孔質で非晶質の石基を有し，石基の鉱物の組合せから岩石系を知り得る場合は少ない．しかし，化学分析の結果から Fe－Mg－Na＋K 図型上に plot すれば，少数の例外を除けば，すべて久野 (1950, 1953) の紫蘇輝石質岩系の区域に入る．紫蘇輝石質岩系は本源岩漿が花崗岩質岩石による混成作用を受け，かつ分別結晶作用を行なつた結果生成したものであると解釈されるから，火砕流を生ぜしめた岩漿の殆んどが混成作用を受けたものであることが知れる．混成作用によつて水その他の揮発性物質が岩漿のなかに濃縮すると見られ，このような揮発性物質を特に多量に含んだ岩漿の噴火により火砕流が生ずるものと考えられる．

火砕流の形成と流動の機巧　[ガス放出の過程] 火砕流堆積物の粒度組成，本質破片の形状，円磨度などから判断して，Krakatoa 型灰流 (および V.T.T.S. 型灰流) では発泡が地下深処から始まり，火道を上昇する間に岩漿の大部分は泡立ち，細かく砕かれ，噴出口から烈しい爆発を伴なわずに流出して火砕流を形成すると解釈される．一方 St. Vincent 型灰流では，発泡は火口内からはじまり，火口の縁では岩漿は一部泡立ち，一部液体のままの状態にあり，噴火は爆発的ではあるが，噴出のガス圧力は著しく高くはなく，噴火雲の内部特に外側で分級を受けた重い物質，すなわち粗粒の軽石と結晶粒とが，その重さのために落下して火砕流を形成すると考えられる．中間型火砕流では，

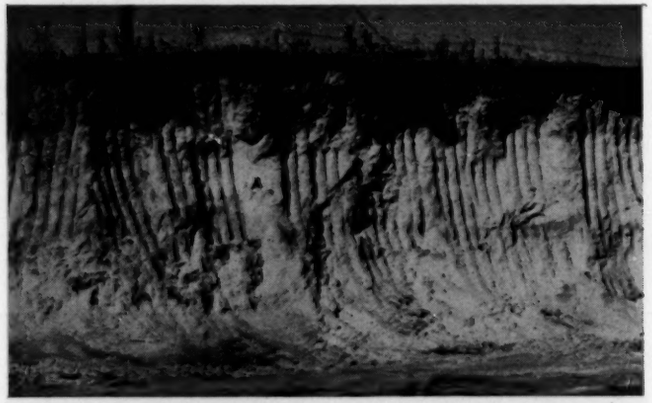

Fig. 16. The Middle Ash-flow of the Kutcharo Volcano. Sp. no. Kc 9, Notoro, Abashiri-shi.

Fig. 17. The Middle Ash-flow of the Kutcharo Volcano. Sp. no. Kc 8, Heiwa, Abashiri-shi.

Fig. 18. The Upper Ash-flow of the Kutcharo Volcano. Sp. no. Kc. 6, Hiushinai, Tanno-mura.

Fig. 19. The Ash-flow of the Mashu Volcano. Sp. no. Ms 3, Minakami, Koshimizu-machi.

Photographs of pyroclastic flow deposits

(震研彙報 第三十九号 図版 村井)

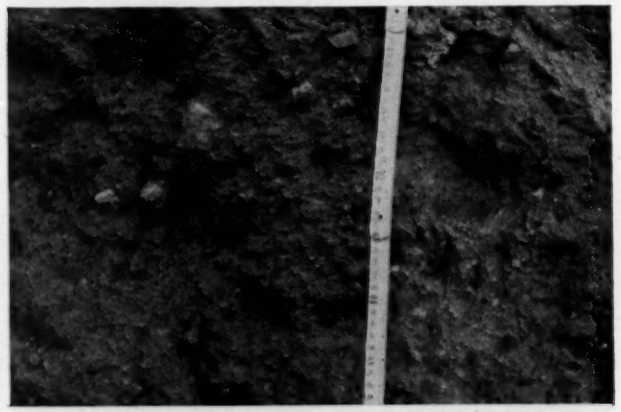

Fig. 20. The Meakandake Pyroclastic Flow of the Akan Volcano. Sp. no. Ak 4, Kamihakuai, Ashoro-machi.

Fig. 22. The 1929 Pyroclastic Flow of the Tokachi-dake Volcano. Sp. no. Tk 6, Bôgakudai.

Fig. 21. Non-welded part of the Tokachi Welded Tuff. Sp. no. TkW 1, Shimizuyama, Furano-machi.

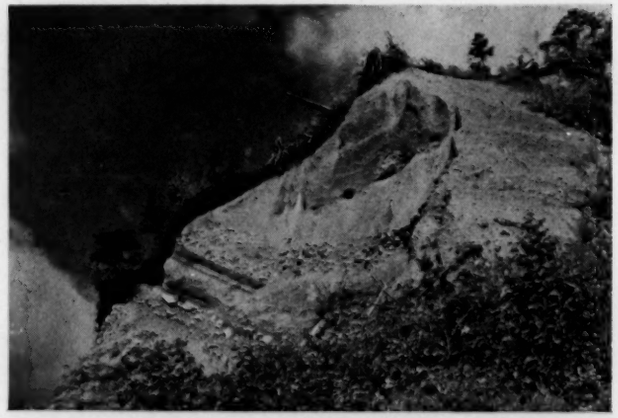

Fig. 23. The Ash-flow and the preceding ash-falls of the Daisetsuzan Volcano. Sp.no. D 2, Ôbako, Kamikawa-machi.

Photographs of pyroclastic flow deposits

（震研彙報 第三十九号 図版 村井）

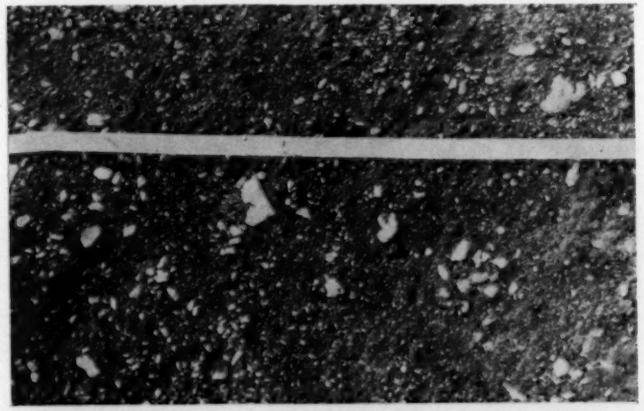

Fig. 24. The Ash-flow of the Shikotsu Volcano. Sp. no. S 7, Tomakomai-shi.

Fig. 26. The Upper Ash-flow of the Toya Volcano. Sp. no. Ty 5, Tateyama, Date-machi.

Fig. 25. The Upper Ash-flow of the Kuttara Volcano. Sp. no. Kt 2, Noboribetsu hot spring.

Fig. 27. The 1929 Ash-flow of the Komagatake Volcano Sp. no. Km 4, Akaigawa, Mori-machi.

Photographs of pyroclastic flow deposits

（震研彙報 第三十九号 図版 村井）

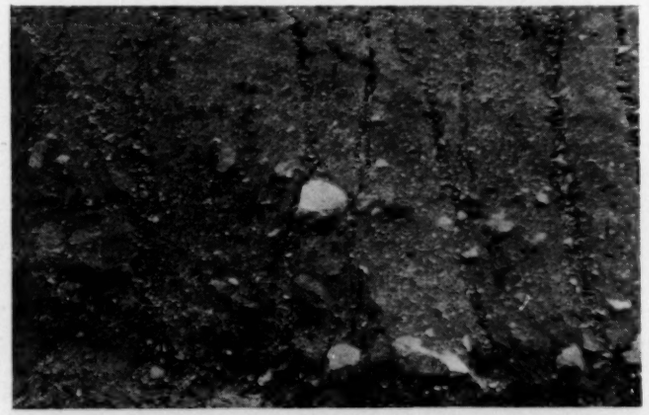

Fig. 28. The Ash-flow of the Towada Volcano. Sp. no. Tw 14,Nigorigawa, Kosaka-machi.

Fig. 30. The Older Ash-flow of the Towada Volcano. Sp. no. Tw 22, Nenokuchi.

Fig. 29. The Ash-flow and the preceding ash-fall of the Towada Volcano. Sp. nos. 17 and 23, Gonohe-machi.

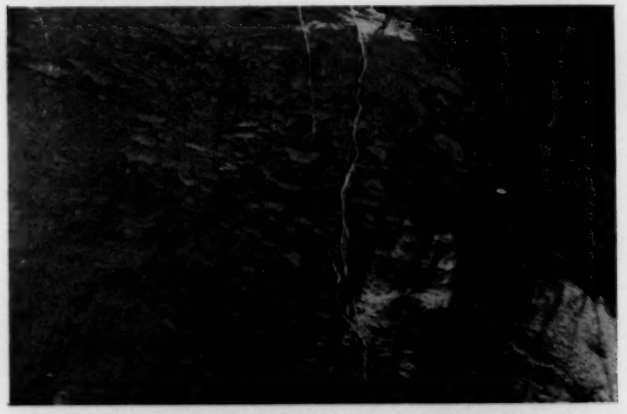

Fig. 31. The Welded Tuff of the Hakkoda Volcano. Sp. no. Hd 1, Moya, Aomori-shi.

Photographs of pyroclastic flow deposits

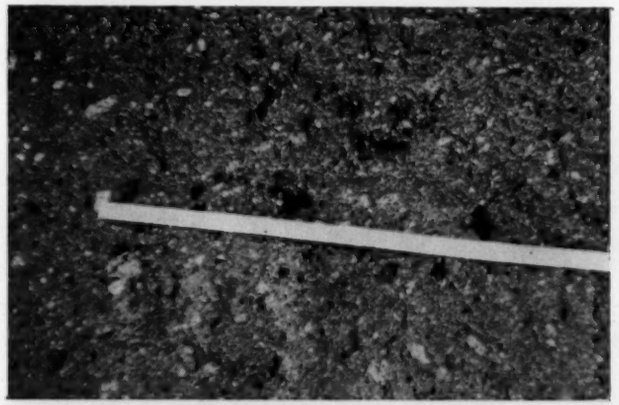

Fig. 32. The Ash-flow of the Osoreyama Volcano. Sp. no. Os 1, Futamata, Mutsu-shi.

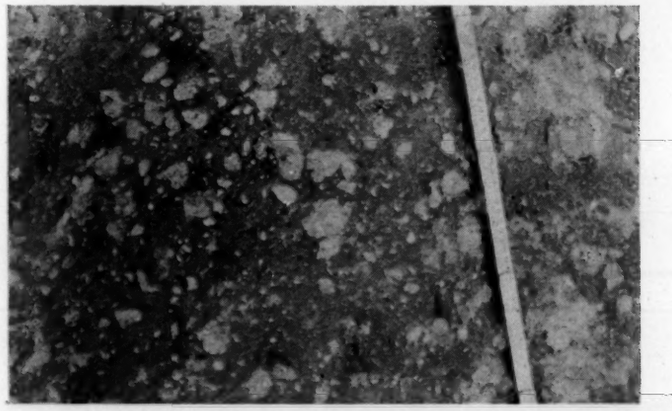

Fig. 34. The Ash-flow of the Onikobe Volcano. Sp. no. On 2, Haguro, Furukawa-shi.

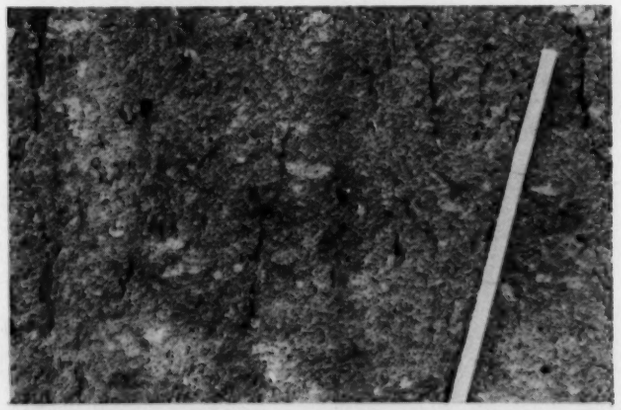

Fig. 33. The Tazawa Welded Tuff. Sendatsu, Obonai-machi.

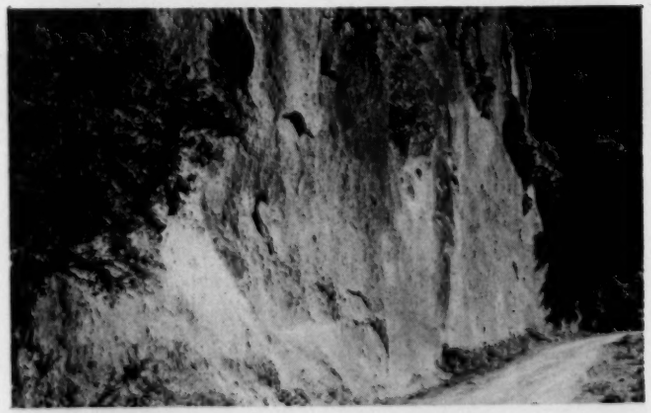

Fig. 35. The Ash-flow of the Hijiori Volcano. Sp. no. Hj 2, Hikage, Ôkura-mura.

Photographs of pyroclastic flow deposits

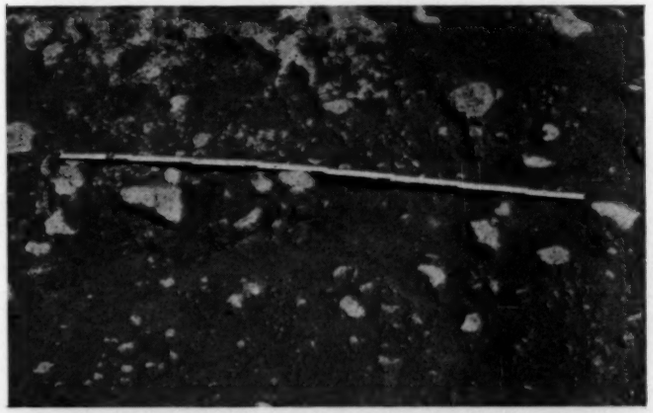

Fig. 36. Non-welded part of the Numajiri Welded Tuff. Sp. no. Nm 1, Nakanosawa, Inawashiro-machi.

Fig. 38. The Scoria-flow of the Nantai Volcano. Sp. no. Nn 1. Misawa, Nikkô-shi.

Fig. 37. The Ash-flow of the Takaharayama Volcano. Sp. no. Th 1, Hariu, Yaita-machi.

Fig. 39. The Pumice-flow of the Nantai Volcano. Sp. no. Nn 3, Arasawa, Nikkô-shi.

Photographs of pyroclatic flow deposits

Fig. 40. The Lower Ash-flow of the Haruna Volcano. Sp. no. Hr 1, Ikaho-machi.

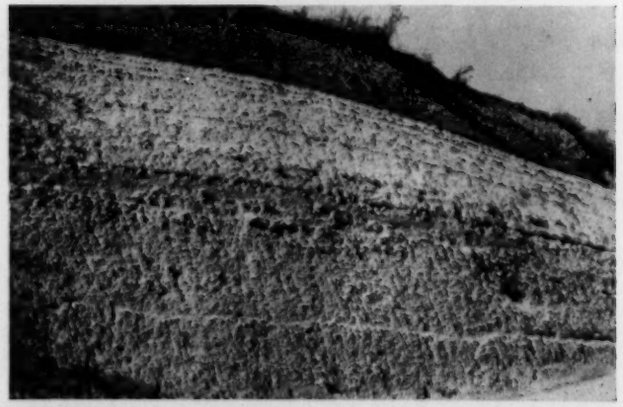

Fig. 41. The Lower and Upper Ash-flows and the preceding pumice-fall of the Haruna Volcano. Sp. nos. Hr 2, 4 and 5, Kurosawa, Shibukawa-shi.

Fig. 42. The Ash-flow of the Kusatsu-Shirane Volcano. Sp. nos. SK 3 and 4, Mihara, Tsumagoi-mura.

Fig. 43. The Pyroclastic Flow of the Myoko Volcano. Sp. no. My 2, Tsubamegawara, Myôkôkôgen-mura.

Photographs of pyroclastic flow deposits

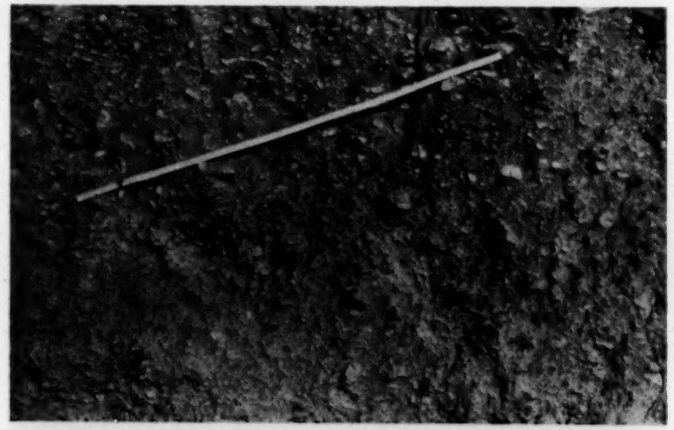

Fig. 44. The Upper Ash-flow of the Asama Volcano. Sp. no. Am 20, Matsubayashi, Komoro-shi.

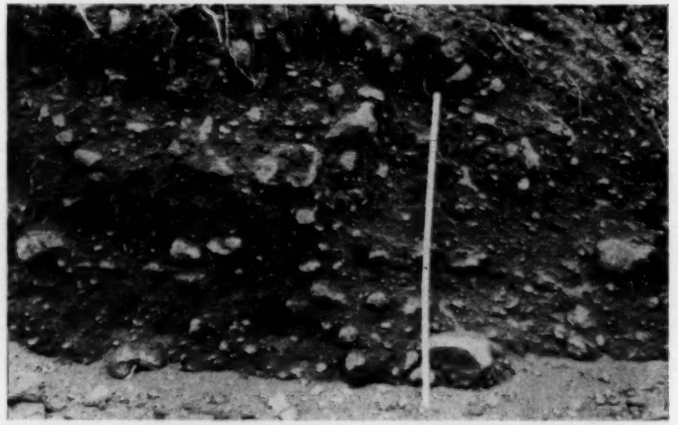

Fig. 46. The Agatsuma Pyroclastic Flow of the 1783 eruption of the Asama Volcano. Sp. no. Am 32, Kuromame-gawara, Naganohara-machi.

Fig. 45. The Oiwake Pyroclastic Flow of the Asama Volcano. Sp. no. Am 28, Mitsuya, Miyota-machi.

Fig. 47. An essential block of the Kambara Nuée Ardente of the 1783 eruption of the Asama Volcano.

Photographs of pyroclastic flow deposits

（震研彙報 第三十九号 図版 村井）

Fig. 48. The Ash-flows of the Hakone Volcano. Sp. nos. Hn 6 and 8, Hakone-machi. The upper layer is scoriaceous and the lower layer is pumiceous.

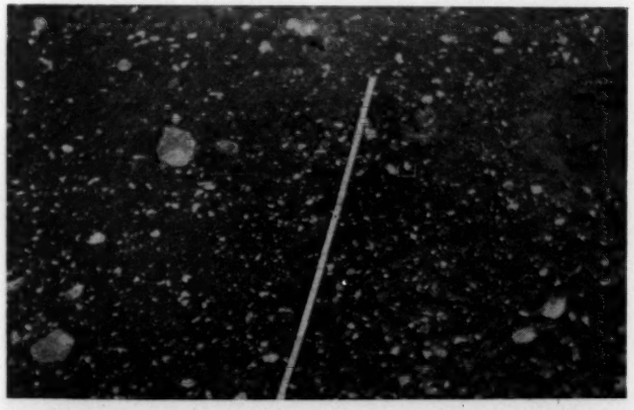

Fig. 50. The Ash-flow (scoriaceous) of the Hakone Volcano. Sp. Hn 10, Mishima-shi.

Fig. 49. The Ash-flow (pumiceous) of the Hakone Volcano. Sp. no. Hn 1, Ashigara, Odawara-shi.

Fig. 51. The Central Cone Pyroclastic Flow of the Hakone Volcano. Sp.Hn 11, Ubako, Sengokuhara-mura.

Photographs of pyroclastic flow deposits

Fig. 52. The Pyroclastic Flow of the Ko-Fuji Volcano. Sp. no. KF 1, Tanukinuma, Fujimiya-shi.

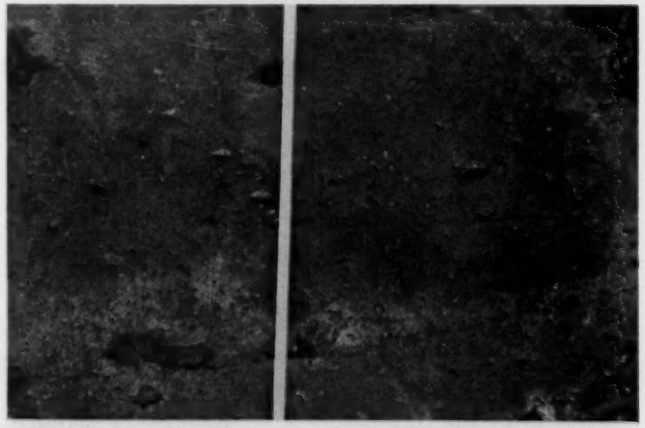

Fig. 53. The Ash-flow of the Aso Volcano. Sp. no. As 2, Hitoyoshi-shi.

Fig. 54. The Middle Ash-flow of the Aira Volcano. Sp. no. Ai 1, Taguchi, Kirishima-mura.

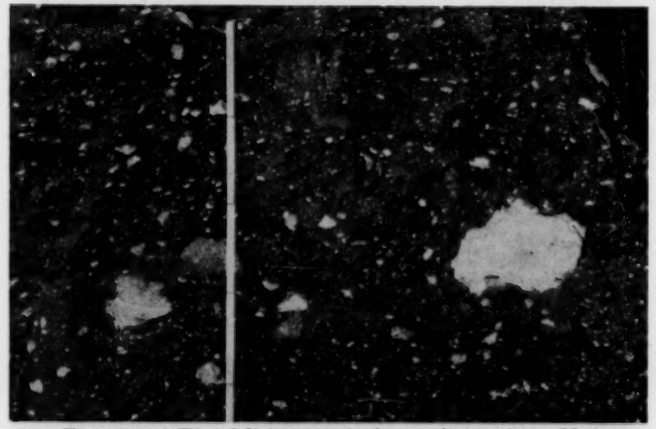

Fig. 55. The Middle Ash-flow of the Aira Volcano. Sp. no. Ai 13, Imaizumi, Ibusuki-shi.

Photographs of pyroclastic flow deposits

Fig. 56. The Sukawa Mud-flow of the Zaô Volcano. Sp. no. Z 1, Zaô hot spring, Yamagata-shi.

Fig. 58. A lava flow of Meakandake. Sp. no. Ak 5, Ashoro-machi.

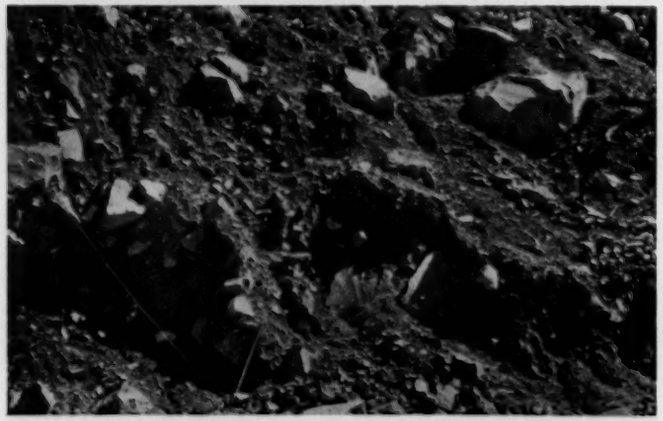

Fig. 57. The 1888 Mud-flow of the Bantai Volcano. Sp. B 3, Kitashiobara-mura.

Fig. 59. A lava flow of the Fuji Volcano. Sp. no. F 2, Shimoawakura, Fujimiya-shi.

Photographs of dry mud-flow deposits and auto-brecciated lava flows

岩漿が火口から噴出するさいおよびその後に発泡が起る．この場合，火山灰が火口から垂直に高く抛出されることはなく，噴出物は一団の泡立つ火砕流となつて山腹を流下する．熱雲の場合も，同様に発泡は火砕流の流動の途中に主として起る．

[火砕流の二体性] 多くの学者によつて指摘されているように，火砕流は二つの部分，すなわち下部の粗粒の物質を含む火砕流の本体と，その上部にひろがる火山塵とガスの雲とに分かれて流下する．このような性質は中間型火砕流と熱雲の場合に特に著しい．これは火砕流の流下の途中で烈しい発泡が起るため，すなわち auto-explosion のためである．放出されたガスは滑剤として働らき，火砕流は非常な速度で流動する．灰流の場合では発泡は主として噴出以前あるいは噴出のさいに起るが，しかしガスの放出は流動の間でも続くと考えられるから，同様の性質を示すと見られる．St. Vincent 型灰流では特にこの性質が顕著に認められる．

[分級作用] 火砕流は乱流の状態で烈しく流下し，分級のかなり悪い堆積物をそのあとに残す．しかしこの間に分級作用はある程度有効に働らき，堆積物は特徴的な粒度組成を持つようになる．分級作用は噴出のさいにも火砕流の流下の途中にも起る．St. Vincent 型灰流では，垂直に上昇する噴火雲のなかで重い粒子が分級作用を受けて落下し，火砕流を形成するが，流下の途中でもガスの放出が続いて細粒物質は上空に運ばれ，粗粒の軽石と結晶粒が特に集中した堆積物を生ずる．中間型火砕流および熱雲でも，流下中に起る auto-explosion により多量の細粒物質が上空に運ばれる．Krakatoa 型灰流および V.T.T.S. 型灰流でもある程度の分級作用が働らくと考えられ，粒度組成は Rosin の法則に適合しなくなる．

[dry mud-flow との中間的性質を有するもの] St. Vincent 型灰流堆積物と共通の性質をもち，類質および異質石質破片の比率が極端に高い堆積物が屢々見られる．これは St. Vincent 型灰流に伴なう場合が多く，特にその最下部を構成する場合が多い，おそらく爆発的噴火によつて火山体の一部が破壊され，同時に多量の本質破片が噴出して火砕流を形成したものと解釈される．このようなものは多くの点で火砕流と dry mud-flow との中間的性質を示している．

BULLETIN OF THE EARTHQUAKE
RESEARCH INSTITUTE
Vol. 39 (1961), pp. 255-283

8. *Crustal Structure in Japan from the Phase Velocity of Rayleigh Waves.*

Part 1. Use of the network of seismological stations operated by the Japan Meteorological Agency.

By Keiiti AKI,

Earthquake Research Institute.

(Read March 28, 1961.—Received March 31, 1961.)

Introduction

The phase velocity of Rayleigh waves was first successfully utilized by Press (1956) in a study of crustal structure in the southern California. The application of this new method has been extended to northern California by Press (1957), and to the entire United States by Ewing and Press (1959). Press (1960) and Oliver, Kovach and Dorman (1961) refined the method with the aid of electronic computers. In Japan, an application of the method has been tried by Shima et al. (1960) with the use of the tripartite stations ; Matsushiro, Tsukuba and Abuyama.

For successful application of the method, it is essential to use purely isolated Rayleigh waves. Press showed that Rayleigh waves with periods from 35 to 15 sec, which have traversed a long oceanic path before entering the area to be studied, are most suitable for this purpose.

In the present study, we used the records of the Samoa shock of April 14, 1957 (19 h 17 m 57 s GCT, 15.5°S, 173°W.) obtained at the network of seismological stations operated by the Japan Meteorological Agency. This is the same earthquake on which Ewing and Press (1959) based their phase velocity measurement for the entire United States. Rayleigh waves with periods 30 to 20 sec from this earthquake are fairly clearly recorded by Wiechert seismographs at many of the J.M.A. stations. The Wiechert seismographs operated at these stations are adjusted to maintain an uniform characteristic (pendulum period 5.0 sec, geometric magnification 70 to 80, and the damping ratio 6 to 8). The dynamic magnification of this instrument at the period of 30 sec is about 1.5. At these long periods the absolute value of the instrumental phase delay is small, and its variation from station to station can be

overlooked. This is the advantage of using a short period instrument

Table 1. List of stations.

Station	Abbreviation	Longitude		Latitude	
		deg.	min.	deg.	min.
Sapporo	SA	141	19.8	43	03.5
Aomori	AO	140	47.0	40	49.0
Hachinohe	HA	141	31.5	40	31.5
Akita	AK	140	06.0	39	43.0
Morioka	MO	141	10.0	39	41.7
Miyako	MY	141	58.0	39	38.6
Sendai	SE	140	54.0	38	15.5
Toyama	TY	137	12.5	36	42.3
Nagano	NA	138	11.7	36	39.5
Utsunomiya	UT	139	52.2	36	32.7
Kumagaya	KU	139	23.0	36	08.7
Mito	MT	140	28.2	36	22.6
Gifu	GI	136	45.8	35	23.8
Nagoya	NY	136	58.0	35	09.8
Kofu	KF	138	33.5	35	39.8
Kameyama	KA	136	27.8	34	51.3
Omaezaki	OM	138	12.7	34	36.1
Shizuoka	SZ	138	24.3	34	58.3
Mishima	MS	138	55.7	35	06.6
Tokyo	TK	139	45.6	35	41.1
Owashi	OW	136	11.6	34	04.0
Yokohama	YO	139	39.2	35	26.1
Tomisaki	TS	139	49.6	34	55.1
Oshima	OS	139	22.6	34	45.6
Toyooka	TO	134	49.1	35	32.1
Kyoto	KY	135	44.0	35	00.6
Hikone	HK	136	14.7	35	16.3
Hiroshima	HR	132	26.1	34	21.7
Osaka	OK	135	32.2	34	38.8
Sumoto	SU	134	54.5	34	20.0
Tomie	TM	128	45.8	32	36.5
Kagoshima	KG	130	33.1	31	34.3
Miyazaki	MZ	131	25.5	31	55.0
Yakushima	YA	130	29.7	30	27.0
Takamatsu	TA	134	03.5	34	19.0
Kochi	KO	133	32.0	33	33.0

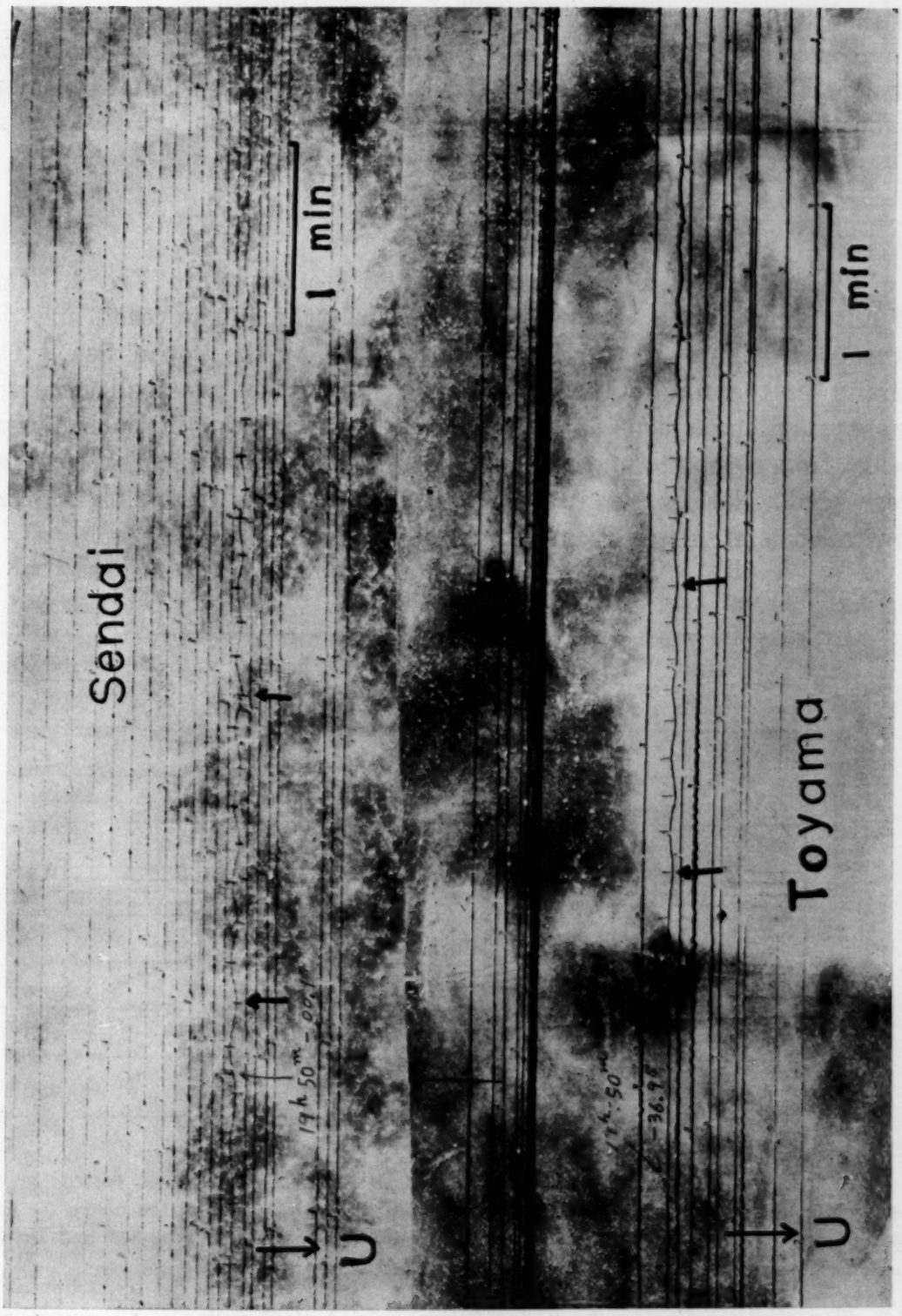

Fig. 1. Rayleigh waves from the Samoa shock of April 14th, 1957 recorded by the seismographs at Sendai (near the Pacific coast) and Toyama (near the Japan Sea coast). The arrows indicate the peaks, of which the wave front charts are given in Figs. 3 and 4.

in the phase velocity study as emphasized by Press.

The seismograms were kindly supplied from about 40 seismological stations through the Seismology Division of the Japan Meteorological Agency. The records of 35 stations are used in the present study. The list of the stations is given in Table 1.

Data

Typical records of the Rayleigh waves are shown in Fig. 1. One of the records was obtained at Sendai near the Pacific coast, and the other was obtained at Toyama near the coast of the Japan Sea. The arrows in the figure indicate the peaks for which we shall trace the propagation throughout Japan. There was no difficulty in tracing these peaks from station to station, because the distances between stations are very small. Misidentification of the peak leads to an impossibly high or low velocity of propagation for Rayleigh waves.

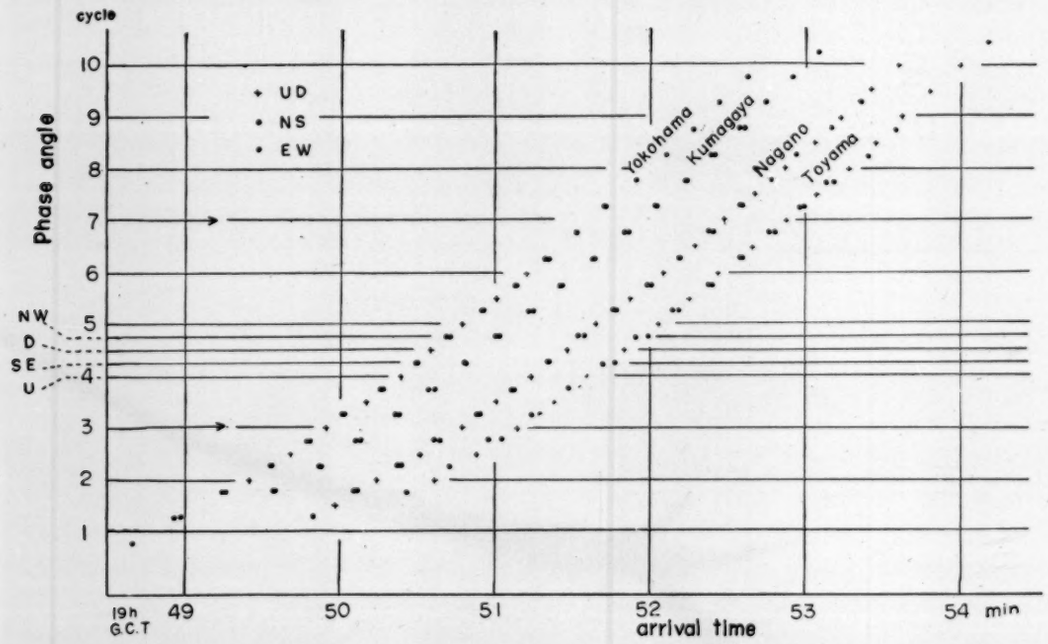

Fig. 2. Arrival times of peaks and troughs in the three component records at the stations in the central part of Japan. A smooth line is drawn to fit the points for each station, and the times at which the smooth line cuts the ordinate for the 3rd and the 7th peak are measured.

The arrival times of all the peaks and troughs are read from the three component records of each station. They are plotted in a figure like Fig. 2, where, the ordinate is the phase angle for the vertical

Table 2. Arrival times and periods of the 3rd and 7th peak at each station.

Station	3rd peak			7th peak		
	period	arrival time		period	arrival time	
	sec.	min.	sec.	sec.	min.	sec.
Sapporo	29.5	51	45.2	23.5	53	22.7
Aomori	29.5	51	13.6	21.8	52	52.6
Hachinohe	28.5	50	55.0	21.7	52	35.3
Akita	28.7	51	04.8	22.5	52	43.1
Morioka	29.0	50	45.5	23.1	52	24.2
Miyako	28.2	50	30.0	22.6	52	09.1
Sendai	28.5	50	23.0	22.8	52	00.5
Toyama	30.0	51	07.1	23.8	52	51.4
Nagano	30.0	50	46.5	23.2	52	29.2
Utsunomiya	28.5	50	09.8	21.1	51	48.0
Kumagaya	29.5	50	14.8	23.5	51	56.2
Mito	28.2	49	56.0	22.2	51	35.0
Gifu	30.0	50	51.4	22.5	52	33.9
Nagoya	29.0	50	43.5			
Kofu	29.0	50	19.7	23.0	52	01.5
Kameyama	29.5	50	47.6	22.2	52	28.3
Omaezaki	28.2	50	07.0	(23.7)	51	49.0
Shizuoka	29.0	50	09.9	22.5	51	49.3
Mishima	29.0	50	01.7	(23.5)	51	41.1
Tokyo	28.5	49	57.8	22.7	51	38.1
Yokohama	28.2	49	55.0	22.3	51	36.2
Tomisaki	28.5	49	40.0	(23.4)	51	19.6
Oshima	28.5	49	44.5	22.0	51	25.2
Toyooka	28.5	51	32.1			
Kyoto	28.5	51	05.5	24.2	52	47.5
Hikone	38.0	50	59.3	20.5	52	39.5
Hiroshima	28.7	52	03.1	22.2	53	45.7
Osaka	28.5	51	04.6	24.0	52	47.5
Sumoto	30.0	51	12.0			
Tomie	29.8	52	55.5	24.8	54	40.0
Kagoshima	30.5	52	02.6			
Miyazaki	28.5	51	47.2	22.6	53	26.3
Yakushima	29.0	51	49.0	24.3	53	30.0
Takamatsu	30.0	51	27.9			
Kochi	28.5	51	27.5			
Average	29.0			22.9		

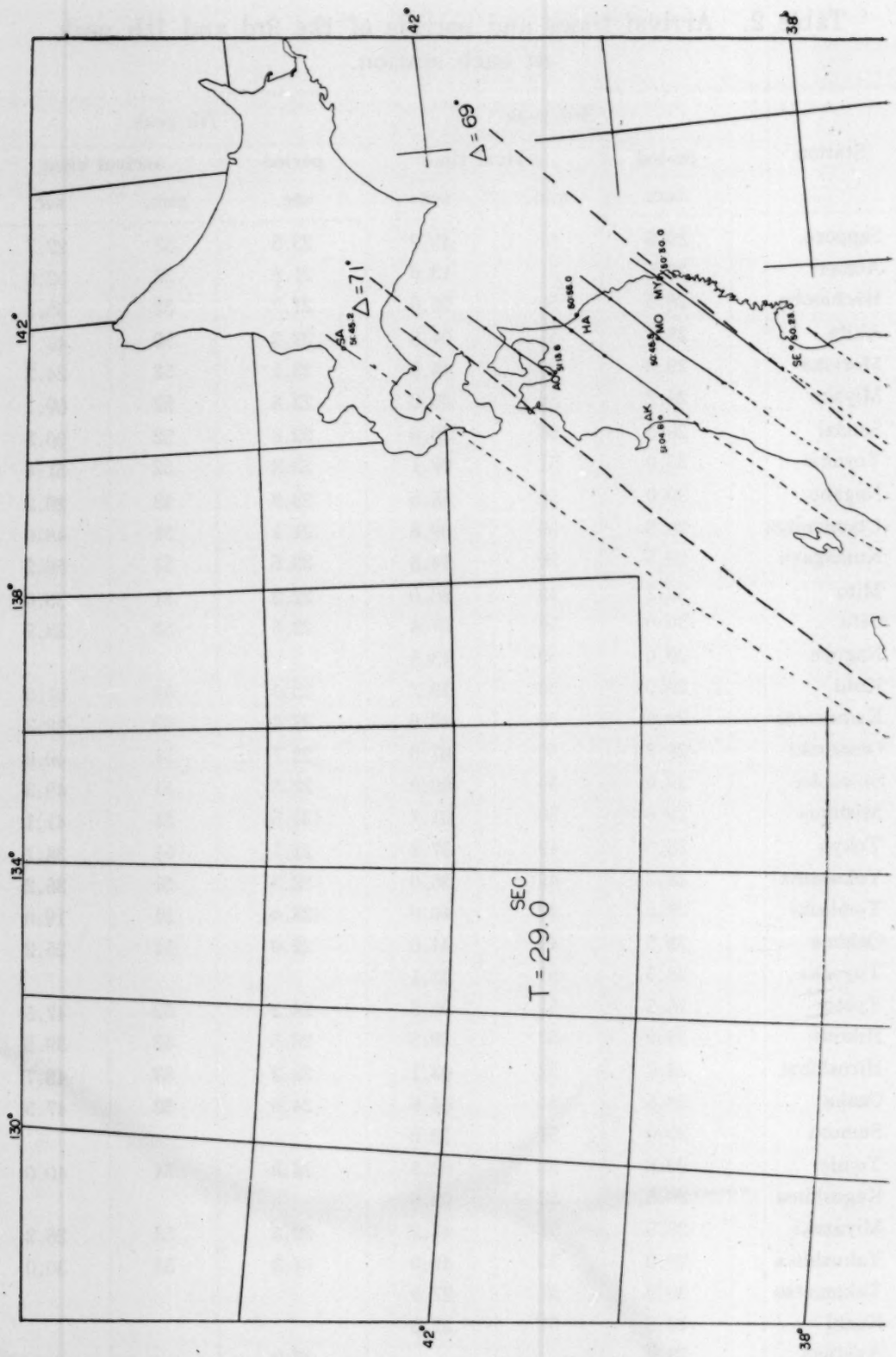

Fig. 3. Wave front of the 3rd peak at every 15 seconds across Japan. The thin dashed
distances of 69° and 71°.

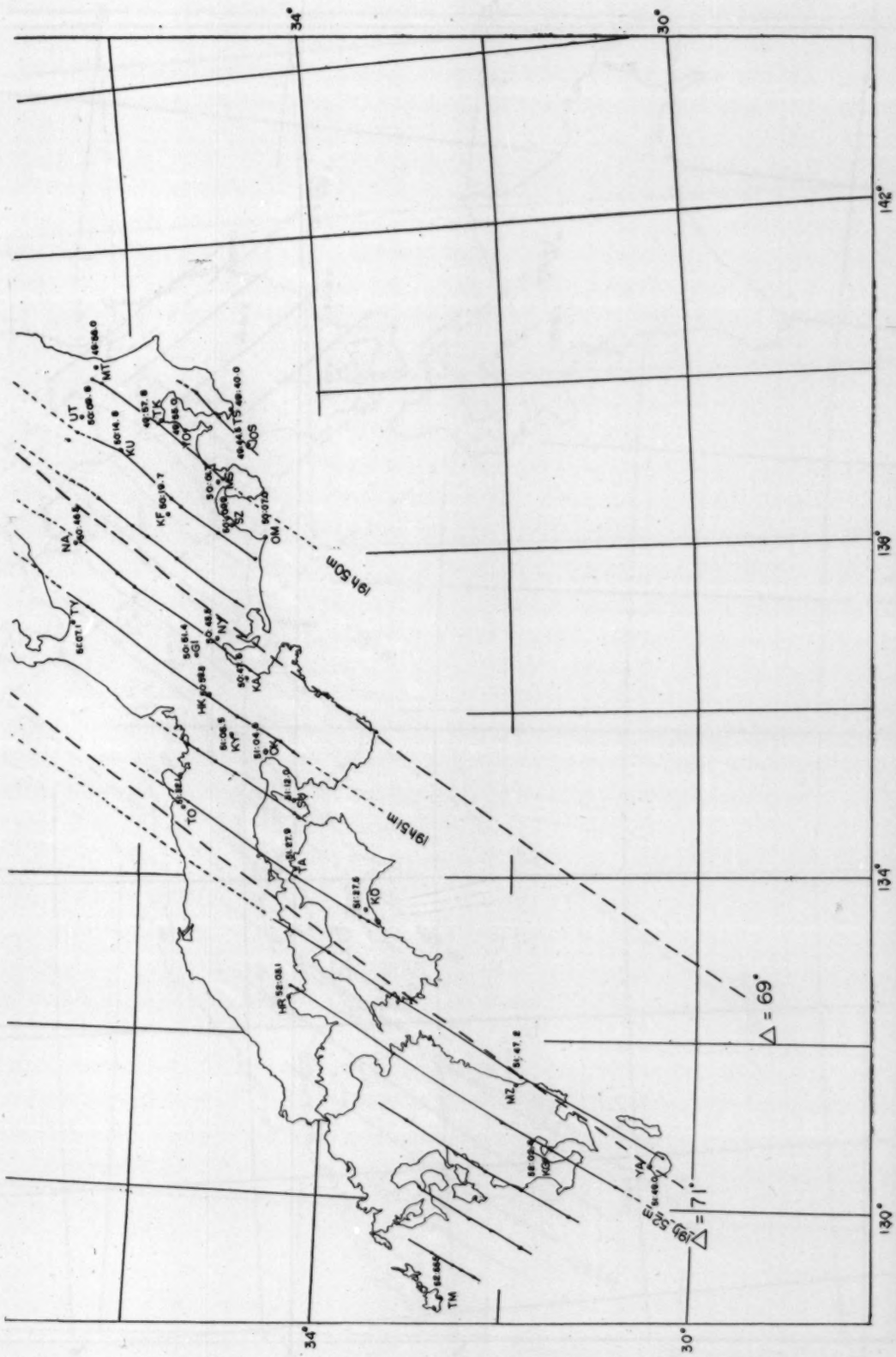

line is used where data are not available. The thick dashed line indicates the epicentral

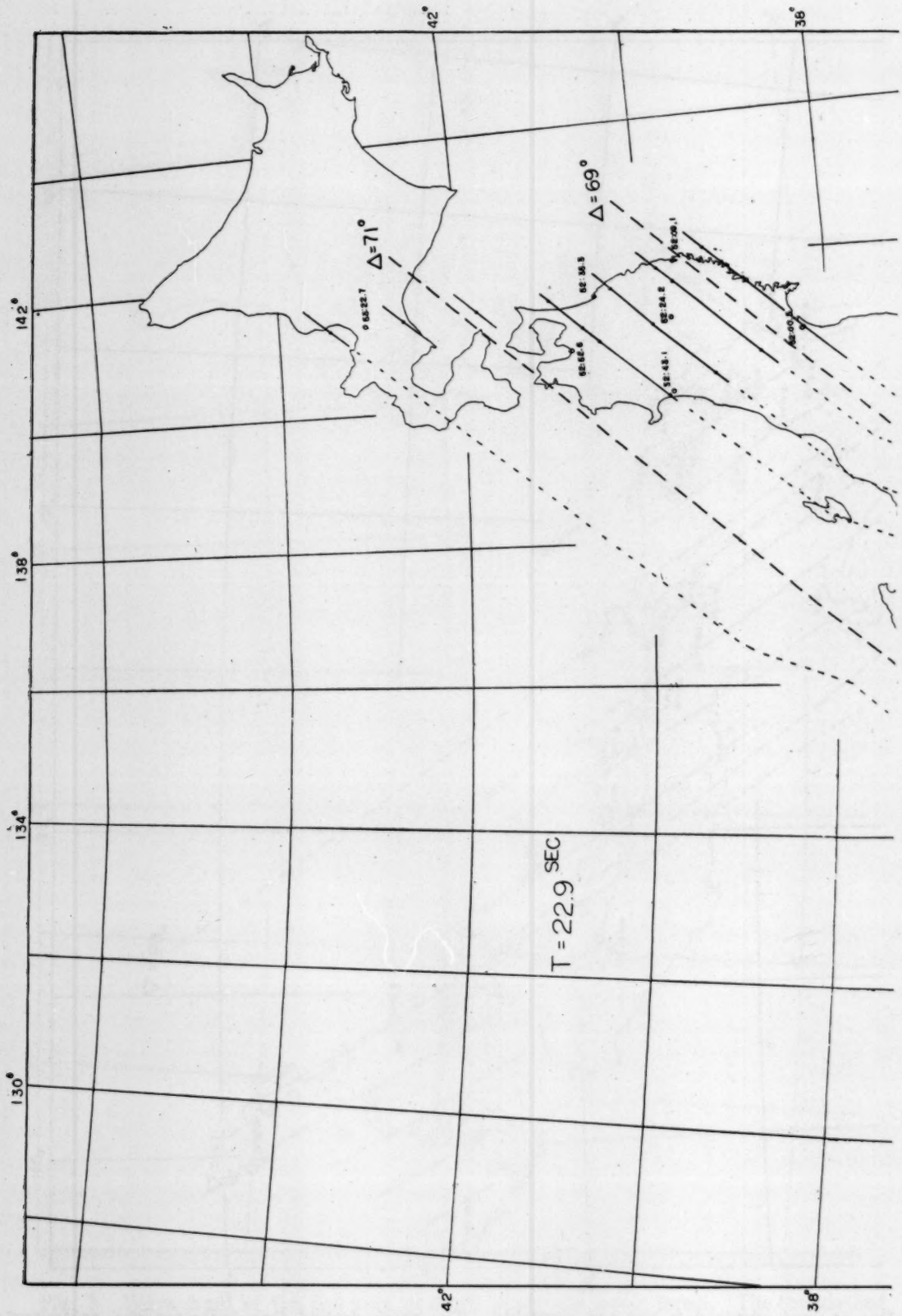

Fig. 4. Wave front of the 7th peak at every 15 seconds across Japan. The thin dashed
distance of 69° and 71°.

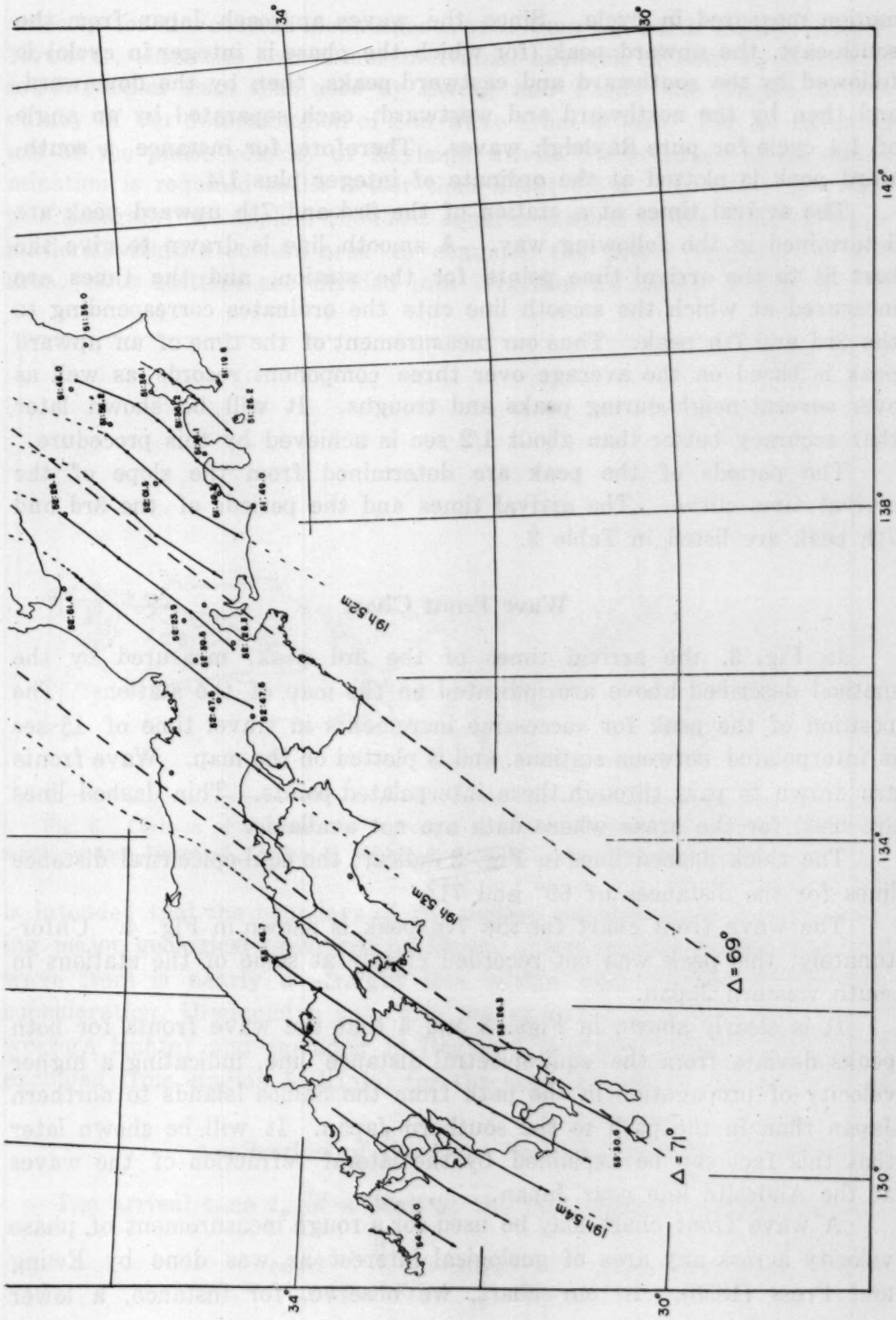

line is used where data are not available. The thick dashed line indicates the epicentral

motion measured in cycle. Since the waves approach Japan from the south-east, the upward peak (for which the phase is integer in cycle) is followed by the southward and eastward peaks, then by the downward, and then by the northward and westward, each separated by an angle of 1/4 cycle for pure Rayleigh waves. Therefore, for instance, a southward peak is plotted at the ordinate of integer plus 1/4.

The arrival times at a station of the 3rd and 7th upward peak are determined in the following way. A smooth line is drawn to give the best fit to the arrival time points for the station, and the times are measured at which the smooth line cuts the ordinates corresponding to the 3rd and 7th peak. Thus our measurement of the time of an upward peak is based on the average over three component records as well as over several neighbouring peaks and troughs. It will be shown later that accuracy better than about 1/2 sec is achieved by this procedure.

The periods of the peak are determined from the slope of the arrival time curve. The arrival times and the periods of the 3rd and 7th peak are listed in Table 2.

Wave Front Chart

In Fig. 3, the arrival times of the 3rd peak, measured by the method described above are indicated on the map of the stations. The position of the peak for successive increments in travel time of 15 sec is interpolated between stations, and is plotted on the map. Wave fronts are drawn to pass through these interpolated points. Thin dashed lines are used for the areas where data are not available.

The thick dashed lines in Fig. 3 indicate the equi-epicentral distance lines for the distances of 69° and 71°.

The wave front chart for the 7th peak is shown in Fig. 4. Unfortunately, this peak was not recorded clearly at some of the stations in south western Japan.

It is clearly shown in Figs. 3 and 4 that the wave fronts for both peaks deviate from the equi-epicetral distance line, indicating a higher velocity of propagation in the path from the Samoa Islands to northern Japan than in the path to the southern Japan. It will be shown later that this fact can be explained by the lateral refraction of the waves at the Andesite line near Japan.

A wave front chart may be used for a rough measurement of phase velocity across any area of geological interest as was done by Ewing and Press (1858). In our chart, we observe, for instance, a lower

velocity for the central mountaneous area than for north eastern Japan. However, since the size of our individual network of stations is mostly much smaller than that used by Ewing and Press, the degree of accuracy of our determination of the wave front is less. For an effective use of the phase velocity of Rayleigh waves, the accuracy of its determination is required to be better than about 1.5%. In order to attain this accuracy, we applied the least squares method to the data of many stations within a certain area to compute the phase velocity for the area. Our stations are divided into 7 regions as shown in Fig. 5. It

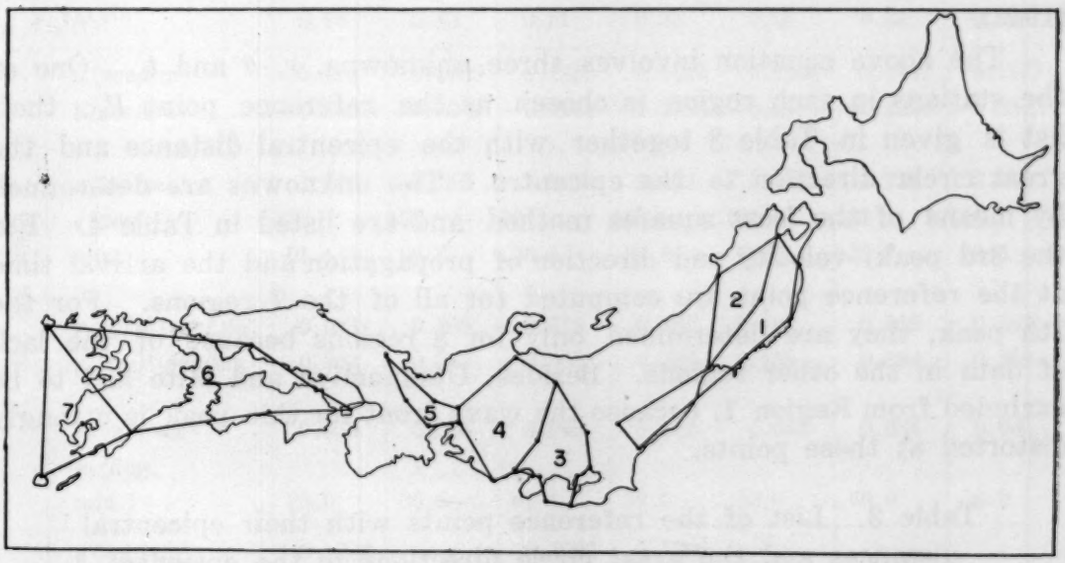

Fig. 5. Division of stations into 7 groups; 1, eastern Tohoku; 2, western Tohoku; 3, south western Kanto; 4, Chubu; 5, Kinki; 6, Seinan; 7, south western Kyushu.

is intended that the boundary of the regions coincides with that separating major geological provinces in Japan. Care is also taken that the wave front is nearly a straight line within each region. From this consideration, Utsunomiya and Mito are excluded from Region 3 (south western Kanto) and included in Region 1 (eastern Tohoku). Osaka is excluded from Region 5 (Kinki) for the same reason.

Application of the Least Squares Method

The arrival time t_m of a peak at the mth station is expressed as

$$t_m=\frac{\cos\theta}{v}(x_m-x_0)+\frac{\sin\theta}{v}(y_m-y_0)+t_0\,,$$

where

v; the velocity of propagation of the peak.
θ; the direction of propagation of the peak measured from the north,
x_m; the latitude of the mth station,
y_m; the longitude of the mth station,
x_0; the latitude of the reference point P_0,
y_0; the longitude of the reference point P_0,
t_0; the arrival time of the peak at the reference point P_0,

x_m-x_0 and y_m-y_0 are measured in km by the use of Richter's table (1942).

The above equation involves three unknowns, v, θ and t_0. One of the stations in each region is chosen as the reference point P_0; their list is given in Table 3 together with the epicentral distance and the great circle direction to the epicentre. The unknowns are determined by means of the least squares mothod and are listed in Table 4. For the 3rd peak, velocity and direction of propagation and the arrival time at the reference point are computed for all of the 7 regions. For the 7th peak, they are determined only for 3 regions because of the lack of data in the other regions. Besides, Utsunomiya and Mito had to be excluded from Region 1, because the wave front for this peak is strongly distorted at these points.

Table 3. List of the reference points with their epicentral distances and the great circle directions to the epicentre.

Station	Region	Epicentral distance		Great circle direction	
		deg.	min.	deg. (from north)	min. (from north)
Sendai	1,2	68	44.5	131	50
Yokohama	3	67	39.1	129	59
Shizuoka	4	68	08.9	128	52
Kameyama	5	69	20.0	127	20
Kochi	6	70	31.9	124	48
Miyazaki	7	71	06.1	122	51

The observed arrival time minus the computed time is shown in Table 5 for all the stations for the 3rd peak, together with the unbiased estimate of the probable error for each region. The probable error ranges from 0 to 0.6 sec., since this error is not only due to the reading error

Table 4. The ratios of the variance of $a=\frac{\cos\theta}{v}$, $b=\frac{\sin\theta}{v}$ and t_0 to the variance of the observed time, the values of a, b, phase velocity v, and direction of propagation θ, and their probable errors for the 3rd and 7th peak.

	Region	1 Eastern Tohoku	2 Western Tohoku	3 South Western Kanto	4 Chubu	5 Kinki	6 Seinan	7 South Western Kyushu
	$r_a^2/r_t^2\times10^4$ (km^{-2})	0.0846	0.252	0.292	0.201	3.025	0.1407	0.438
	$r_b^2/r_t^2\times10^4$ (km^{-2})	0.8429	2.154	0.453	0.359	0.453	0.0982	0.205
	$r_{t_0}^2/r_t^2$	0.16	0.83	0.21	0.35	0.56	0.24	0.91
the 3rd peak	a (sec/km)	0.1707	0.1709	0.1860	0.1684	0.1548	0.1407	0.1177
	b (sec/km)	−0.2033	−0.2042	−0.2102	−0.2356	−0.2174	−0.2290	−0.2362
	v (km/sec)	3.767	3.755	3.563	3.453	3.747	3.722	3.789
	θ (deg.	130	129	131	125	125	121	116
	min.)	01.1	55.5	30.5	32.9	27.4	33.7	28.6
	$r_a\times10^2$ (sec/km)	0.083	0.255	0.316	0.287	0.480	0.519	0.337
	$r_b\times10^2$ (sec/km)	0.263	0.747	0.393	0.383	0.185	0.289	0.230
	r_v (km/sec)	0.030	0.084	0.046	0.042	0.044	0.034	0.030
	r_θ (deg.		1					
	min.)	23.0	06.6	43.1	38.0	52.0	40.0	38.0
the 7th peak	a (sec/km)	0.1782		0.1992	0.1786			
	b (sec/km)	−0.1973		−0.2111	−0.2449			
	v (km/sec)	3.761		3.445	3.299			
	θ (deg.)	132		133	126			
	min.)	05.3		22.2	06.6			
	$r_a\times10^2$ (sec/km)	0.196		0.270	0.420			
	$r_b\times10^2$ (sec/km)	0.518		0.335	0.561			
	r_v (km/sec)	0.058		0.036	00.56			
	r_θ (min.)	48.6		35.8	53.8			

and the error in time keeping at the stations, but is also due to the real irregularity of the wave front, because the computed time is based on the assumption of plane waves. We may, therefore, conclude that

Table 5. List of the observed arrival time minus the computed time.

1. E. Tohoku

Sendai	+0.1 sec
Utsunomiya	−0.5
Mito	+0.5
Miyako	−0.4
Hachinohe	+0.1
Aomori	+0.2
Morioka	+0.0
	r_t=0.29

2. W. Tohoku

Sendai	0.0
Morioka	0.0
Akita	0.0
Aomori	0.0
	r_t=0.00

3. S. W. Kanto

Yokohama	+0.6
Tomisaki	−0.4
Oshima	−1.3
Mishima	+0.1
Shizuoka	+1.2
Kofu	−0.3
Nagano	−0.8
Kumagaya	+0.6
Tokyo	+0.3
	r_t=0.59

4. Chubu

Shizuoka	−0.1
Omaesaki	−0.3
Nagoya	−1.0
Gifu	+1.3
Toyama	−0.8
Nagano	+0.5
Kofu	+0.1
	r_t=0.64

5. Kinki

Kameyama	−0.4
Kyoto	+0.5
Toyooka	−0.1
Hikone	−0.2
Gifu	0.0
Nagoya	−0.2
	r_t=0.28

6. Seinan

Kochi	−0.2
Miyazaki	−0.3
Tomie	+0.5
Hiroshima	−0.5
Takamatsu	−0.7
Sumoto	+1.2
	r_t=0.62

7. S. W. Kyushu

Kagoshima	+0.2
Yakushima	−0.1
Tomie	−0.1
Miyazaki	−0.1
	r_t=0.18

both the accuracy of reading and the accuracy of time keeping at the J.M.A. stations are better than about 1/2 sec.

In estimating the error of the velocity and direction of propagation,

first, the variance of $a=\frac{\cos\theta}{v}$ and $b=\frac{\sin\theta}{v}$ are computed from the variance of the observed time. Since the number of stations is too small for Region 2 and 7, an average of the variance of the observed time for the other regions was used instead of the estimate from their own values. Table 4 lists the ratios of the variances of a, b and t_0 to the variance of the observed time. The ratio is a constant for a given net of stations, and can be used in future study.

The probable errors of the velocity and direction of propagation are then determined by the formulas,

$$r_v=\frac{1}{(a^2+b^2)^{3/2}}\sqrt{a^2r_a^2+b^2r_b^2}$$

$$r_\theta=\frac{1}{a^2+b^2}\sqrt{a^2r_b^2+b^2r_a^2}$$

where

r_v ; the probable error of the velocity of propagation,
r_θ ; the probable error of the direction of propagation,
a ; $\cos\theta/v$
b ; $\sin\theta/v$
r_a ; the probable error of a,
r_b ; the probable error of b.

r_v and r_θ are given in Table 4 together with a, b, r_a and r_b for various regions.

These probable errors indicate that the accuracy of our determination of the phase velocities is 1 to 1.5%, which is sufficient for their effective use in the study of crustal structure.

Application of Press' Standard Phase Velocity Curve

In determining the crustal structure from the phase velocity of Rayleigh waves, Press (1956) used a set of reference phase velocity curves, to each of which the thickness of the crust is assigned as a parameter. In his first construction of the reference curves, the observed group velocity curve for Africa is integrated with the integration constant determined from the assumption that the African continent is made of a crustal layer 35 km thick with shear velocity 3.51 km/sec overlying a mantle with shear velocity 4.68 km/sec. Later, Press (1960) reconstructed the standard phase velocity curves from a crust-mantle

model based on a refraction result in Africa (Hales and Sachs, 1956) and Gutenberg's study (1959) on the mantle under continents. This is the model 6EG, for which the shear velocity distribution is reproduced in Fig. 7. In this model, the crust consists of the top layer 22 km thick with shear velocity 3.53 km/sec and the intermediate layer 15 km thick with shear velocity 3.80 km/sec overlying a mantle with shear velocity 4.60 km/sec. Press showed that this structure explains very well the observed group velocity of Rayleigh waves for Africa. The standard phase velocity curves based on the above structure are shown in Fig. 6.

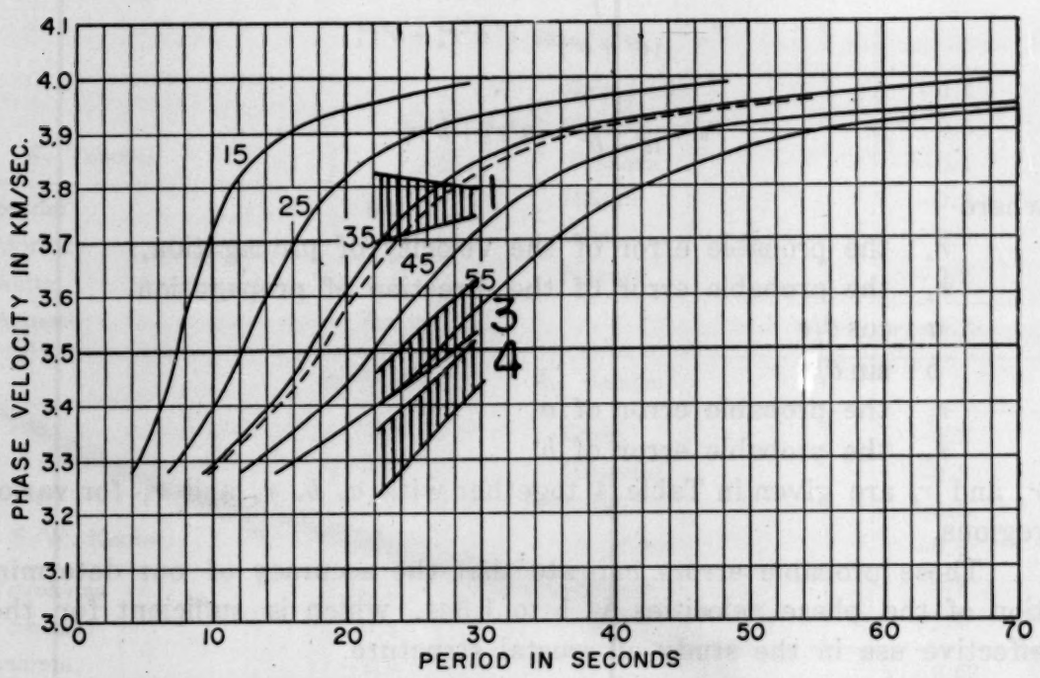

Fig. 6. Press' standard phase velocity curves (Press, 1960). The phase velocity data for Region 1, 3, and 4 are shown with the range of probable errors.

In the standard phase velocity curves, the thickness of the crust is the only parameter that varies from place to place, and it is implicitly assumed that the compressional and shear velocities in all the layers, as well as the density ratios and the proportion of the thickness of the layers, do not vary. This is certainly an oversimplification, but the success of their use in a rough determination of crustal thickness in the United States tempt us to apply the standard curves to our phase velocity data.

The thickness of the crust obtained by the application of Press' standard curves to the phase velocities of our 3rd and 7th peaks are

given in Table 6 for various regions. These values are significantly greater than those determined by the refraction study.

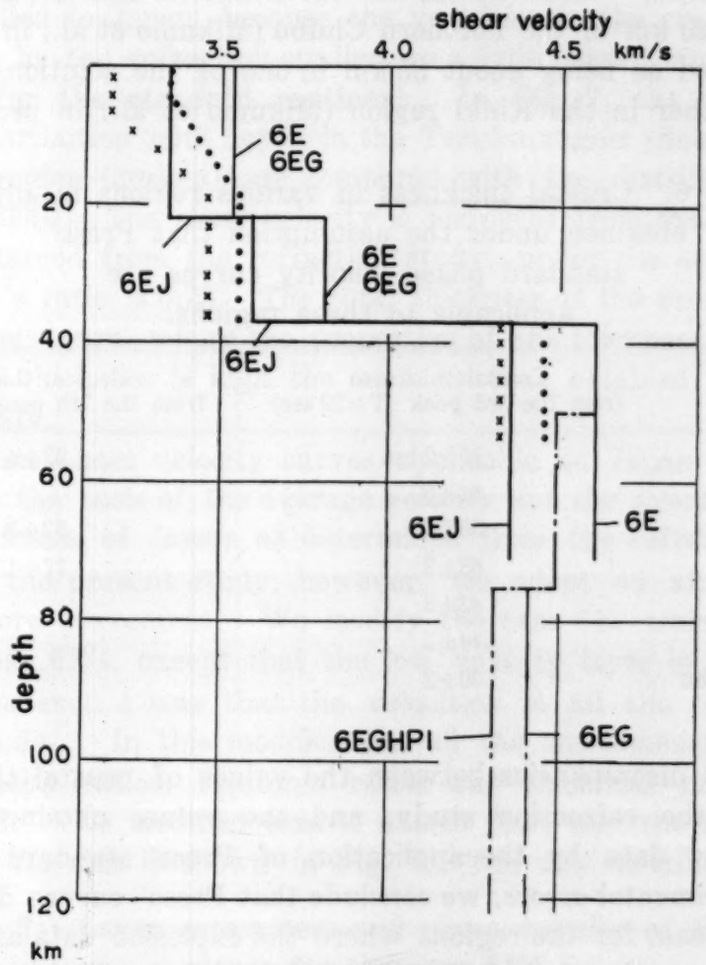

Fig. 7. Shear velocity distribution at depths for various crust-mantle models. 6EG is the model adopted by Press in his construction of standard phase velocity curves. 6EJ is adopted to intepret the phase velocity data in Japan. 6EGHPI represents the mantle under the Pacific ocean (Aki and Press, in press).

The study of the crustal structure in Japan by means of the explosion generated seismic waves has been carried out by the Research Group for Explosion Seismology since 1950. By the effort of the members of the group, the crustal structures in the Tohoku, the northern Kanto, the northern Chubu and the Kinki regions have been determined. The crust usually consists of a relatively thin upper layer with compressional velocity 5.8 km/sec (for Tohoku) or 5.5 km/sec (for others) and a lower layer with compressional velocity 6.0 to 6.2 km/sec, which over-

lies the mantle with relatively low velocity of 7.5 to 7.7 km/sec. The crustal thickness was obtained as 20 to 25 km in the Tohoku region (Matuzawa, 1959), about 25 km in the northern Kanto (Usami et al., 1958), about 40 km in the northern Chubu (Mikumo et al., in press), and it was obtained as being about 35 km in one of the solutions and about 28 km in another in the Kinki region (Mikumo et al., in press).

Table 6. Crustal thickness in various regions in Japan obtained under the assumption that Press' standard phase velocity curves are applicable to these regions.

Region	Crustal thickness from the 3rd peak (T=29 sec)	Crustal thickness from the 7th peak (T=23 sec)
1. e. Tohoku	40±2 km	33±4 km
2. w. Tohoku	41±6	
3. s. w. Kanto	55±3	52±3
4. Chubu	63±3	77±15
5. Kinki	42±3	
6. Seinan	44±2	
7. s. w. Kyushu	39±2	

Since the discrepancies between the values of crustal thickness obtained from the refraction study, and the values obtained from the phase velocity data by the application of Press' standard curves, are beyond experimental errors, we conclude that Press' curves do not apply to Japan at least for the regions where the explosion data are available. It should be mentioned that the discrepancy for the Kinki region, if we adopt one of the solutions from the refraction study, is not as great as for the Tohoku and the Chubu region.

In the United States, Press' standard curves give the crustal thickness that agrees well with that obtained in most of the areas from the refraction study. There is, however, an area where they do not agree. That is the high plateau area (Utah, Nevada, and New Mexico), where the thickness from the refraction measurements average close to 35 km, while Press' curves, applied to the phase velocity data, yield the an average thickness of about 48 km. Woollard (1959) attributes this discrepancy to the masking of layering within the crust in the refraction measurements. A similar discrepancy for the California-Nevada area was discussed by Press (1960).

Modified Standard Curves Applicable to Japan

It is not unexpected that Press' standard phase velocity curves may not be applied to Japan, because the velocities in the crust and mantle determined by the refraction studies are a little lower than those adopted by Press for the standard continent. In Fig. 7, the average shear velocity distribution with depth in the Tohoku region (dots) and that in the Kinki region (crosses) are compared with the distribution adopted by Press (6EG). The shear velocity is computed from the compressional velocity obtained from the refraction study, under the assumption that the Possion's ratio is 0.25. The total thickness of the crust is taken as 37 km in the figure, where the proportion of the thickness of each layer to the total thickness is kept the same as that obtained from the refraction study.

Reference phase velocity curves applicable to Japan may be constructed on the basis of the average velocity and the average proportion of the thickness of layers as determined from the refraction study in Japan. In the present study, however, we adopt an alternative way which is more convenient. We modify the case 6E, which is identical with the case 6EG, except that the low velocity layer in the mantle is neglected, in such a way that the velocities in all the layers are reduced by 5.5%. In this modification, all the non-dimensional products such as density ratios, Poisson's ratios and thickness proportions are not changed. This modified case is named 6EJ, and the shear velocity distribution for this is shown in Fig. 7. The new distribution is much

Table 7. Layer parameters and phase velocity of Rayleigh waves for the case 6*EJ*.

Layer	Thickness	Compressional velocity	Shear velocity
1	22 km	5.698 km/sec	3.336 km/sec
2	15	6.332	3.591
3	∞	7.522	4.347

Period	Phase velocity	Period	Phase velocity
70.44 sec	3.853 km/sec	22.74 sec	3.436 km/sec
42.48	3.770	20.22	3.353
33.64	3.686	17.65	3.269
28.85	3.603	14.72	3.186
25.49	3.519	10.55	3.102

closer to the observed one in Japan and probably a sufficient satisfactory approximation for the present purpose. The numerical values for the case 6EJ, which are obtained from the values for 6E given by Press (1960), are listed in Table 7.

The reference phase velocity curves based on the new model 6EJ are shown in Fig. 8, together with the observed velocities for Region 1, 3, and 4, where the shaded area represents the range of probable error. If this figure is compared with Fig. 6, it can be seen that not only the thickness of crust is adequately reduced for each region, but also the agreement between the theoretical and experimental curves is much improved.

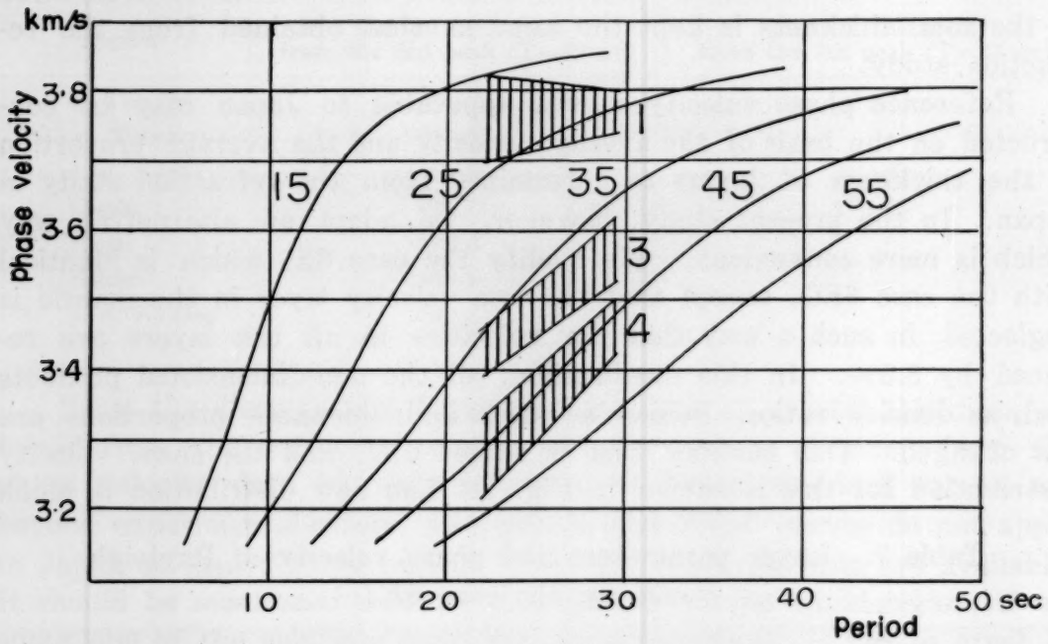

Fig. 8. Modified standard phase velocity curves applicable to Japan based on the case 6EJ. The phase velocity data for Regions 1, 3, and 4 are shown with the range of probable errors.

Table 8 lists the crustal thickness for various regions obtained by the application of the modified standard curves to our phase velocity data. The thickness of 20 to 25 km for the Tohoku region agrees with the thickness obtained from the refraction study (Matuzawa, 1959). The thickness of 27 km for the Kinki region also agrees well with the thickness in one of the solutions obtained by Mikumo *et al* (in press). The crustal thickness in northern Chubu amounts to 43.5 km in one of the solution obtained by Mikumo *et al*. This value is not far from our

value of 46 km for the entire Chubu. Our result also agrees very well with the result of Kishimoto and Kamitsuki's (1956) study on the fore-runners of near earthquakes in central and south western Japan. Our result is also consistent with the distribution of anomalies in the travel time of *P* waves observed by many investigators (e.g. Honda, 1932).

Table 8. Crustal thickness in various regions in Japan obtained by the use of modified standard phase velocity curves which are based on the case 6*EJ*.

Region	Crustal thickness from the 3rd peak (T=29 sec)	Crustal thickness from the 7th peak (T=23 sec)
1. e. Tohoku	25±3 km	20±5 km
2. w. Tohoku	26±10	
3. s. w. Kanto	39±3	37±3
4. Chubu	46±3	46±5
5. Kinki	27±4	
6. Seinan	29±3	
7. s. w. Kyushu	23±4	

We may therefore, conclude that the case, 6EJ is a closer approximation to the crustal structure in Japan than the case 6EG. In other words, the elastic wave velocities in the crust and at the top of the mantle in Japan are about 5.5% lower than those in the standard continents. The shear velocity in the mantle, adopted in the case 6EJ is as low as the volocity at Gutenberg's asthenosphere low velocity channel as shown in Fig. 7, where 6EG represents the mantle under continents and 6EGHPl represents the mantle under the Pacific ocean (Aki and Press, in press). It is of extreme interest to find out if, in Japan, the shear velocity is kept constant from the top of the mantle down to the low velocity channel, (in other words, the low velocity channel reaches the Mohorovicic discontinuity in this techtonically active area,) or the shear velocity increases to the value for the standard Moho before it decreases at the channel. The latter case is more likely in the California-Nevada area, according to Press (1960). In order to study this, we have to extend our measurements to longer periods.

It should be mentioned here that the application of our modified standard phase velocity curves to the data for the high plateau area in the United States give the crustal thickness as very close to the value obtained from the refraction study. This suggests that the crustal velocities in this area are also lower than those in other parts of the

continent. The problem there is, however, rather complicated as discussed by Press (1960). Press studied the crustal structure in the California-Nevada area by means of both the refraction method and the phase velocity method, and suggests the existence of a low velocity zone in the intermediate layer or an unusually high Poisson's ratio for this layer.

The Bouguer Gravity Anomaly and the Phase Velocity of Rayleigh Waves

Ewing and Press (1959) found a remarkable correlation between the phase velocity of Rayleigh waves, topography, and the Bouguer gravity anomaly for various regions in the United States. This implies that the crustal thickness determined from the phase velocity agrees with that from the gravity data and that the isostatic compensation is realized in these regions (Woollard, 1959).

We observed a similar correlation for Japan as shown in Fig. 9, where the phase velocities of Rayleigh waves for the period of 29 sec are shown for various regions in Japan, together with a rough sketch of the topography and the Bouguer anomaly, based on the map compiled by Tsuboi (1959). It can be seen in the figure that, as a general trend,

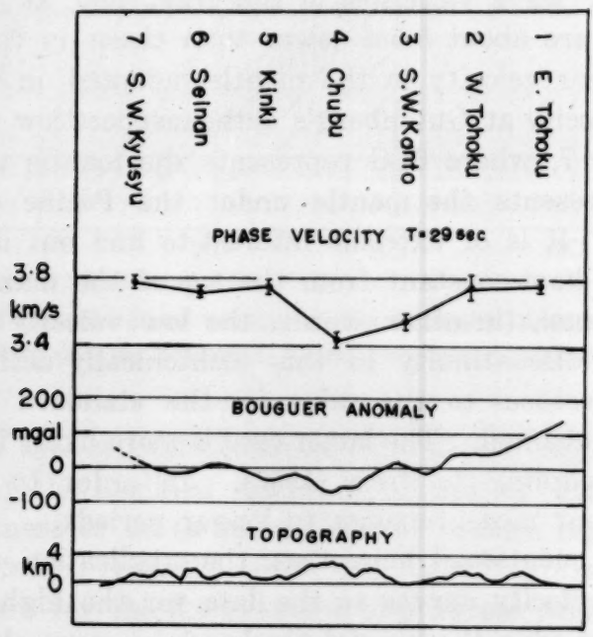

Fig. 9. Phase velocity of Rayleigh waves with a period of 29 sec, Bouguer gravity anomaly and topography for various regions in Japan.

the higher the phase velocity the greater the Bouguer positive anomaly. If we examine it more carefully, however, it seems that the relation between them for south western Japan is a little different from that for central and north eastern Japan. To show this more clearly, we plotted the phase velocity for the period of 30 sec against the average Bouguer anomaly for each region in Fig. 10. We also plotted the data for the United States obtained by Ewing and Press in the same diagram.

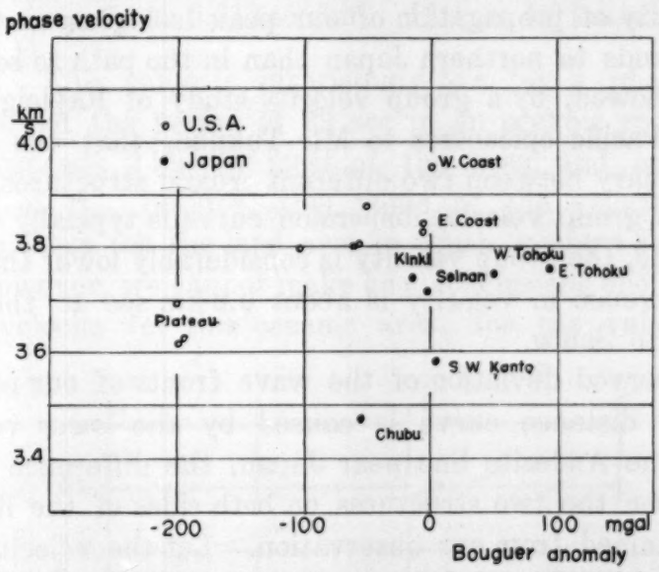

Fig. 10. Relation between the phase velocity of Rayleigh waves with a period of 30 sec and the average Bouguer anomaly for various regions in Japan and the United States. The data for the United States are obtained by Ewing and Press (1959).

The points for central and north eastern Japan in Fig. 10 lie on a straight line, departing considerably from the line for the data in the United States. It is remarkable that both lines are very nearly parallel to each other. The points for south western Japan do not lie on the line for central and north eastern Japan, deviating from it in the sense toward the line for the United States. This fact may have an important bearing on the apparent difference between north eastern and the south western Japan in geology and geotechtonics. Dr. Tsuboi pointed out to the writer that the effect of the neighbouring suboceanic mass must be removed from the Bouguer anomaly in Japan before any detailed discussion of such a diagram is made, and that the reduction will shift the points for Japan in Fig. 10 to the left, closer to the points for the United States. Unfortunately, at present, we do not have enough gravity observations on the ocean near Japan which are necessary

for the reduction. If the reductions are applied to the Bouguer anomaly, the diagram will be very useful in discussing the geological conditions at various places, with the aid of the velocity-density relation for various materials under various physical conditions.

Lateral Refraction of Rayleigh Waves at the Andesite Line

The wave front charts shown in Figs. 3 and 4 clearly demostrate that the velocity of propagation of our peak is higher in the path from the Samoa Islands to northern Japan than in the path to southern Japan. Santo (1961) showed, by a group velocity study of Rayleigh waves from many circum Pacific epicentres to Mt. Tukuba, that the Andesite line may be a boundary between two different crustal structures. On the east side of it, the group velocity dispersion curve is typically oceanic, while on the west side, the group velocity is considerably lower than that on the east; the difference in velocity is about 0.2 km/sec at the period of 30 sec according to Santo.

If the observed deviation of the wave fronts of our peaks from the equi-epicentral distance curve is caused by the lower velocity on the west side of the Andesite line near Japan, the difference in the phase velocity between the two structures on both sides of the line can be accurately determined from our observation. Let the velocity of propagation of a peak with period T be c_0 on the east side of the Andesite line and that on the west be c_1, then the arrival time t_m of the peak at the mth station can be written as (Brune, Nafe and Oliver, 1960)

$$t_m=\frac{\Delta_m-x_m}{c_0}+\frac{x_m}{c_1}+(n+\varepsilon)T$$

where n is an integer, ε is a constant, Δ_m is the epicentral distance to the mth station, and x_m is the portion of the distance from the Andesite line. Since the period of our peak is almost the same for all of our stations (Table 2),

$$t_m-\left(\frac{\Delta_m-x_m}{c_0}+\frac{x_m}{c_1}\right)$$

must be approximately constant. Therefore, $t_m-\frac{\Delta_m}{c_0}$ must be proportional to $\left(\frac{1}{c_1}-\frac{1}{c_0}\right)x_m$, and if we plot $t_m-\frac{\Delta_m}{c_0}$ against x_m, the slope of

the plotted points will be equal to $\left(\frac{1}{c_1}-\frac{1}{c_0}\right)$. Assuming that c_0 is 4.0 km/sec for the period 29 sec, which is very close to the value for the case 8099 of Dorman, Ewing and Oliver (1960), we computed $t_m-\frac{\Delta_m}{c_0}$ for the 3rd peak for the stations listed in Table 3, and plotted them against x_m in Fig. 11. Fitting a straight line to the points, we obtain the value of $\frac{1}{c_1}-\frac{1}{c_0}$ as 0.012 sec/km. If c_0 is 4.0 km/sec, therefore, c_1 is 3.82 km/sec. This value is surprisingly low for a phase velocity of Rayleigh waves of the period of 29 sec in an oceanic region where the water depth exceeds 2 km in most of the area, and exceeds 4 km in about a half of it. Besides, this value of the velocity is not much different from those for the land area in south western Japan (Table 4). At present, however, we cannot make any conclusions about the absolute value of the velocity for this oceanic area, for the value depends on

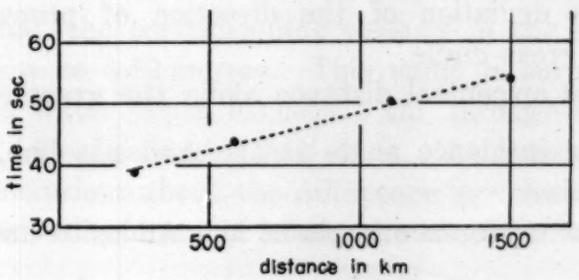

Fig. 11. $t_m-\Delta_m/C_0$ against the distance x_m from the Andesite line to several stations on the Pacific coast (for the 3rd peak.)

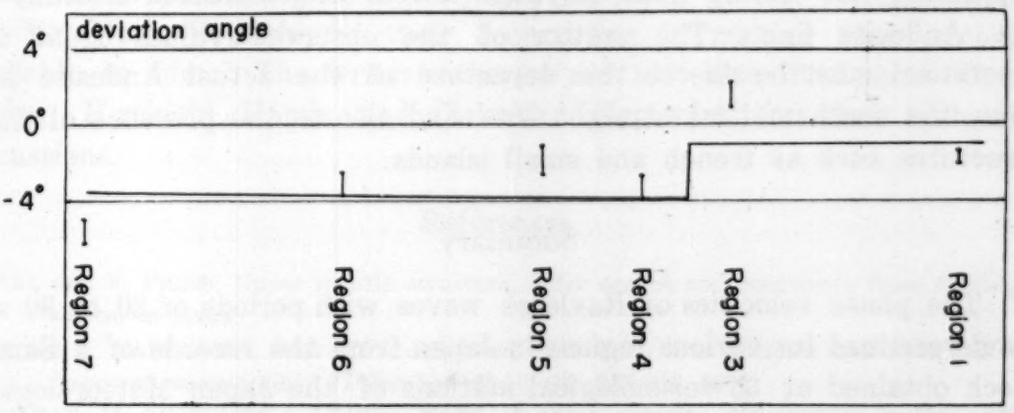

Fig. 12. Theoretical and observed deviations of the direction of propagation of the 3rd peak from the great circle direction to the epicentre.

the assumption on the velocity c_0 for a typical Pacific oceans.

The direction of propagation of Rayleigh waves will also be affected by the lateral refraction at the Andesite line. Fig. 12 shows the deviation of the observed direction from the great circle direction to the epicentre, with the range of its probable error. Assuming that the Andesite line is straight, and c_0 is 4.0 km/sec, and c_1 is 3.8 km/sec, we computed a theoretical deviation of the direction of propagation from the great circle by a refraction at the Andesite line. The following formulas are used in the computation.

$$\sin\delta=\sin(i_1-i_0)\frac{\sin\Delta'}{\sin\Delta}\ ,$$

and

$$\frac{\sin i_0}{\sin i_1}=\frac{c_0}{c_1}\ ,$$

where

δ ; the deviation of the direction of propagation from the great circle,

Δ ; the epicentral distance along the great circle path,

$\frac{\pi}{2}-i_0$; the incidence angle at the Andesite line,

$\frac{\pi}{2}-i_1$; the emergence angle at the Andesite line,

Δ' ; the distance between the incident point and the epicentre.

As shown in Fig. 12, the agreement between the observed deviation angle and the theoretical angle seems good as a first approximation, supporting the theory that Rayleigh waves are refracted laterally at the Andesite line. The scatter of the observed values from the theoretical must be due to the departure of the actual Andesite line from the mathematical straight line and also to the presence of finer structures such as trench and small islands.

Summary

The phase velocities of Rayleigh waves with periods of 20 to 30 sec are determined for various regions in Japan from the records of a Samoa shock obtained at 35 seismological stations of the Japan Meteorological Agency. By means of the least squares method, the velocities are determined with the accuracy of 1 to 1.5%. Examining these velocities

in the light of Press' standard phase velocity curves for the standard continents, and taking into account the result of refraction studies in Japan, we conclude that Press' curves do not apply to Japan. We modified the standard curves in such a way that the velocities in the crust and at the top of the mantle are reduced by 5.5%. The new velocities are much closer to the values obtained from the refraction study in Japan. The application of the new standard curves gives crustal thicknesses which agree very well with those determined from refraction and other studies.

We found a similar positive correlation between the phase velocity of Rayleigh waves and the positive Bouguer gravity anomaly as Ewing and Press (1959) found in the United States. It seems, however, that the relation depends on the geology of the region, and a single relation does not cover the whole earth.

Our wave front chart suggests that Rayleigh waves are laterally refracted at the Andesite line near Japan. If we assume that the phase velocity for a period of 29 sec is 4.0 km/sec in the oceans to the east of the Andesite line, the corresponding velocity in the area on its west side must be as low as 3.82 km/sec. This value is surprisingly low for an area where the water depth exceeds 2 km throughout most of the area and exceeds 4 km in about a half of it. At present, however, we can only make conclusions about the difference in velocity between both sides of the Andesite line but not about the absolute value of velocity.

Acknowledgment

The writer's thanks are owing to all the seismologists at the stations of the Japan Meteorological Agency and especially to Dr. Takuzo Hirono and Mr. Norio Noguchi for their cooperation in making their records available to him. The writer's thanks are also due Professors Chuji Tsuboi, Hirokichi Honda and Takahiro Hagiwara for their valuable discussions.

References

K. AKI, and F. PRESS, Upper mantle structure under oceans and continents from Rayleigh waves, in press.

J. BRUNE, J. NAFE and J. OLIVER, A simplified method for the analysis and synthesis of dispersed wave trains, *J. Geophys. Res.*, **65**, 287-304, 1960.

J. DORMAN, M. EWING and J. OLIVER, Study of shear velocity distribution in the upper mantle by surface wave analysis, Part 1: mantle Rayleigh waves, *Bull. Seis. Soc. Am.* **50** 87-115, 1960.

M. EWING and F. PRESS, Determination of crustal structure from phase velocity of Rayleigh waves, Part 3, the United States, *Bull. Geol. Soc. Am.*, **70**, 229-224, 1959.

B. GUTENBERG, The asthenosphere low velocity layer, *Annali di Geofisica*, **12**, 439-460, 1959.

A. L. HALES and I. S. SACHS, Evidence for an intermediate layer from crustal structure studies in Eastern Transvaal, *Geophys. J.*, **2**, 15-33, 1959.

H. HONDA, A note on the anomaly of the velocity of seismic waves, *Geophys. Mag.*, **6**, 189-192, 1932.

Y. KISHIMOTO and A. KAMITSUKI, On the crustal structure as deduced from forerunner analysis, *Zisin, Ser. 2*, **9**, 200-208, 1956.

T. MATUZAWA, On the crustal structure in north east Japan by explosion seismic observations, *Bull Earthq. Res. Inst.*, **37**, 123-154, 1959.

T. MIKUMO, M. OTSUKA, T. ŌTSU T. TERASHIMA and A. OKADA, Crustal structure in central Japan as deduced from the Miboro explosion seismic observations, in press.

J. OLIVER, R. KOVACH and J. DORMAN, Crustal strucutre of the New York-Pennsylvania Area, *J. Geophys. Res.* **66**, 215-226, 1961.

F. PRESS, Determination of crustal structure from phase velocity of Rayleigh waves, Part 1: southern California, *Bull. Geol. Soc. Am.*, **67**, 1647-1658, 1956. Part 2 San Francisco Bay Region, *Bull. Seis. Soc. Am.*, **47**, 87-88, 1957.

F. PRESS, Crustal structure in California-Nevada Region, *J. Geophys. Res.*, **65**, 1039-1051, 1960.

C. F. RICHTER, Calculation of small distances, *Bull. Seis. Soc. Am.*, **33**, 243-250, 1943.

T. A. SANTO, Rayleigh wave dispersion across the oceanic basin around Japan, Part 3, on the crust of the south-western Pacific ocean, *Bull. Earthq. Res. Inst.*, **39**, 1-22, 1961.

T. SHIMA, S. IZUMI and T. SHIBATA, On the coda portion of surface waves, reported at the meeting of the Seismological Society of Japan, May, 1960.

C. TSUBOI, Gravity survey along the lines of precise levels throughout Japan by means of a Worden gravimeter, Part 4, Map of Bouguer anomaly distribution in Japan based on approximately 4,500 measurements, *Bull. Earthq. Res. Inst., Suppl.* Vol. **4**, part 3, 1954.

T. USAMI, T. MIKUMO, E. SHIMA, I. TAMAKI, S. ASANO, T. ASADA and T. MATUZAWA, Crustal structure in northern Kanto district by explosion seismic observations, part, 2, models of crustal structure, *Bull. Earthq. Res. Inst.*, **36**, 349-357, 1958.

G. P. WOOLLARD, Crustal structure from gravity and seismic measurements, *J. Geophys. Res.*, **64**, 1921-1544, 1959.

8. レーリー波位相速度法による日本の地下構造の研究 第1報

地震研究所 安芸敬一

1957年4月15日（日本時間）のサモア島の地震による，周期20秒から30秒のレーリー波は，気象庁のヴィーヘルト地震計網によつてかなりよく記録された（第1図）．気象庁の御好意で集められた記録のうち，35カ所の記録を解析して，日本各地でのレーリー波位相速度が求められた．位相速度の測定には，3成分記録を用い，最小自乗法を応用して，1ないし1.5%の精度が得られた．

Pressがアメリカ大陸の地殻の厚さを求めるのに用いた標準の位相速度曲線を，われわれの測定値に応用すると，爆破などから知られている地殻の厚さより，著しく大きい値が出た．つまり，標準の大陸に適用するプレスの位相速度曲線は，日本には適用されない．

日本の地殻およびマントル上部の弾性波速度として，標準の大陸のものより5.5%小さいものを仮定すると，爆破の結果とよく一致する地殻の厚さが，レーリー波から求められる．日本の弾性波速度が大陸の標準よりも小さいことは，爆破の結果にも示されていることであり，興味ある重要な事実であることを強調したい．また，この結果，日本のモホ直下のS波速度が，Gutenbergのマントル内の低速層の速度とほとんど同じことによる（第7図）．日本のような所では，低速層がホモまで達しているのかも知れない．このことをはつきりさせるには，より長周期のレーリー波をしらべる必要がある．

EwingとPressは，重力のブーゲー異常とレーリー波位相速度の間の著しい相関関係をアメリカ大陸について見出している．われわれも同様の結果をえた（第9図，第10図）．ただしその関係は，日本とアメリカで異なり，また日本のなかでも中部および東日本と西日本で異なるように見える．同じ地殻の厚さに対して中部および東日本は，アメリカより位相速度が小さく，ブーゲー異常が大きいように見える．これは大変興味のあることであるが，この関係を詳細に議論するには，重力異常に対する海の影響をとり除く必要があり，今後の問題である．

われわれのレーリー波の第3および第7の山の波面図（第3図，第4図）にはつきりあらわれているように，日本北部には，日本南部より同じ震央距離に対して，約20秒だけ波がはやくついている．このことが三東のいうような安山岩様の東と西の速度差によるとすると，速度差として，約0.2 km/secの値が得られる．東側の海について，Dormanらの求めた位相速度を正しいとすると，西側では，29秒の周期の波の位相速度が3.82 km/secとなる．この値は海として驚くほど小さい値であつて，西南日本の値とほとんどひとしい．南方の島に長周期地震計をおけば，このことを確かめることができるであろう．

Bulletin of the Earthquake Research Institute
Vol. 39 (1961), pp. 285-326

9. *Crustal Structure in Central Japan as Derived from the Miboro Explosion-Seismic Observations.*

Part 1. Explosions and Seismic Observations.

By The Research Group for Explosion Seismology.

(Read Jan. 24, 1961.—Received June 30, 1961.)

1. Introduction

Since September 1957, several scores of tons of explosives have been detonated many times by the Dengen Kaihatu Co., for quarrying purposes connected with the construction of a rock-fill dam at the site of Miboro-valley, Sirakawa-village, Gihu Prefecture. The Research Group for Explosion Seismology, making the best use of these opportunities, has carried out six large scale systematic seismic observations. Our aim was to get precise information about the crustal structure in central Japan, over the Kwantô-, Tyûbu-, Kinki- and Tyûgoku-Districts.

An outline of the explosion-seismic observations and the observed results will be given in the following.

2. Description of Explosions

Quarry area where the shots were fired is situated in Hukusima-valley, a gorge of a branch of the Syôgawa, 800–900 m high above sea level, and is adjacent to the south-eastern foot of Mt. Hakusan. From a geological point of view, it consists mainly of granite-porphry. Topographical features near the Miboro dam-site and Hukusima-valley are shown in Fig. 1, and a detail map near the shot points in Fig. 2, and those of six explosion features are outlined in Fig. 3.

As can be seen in the above figures, a coyote-tunnel blast system was adopted in the I–V explosions, and a bench-cut blast system only in the VI detonation, respectively. In the former system, dynamite was detonated in many coyote-tunnels drilled horizontally in the hillsides, and so the exploded area occupied a certain spatial extent, while in the latter system, explosives concentrated in vertically drilled six blast holes, each 10″ in diameter and 25–30 m deep, were fired simultaneously. Only

the last was blasted at midnight. The ignition method was as follows. The initiating fuses extending outside from the dynamite charges in the tunnels or the blast holes, were gathered to an electric blasting cap. This cap was ignited through AC 200 V by operating a knife-switch on a switch-board set up at a spot 200–300 m distant. Shot times were directly registered on the oscillogram. The shot times thus determined and the amount of explosives in the six explosions mentioned above are tabulated in Table 1.

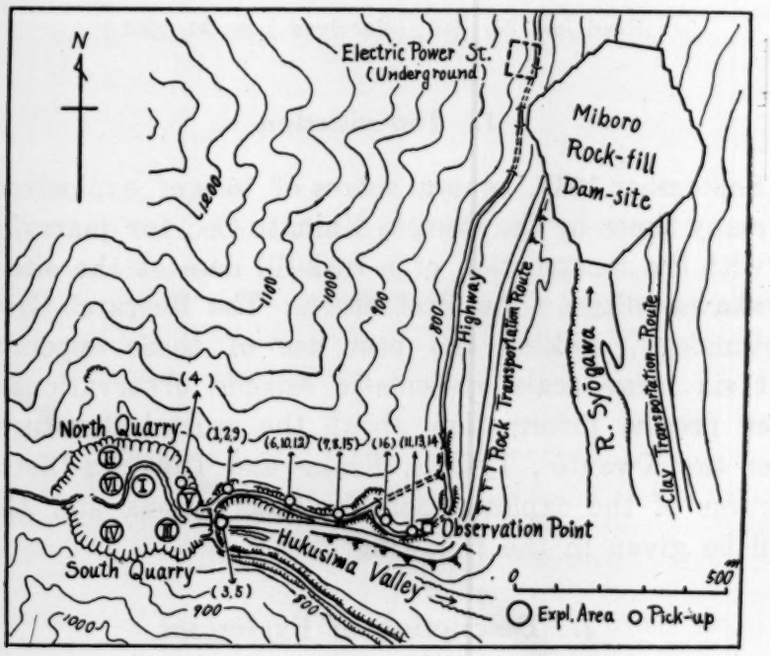

Fig. 1. Topographical map of Miboro dam-site and quarry area in Hukusima-valley.

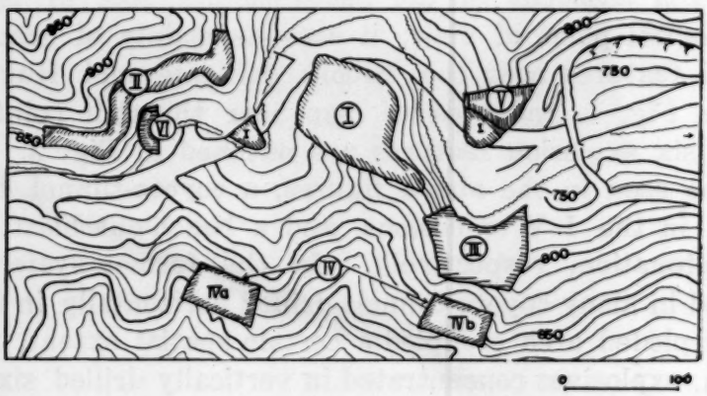

Fig. 2. View of I–VI explosion areas in Hukusima-valley.

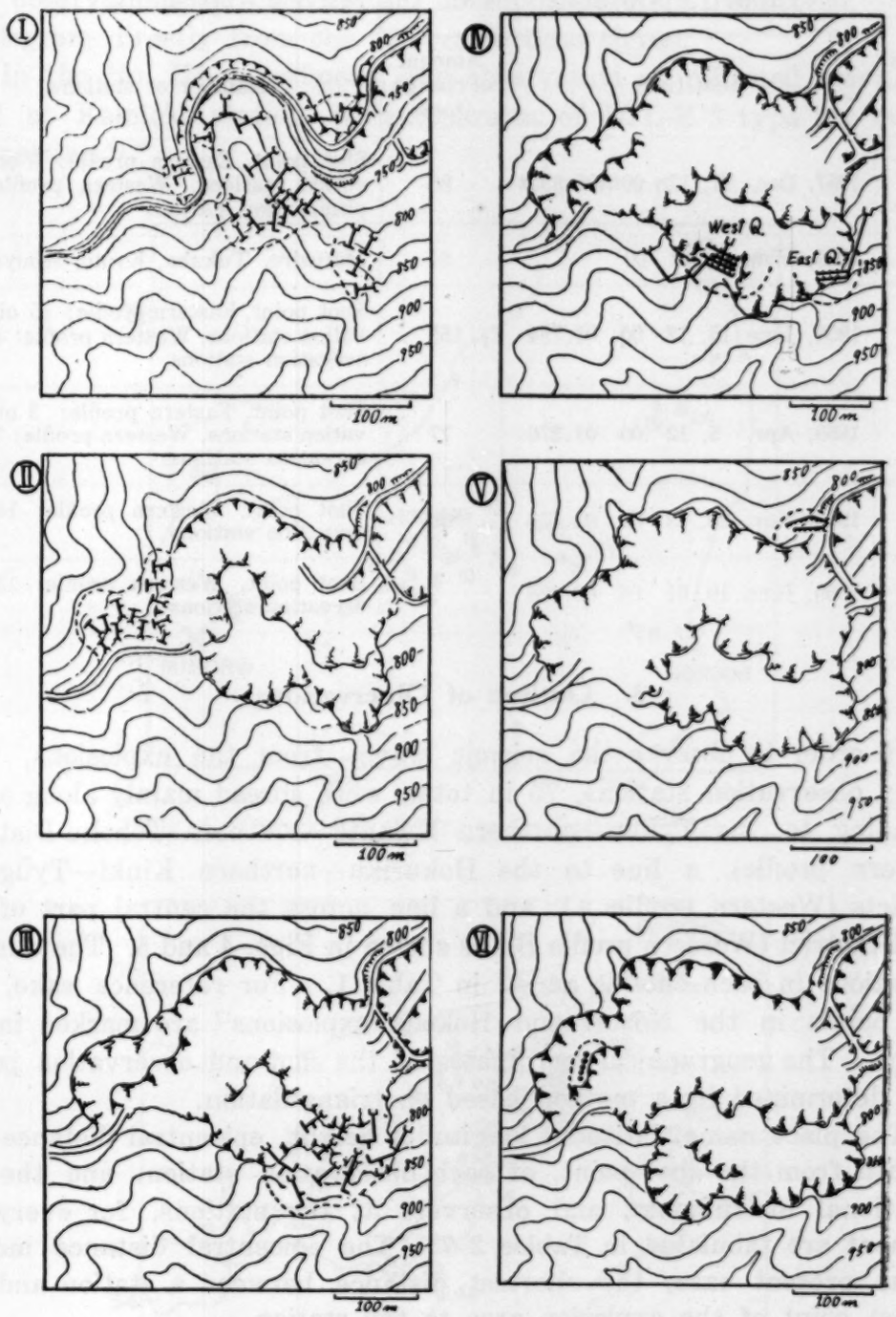

Fig. 3. Details of explosion feature (I–VI).

⊢⊢ Coyote-tunnel blast system.
●●● Bench-cut blast hole system.
--- Quarry area.

Table 1. Observations of the Miboro explosions.

No. of Explosion	Shot time	Amount of charge (tons)	Number of stations
I	1957, Dec. 21, 12h 00m00.831s	86	Shot point, Eastern profile: 8 observation stations, Western profile: 8 observation stations
II	1958, Mar. 5, 12 00	81	Matusiro, Tukuba, Kyoto, Abuyama
III	1958, June 15, 12 00 01.754	155	Shot point, Eastern profile: 15 observation stations, Western profile: 4 observation stations
IV	1959, Apr. 5, 12 00 01.276	77	Shot point, Eastern profile: 3 observation stations, Western profile: 7 observation stations
V	1959, Nov. 20, 12 00 01.173	30	Shot point, Western profile: 14 observation stations
VI	1960, June 10, 01 05 00.906	2.67	Shot point, Western profile: 12 observation stations

3. Outline of Observations

In order to observe the seismic waves from the explosions, temporary observation stations, 75 in total, were spread mainly along a line extending to the Tyûbu—northern Kwantô—southern Tôhoku-Districts (Eastern profile), a line to the Hokuriku—northern Kinki—Tyûgoku-Districts (Western profile A), and a line across the central part of the Kinki-District (Western profile B), as shown in Figs. 4 and 5. The number of stations in each shot is added in Table 1. For reference sake, the shot points in the Nozori and Hokoda explosions[1] are marked in the figures. The geographical coordinates of the shot and observation points were determined by a method based on triangulation.

The place name, latitude, longitude, height, epicentral distance and azimuth from the shot point, of each observation station, and the observational instruments, and observers at the stations, for every experiment are tabulated in Tables 2–7. The epicentral distance means, in the present case, the shortest distance between a station and the nearest point of the explosion area to the station.

Most of the stations were equipped with electromagnetic transducers with a natural frequency of 3 c/s, amplifiers and oscillographs, as in

1) The Research Group for Explosion Seismology, *Bull. Earthq. Res. Inst.*, **36** (1958), 329-348; **37** (1959), 495-508.

past observations of this kind. Time marks were registered on the oscillogram directly from the JJY radio time signal.

In the No. III experiment, the observation of reflected waves was tried at Kamioka station, with apparatus of ETL-M-3 type for seismic prospecting.[2)]

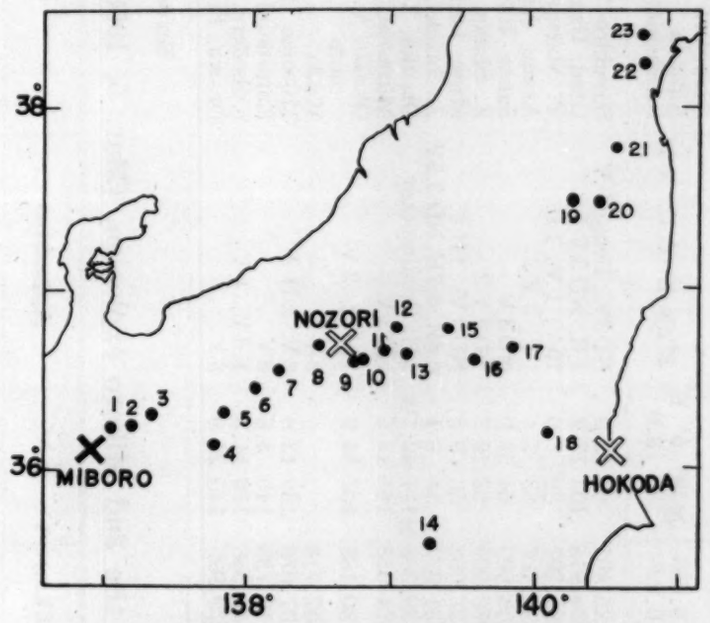

Fig. 4. Observation stations in the Eastern profile.

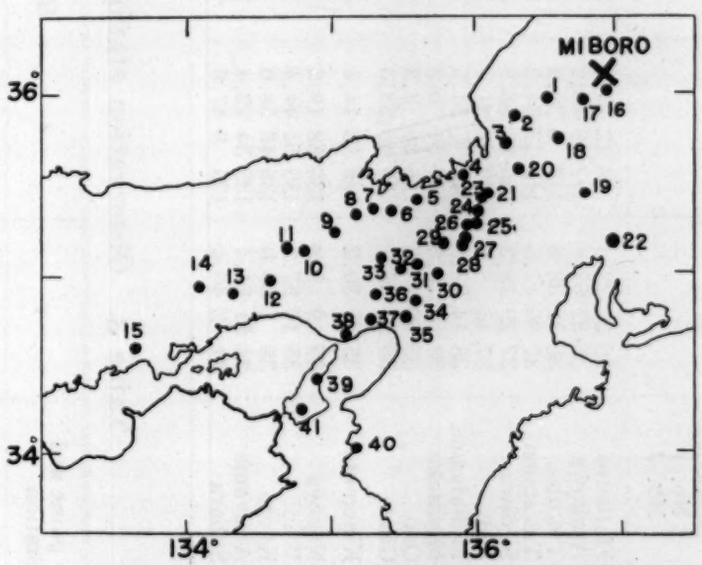

Fig. 5. Observation stations in the Western profile.

2) Report R.G.E.S., No. 17 (1958), 8-10.

Table 2. Observation stations in the 1st Miboro explosion. (Dec. 21, 1957)

Shot point and Station		φ	λ	H(m)	Δ(km)	Θ	Apparatus	Observer
0	(shot point) Miboro	36° 7′22″6N	136°54′26″5E	790~840	0.000			
	(stations)							Ninagawa
	No. 1				0.039	N48° 0′ E	27 c/s E. T. L. ×3	Kamata
	No. 2				0.225	59 8.0		Kawashima
E 7	Matusiro	36 32 22.4	138 12 23.6	383	125.401	68 22.9	ND 3V, Benioff V	Suyehiro Yamagishi
E 14	Asakawa	35 37 52.7	139 16 45.2	195	220.915	104 17.2	1 H, ND 3 V 2	Utsu, Usami
E 18	Tukuba	36 12 38.6	140 6 39.9	286	288.297	88 3.9	10 V, 1 V, 1 H	T. Matsumoto
E 19	Takatama	37 30 17.5	140 17 54.5	516	339.197	63 7.4	1 V, 3 V 2	Asano, Asanuma
E 20	Siroiwa	37 29 28.3	140 28 53.2	344	353.003	64 32.9	ND 3 V	Santo, Karakama, Goto
E 21	Isida	37 46 5.8	140 38 11.7	163	378.909	62 12.7	ND 3 V 2	E. Shima, Sibano
E 22	Mukaiyama	38 14 32.9	140 17 54.5	128	422.052	56 9.3	ND 3 V, 3 H 2	Mine, Ishigaki
E 23	Miyatoko	38 24 0.6	140 51 0.3	49	431.327	54 9.1	0.8H, 0.7H, ND 3.5V	Z. Suzuki, T. Sato
W 1	Ôno	35 59 30.2	136 30 2.2	171	39.368	N111 40.1W	2 H, Strainmeter	Ôtsuka, T. Tanaka
W 19	Gihu	35 27 35.1	136 46 53.3	50	74.358	161 12.5	ND 3 V	Muramatsu, Yabashi
W 20	Kinomoto	35 35 30.2	136 18 14.4	340	80.185	137 14.6	14 V 2, 3 V	Okano, Y. Kobayashi, Kawamoto
W 22	Nagoya	35 9 9.9	136 58 19.5	53	107.716		3 V 2	Wada
W 28	Wani	35 10 52.2	135 54 44.4	128	137.878	139 13.6	2 V, 2 H 2	Mikumo, Funabiki
W 30	Kyoto	35 1 30.0	135 46 58.0	54	158.735	140 4.5	2 V	Kamitsuki, Okamoto
W 34	Abuyama	34 51 24.4	135 34 22.4	215	185.356	139 14.3	1.3 V, 1 V	Kubodera,
W 40	Suhara	34 2 40.4	135 9 47.0	5	279.995	145 23.9	3 V	Ozawa, Fujiwara

Surveyer: A. Okada

Table 3. Observation stations in the 2nd Miboro explosion. (Mar. 5, 1958)

Shot point and Station		φ	λ	H(m)	Δ(km)	Θ	Apparatus	Observer
0	Miboro	36° 7′24″3N	136°54′17″1E	895	0			
E 7	Matusiro	36 32 22.4	138 12 23.6	383	125.691	N 68° 19′ E	ND 3 V 2	Suyehiro
E 18	Tukuba	36 12 38.6	140 6 39.9	286	288.599	88 2	3 V 2, 1 H	T. Matsumoto
W 30	Kyoto	35 1 30.0	135 46 58.0	54	158.593	N140 5 W	2 V 2	Mikumo, Ôtsuka
W 34	Abuyama	34 51 24.4	135 34 22.4	215	185.208	139 14	3 V, 1 V	Okano

Table 4. Observation stations in the 3rd Miboro explosion. (June 15, 1958)

Shot point and Station		φ	λ	H(m)	Δ(km)	Θ	Apparatus	Observer
0	Miboro	36° 7′18″7 N	136°54′29″3 E	815	0	N E	S. S. C ×3	Ninagawa, Hirasawa, Kawashima, Furuya
	No. 1				0.124	19°		
	No. 2				0.277	28		
	No. 3				0.526	59		
E 1	Myôgase	36 13 30.7	137 1 16.2	650	15.239	41° 34′0	15V (E.T.L.), 3V, 3H	Wada, Shichi
E 2	Kotakari	36 14 22.2	137 9 30.0	530	25.930	59 53.2	2V, 2H, Strainmeter	Ôtsuka, T. Tanaka
E 3	Kamioka	36 17 53.1	137 19 3.3	568	41.585	62 3.9	E. T. L. ×12	Murauchi, Asanuma
E 4	Inekoki	36 9 29.5	137 45 57.6	831	77.222	87 0.6	4 V, 2 V	Muramatsu, Yabashi
E 5	Hotako	36 19 39.2	137 49 21.1	988	85.224	74 29.0	3 V 3	Nakajima, Yamazaki
E 6	Omi	36 27 47.0	138 2 34.6	756	108.614	69 40.1	3 V	H. Okada, Takeuchi
E 7	Matusiro	36 32 22.4	138 12 23.6	383	125.354	68 19.1	Benioff	
E 8	Hoppo	36 43 39.1	138 30 39.8	1670	158.578	64 56.6	3 V	Suyehiro, Takeyama
E 10	Sawatari	36 37 1.6	138 46 39.8	515	176.440	71 51.9	3 V 2	E. Shima, Yanagisawa
E 11	Takayama	36 37 40.6	138 58 7.0	604	193.124	73 6.4	3 V 2	Asada, Terashima, Kurimoto
E 12	Hujiwara	36 48 5.8	139 2 56.7	604	206.080	68 32.7	3 H, 1.3 V, 2.8 V	Santo, Karakama
E 13	Kawaba	36 40 11.2	139 6 30.0	497	206.418	72 52.9	3 V 3	Asano, Oguchi
E 15	Yumoto	36 18 6.9	139 25 19.5	1498	237.510	71 29.5	3.4 V, 2 H 2	Z. Suzuki, H. Shima, Emura
E 16	Nisioasi	36 37 48.0	139 36 32.2	405	248.702	76 54.3	3 V, 6 V, 6 H	Utsu, Usami
E 18	Tukuba	36 12 38.6	140 6 39.9	286	288.218	88 2.4	3 V, 1 V	T. Matsumoto, Saito
W24	Sin'asahi	35 21 8.2	136 0 59.4	148	117.353	N W 136 37.8	1.5 V	Ozawa, Fujiwara
W34	Abuyama	34 51 24.4	135 34 22.4	215	185.303	139 11.8	1 V	Kubodera, H. Watanabe
W37	Rokkô	34 45 52.7	135 14 56.6	868	212.866	134 59.3	3 V	Okano, Nishi
W39	Sizuki	34 25 52.9	134 53 50.6	20	261.860	135 42.6	3 V, 2 V	Mikumo Kamitsuki

Surveyer: A. Okada

Table 5. Observation stations in the 4th Miboro explosion. (Apr. 5, 1959)

Shot point and Station		φ	λ	H(m)	Δ(km)	θ N E	Apparatus	Observer
0	Miboro (a)(*)	36° 7′18″8N	136°54′20″2E	850	0 (*)			Furuya, Hirasawa, Kamata
	(b)(*)	36 7 18.0	136 54 31.3	815	0 (*)			
	No. 1			770	0.192	17°	(made in NEC) 28 c/s	
	No. 2			775	0.385	41	〃	
	No. 3			775	0.575	55	〃	
W10	Ikuno	35 9 42.5	134 48 18.1	355	218.008	240°45′5	3 V	Okano
W12	Yamazaki	34 58 41.4	134 33 24.4	86	247.874	249 13.0	3 V 2	Usami, Utsu, Asanuma
W26	Takasima	35 17 4.9	135 56 40.6	282	127.233	223 6.9	Den 1V2, Den 3.5 H 2	Terashima, Oguchi, Den
W32	Kameoka	35 2 0.7	135 28 22.3	355	177.306	226 59.0	3 V 1	Muramatu, Kajita
W33	Taki	35 6 58.6	135 20 30.3	298	180.312	231 46.8	3 V, 3 H 2	Tamaki, Kawamoto
W38	Tainohata	34 39 31.6	135 5 54.4	110	230.849	225 19.7	3 V 2	Mikumo, Ôtsuka, Nakajo
W41	Kitaama	34 16 9.9	134 46 53.2	125	282.195	223 16.3	3 V 3, 1 V	Santo, Tsujiura, Maruyama
E 7	Matusiro	36 32 22.4	138 12 23.6	383	125.418	68 19.0	Benioff	
E 9	Ôiwa	36 36 19.4	138 43 37.5	696	171.774	71 47.7	3 V 3	Nakajima, Yamazaki
E17	Sinoi	36 41 15.8	139 50 4.6	355	274.064	73 14.1	3 V 2	Asano, Yanagisawa

(*) (a) is a standard point for western stations.
(b) is a standard point for eastern and near-by stations.

Surveyer: A. Okada

Table 6. Observation stations in the 5th Miboro explosion. (Nov. 20, 1959)

Shot point and Station		φ	λ	H(m)	Δ(km)	Θ	Apparatus	Observer
0	Miboro	36°7′26″28 N	136°54′29.76 E	770		N E		Ninagawa, Ichikawa, Tamura
	No. 1				0.114	56°		
	No. 2				0.334	71		
	No. 3				0.483	73		
						N ° ′ W		
W 2	Nakai	35 52 56.5	136 16 38.1	104	62.886	115 13.8	3 V 2	Asanuma, Iino
W 3	Utuo	35 43 37.0	136 13 47.4	201	75.421	125 44.1	3 V	Nakajima, Yamazaki
W 5	Ôi	35 26 45.4	135 36 14.4	45	139.853	122 32.2	3 V 3	Muramatu, Komatu
W 6	Yatuai	35 21 6.5	135 24 58.2	197	159.851	122 24.2	3 V 2	T. Matsumoto, Karakama
W 7	Yasiro	35 22 52.3	135 18 4.9	125	167.055	119 33.3	1 H, 1 V	Terashima, Noguti
W 8	Hukutiyama	35 20 19.5	135 10 15.8	155	179.672	118 59.9	ND 3, DK 1 V	Onda, Seino, Hotta
W 9	Aogaki	35 14 11.4	135 1 34.1	179	196.761	120 1.6	3 V 2	Sakai, Hamamatsu
W11	Kawakami	35 9 4.5	134 42 45.0	466	226.243	118 29.1	3 H 2, 3 V	Kawamoto and two others
W13	Kamigori	34 53 51.2	134 21 12.0	189	268.723	120 24.8	3 V, 1 H 2	Hori, Tsujiura, Ando
W14	Yanahara	34 57 5.8	134 4 32.5	122	287.882	116 51.1	3 V, 1 H 2	Santo, H. Matsumoto, Saito
W15	Yakage	34 35 12.6	133 38 17.4	105	342.602	119 50.4	4 V 2	E. Shima, Asano, Oguchi
W21	Kaizu	35 26 45.3	136 5 22.1	86	105.533	135 27.8		Takagi, Ito
W29	Bessyo	35 10 2.6	135 46 56.2	640	147.168	136 8.6	3 V	Okano, Wada
W31	Sikibigahara	35 3 47.5	135 36 49.5	498	166.155	135 5.5	3 V	Mikumo, Ôtsuka

Surveyer: A. Okada

Table 7. Observation stations in the 6th Miboro explosion. (June 10, 1960)

Shot point and Station		φ	λ	H(m)	Δ(km)	Θ	Apparatus	Observer
						N E		
0	Miboro	36° 7′23″4N	136°54′18″8E	794~812				Chujo, Mori, Kawashima
	No. 1			780	0.170	51.9	S.S.G 26 c/s	
	No. 2			775	0.373	77.8	〃	
	No. 3			770	0.487	77.1	〃	
	No. 4			770	0.646	79.6	〃	
	No. 5			770	0.755	79.0	〃	
W 2	Nakai	35 52 58.1	136 16 37.3	107	62.596	115°12.9′	3 V 2	Asanuma, Terashima
W 4	Mikata	35 32 52.0	135 55 7.6	90	109.619	125 36.9	3 V 2	Onda, Hotta
W 9	Aogaki	35 14 11.4	135 1 34.1	179	196.480	120 2.4	3 V 2, 2/3 H	Utsu, Hamamatsu
W16	Arabuti	36 1 43.9	136 57 33.8	789	11.545	165 0.9		Kumazawa, Aoki
W17	Itosiro	35 58 10.5	136 46 28.4	685	20.711	145 21.5	3 V 2, 1 V	Oguchi, Asano
W18	Ôgawara	35 44 53.7	136 34 53.0	452	50.832	144 54.9	3 V 2, 3 H	Muramatus, Kajita
W23	Kitoge	35 25 7.3	136 2 3.4	87	110.945	134 47.1	3 V 3	Nakajima, Yamazaki
W25	Sirahige	35 16 19.2	136 0 48.4	98	124.215	139 28.9	3 V 2	Saito, Karakama
W27	Kido	35 11 54.9	135 55 2.0	72	137.040	138 54.5	3 V	Ôtsuka, Mikumo
W34	Abuyama	34 51 24.4	135 34 22.4	215	185.333	139 17.3	3 V 2	Okano, H. Watanabe
W35	Senriyama	34 46 8	135 30 46	70	196.330	139 55.1	3 V	Kamitsuki
W36	Ôharano	34 54 26.4	135 18 24.2	210	198.020	132 55.8	3 V, 3 H 2	Tamaki, Kawamoto

Surveyer: A. Okada

4. Observed Results

Observations were carried out successfully, obtaining satisfactory seismograms at most of the stations. The seismograms are shown in Fig. 9. These records were read independently by several members of our group, and then the arrival times of various phases were determined only when satisfactory agreement was found. For the sake of convenience, the accuracy of the adopted values was classified into four grade, taking the clarity of the initial motion and time marks into consideration :

a : $\Delta t \leqq 0.02$ sec
b : $0.02 < \Delta t \leqq 0.05$ "
c : $0.05 < \Delta t \leqq 0.1$ "
d : $0.1 < \Delta t$ "

where Δt is the expected errors in the time determination.

Tables 8–13 indicate the arrival times of the first P wave and prominent later phases observed at all stations in the six observations. They are reduced to the travel times and rearranged in Tables 14, 15

Table 8. Observational data of the 1st Miboro explosion. (Dec. 21, 1957)

Station		P	Direction	Accuracy	Later phases			
0	Miboro	12h 00m 00.s831						
	No. 1	00.855	U	a				
	No. 2	00.933	U	a				
E 7	Matusiro	22. 70	U	b	28.37	41.5		
E14	Asakawa	37. 16	D	a	43.18	44.98	01 m 04.00	
E18	Tukuba	45. 04	D	b	48.31			
W 1	Ôno	07. 93	D	b	13.39			
W19	Gihu	13. 95	U	a	15.22	16.30	18.11	23.65
W20	Kinomoto	14. 91	U	b	17.10	24.67		
W28	Wani	24. 7	U	d	42.5			
W30	Kyoto	28. 3	D	d	48.3			
W34	Abuyama	32. 18	U	a	32.43	54.98		
W40	Suhara	44. 6	D	d	01m 19.2	20.7		

Table 9. Observational data of the 2nd Miboro explosion. (Mar. 5, 1958)

Station		P	Direction	Accuracy	Later phases
E 7	Matusiro	12h 00m 20s.42	D	b	20.80 21.70 37.88
W34	Abuyama	30.06	U	b	31.15 33.42

Table 10. Observational data of the 3rd Miboro explosion. (June 15, 1958)

Station		P	Direction	Accuracy	Later phases
0	Miboro	12h 00m 01s.754			
	No. 1	01.874	U	a	
	No. 2	01.864	U	a	
	No. 3	01.903	U	a	
E 1	Myôgase	04. 66	U	a	09.66 10.33 12.41 14.35 19.78
E 2	Kotakari	06. 57	U	a	06.88 10.90
E 3	Kamioka	09. 12	U	a	09.89 10.29 11.13 12.60 12.99 14.47 15.15
E 4	Inekoki	15. 41	D	a	16.53 21.27 25.37
E 5	Hotaka	16. 60	D	b	17.56
E 6	Omi	20. 7	D	d	20.9 23.0 34.1 39.2
E 7	Matusiro	22. 9	D	d	
E 8	Hoppo	28. 97	D	b	29.45 32.68 36.08 49.25 49.80
E10	Sawatari	32. 3	D	d	
E11	Takayama	34. 33	D	a	
E12	Hujiwara	35. 73	U	b	35.95
E13	Kawaba	35. 84	U	b	36.24 38.40 42.03 01m 00.43 01.43
E15	Yumoto	40. 13	D	a	42.04 49.68 01m 08.81
E16	Nisioasi	41. 36	D	b	41.55 45.74
E18	Tukuba	45. 92	D	b	47.66 48.73 55.90 01m 07.26 20.65 27.75
W24	Sin'asahi	22. 0	U	d	23.1 30.5 39.3 42.2
W34	Abuyama	32. 6	U	d	
W37	Rokkô	37. 80	U	a	01m 03.90 04.07
W39	Sizuki	46. 35	U	b	01m 17.23 18.68

Table 11. Observational data of the 4th Miboro explosion. (Apr. 5, 1959)

Station		P	Direction	Accuracy	Later phases				
0	Miboro	12h 00m 01s.276							
	No. 1	01.382		a					
	No. 2	01.385		a					
	No. 3	01.422		a					
W10	Ikuno	36. 36	U	d	36.65				
W12	Yamazaki	40. 35	U	a	42.58	43.52	72.02		
W26	Takasima	22. 28	D	c	23.78	40.27	40.58	40.82	41.10
W32	Kameoka	30. 94	U	c	31.05	31.57	53.15		
W33	Taki	31. 54	U	c	32.32				
W38	Tainohata	38. 38	U	c	38.42	40.78			
W41	Kitaama	44. 48	D	a	53.37				
E 7	Matusiro	23. 4	U	d					
E 9	Ôiwa	30, 29	D	d	31.35				
E17	Sinoi	44. 5	D	d					

Table 12. Observational data of the 5th Miboro explosion. (Nov. 20, 1959)

Station		P	Direction	Accuracy	Later phases				
0	Miboro	12h 00m 1s.73(*)							
	No. 1	1.762	U	a					
	No. 2	1.814	U	a					
	No. 3	1.846	U	a					
W 2	Nakai	12. 48	U	a	13.13				
W 3	Utuo	14. 77	D	a	14.95	15.28	24.09		
W 5	Ôi	25. 26	D	c	25.44	25.53	25.73	42.62	
W 6	Yatuai	28. 99	U	b					
W 7	Yasiro	29. 79	Pull	b	29.79	30.03	49.7		
W 8	Hukutiyama	31. 38		b	32.06	32.14	52.88		
W11	Kawakami	37. 64	D	a	37.97	39.34	65.66		
W13	Kamigori	43. 44	U	b	77.69				
W14	Yanahara	45. 99	D	b	46.45	46.54	49.98		
W15	Yakage	51. 34	U	d					
W21	Kaizu	19. 64	U	b	19.89	20.00	20.42	20.71	21.33
W29	Bessyo	26. 98	D	c	27.35	27.66	27.72	46.35	
W31	Sikibigahara	30. 13	D	a	30.45	50.3			

* The shot time is checked using the data of Nakai station in the 6th Miboro explosion.

Table 13. Observational data of the 6th Miboro explosion.
(June 10, 1960)

Station		P	Direction	Accuracy	Later phases				
0	Miboro	$01^h\ 05^m\ 0^s.906$							
	No. 1	0.955	U	a					
	No. 2	0.999	U	a					
	No. 3	1.020	U	a					
	No. 4	1.052	U	a					
	No. 5	1.075	U	a					
W 2	Nakai	11. 61	U	a	12.27				
W 4	Mikata	19. 94	U	a	19.97	20.38	20.40	20.44	21.00
W 9	Aogaki	33. 25	U	a	34.32	34.36	57.35		
W16	Arabuti	3. 00	U	a	4.65	4.89			
W17	Itosiro	4. 64	U	a	7.46	7.69			
W18	Ôgawara	9. 65	U	a	10.20	13.11			
W23	Kitoge	20. 38	D	b	21.13	21.16			
W25	Sirahige	22. 48	U	c	23.09				
W27	Kido	25. 86	D	c					
W34	Abuyama	31. 60	U	b	32.53	55.84	56.55		
W36	Ôharano	33. 64	U	c	33.79	34.37	58.09	58.13	

and 16 for the said three profiles, respectively. Travel-time graphs are shown in Figs. 6 and 7.

In order to obtain knowledge about the superficial structure, pickups were set up within a distance of 800 m from the shot points. The results are shown in Table 17 and Fig. 8. But the here-mentioned distance must be corrected in the travel-time calculation, taking the topographical effects into account.

It is to be added here that fairly distinct phases were observed at Kamioka station[3]. The observed data are listed in Table 18.

Crustal structure in central Japan, derived from the above observed data will be discussed in Part 2 of this paper under the same title[4].

3) S. MURAUCHI, *Report R.G.E.S.*, No. 17 (1958), 9.
4) T. MIKUMO *et al.*, *Bull. Earthq. Res., Inst.*, **39** (1961) 321-343.

Table 14. Travel times for the Eastern profile.

No. of Station	No. of observation	Station	Δ(km)	$P-O$(see)	$(P-O)-\Delta/6$(sec)
E 1	III	Myogase	15.24	2.91	+0.37
〃 2	〃	Kotakari	25.93	4.82	+0.50
〃 3	〃	Kamioka	41.59	7.37	+0.44
〃 4	〃	Inekoki	77.22	13.66	+0.79
〃 5	〃	Hotoka	85.22	14.85	+0.65
〃 6	〃	Omi	108.61	18.8	+0.7
〃 7	I	Matusiro	125.40	21.87	+0.98
〃 8	III	Hoppo	158.58	27.22	+0.70
〃 9	IV	Ôiwa	171.77	29.01	+0.38
〃 10	III	Sawatari	176.44	30.4	+1.0
〃 11	〃	Takayama	193.12	32.58	+0.40
〃 12	〃	Huziwara	206.08	33.98	−0.36
〃 13	〃	Kawaba	206.42	34.09	−0.31
〃 14	I	Asakawa	220.92	36.33	−0.48
〃 15	III	Yumoto	237.51	38.38	−1.20
〃 16	〃	Nisioasi	248.70	39.61	−1.84
〃 17	IV	Sinoi	274.06	43.2	−2.5
〃 18	III	Tukuba	288.22	44.17	−3.87

Table 15. Travel times for the Western profile (A).

No. of Station	No. of observation	Station	Δ(km)	$P-O$(sec)	$(P-O)-\Delta/6$(sec)
W 1	IV	Ôno	39.37	7.10	+0.54
〃 2	I	Nakai	62.89(V) 62.60(VI)	10.75(V) 10.70(VI)	+0.27
〃 3	VI	Utuo	75.42	13.04	+0.47
〃 4	V VI	Mikata	109.62	19.03	+0.76
〃 5	V	Ôi	139.85	23.53	+0.22
〃 6	VI	Yatuai	159.85	27.26	+0.62
〃 7	V	Yasiro	167.06	28.06	+0.22
〃 8	V	Hukutiyama	179.67	29.65	−0.29
〃 9	VI	Aogaki	196.48	32.34	−0.41
〃 10	IV	Ikuno	218.01	35.07	−1.26
〃 11	V	Kawakami	226.24	35.91	−1.80
〃 12	IV	Yamazaki	247.87	39.07	−2.24
〃 13	V	Kamigōri	268.72	41.71	−3.07
〃 14	V	Yanahara	287.88	44.26	−3.72
〃 15	V	Yakage	342.60	49.61	−7.49

Table 16. Travel times for the Western profile (B).

No. of Station	No. of observation	Station	Δ(km)	$P-O$(sec)	$(P-O)-\Delta/6$(sec)
W 16	VI	Arabuti	11.55	2.09	+0.17
〃 17	VI	Itosiro	20.71	3.73	+0.28
〃 18	VI	Ôgawara	50.83	8.74	+0.27
〃 19	I	Gihu	74.36	13.12	+0.71
〃 20	I	Kinomoto	80.19	14.08	+0.72
〃 21	V	Kaizu	105.53	17.91	+0.32
〃 23	VI	Kitoge	110.95	19.47	+0.98
〃 24	III	Imazu	117.35	20.2	+0.6
〃 25	VI	Sirahige	124.21	21.57	+0.87
〃 26	IV	Takasima	127.23	22.00	+0.79
〃 27	VI	Kido	137.04	23.95	+1.11
〃 28	I	Wani	137.88	23.9	+0.9
〃 29	V	Bessyo	147.17	25.25	+0.72
〃 30		Kyôto	158.74	27.20*	+0.74
〃 31	V	Sikibigahara	166.16	28.40	+0.71
〃 32	IV	Kameoka	177.31	29.66	+0.11
〃 33	IV	Taki	180.31	30.26	+0.21
〃 34	I VI	Abuyama	185.36(I) 185.33(VI)	31.35 (30.69)	+0.46 (−0.20)
〃 36	VI	Ôharano	198.02	32.73	−0.27
〃 37	III	Rokkô	212.87	36.05	+0.57
〃 38	IV	Tainohata	230.85	37.10	−0.37
〃 39	III	Sizuki	261.86	44.60	+0.96
〃 40	I	Suhara	280.00	43.9	−3.83
〃 41	IV	Kitaama	282.20	43.20	−2.8

* This was obtained in the explosion of Nov. 2, 1958.

Table 17. Travel times near the shot point.

No. of Explosion	P. U. Number	Δ (m)	$P-O$ (msec)
I	1	39	24
V	1	114	32
III	1	124	93
VI	1	170	49
IV	1	192	106
I	2	225	102
III	2	277	110
V	2	334	84
VI	2	373	93
IV	2	385	109
V	3	483	116
VI	3	487	114
III	3	526	149
IV	3	575	146
VI	4	646	146
VI	5	755	169

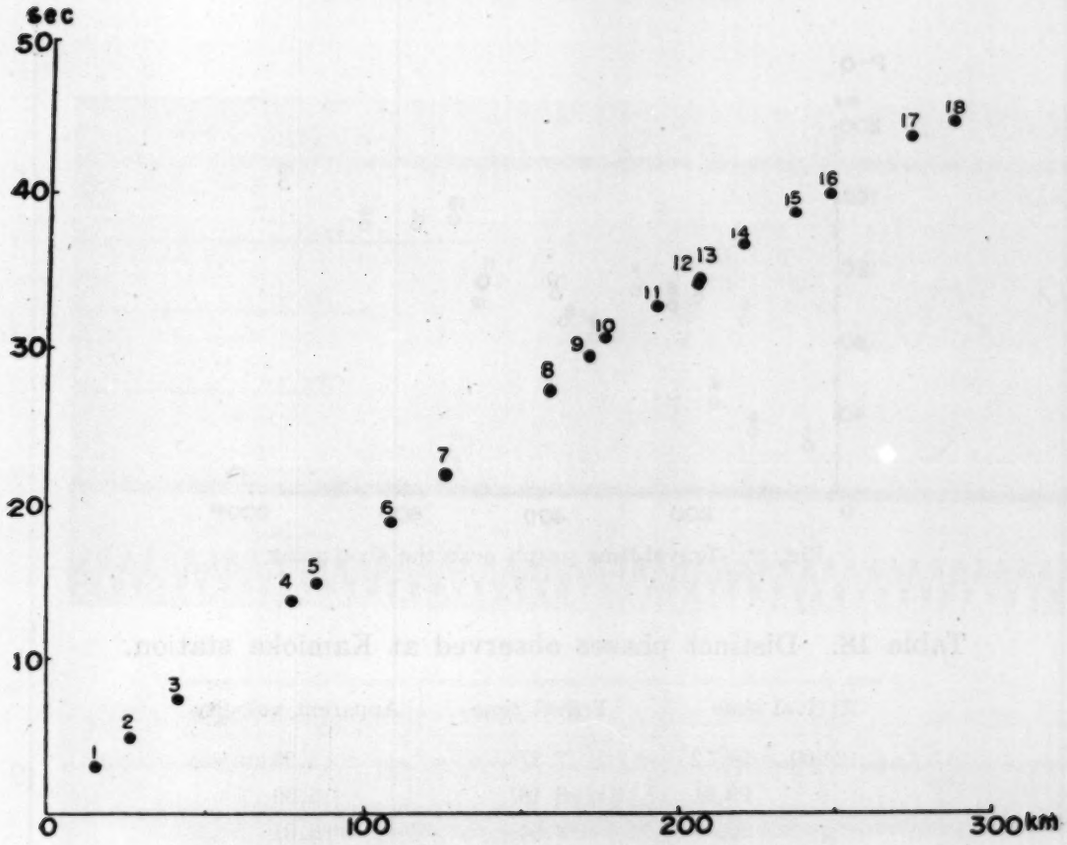

Fig. 6. Travel-time graph in the Eastern profile.

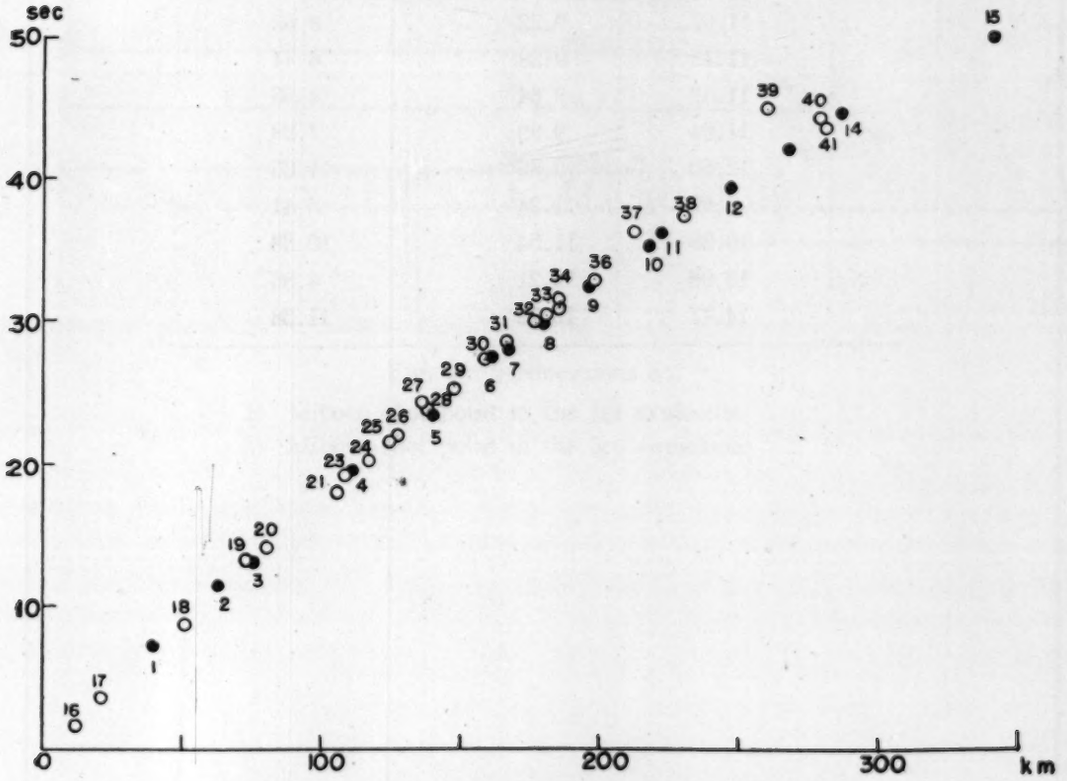

Fig. 7. Travel-time graph in the Western profile.

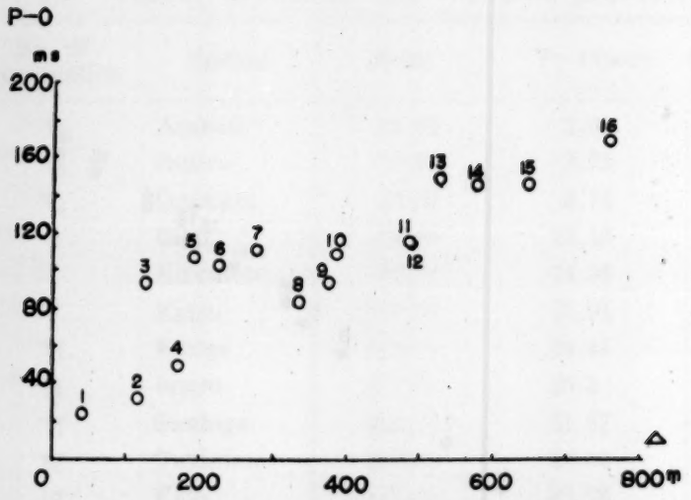

Fig. 8. Travel-time graph near the shot point.

Table 18. Distinct phases observed at Kamioka station.

Arrival time	Travel time	Apparent velocity
$12^h\ 00^m\ 09^s.12$	$7^s.37$	5.98 km/sec
09.91	8.16	5.30
10.29	8.54	6.01
10.48	8.73	5.11
11.07	9.32	8.63
11.13	9.38	6.44
11.39	9.64	4.95
11.64	9.89	7.98
12.60	10.85	11.25
12.99	11.24	8.41
13.29	11.54	10.38
13.96	12.21	6.86
14.47	12.72	11.38

1)

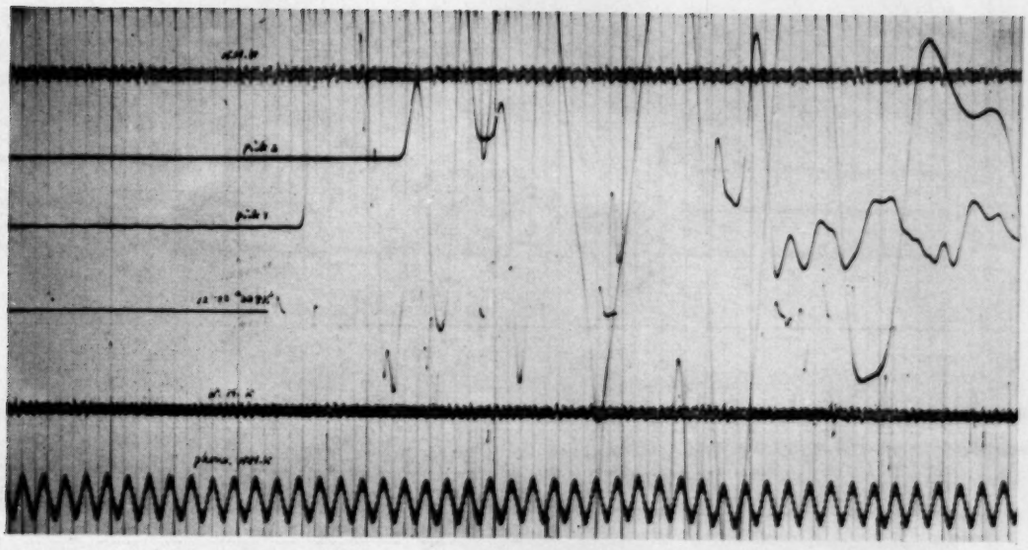

2)

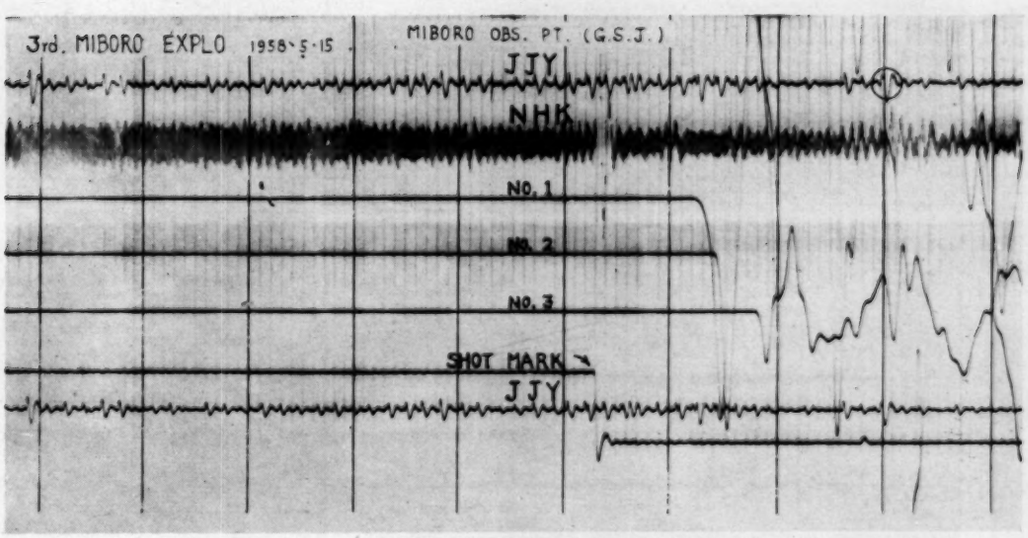

Fig. 9. Seismograms at:

1) Miboro shot point in the 1st explosion.
2) Miboro shot point in the 3rd explosion.

3)

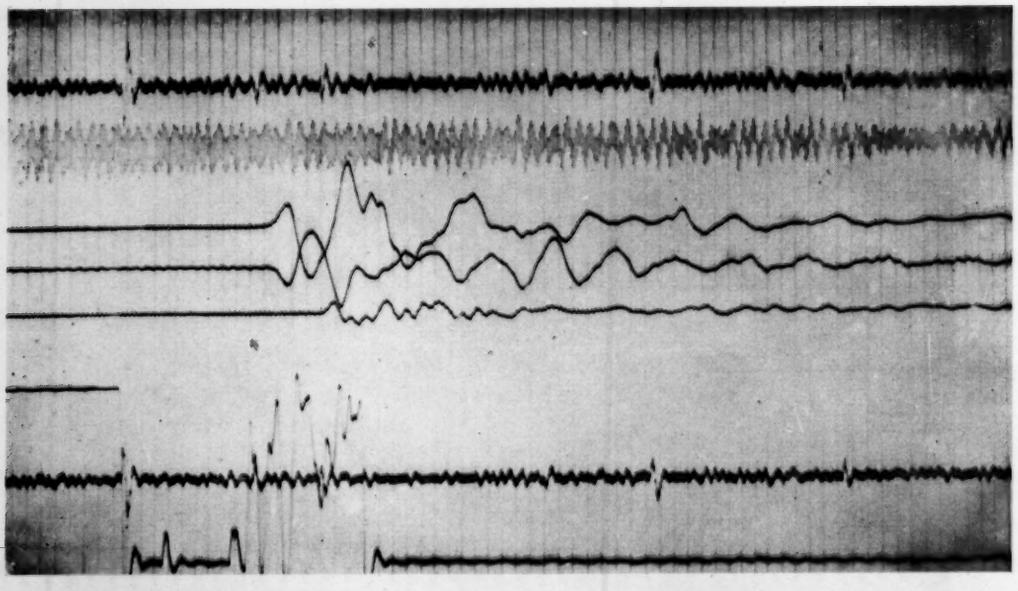

4)

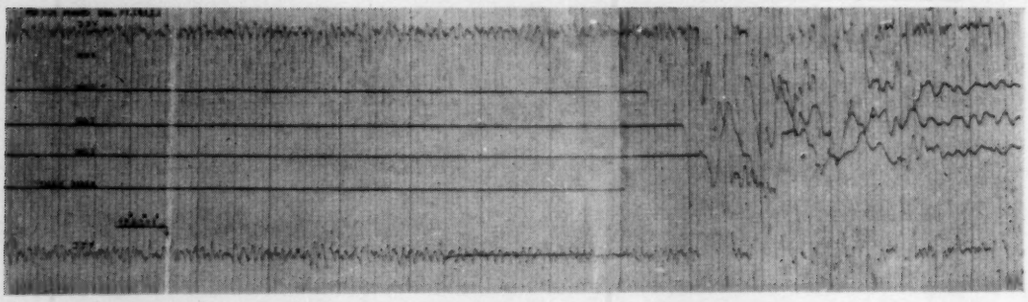

5)

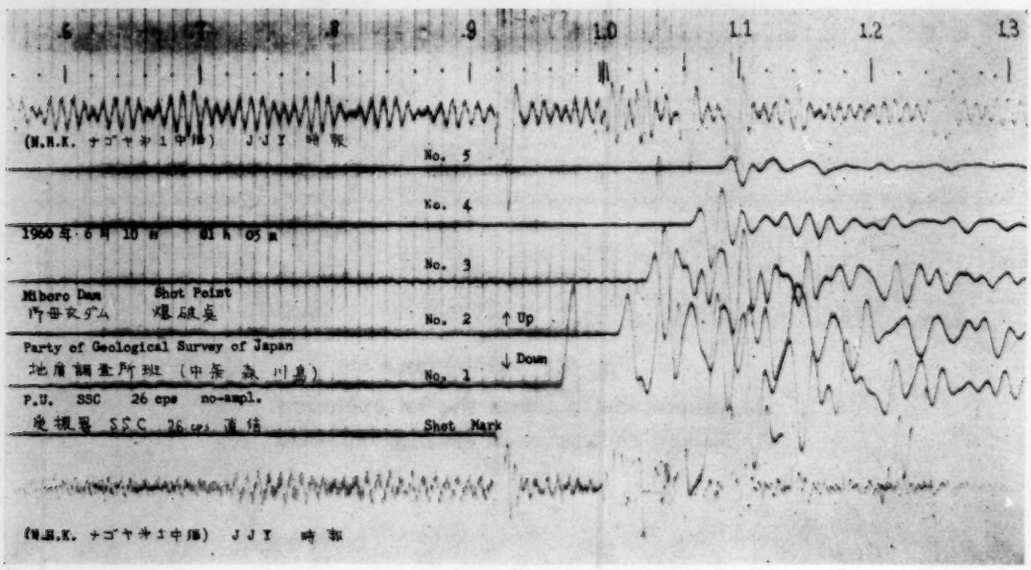

Fig. 9. Seismograms at:

3) Miboro shot point in the 4th explosion.
4) Miboro shot point in the 5th explosion.
5) Miboro shot point in the 6th explosion.

6)

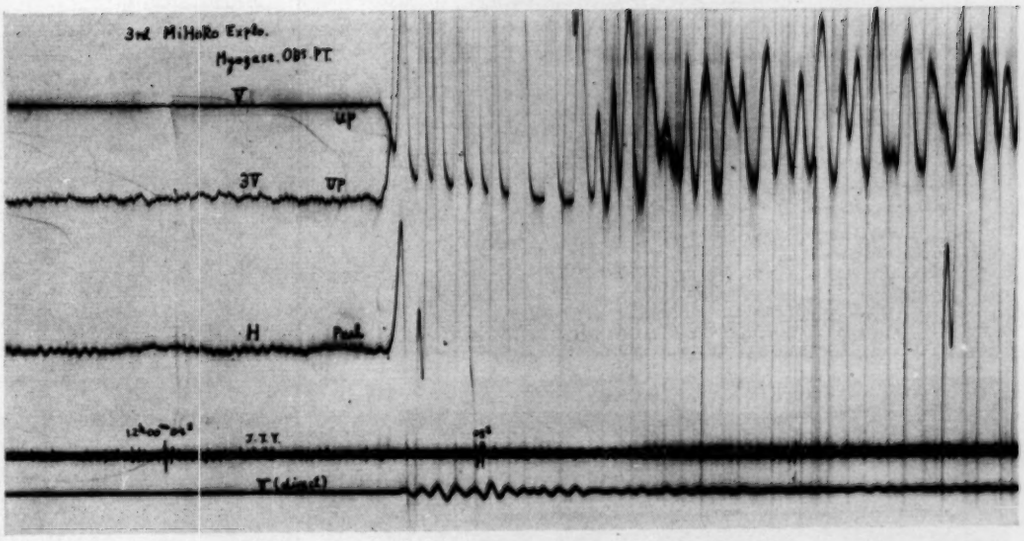

7)

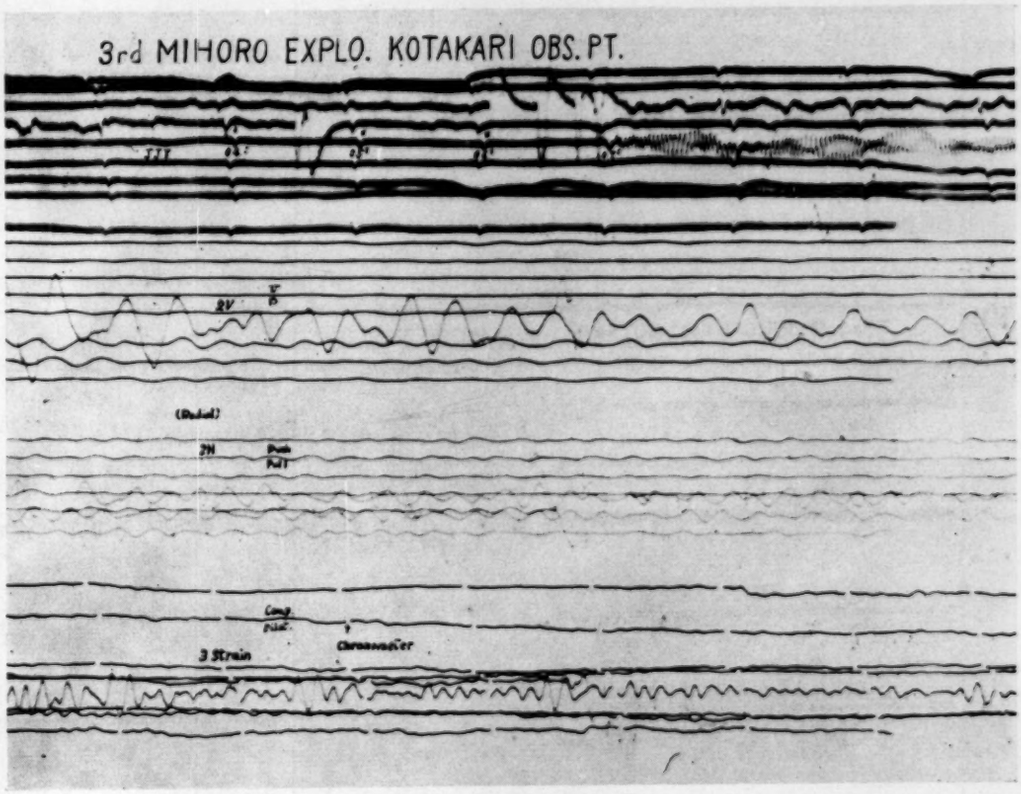

Fig. 9. Seismograms at:

6) E-1 Myôgase in the 3rd explosion.
7) E-2 Kotakari in the 3rd explosion.

8)

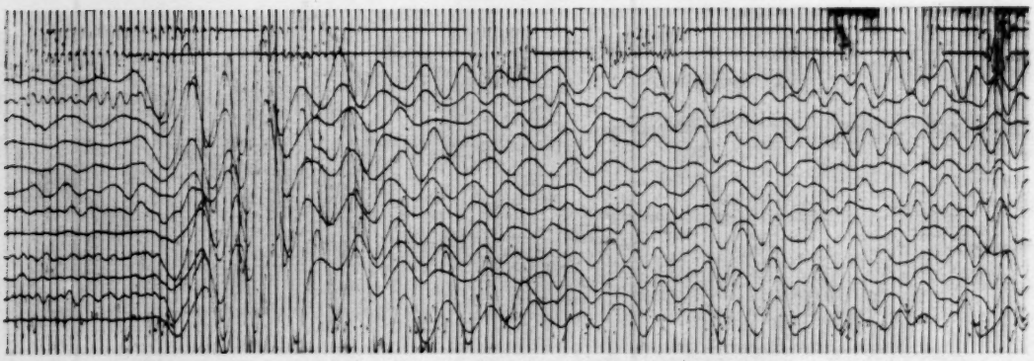

9)

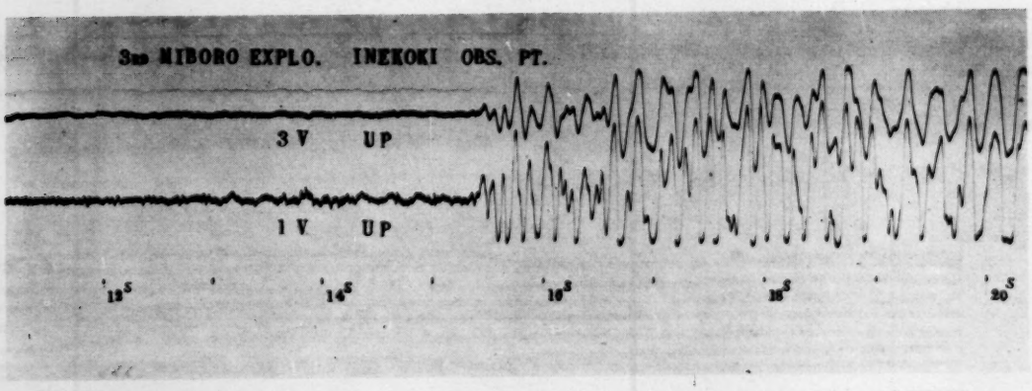

10)

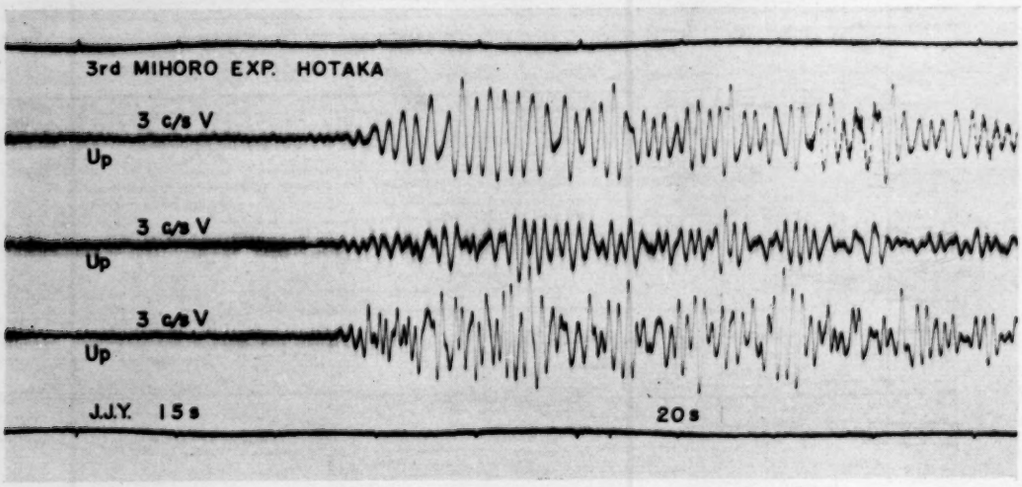

Fig. 9. Seismograms at:

8) E-3 Kamioka in the 3rd explosion.
9) E-4 Inekoki in the 3rd explosion.
10) E-5 Hotaka in the 3rd explosion.

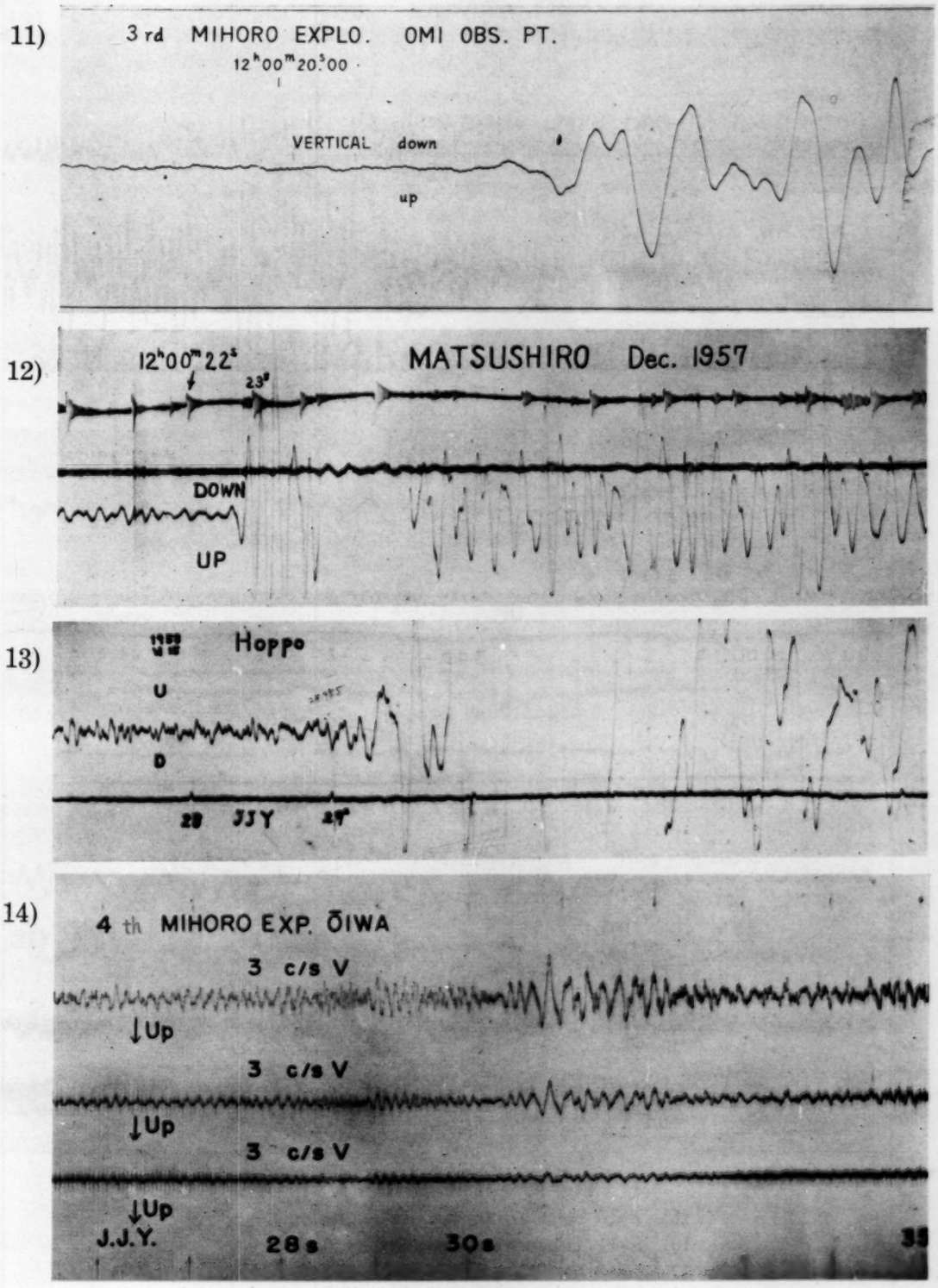

Fig. 9. Seismograms at:

11) E-6 Omi in the 3rd explosion.

12) E-7 Matushiro (Matsusiro) in the 1st explosion.

13) E-8 Hoppo in the 3rd explosion.

14) E-9 Ōiwa in the 4th explosion.

15)

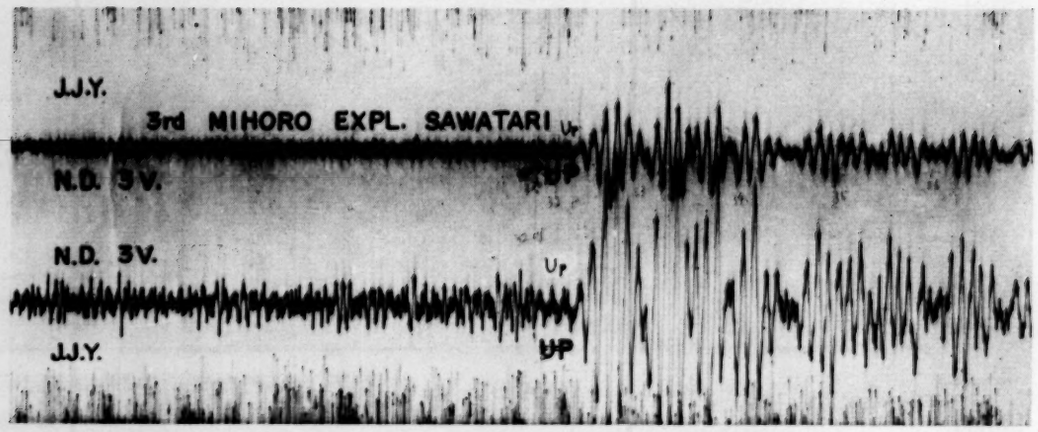

16)

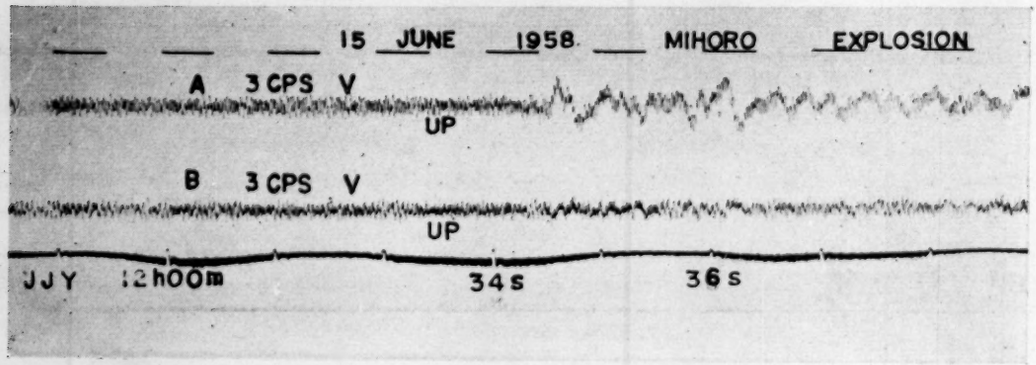

17)

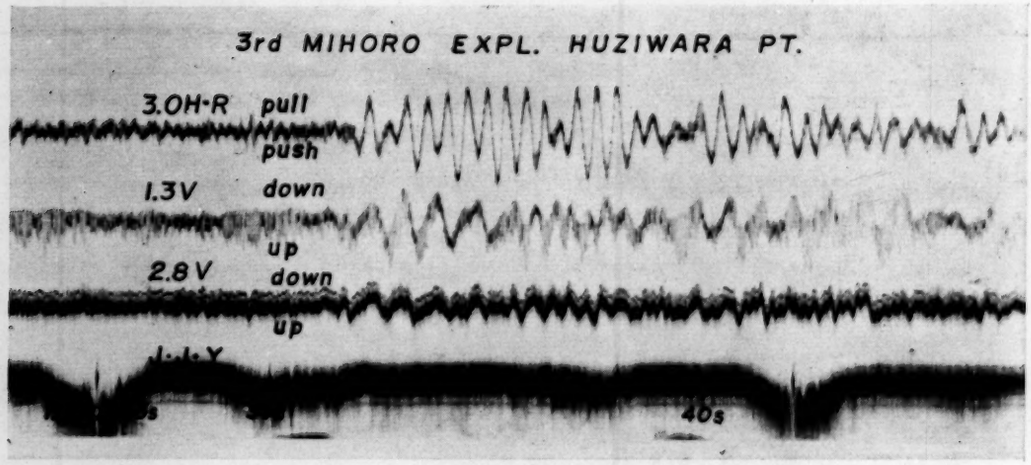

Fig. 9. Seismograms at:
15) E-10 Sawatari in the 3rd explosion.
16) E-11 Takayama in the 3rd explosion.
17) E-12 Huziwara in the 3rd explosion.

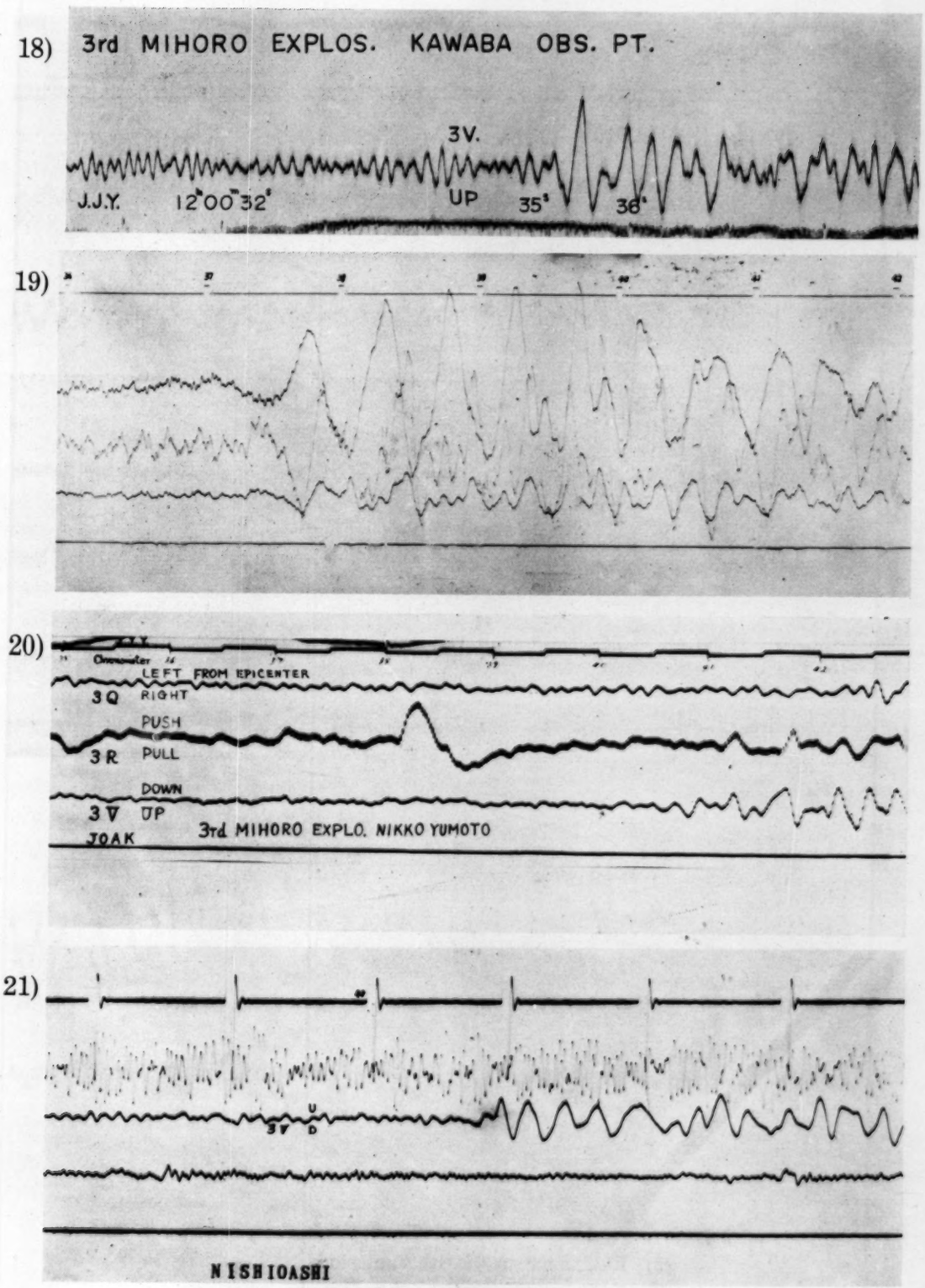

Fig. 9. Seismograms at:

18) E-13 Kawaba in the 3rd explosion.
19) E-14 Asakawa in the 1st explosion.
20) E-15 Yumoto in the 3rd explosion.
21) E-16 Nisiôasi (Nishiōashi) in the 3rd explosion

22)

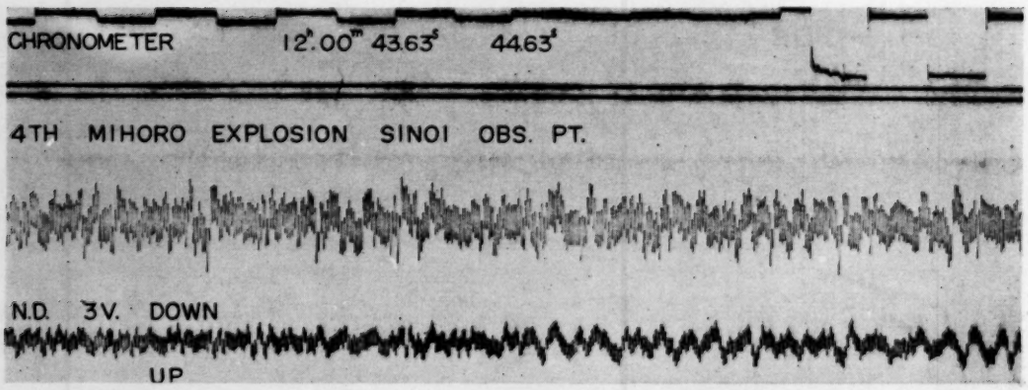

23)

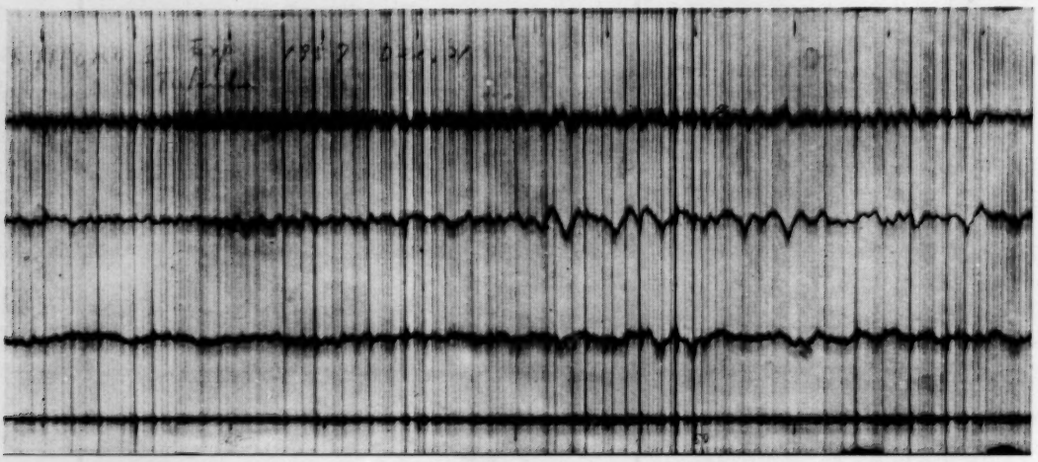

24)

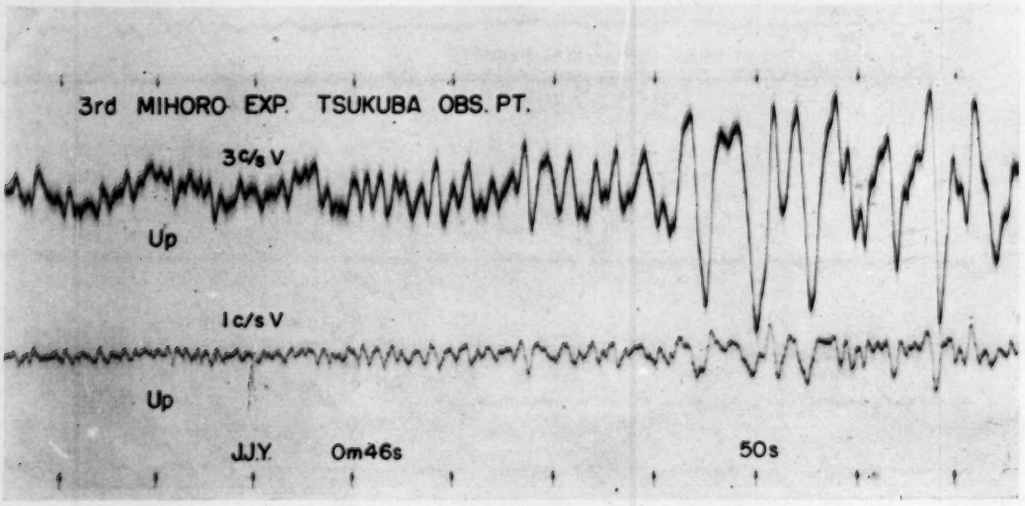

Fig. 9. Seismograms at:

22) E-17 Sinoi in the 4th explosion.
23) E-18 Tukuba in the 1st explosion.
24) E-18 Tukuba (Tsukuba) in the 3rd explosion.

25)

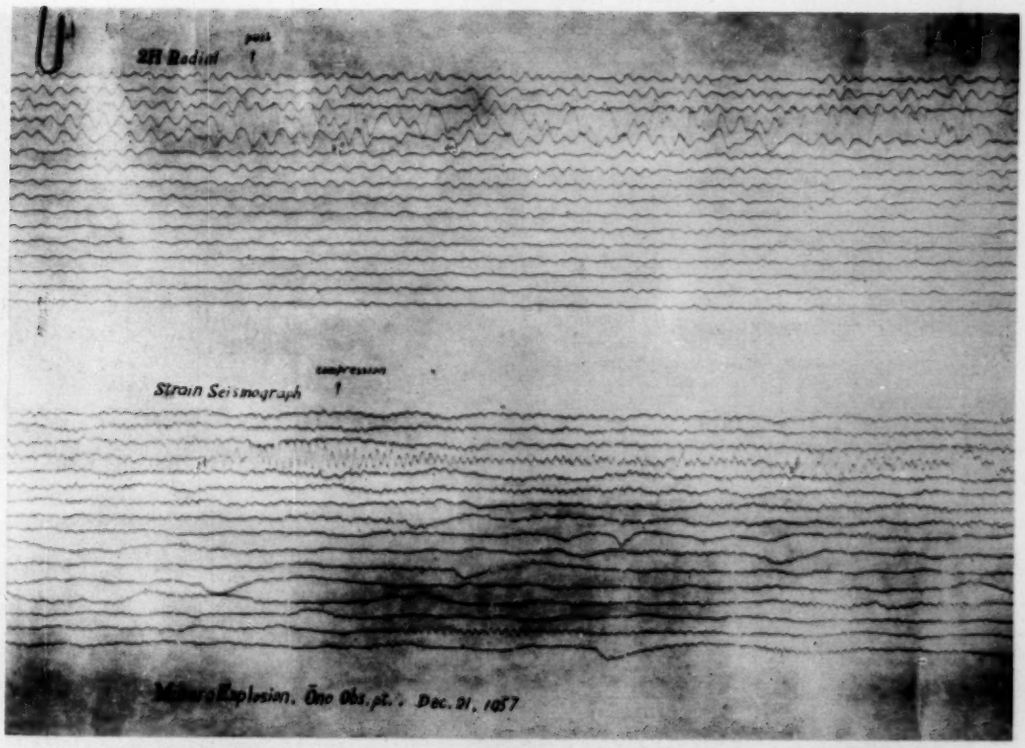

26)

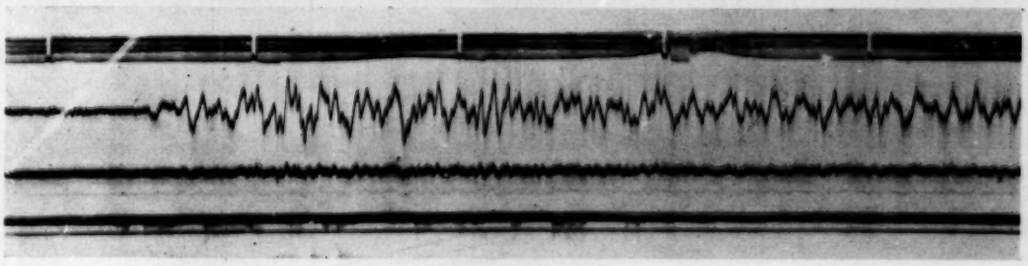

27)

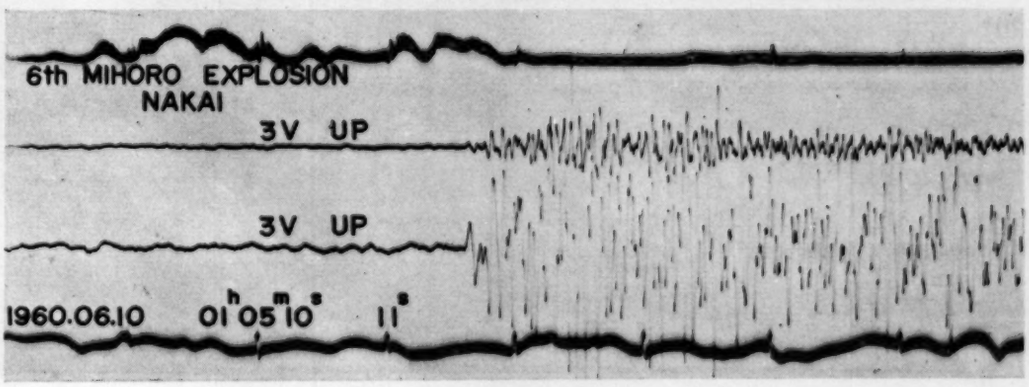

Fig. 9. Seismograms at:

25) W(A)-1 Ōno in the 1st explosion.

26) W(A)-2 Nakai in the 5th explosion.

27) W(A)-2 Nakai in the 6th explosion.

28)

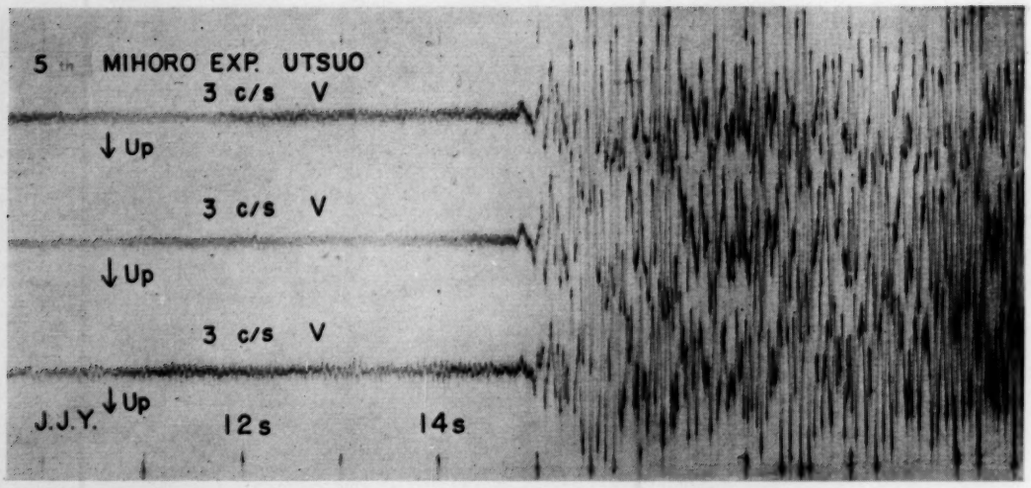

29)

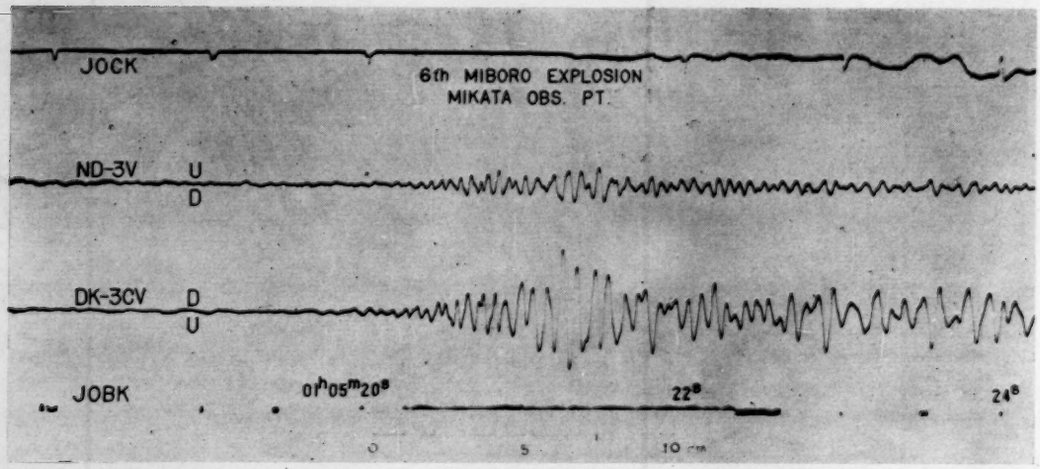

30)

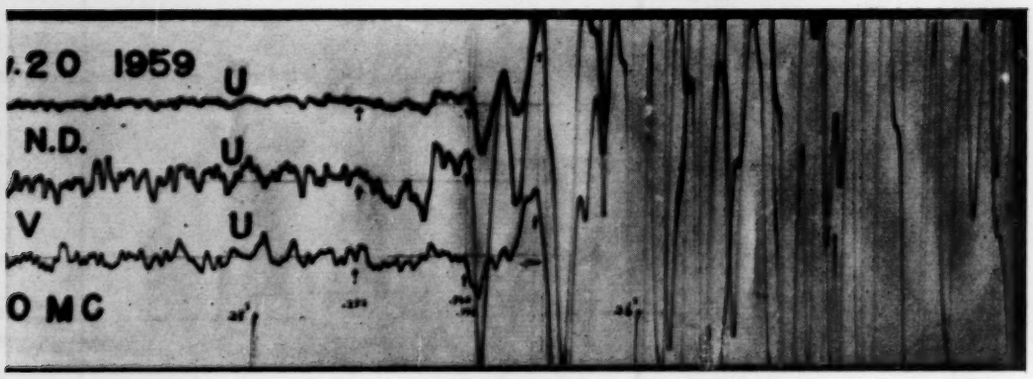

Fig. 9. Seismograms at:

28) W(A)-3 Utuo (Utsuo) in the 5th explosion.

29) W(A)-4 Mikata in the 5th explosion.

30) W(A)-5 Ôi in the 5th explosion.

31)

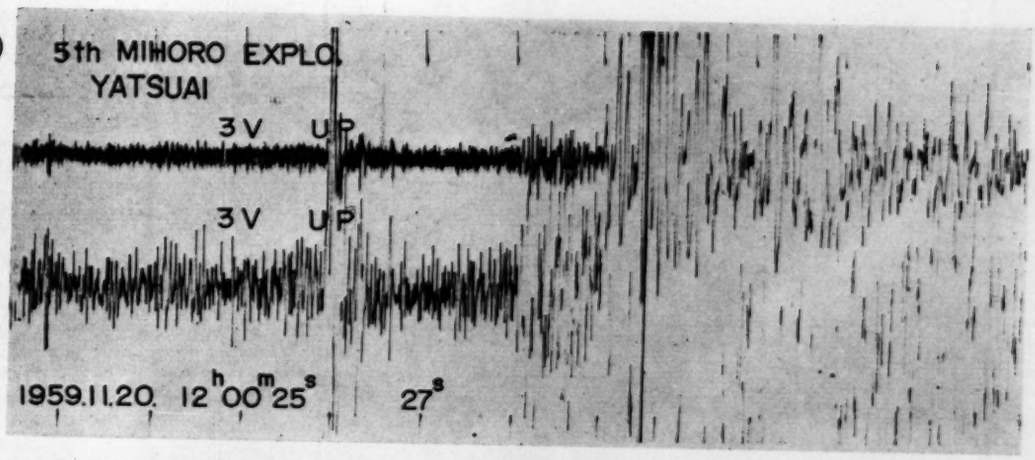

32)

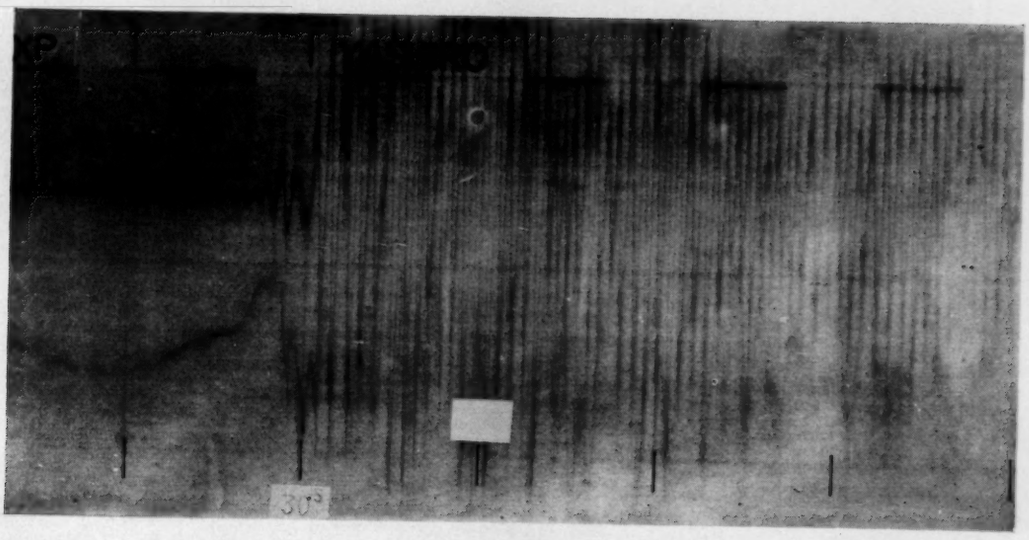

33)

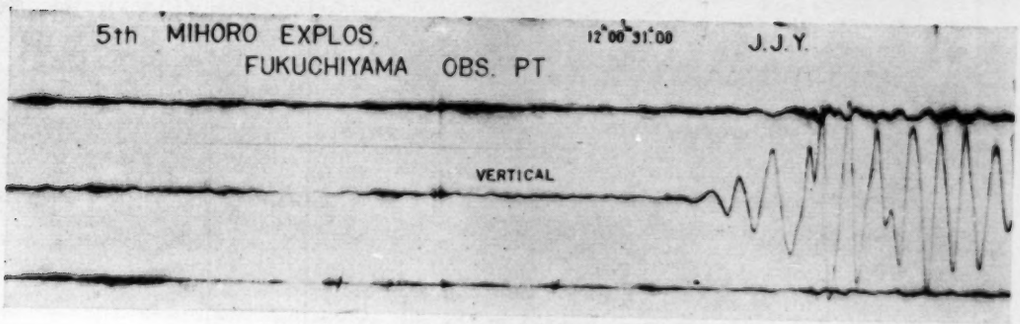

Fig. 9. Seismograms at:
31) W(A)-6 Yatuai (Yatsuai) in the 5th explosion.
32) W(A)-7 Yasiro (Yashiro) in the 5th explosion.
33) W(A)-8 Hukutiyama (Fukuchiyama) in the 5th explosion.

34)

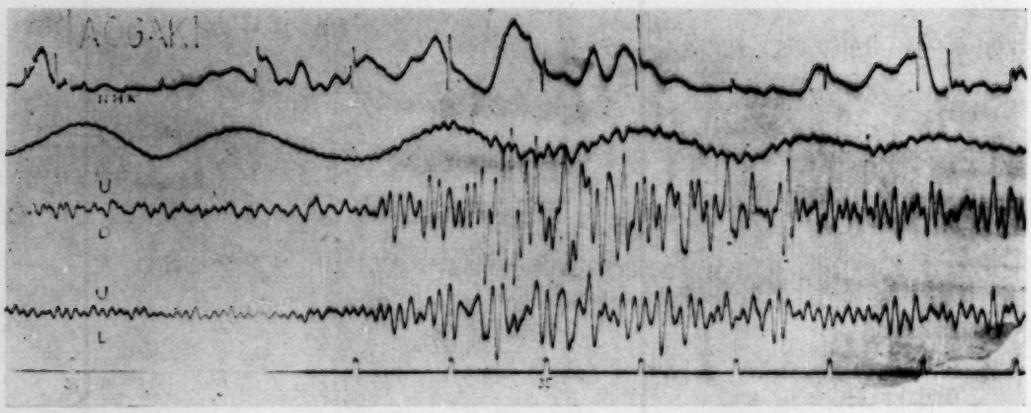

35)

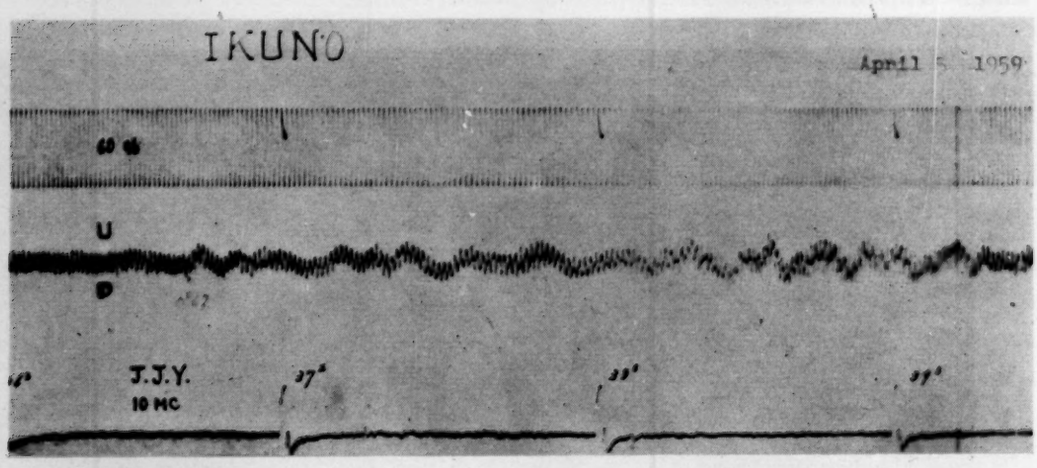

36)

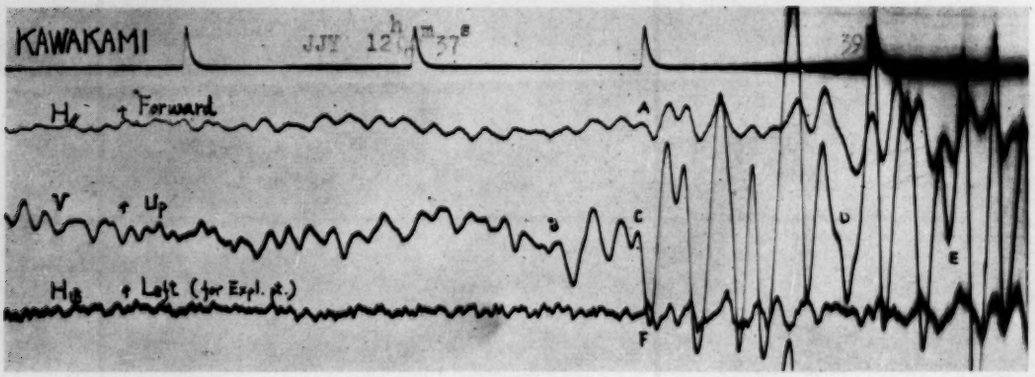

Fig. 9. Seismograms at:

34) W(A)-9 Aogaki in the 6th explosion.

35) W(A)-10 Ikuno in the 4th explosion.

36) W(A)-11 Kawakami in the 5th explosion.

37)

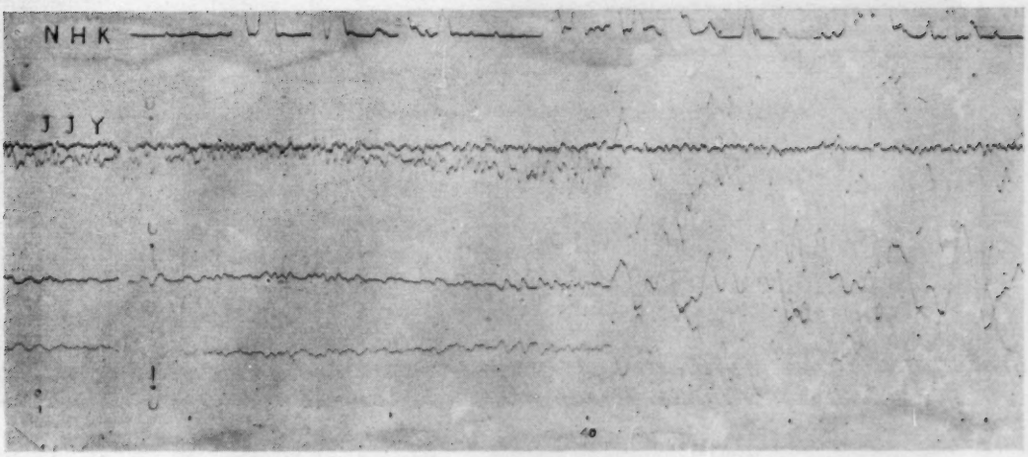

38)

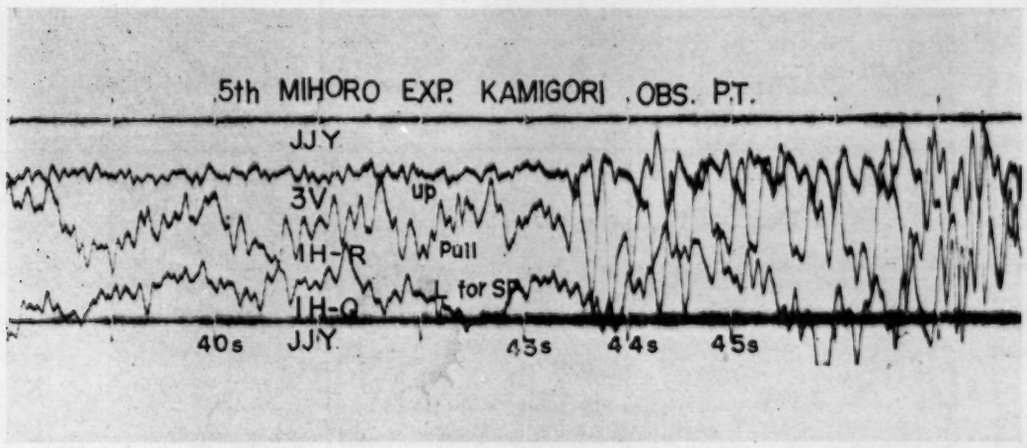

39)

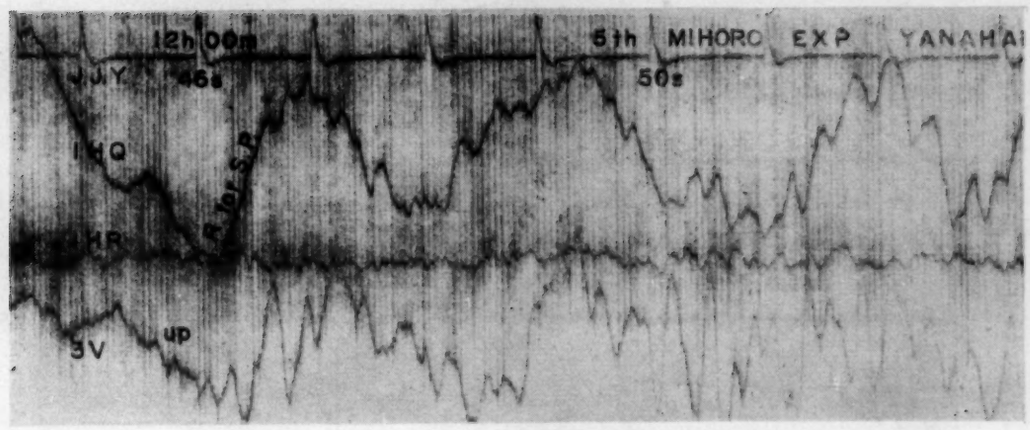

Fig. 9. Seismograms at:

37) W(A)-11 Yamazaki in the 4th explosion.
38) W(A)-13 Kamigôri in the 5th explosion.
39) W(A)-14 Yanahara in the 5th explosion.

40)

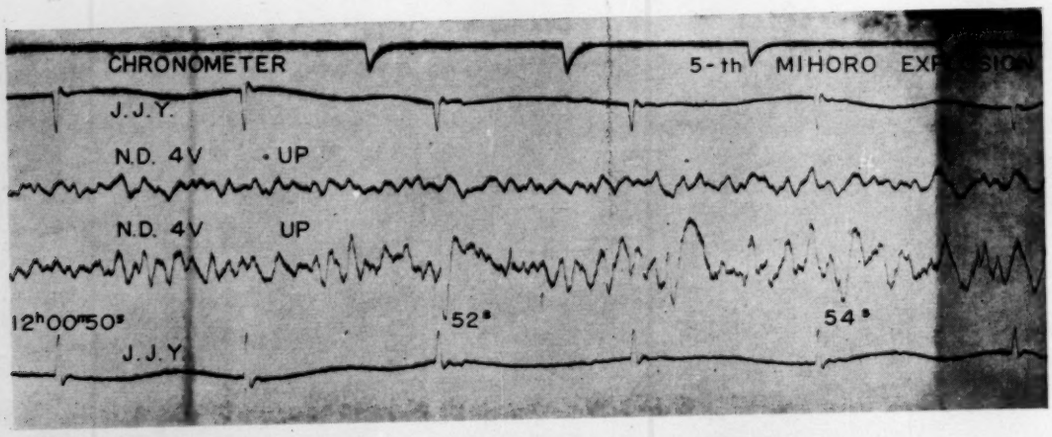

41)

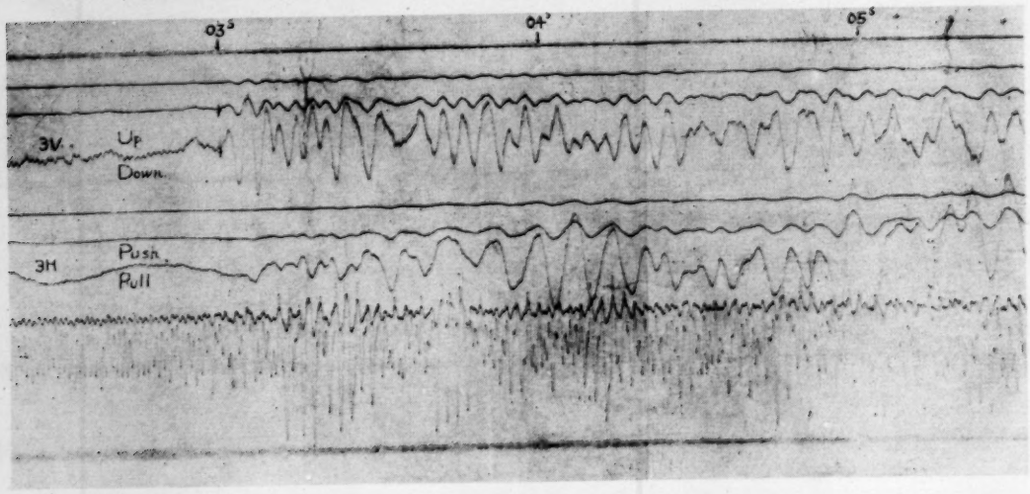

42)

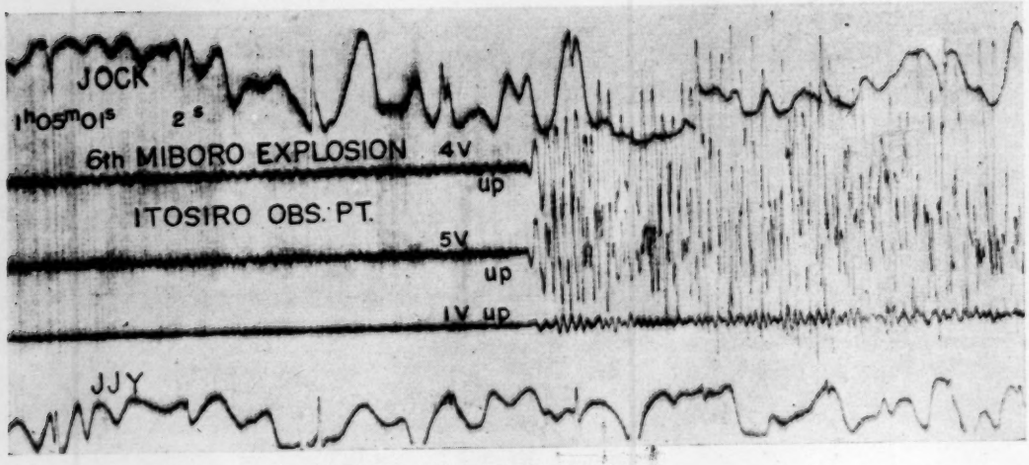

Fig. 9. Seismograms at:

40) W(A)-15 Yakage in the 5th explosion.
41) W(B)-16 Arabuti in the 6th explosion.
42) W(B)-17 Itosiro in the 6th explosion.

43)

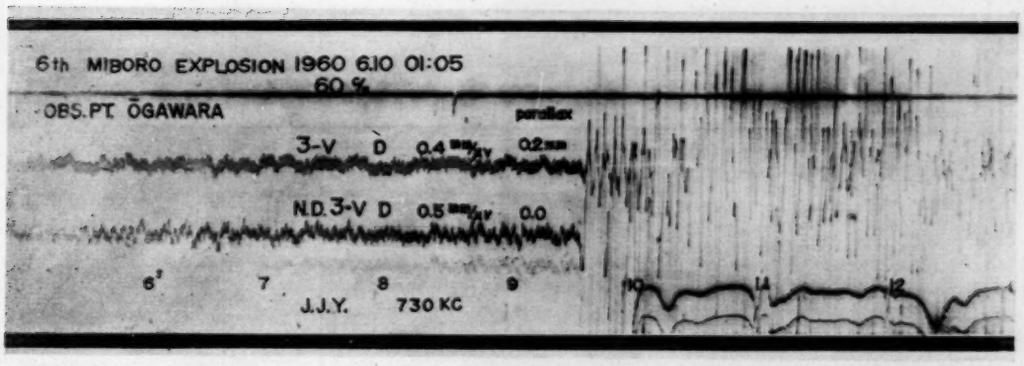

44)

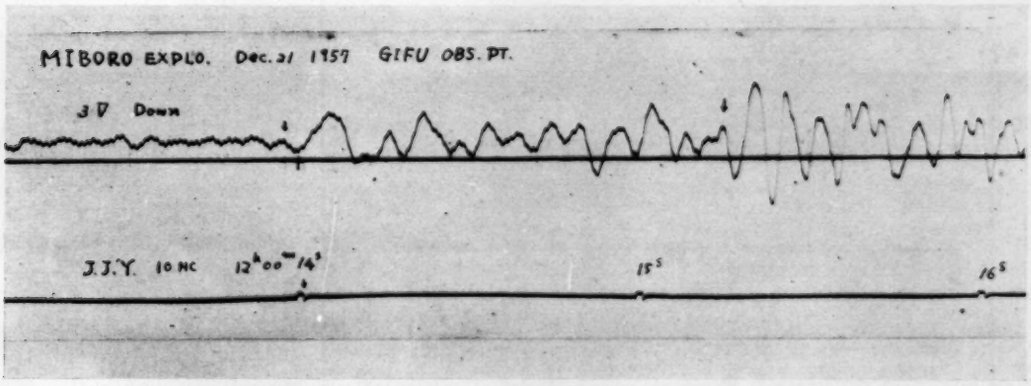

45)

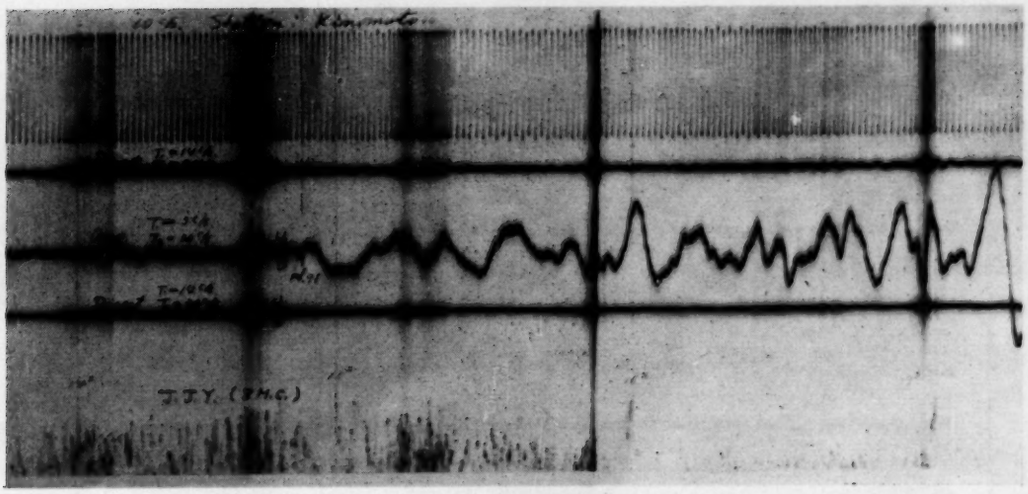

Fig. 9. Seismograms at:
43) W(B)-18 Ôgawara in the 6th explosion.
44) W(B)-19 Gihu (Gifu) in the 1st explosion.
45) W(B)-20 Kinomoto in the 1st explosion.

46)

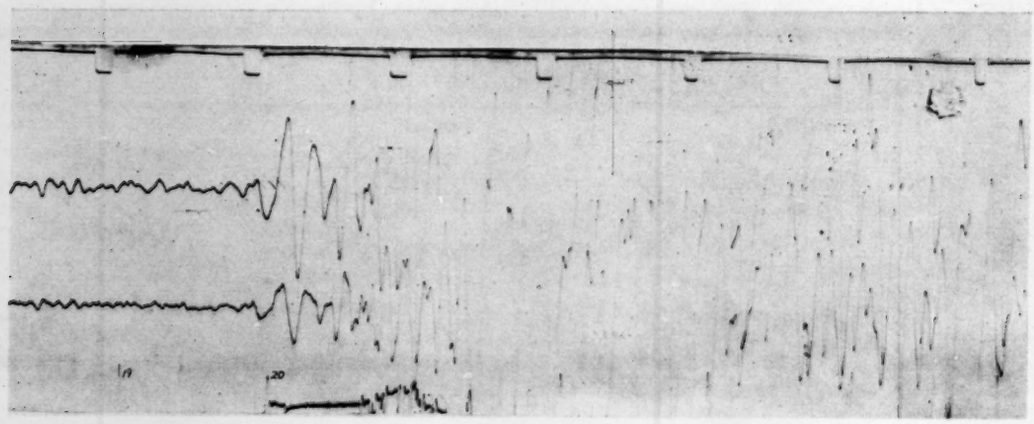

47)

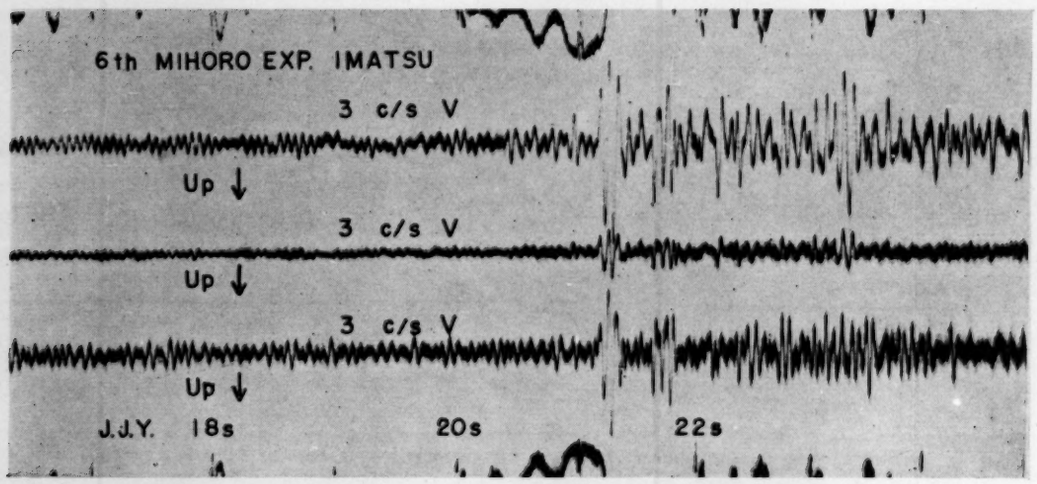

48)

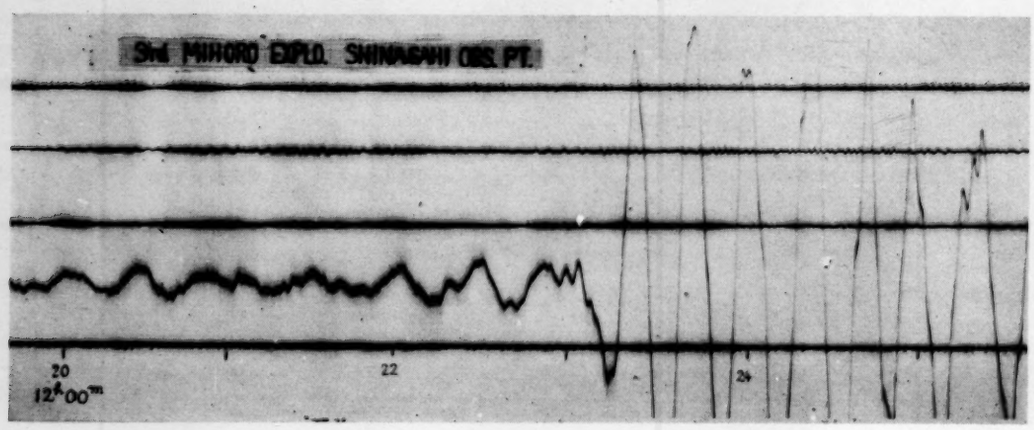

Fig. 9. Seismograms at:
46) W(B)-21 Kaizu in the 5th explosion.
47) W(B)-22 Kitoge (Imatsu) in the 6th explosion.
48) W(B)-24 Imazu (Shin'ashi) in the 3rd explosion.

49)

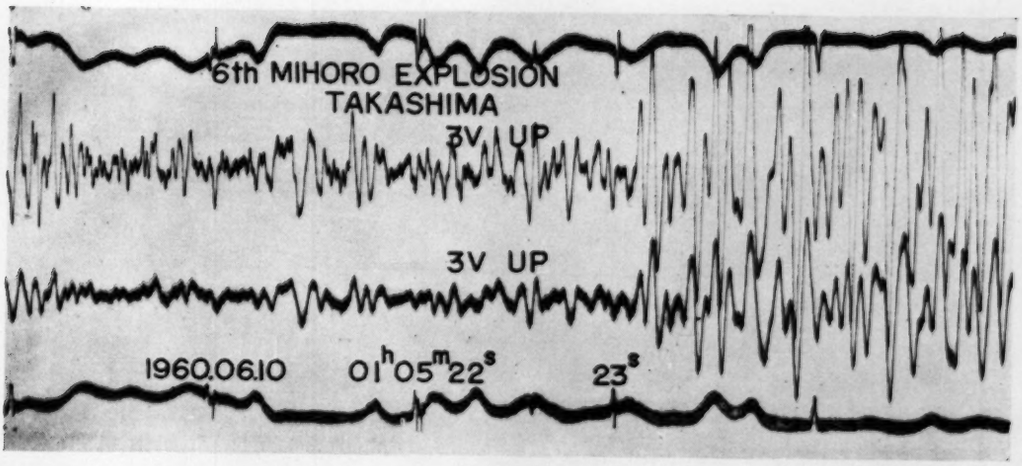

50)

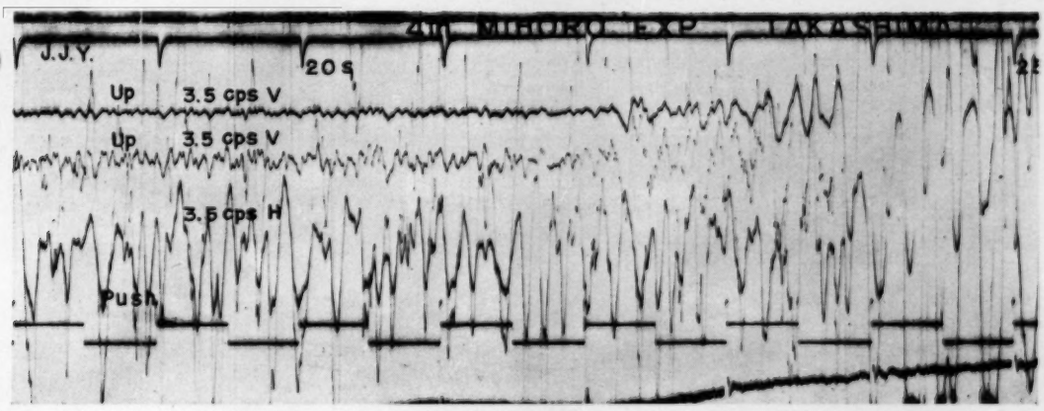

51)

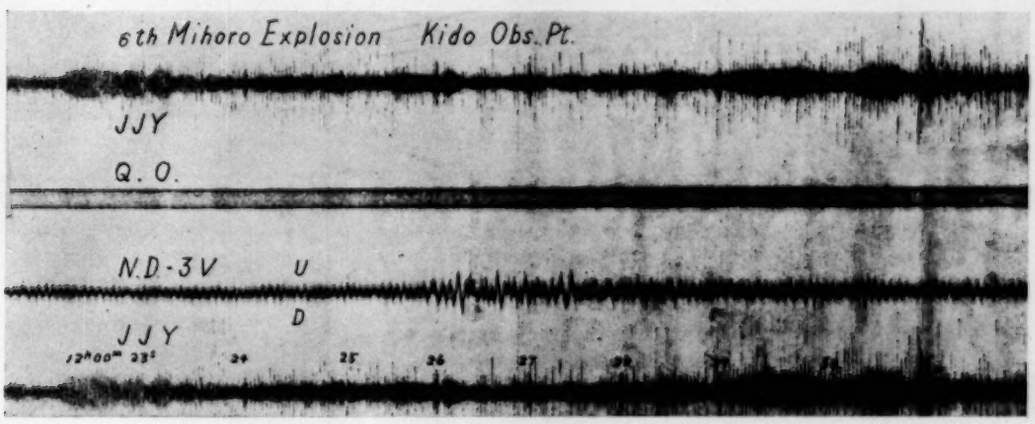

Fig. 9. Seismograms at:

49) W(B)-25 Sirahige (Takashima) in the 6th explosion
50) W(B)-26 Takasima (Takashima) in the 4th explosion.
51) W(B)-27 Kido in the 6th explosion.

52)

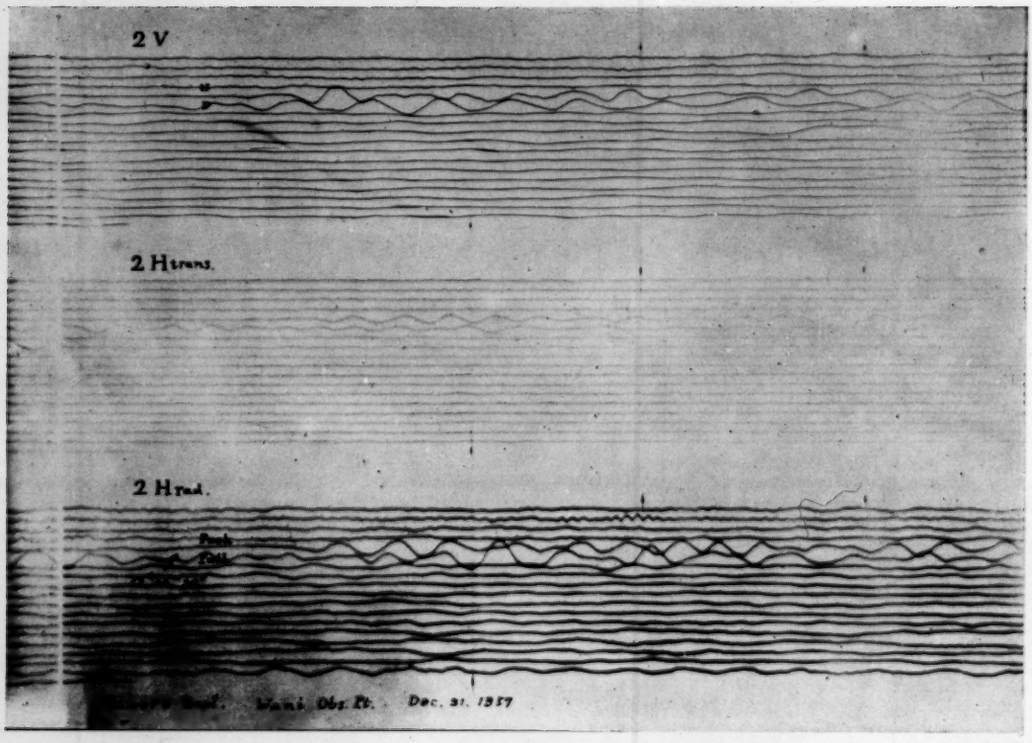

53)

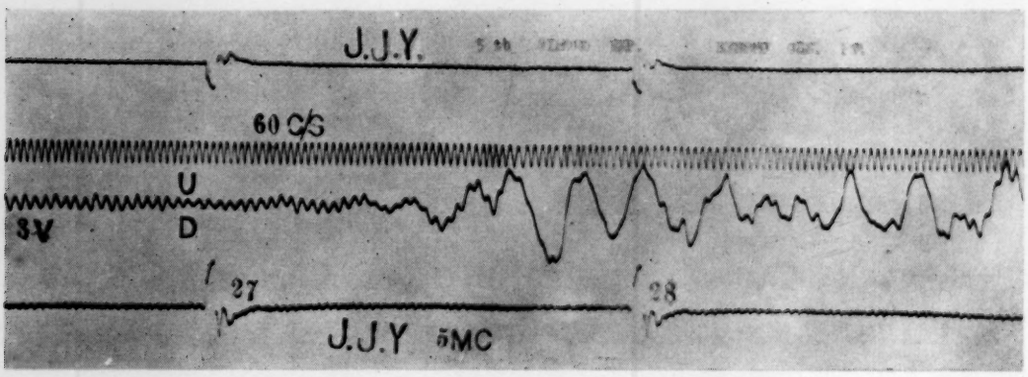

Fig. 9. Seismograms at:
52) W(B)-28 Wani in the 1st explosion.
53) W(B)-29 Bessyo in the 5th explosion.

54)

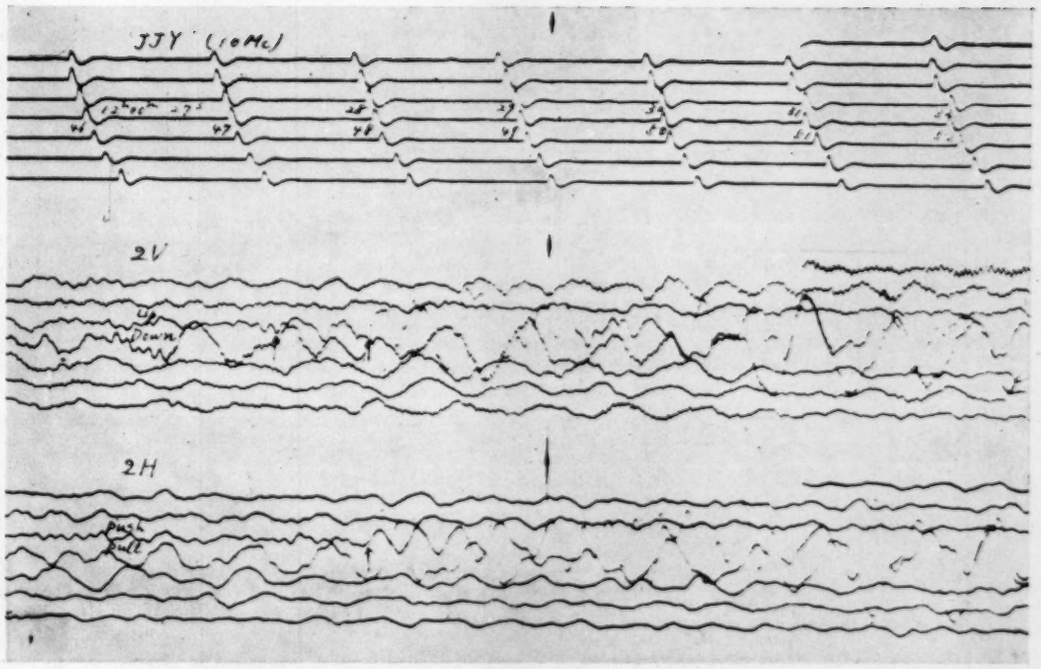

55)

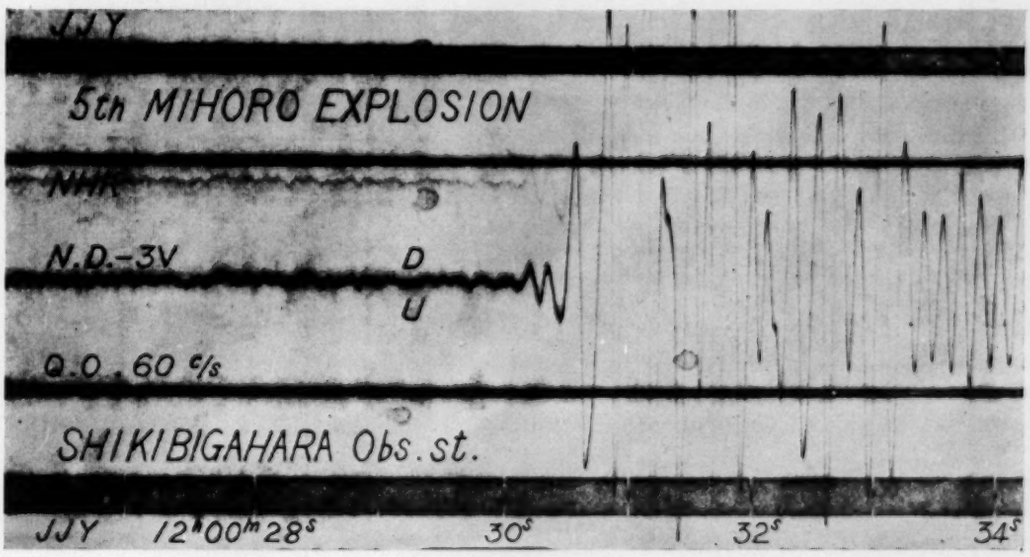

Fig. 9. Seismograms at:

54) W(B)-30 Kyôto in the explosion of Nov. 2, 1958.

55) W(B)-31 Sikibigahara (Shikibigahara) in the 5th explosion.

56)

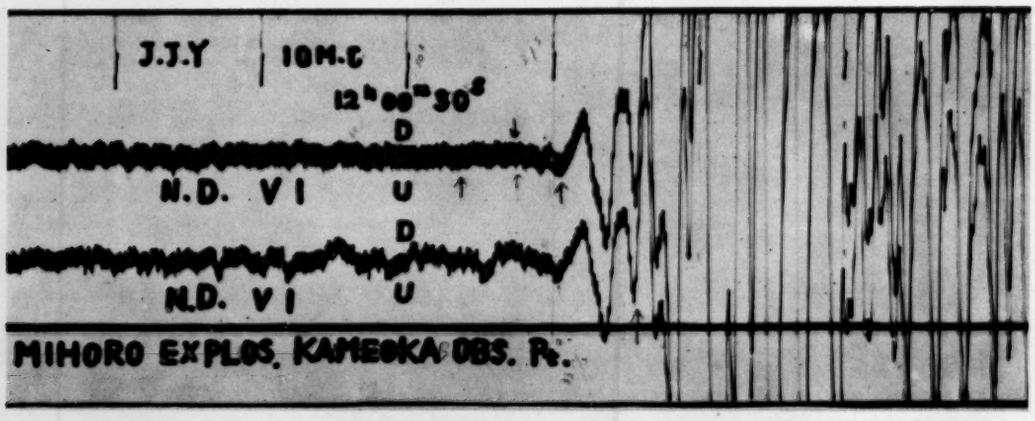

57)

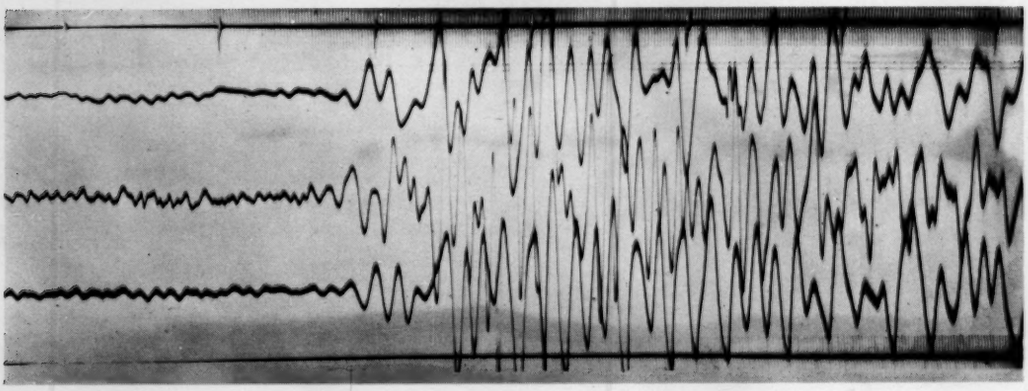

58)

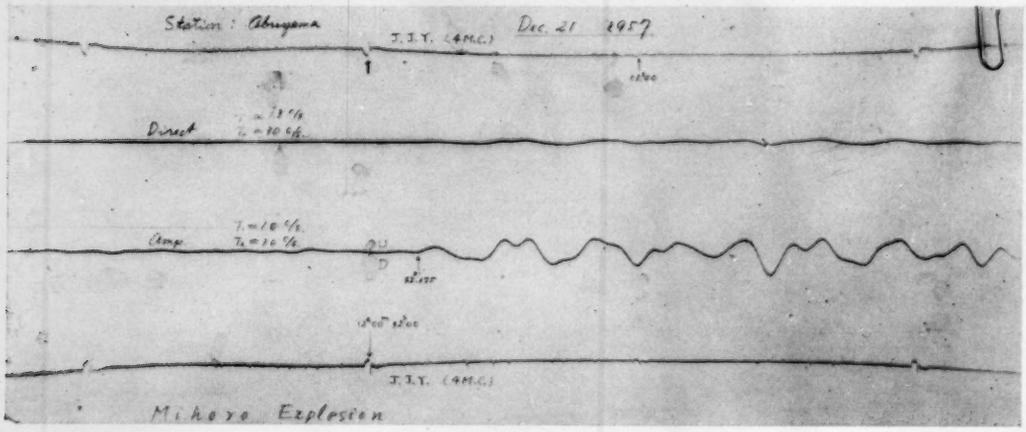

Fig. 9. Seismograms at:

56) W(B)-32 Kameoka in the 4th explosion.
57) W(B)-33 Taki in the 4th explosion.
58) W(B)-34 Abuyama in the 1st explosion.

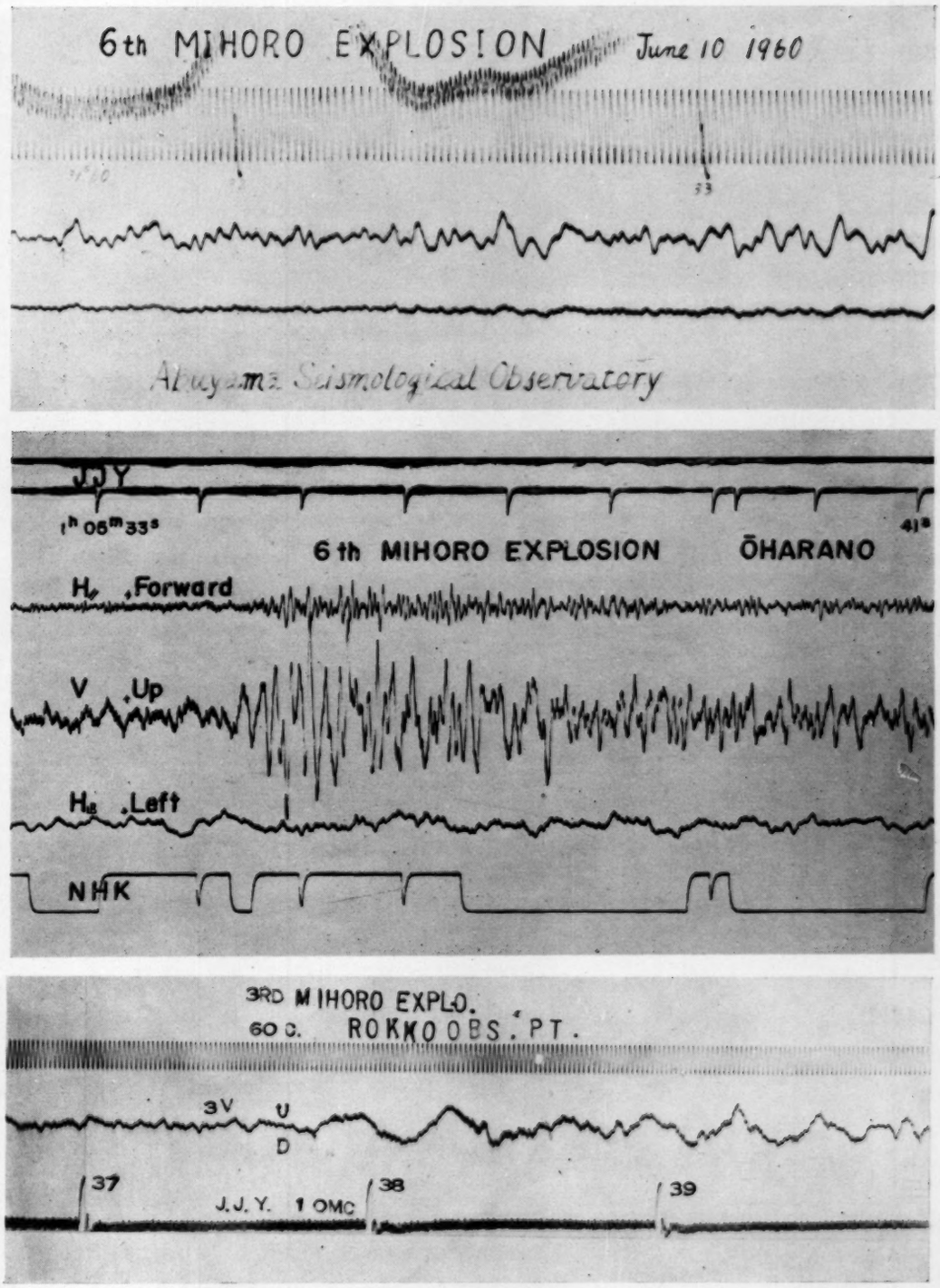

Fig. 9. Seismograms at:
59) W(B)-35 Abuyama in the 6th explosion.
60) W(B)-36 Ôharano in the 6th explosion.
61) W(B)-37 Rokkô in the 3rd explosion.

62)

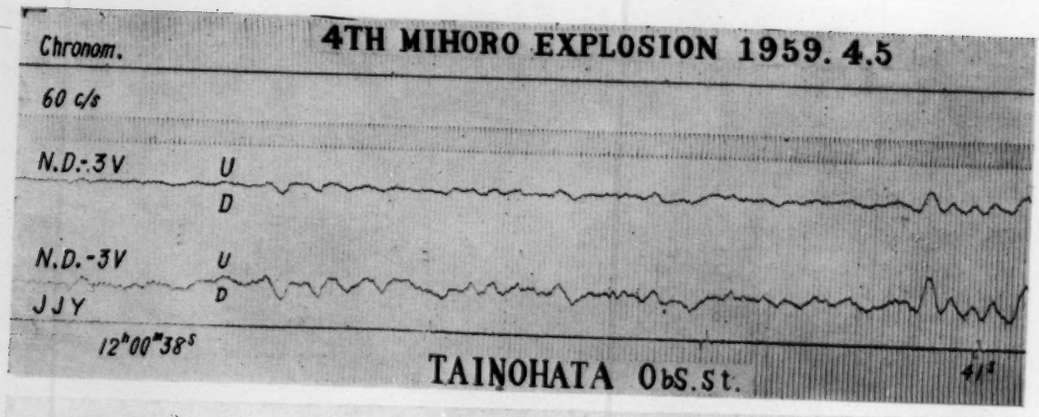

63)

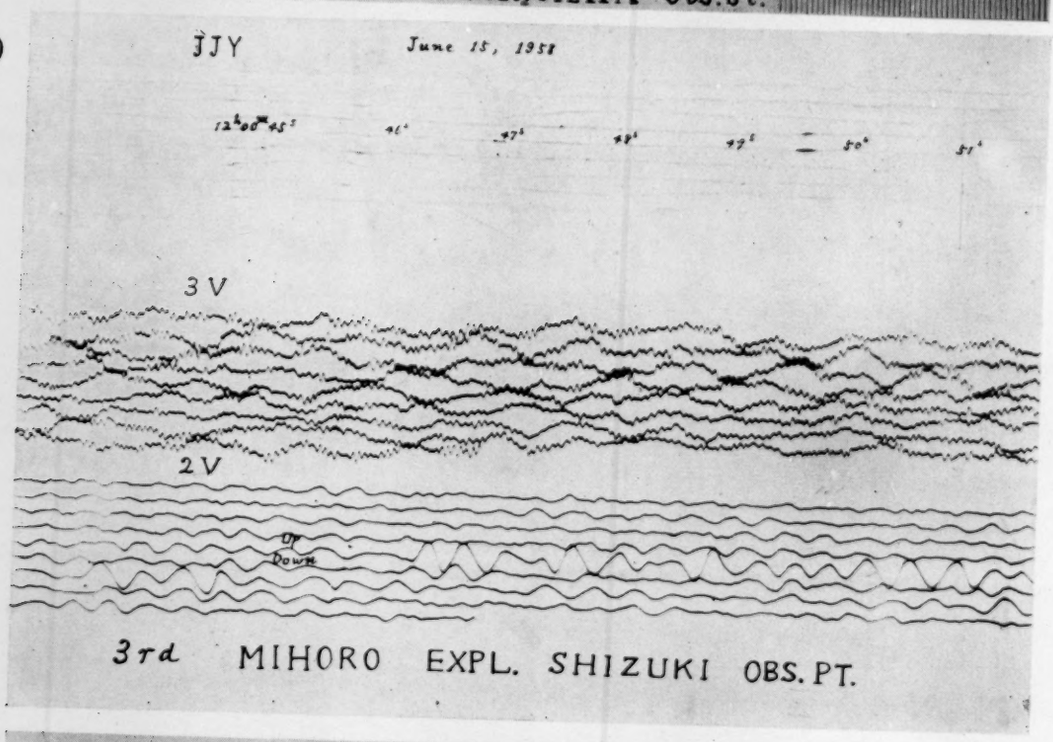

64)

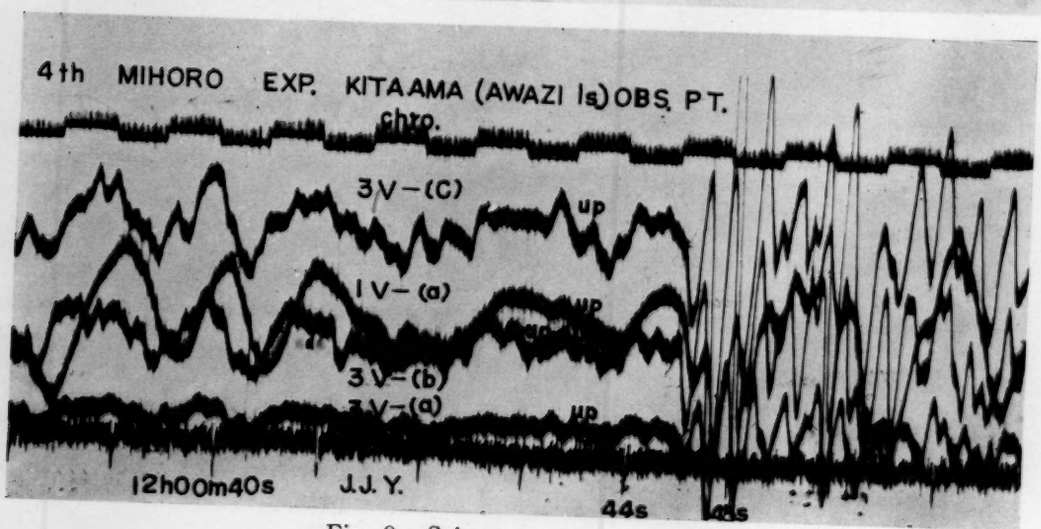

Fig. 9. Seismograms at:
62) W(B)-38 Tainohata in the 4th explosion
63) W(B)-39 Sizuki (Shizuki) in the 3rd explosion
64) W(B)-41 Kitaama in the 4th explosion.

5. Acknowledgement

We wish to express our sincere thanks to the Dengen Kaihatu Company and Hazama-gumi Company, which gave us important help in our experiments, without which successful results could not have been obtained. Our thanks go also to the Nippon Hôsô Kyôkai (NHK); the Tôhoku-, Tôkyô-, Tyûbu, Hokuriku-, and Kansai- Electric Power Companies; the Prefectural Administration Offices and Police Headquarters concerned; provincial authorities and police stations where our observation stations were installed.

Financial aid was granted by the fund for special works of the Earthquake Research Institute in these observation.

Our thanks are due to Prof. R. Takahasi, the director of the Institute, Profs. F. Kishinouye, H. Kawasumi and T. Hagiwara, for their kind help in the project.

Members of the group, who participated in the project are as follows (in Alphabetic order). (1960, 4)

Geophysical Institute, Hokkaidô University: N. Den, H. Hotta, T. Matuzawa, H. Okada, M. Seino, K. Tazime.

Geophysical Institute, Tôhoku University: K. Emura, A. Ishigaki,* E. Mine, Y. Nakamura, Z. Suzuki, A. Takagi.

Akita University: K. Noritomi.

Mizusawa Latitude Observatory: T. Sugawa.

Japan Meteorological Agency: O. Hamamatsu, M. Ichikawa, M. Katsumata, S. Suyehiro, T. Usami, T. Utsu.

Geophysical Institute, Tokyo University: T. Asada, Y. Oguchi, K. Takano, T. Terashima.

Earthquake Research Institute, Tokyo University: S. Asano, M. Hori, I. Karakama, H. Kawasumi, S. Komaki, H. Matsumoto, T. Matumoto, S. Miyamura, N. Nakajima, A. Okada, I. Onda, S. Saitô, T. Santô, M. Sibano, E. Shima, K. Tsujiura, Y. Yamazaki, M. Yanagisawa.

Natural Science Museum: T. Asanuma, S. Murauchi.

Arabia Oil Company: T. Tateishi.

Geological Survey Institute: M. Hayakawa, K. Hirasawa, S. Honjyô, S. Huruya, K. Ichikawa, S. Kamata, T. Kaneko, T. Kawashima, K. Mori, S. Nagumo, S. Ninagawa, J. Tyûjyô.

Matsushiro Seismological Observatory: K. Aihara, T. Shima.*

* Previous members.

Faculty of Science, Nagoya University: H. Aoki, K. Iida, M. Kumazawa.
Gihu University: S. Kajita, I. Muramatsu, T. Yabasi.
Geophysical Institute, Kyôto University: A. Kamitsuki,* A. Kubotera,* E. Nishimura, M. Ôtsuka, I. Ozawa.*
Disaster Prevention Research Institute, Kyôto University: T. Mikumo, S. Yoshikawa.
Abuyama Seismological Observatory, Kyôto University: K. Okano, T. Wada.*
Aso Volcanological Laboratory, Kyôto University: K. Kamo.
Osaka Institute of Technology: O. Kawamoto, I. Tamaki.

Postscript

Inscriptions on seismograms, "Mihoro" should be corrected to "Miboro", but they are left as hitherto used.

Romanization for place names follows the modern Japanese system instead of the Hepburn style.

---

9. 御母衣爆破地震動観測による日本中部の地殻構造

第1部 御母衣爆破地震動の観測

爆破地震動研究グループ

1957 年9月以来，岐阜県大野郡白川村御母衣においては，電源開発株式会社によつて，ロックフィルダム建設工事に伴なう大爆破が度々実施されてきた．爆破地震動研究グループは，これらの爆破を利用して，関東，中部，近畿，中国の各地域にわたる地殻構造を研究するために，6 回にわたる組織的な地震動観測を行なつた．

各回の爆破点の位置，爆破時刻，火薬量，および観測点の詳細な位置は Table 1~7 に示された通りである．

観測点は総計 75 に上るが，Fig. 4 および 5 に示されるように，主として中部—関東北部—東北南部地方に到る測線（東方測線），北陸—近畿北部—中国地方に伸びる測線（西方A測線）および近畿地方中部を横切る測線（西方B測線）上に配置された．

観測の結果は，数点を除いて良好な記録を得ることができた．観測値は Table 8~18 に与えられ，これにもとづく走時図は Fig. 6, 7 および 8 に示されている．

本観測は御母衣ダム建設工事担当の電源開発株式会社および間組の御協力により実施されたものである．また日本放送協会，東北，東京，中部，北陸，関西各電力会社および関係府県庁当局，警察本部ならびに観測点所在の市町村役場，警察署からも多くの御便宜をはかつて頂いた．これらの各位に対して厚く感謝の意を表する次第である．

なお，この観測は東京大学地震研究所特別事業の一部として行なわれたもので，高橋所長 および岸上，河角，萩原各教授の御助力をいただいた．記して感謝する次第である．

BULLETIN OF THE EARTHQUAKE
RESEARCH INSTITUTE
Vol. 39 (1961). pp. 327-349

10. *Crustal Structure in Central Japan as Derived from the Miboro Explosion-Seismic Observations.*

Part 2. On the Crustal Structure.

By Takeshi MIKUMO*, Michio ÔTSUKA**, Tokuji UTSU***,
Tsutomu TERASHIMA**** and Atusi OKADA.*****

(Read Jan. 24, 1961.—Received June 30, 1961).

1. Introduction

This is one of a series of papers under the same title[1].

Crustal structure in central Japan, over the Kwantô, Tyûbu, Kinki and Tyûgoku Districts, will be discussed in some detail, making use of the data obtained by our group.

Detailed investigation of the underground structure by the refraction method generally requires repeated observations of seismic waves from two blasts at both sides of the profile along which observation stations are closely spread. Seismic waves from the Miboro Explosions were observed at the stations spreading along the Eastern and Western profiles, but no corresponding blast at the other end has yet been fired. The data obtained were one-sided.

Under these circumstances two standpoints may be possible in the way of analysis. One is as follows; some of unknown factors, such as propagation velocities in the crustal layers and the layer's thickness, will be assumed from previous knowledge based on past observational data, and then observed travel times will be interpreted so as to be consistent with these assumptions. The other is that; the apparent velocities of wave groups obtained from time-distance curves will be assumed to approximate the true ones in the respective crustal layers bounded by refracting horizons. The structure derived the from former standpoint is named by us Model I and the one from the latter Model II.

* Disaster Prevention Research Institute, the University of Kyôto.
** Geophysical Institute, Faculty of Science, the University of Kyôto.
*** Japan Meteorological Agency.
**** Geophysical Institute, Faculty of Science, the University of Tokyo.
***** Earthquake Research Institute, the University of Tokyo.

1) The Research Group for Explosion Seismology, *Bull. Earthq. Res. Inst.*, **39** (1961), 279-319.

Two of the probable models of crustal structure in each of the said profiles will be given. In the following analysis, travel times of the first compressional arrivals observed at the mentioned stations are mainly used with some reference to the later phases including S waves.

2. Travel Times near the Shot Point

As described in Part 1 of this paper, in the vicinity of the shot point at Miboro, pick-ups were set up along the left bank of Hukusima-valley, a quarrying site. The observed data at a total of 16 points in the I–VI explosions, except the No. II blast, are shown in Table 17 and Fig. 8 in the previous report. Looking at these results, analysis from the raw data seems to be difficult, owing to complicated factors, such as a certain extent of the shot area, the shooting procedure and topographical effects of the shot point and its environs.

An attempt will therefore be made here to reexamine the data, taking these effects into consideration.

1. On the shot time

The shot mark was registered through a lead-in wire connected

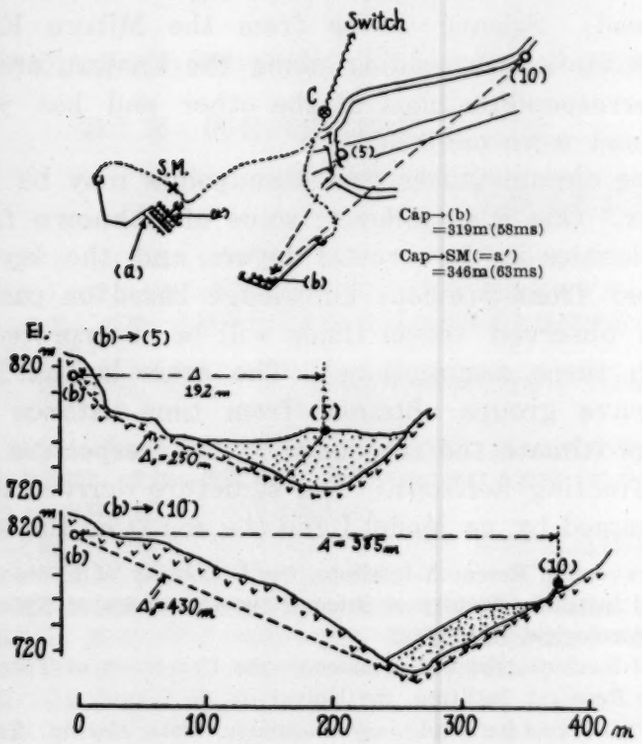

Fig. 1. An example of the explosion system and its profile.

with the point adjacent to an electrical blasting cap at the junction of detonating fuses leading to dynamite chambers or tunnels, except in the case of the No. VI explosion. Hence, the registered shot time should be corrected, taking the time delay into account, which elapsed in the detonating fuse between the cap and the nearest chamber. The delay is caused by the finite speed of firing. The value of 5.5 km/sec provided in JIS is adopted here as the detonation velocity in the prima chord. Using this value, the ignition time (O') in the earlist detonated chamber can be deduced from the registered shot time (O) for each of the explosions.

2. On Δ

The distance (Δ_0) between the earliest ignited chamber and the pick-up does not coincide in general with the distance on plane (Δ) between the nearest chamber and the pick-up. In the profile along a steep valley, the results may be much influenced by elevations and topography. For the present case the virtual distance (Δ_0') along the wave path between the nearest shot point and the pick-up was determined graphically for each of the profiles on a topographical map of 1/2000 precision. Fig. 1 shows a example of the profiles in the No. IV explosion.

3. Travel time analysis

Table 1. Reduced travel times near the shot point.

No.	Obs. No.	P.U. No.	Δ	Δ_0'	(Corr.)	$P-O$	$P-O'$	(Corr.)
1	I	1	39^{m}	50^{m}	+11^{m}	24^{ms}	30^{ms}	+ 6^{ms}
2	V	1	114	118	+ 4	32	30	− 2
3	III	1	124	173	+49	93	74	−19
4	VI	1	170	170	0	49	45	− 4
5	IV	1	192	250	+68	106	101	− 5
6	I	2	225	260	+35	102	108	+ 6
7	III	2	277	343	+67	110	91	−19
8	V	2	334	338	+ 4	84	82	− 2
9	VI	2	373	375	+ 2	93	89	− 4
10	IV	2	385	430	+45	109	104	− 5
11	V	3	483	490	+ 7	116	114	− 2
12	VI	3	487	489	+ 2	114	110	− 4
13	III	3	526	590	+64	149	130	−19
14	IV	3	575	623	+48	146	141	− 5
15	VI	4	646	652	+ 6	146	142	− 4
16	VI	5	755	777	+22	169	165	− 4

The corrected results of the travel time and the distance, after the above stated procedure, P—O' and Δ' are collectively listed in Table 1. In this treatment, the relative difference between the speed of waves from the nearest dynamite chamber and that from the earliest ignited one was examined from each observation point. The travel times shown in Table 1 are plotted versus distance in Fig. 2. Except for the data obtained at 6 points within a distance of 250 m, the relation between the travel times and the distances is given by the following formula, determined by the method of least squares.

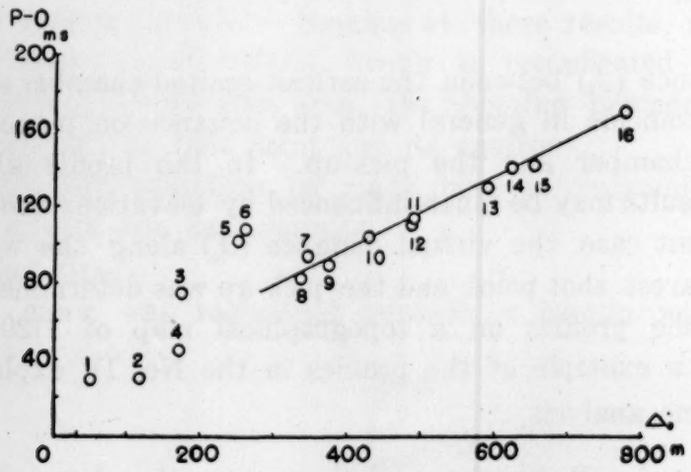

Fig. 2. Reduced travel time curves near the shot point.

$$T=\Delta'_0/5.53+0.025 \qquad \text{for pick-ups No. 7–16 in } 250<\Delta<760 \text{ m.}$$

The velocity of compressional waves in the said range is about 5.5 km/sec. It seems difficult to find a reasonable explanation for the scattering of the plots for $\Delta'_0<250$ m, but this may probably be attributed to the effects of the irregular weathered layer on which the pick-ups were set.

3. Crustal Structure in the Tyûbu and Kwantô Districts (the Eastern Profile)

§ 1. Time-Distance Curves

The reduced time-distance graph in the Eastern profile is shown in Fig. 3, by the use of the data tabulated in Table 14 in Part 1 of this paper. In this figure $P-O-\Delta/6$ is taken as the ordinate to study detailed features of the travel times.

There may be some ways of drawing reasonable curves, but two

cases are adopted here from the representative standpoints mentioned before.

The travel times fitted to each of the branches are represented as the following formulae for Models I and II.

$$\text{M-I}\begin{cases} P_1;\ T_1=\Delta/5.55+0.16 & \text{for Myôgase-Kotakari } (\ \Delta<28\text{ km}) \\ P_{21};\ T_{21}=\Delta/5.86+0.43 & \text{for Kamioka-Matusiro } (28<\Delta<130\text{ km}) \\ P_{22};\ T_{22}=\Delta/6.33+2.07 & \text{for Matusiro-Ôiwa } (130<\Delta<175\text{ km}) \\ P_3;\ T_3=\Delta/7.91+8.18 & \text{for Takayama-Nisioasi } (185<\Delta\ \text{km}) \end{cases}$$

$$\text{M-II}\begin{cases} P_1;\ T_1=\Delta/5.55+0.16 & \text{for Myôgase-Kotakari } (\ \Delta<38\text{ km}) \\ P_2;\ T_2=\Delta/6.00+0.68 & \text{for Kamioka-Ôiwa } (38<\Delta<185\text{ km}) \\ P_3;\ T_3=\Delta/7.90+8.13 & \text{for Takayama-Nisioasi } (185<\Delta\ \text{km}) \end{cases}$$

Analysis will be made solely by using the travel time equations[2].

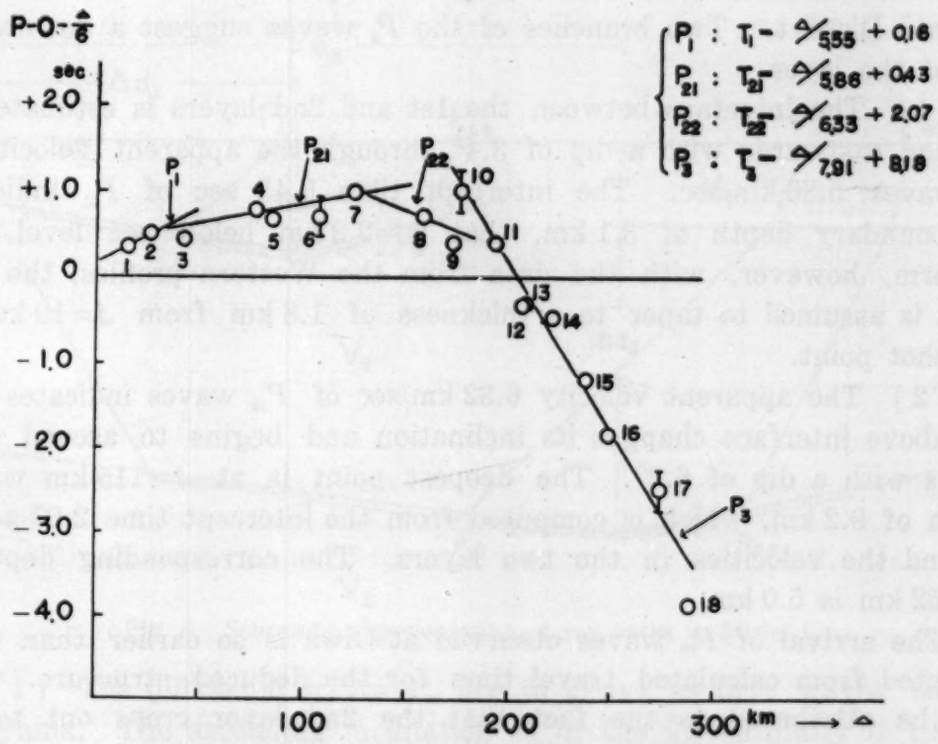

Fig. 3. Reduced travel time curves in the Eastern profile.

§ 2. Model I

1. Travel times of P_1 and the superficial layer

The apparent velocity of P_1 waves, 5.55 km/sec, is adopted as the true velocity in the 1st layer. This value agrees well with the corresponding velocity in the Western profile, the data from observation

2) Report R. G. E. S., (1961), in preparation.

near the shot point and the result obtained in the Kwantô District[3].

The intercept time of P_1, 0.16 sec, suggests the possible existence of a superficial layer with a lower velocity overlying the 1st layer. Near the shot point, however, the velocity of 5.53 km/sec corresponding to that in the 1st layer is observed beyond a distance of 250 m. On the contrary, the intercept time is nearly zero in the case of the Western profiles. These facts indicate that the weathered layer may be negligibly thin beneath the shot point at Miboro. The superficial layer with unknown low velocity is assumed to exist only near Myôgase and Kotakari stations.

2. Travel times of P_2 and the thickness of the first layer

The true velocity of longitudinal waves in the 2nd layer is assumed to be 6.00 km/sec, from the results of explosion observation in the Kwantô District. Two branches of the P_2 waves suggest a downwarping of the layer.

(1) The interface between the 1st and 2nd layers is estimated to descend eastwards with a dip of 3.4° through the apparent velocity of P_{21} waves, 5.86 km/sec. The intercept time 0.43 sec of P_{21} indicates the boundary depth of 3.1 km, that is, 2.3 km below sea level. To conform, however, with the data from the Western profiles, the first layer is assumed to taper to a thickness of 1.8 km from $\Delta=10$ km to the shot point.

(2) The apparent velocity 6.32 km/sec of P_{22} waves indicates that the above interface changes its inclination and begins to ascend eastwards with a dip of 6.2°. The deepest point is at $\Delta=115$ km with a depth of 9.2 km, which is computed from the intercept time 2.07 sec of P_{22} and the velocities in the two layers. The corresponding depth at $\Delta=152$ km is 5.0 km.

The arrival of P_{22} waves observed at Ôiwa is so earlier than to be expected from calculated travel time for the deduced structure. This may be attributed to the fact that the 2nd layer crops out to the earth's surface between Hoppo and Ôiwa. This is confirmed also by the results of Kwantô explosions.

(3) As for the thickness of the 1st layer with the velocity of 5.55 km/sec beyond Takayama station, the value of 6 km is adopted so as to be consistent with the explosion data in the Kwantô region.

3. Travel times of P_3 and the thickness of the second layer

The true velocity in the 3rd layer is assumed to be 7.70 km/sec in

3) T. USAMI *et al.*, *Bull. Earthq. Res. Inst.*, **36** (1958), 349-357.

accordance with the observational data from the Kwantô District. The discontinuity surface between the 2nd and 3rd layers is considered to ascend eastwards with a dip of 1.8°, in view of the apparent velocity 7.91 km/sec of P_3 waves. A tentative estimation gives a round value of 38 km for the boundary depth beneath Miboro. From the data for the Western profiles, however, the depth in various probable models is estimated to be 27–29 km under any assumption. On the other hand, the boundary has already been found to be about 25–30 km in the Kwantô region. These data suggest a downward warping of the 2nd layer. That is, the discontinuity surface along the said profile is supposed to descend eastwards from Miboro and in turn begin to ascend toward the Kwantô area. The ray paths of the mentioned waves in this profile are schematically represented in Fig. 4.

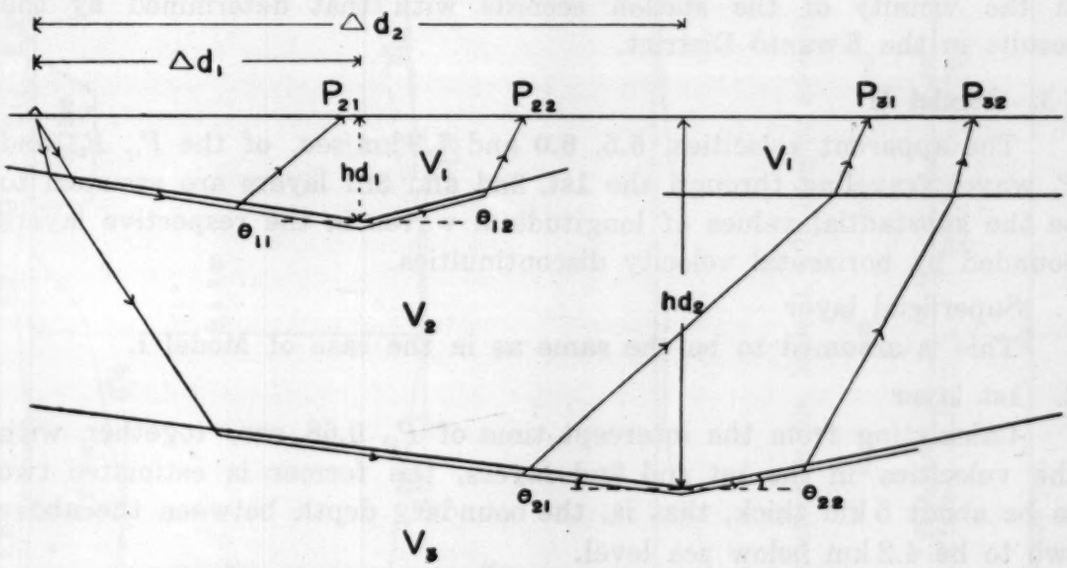

Fig. 4. Schematic representation of ray paths in Model I.

(1) The diffracted waves P_{32} are to arrive as first waves beyond Takayama. The ascending inclination θ_{22} of the discontinuity is 1.8° as determined above. The boundary depth beneath Miboro is assumed to be 27.7 km below sea level, so as to be consistent with the Western profile data.

(2) Concerning a descending dip θ_{21}, no direct evidence is found. For this reason, therefore, a possible limit of θ_{21} is estimated only from the following simultaneous conditions.

One is a geometric condition that the P_{32} waves emerge first beyond Takayama. The other is the condition keeping the intercept time of

P_{32} 8.18 sec. The limit is determined as $\theta_{21} \geqq 3.9°$. The value of 4.0° is adopted in the present case with a view to minimizing the inclination.

(3) Using the intercept time and the velocities in the respective layers, the deepest boundary is found to occur at $\Delta = 149$ km, and its depth is 38.1 km. The depth at a distance of 250 km is 35.0 km.

(4) The arrivals of P_3 waves observed at Huziwara, Kawaba and Tukuba are earlier than to be expected from calculation of this model. These are attributable to outcrop of the 2nd layer near the stations. The anomalous delay at Asakawa indicates the possible existence of material characterized by a low velocity at the surface. Along a profile including Miboro and Tukuba, the interface between the 2nd and 3rd layers is believed to ascend from the deepest point with a dip of 3.9°, and to have a value of 28.0 km beneath Tukuba. The crustal structure in the vicinity of the station accords with that determined by the results in the Kwantô District.

§ 3. Model II

The apparent velocities, 5.5, 6.0 and 7.9 km/sec, of the P_1, P_2, and P_3 waves traveling through the 1st, 2nd and 3rd layers are assumed to be the substantial values of longitudinal waves in the respective layers bounded by horizontal velocity discontinuities.

1. Superficial layer

This is assumed to be the same as in the case of Model I.

2. 1st layer

Calculating from the intercept time of P_2, 0.68 sec, together with the velocities in the 1st and 2nd layers, the former is estimated two to be about 5 km thick, that is, the boundary depth between the above two to be 4.2 km below sea level.

The early arrivals of P_2 waves observed at Kamioka and Ôiwa would be indicative of exposure of the 2nd layer to the surface near the stations. A possible explanation of the late arrival at Matusiro is a local velocity irregularity. As for the thickness of the 1st layer at a great distance, the already determined value of 6 km in the Kwantô region is adopted here.

3. 2nd layer and 3rd layer

The P_3 waves emerge as initial arrivals beyond the distance of Takayama. The intercept time 8.13 sec of P_3, the afore-mentioned 1st layer's thickness and the velocities indicate that the depth of the interface between the 2nd and 3rd layers is 35.6 km beneath sea level.

km 300 250 200 150 100 50 0

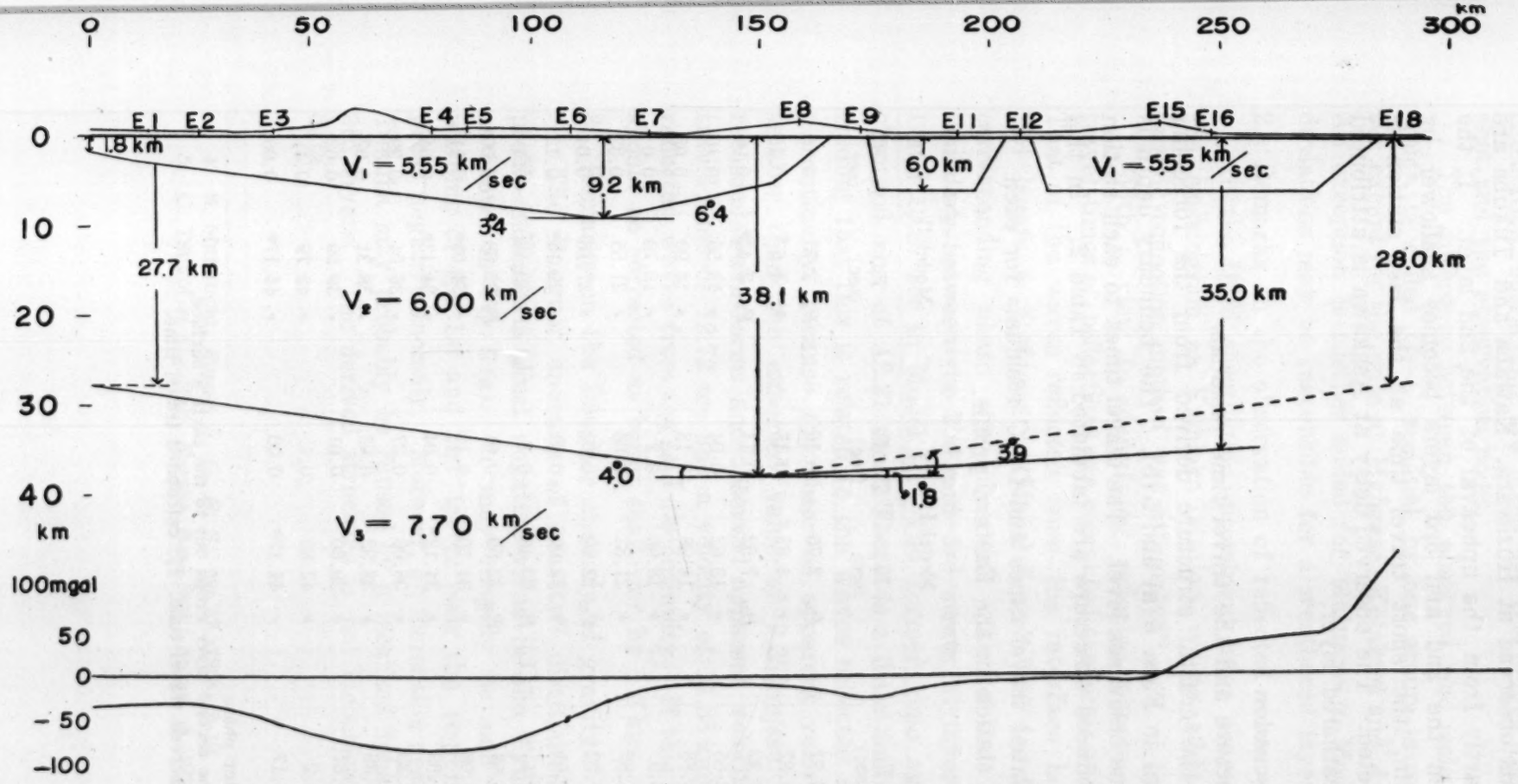

Fig. 5(a). Crustal structure in the Eastern profile. Model I, with Bouguer anomaly of gravity along the profile.

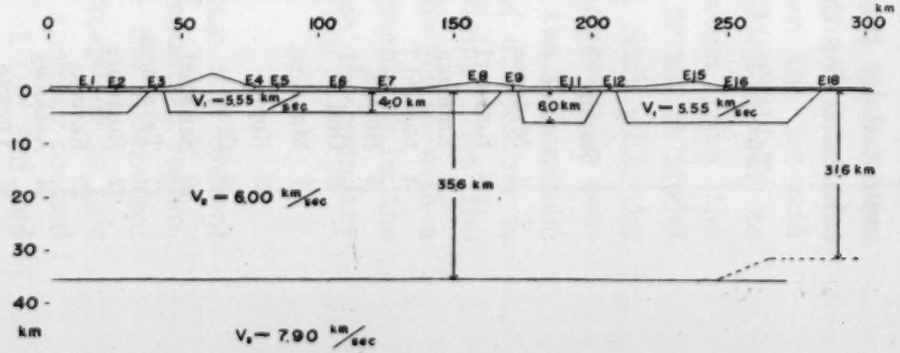

Fig. 5(b). Crustal structure in the Eastern profile. Model II.

The early arrivals observed at Huziwara, Kawaba and Tukuba are believed to result partly from the upheaval of the 2nd layer. If the discontinuity between the 2nd and 3rd layers becomes shallower by 4 km from $\Delta=250$ km, the short travel time at the last station is satisfactorily interpreted. The observed delay at Asakawa is attributed to a low velocity weathered layer.

§ 4. Results and Discussion

1. The derived structure and the travel time residuals

Two models of the crustal structure derived from the foregoing analysis are presented in Figs. 5 (a) and 5 (b). The boundary depth is indicated by the value below sea level. The travel times to each station calculated for the deduced structure are tabulated in Table 2. In this

Table 2. Calculated travel times and $O-C$ residuals for each station in the Eastern profile.

	Station		Model I			Model II		
		T_0 (sec)		T_c (sec)	T_0-T_c (sec)		T_c (sec)	T_0-T_c (sec)
E	1 Myôgase	2.91		P_1 2.75	0.16		P_1 2.75	0.16
	2 Kotakari	4.82		〃 4.67	0.15		〃 4.67	0.16
	3 Kamioka	7.37		P_{21} 7.52	−0.14		P_2 7.43*	−0.06
	4 Inekoki	13.66		〃 13.62	0.04		〃 13.56	0.10
	5 Hotaka	14.85		〃 14.98	−0.13		〃 14.90	−0.05
	6 Omi	18.8		〃 18.96	−0.2		〃 18.79	0.0
	7 Matusiro	21.87		〃 21.82	0.06		〃 21.55	0.32
	8 Hoppo	27.22		P_{22} 27.19	0.03		〃 27.18	0.04
	9 Ôiwa	29.01		〃 29.00*	0.01		〃 29.13*	−0.12
	10 Sawatari	30.4	(L)	P_{31} 30.48	−0.1	(L)	P_3 30.45	−0.1
	11 Takayama	32.58		P_{32} 32.59	−0.01		P_3 32.58	0.00
	12 Huziwara	33.98		〃 34.10*	−0.12		〃 34.09*	−0.11
	13 Kawaba	34.09		〃 34.13*	−0.04		〃 34.13*	−0.04
	14 Asakawa	36.33		〃 36.06	0.27		〃 36.04	0.29
	15 Yumoto	38.38		〃 38.33	0.05		〃 38.31	0.07
	16 Nisioasi	39.61		〃 39.60	0.01		〃 39.59	0.02
	17 Sinoi	43.2 ?		〃 42.80	(0.4)		〃 42.79	(0.4)
	18 Tukuba	44.17		〃 44.17*	0.00		〃 44.17*	0.00

Remarks: 1) (L); later phase
2) * ; The second layer crops out to the earth's surface.
3) T_0; observed travel time, T_c; calculated travel time.

calculation, corrections are made for the height difference between the shot and the observation point.

The difference between the observed and calculated travel times, which is called $O-C$ residual by our group, is reconciled within 0.15 sec except for the ones at Myôgase, Kotakari and Asakawa, in Model I. An exception is further added for Matusiro to Model II. All of these deviations may be responsible for a weathered layer.

2. Remarks on the observation of reflected waves

In the third observation, prominent later phases were recorded on the seismogram at Kamioka station where additional study of the seismic reflection method was attempted[4].

With a view to identifying reflected phases in the seismogram, travel times of reflections are computed concerning the derived structure. That of the waves reflected from the interface between the 1st and 2nd layers is 7.46 sec in Model I and 7.68 sec in Model II, but no corresponding phase was observed. As to the reflection from the boundary between the 2nd and 3rd strata, it takes 12.20 sec in Model I and 13.87 sec in Model II. The former time agrees well with the observed one of 12.21 sec. There is a little doubt, however, in concluding that this is related to the waves reflected from the Mohorovičić discontinuity, because the observed apparent velocity of 6.86 km/sec is smaller than the expected value of 9.35 km/sec. Judging from the recorded wave forms and observed apparent velocity, the phase with a travel time of 12.72 sec and a velocity of 11.38 km/sec seems to be the reflected waves from the said discontinuity. If this is true, the boundary should be corrected as being shallower by 1.3 km.

3. Remarks on the Bouguer anomaly of gravity

The Bouguer anomaly of gravity[5] distributed along the present profile indicates a great negative value in the Tyûbu mountain region, as shown in Fig. 5 (a). It may roughly be said that the downward warping of the 1st and 2nd layers near the region corresponds to this great negative anomaly. Morever, an increasing positive anomaly toward Tukuba may probably be caused by a localized upheaval of the 2nd and 3rd layers. The derived structure is not inconsistent with the gravity data.

4) S. MURAUCHI, *Report R. G. E. S.*, No. 17 (1958), 9–10.

5) C. TSUBOI *et al.*, *Bull. Earthq. Res. Inst., Suppl.* **4** (1955), Part 5; (1956), Part 7.

4. Crustal Structure in the Tyûbu, Kinki and Tyûgoku Districts (the Western profile)

§ 1. Time-Distance Curves

Reduced travel times in the Western profiles are plotted in Figs. 6 and 7, by the use of the data listed in Tables 15 and 16 in Part 1 of this paper.

The travel times of each wave group are represented as the following formulae for Models I and II in two Western profile. Profile A designates the northern section including the Hokuriku—northern Kinki—Tyûgoku regions and Profile B indicates the southern section traversing the central part of the Kinki District.

1. Profile A

M–I	P_{21}; $T_{21}=\Delta/5.92+0.31$	for	Nakai-Mikata	($28<\Delta<102$ km)
	P_{22}; $T_{22}=\Delta/6.32+1.41$	for	Mikata-Yasiro	($102<\Delta<165$ km)
	P_3; $T_3=\Delta/7.52+5.98$	for	Hukutiyama-Yanahara	($165<\Delta$ km)
M–II	P_2; $T_2=\Delta/6.00+0.46$	for	Nakai-Ôi	($50<\Delta<160$ km)
	P_3; $T_3=\Delta/7.50+5.82$	for	Yatuai-Yanahara	($160<\Delta$ km)

2. Profile B

M–I	P_1; $T_1=\Delta/5.55$	for	Arabuti-Itosiro	($\Delta<28$ km)
	P_{21}; $T_{21}=\Delta/5.81+0.31$	for	Ôgawara-Kitoge	($28<\Delta<112$ km)
	P_{22}; $T_{22}=\Delta/6.16+1.40$	for	Sirahige–Sikibi.	($112<\Delta<168$ km)
	P_3; $T_3=\Delta/7.45+6.13$	for	Taki-Tainohata	($168<\Delta$ km)
M–II	P_1; $T_1=\Delta/5.50$	for	Arabuti-Ôno	($\Delta<45$ km)
	P_2; $T_2=\Delta/6.00+0.46$	for	Ôgawara	
	P_2'; $T_2'=\Delta/6.00+0.70$	for	Gihu-Kyoto	($70<\Delta<165$ km)
	P_3; $T_3=\Delta/7.50+6.21$	for	Sikibi.-Kitaama	($165<\Delta$ km)

§ 2. Model I

2–1. Profile A (Northern Section)

1. Travel times of P_1 and the superficial layer

As is the case in the Eastern profile, the apparent velocity of the P_1 waves, 5.55 km/sec, is adopted as the true one for the longitudinal waves in the 1st layer, common to both of the Profiles A and B. The superficial layer overlying the 1st one, near the shot point, can be omitted in the present case, considering that the intercept time of P_1 is negligibly small.

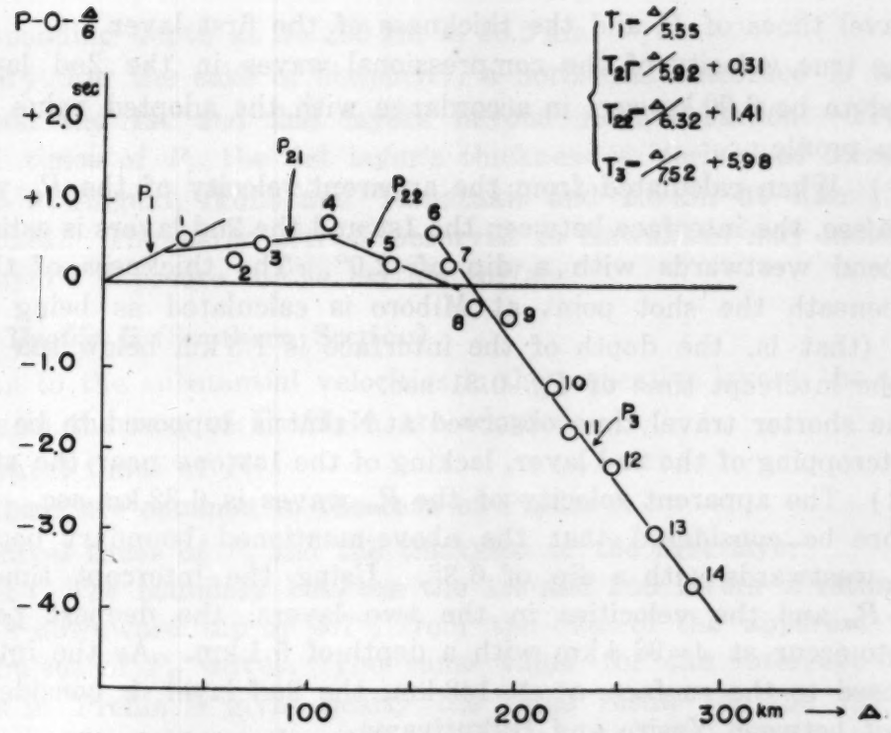

Fig. 6. Reduced travel time curves in the Western profile A.

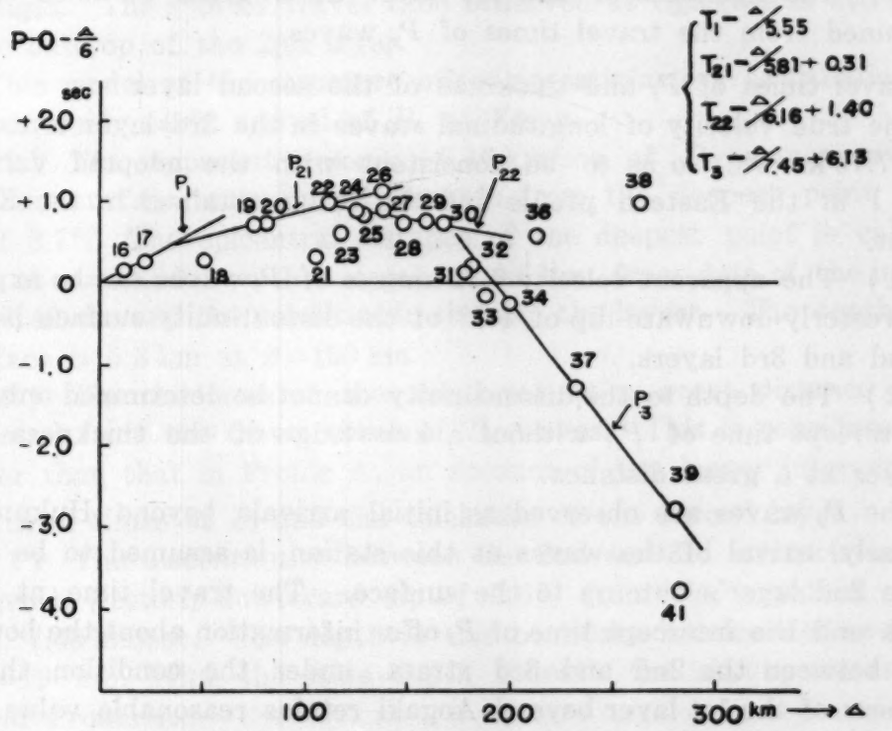

Fig. 7. Reduced travel time curves in the Western profile B.

2. Travel times of P_2 and the thickness of the first layer

The true velocity of the compressional waves in the 2nd layer is assumed to be 6.00 km/sec, in accordance with the adopted value in the Eastern profile.

(1) When calculated from the apparent velocity of the P_{21} waves, 5.92 km/sec, the interface between the 1st and the 2nd layers is estimated to descend westwards with a dip of 2.0°. The thickness of the 1st layer beneath the shot point at Miboro is calculated as being about 2.6 km (that is, the depth of the interface is 1.8 km below sea level), from the intercept time of P_{21}, 0.31 sec.

The shorter travel time observed at Nakai is supposed to be due to the outcropping of the 2nd layer, lacking of the 1st one near the station.

(2) The apparent velocity of the P_{22} waves is 6.32 km/sec. It can therefore be considered that the above-mentioned boundary begins to ascend westwards with a dip of 6.3°. Using the intercept time 1.41 sec of P_{22} and the velocities in the two layers, the deepest point is found to occur at $\Delta=96.4$ km with a depth of 5.1 km. As the interface is exposed to the surface at $\Delta=143$ km, the 2nd layer is considered to crop out between Yasiro and Hukutiyama.

(3) The thickness of the 1st layer at a great distance will be determined from the travel times of P_3 waves.

3. Travel times of P_3 and thickness of the second layer

The true velocity of longitudinal waves in the 3rd layer is assumed to be 7.70 km/sec, so as to be consistent with the adopted value for Model I in the Eastern profile and the result obtained in the Kwantô District.

(1) The apparent velocity 7.52 km/sec of P_3 waves can be explained by a westerly-downward dip of 1.7° of the discontinuity surface between the 2nd and 3rd layers.

(2) The depth to the discontinuity cannot be determined only from the intercept time of P_3, without a knowledge of the thickness of the 1st layer at a great distance.

The P_3 waves are observed as initial arrivals beyond Hukutiyama. The early arrival of the waves at this station is assumed to be caused by the 2nd layer's outcrop to the surface. The travel time at Hukutiyama and the intercept time of P_3 offer information about the boundary depth between the 2nd and 3rd strata, under the condition that the thickness of the 1st layer beyond Aogaki retains reasonable value. This consideration leads to 27.7 km in the mean depth below sea level. The

corresponding depth at $\Delta=290$ km is 36.5 km.

(3) For the sake of simplicity, a horizontal interface is assumed between the 1st and 2nd layers beyond Aogaki station. From the travel times of P_3, the 1st layer's thickness is derived as being about 8.5 km at Aogaki, Ikuno and Yamazaki, and 2.5 km at Kamigôri and Yanahara. The early arrival observed at Kawakami may indicate the 2nd layer's exposure to the earth's surface.

2-2. Profile B (Southern Section)

As to the substantial velocities in the respective layers, the assumed values in the case of Profile A are adopted.

1. Travel times of P_1

These are common to the case of Profile A.

2. Travel times of P_2 and the thickness of the first layer

(1) The boundary between the 1st and 2nd layers is estimated to have a downward dip of 5.7°, from the data of the apparent velocity 5.81 km/sec of P_{21} waves. The same value for the intercept time of P_{21} as in Profile A gives nearly the same result for the 1st layer's thickness beneath the shot point, in spite of a slight difference in the dip angle. The shorter travel time observed at Ôgawara is attributable to the outcrop of the 2nd layer.

This model of the structure offers no satisfactory explanation as to the extremely early arrival of P_{21} at Kaizu.

(2) The apparent velocity 6.16 km/sec of P_{22} waves gives the boundary surface ascending westwards from the deepest point with a dip of 3.7°. The epicentral distance of the deepest point is calculated to be at $\Delta=86.8$ km with a depth of 9.5 km, from data of the intercept time 1.40 sec and the velocities in the two the layers. The depth of the interface is 5.3 km at $\Delta=160$ km.

(3) The thickness of the 1st layer at a great distance will be estimated from the travel times of P_3 waves. This is considered to be thicker than that in Profile A, on account of the larger intercept time.

3. Travel times of P_3 and the thickness of the second layer

(1) The discontinuity between the 2nd and 3rd strata is estimated to have a westerly-downward dip of 2.6°, from the apparent velocity of P_3, 7.45 km/sec. The depth to this boundary is calculated as 36.4 km at $\Delta=190$ km, being the same depth beneath the shot point as in the case of Profile A.

(2) The P_3 waves are observed as initial arrivals beyond Kameoka.

The intercept time of P_3, 6.13 sec indicates a thickness of 9.5 km for the 1st layer beyond Ôharano, under the assumption of a horizontal interface.

The earlier arrivals observed at Kameoka, Taki and Abuyama stations are believed to be the result of an outcrop of the 2nd layer to the surface. The observed times at Rokkô and Sizuki are interpreted to be those of the later phase P_{22}, judging from calculated results of the wave propagation.

(3) A possible explanation of the early arrival at Kitaama (Awazi Isl.) is that the discontinuity between the 2nd and 3rd strata ascends westwards with a dip of 6.8° from a distance of 194 km having a depth of 25.2 km below the station.

§ 3. Model II

The apparent compressional velocities, 5.5, 6.0 and 7.5 km/sec, of the P_1, P_2 and P_3 waves traveling through the 1st, 2nd and 3rd layers are assumed to be the true ones in the respective layers, common to both of the Profiles A and B.

As in the case of Model I, the superficial layer is neglected because of the zero intercept of P_1 waves.

3-1. Profile A (Northern Section)

1. 1st layer

The depth to the boundary between the 1st and 2nd layers is calculated as 3.2 km below the shot point, that is, 2.4 km below sea level, from the data of the intercept time of P_2 and the wave velocities.

The arrival times observed at Nakai and Ôi are earlier than those expected from the derived structure, and that at Mikata is later than the calculated times. To give a possible explanation to these deviations, it is considered that the 2nd layer crops out to the surface at Nakai with a tapering of the 1st layer from $\Delta=50$ km, that the 1st layer's thickness increases to 6 km from $\Delta=90$ km, and that it again tapers from $\Delta=105$ km with an outcrop of the 2nd layer at Ôi.

2. 2nd layer and 3rd layer

The longitudinal waves P_3 passing through the 3rd layer emerge as initial arrivals beyond Yatuai. From the standard equations of the travel times, the 2nd layer is found to be as thick as 25.2 km below the shot point, namely, the boundary depth between the 2nd and 3rd layers is 27.6 km.

The assumed thickness of 2.4 km for the 1st layer between Yatuai and Hukutiyama gives an earlier arrival in the calculation than the observed time for the former station. It is believed that the observed arrival is related to the later phase. The delayed arrivals observed at Aogaki, Ikuno and Yamazaki are considered to be attributable to increased thickness of the 1st layer to about 13 km.

Calculating from the observed travel times of P_3, the 1st layer's thickness is estimated to be 2.4 km below Kawakami and 6 km below Kamigôri and Yanahara stations.

3-2. Profile B (Southern Section)

1. 1st layer

The early arrival observed at Ôgawara may be the result of the 1st layer tapering from $\Delta=30$ km and the 2nd one cropping out to the surface near the station.

Beyond Gihu, the thickness of the 1st layer is estimated as 5.7 km from the intercept time of P_2, which is a little larger than the previously determined value at a short distance.

To interpret the observed early arrival at Kaizu, it is necessary to consider that the 2nd layer is exposed to the surface at the station with a tapering of the 1st layer from $\Delta=80$ km. If we approve of this point-of-view, however, we find it difficult to give a satisfactory explanation to the delayed arrivals observed at several points between Kitoge and Wani. The onset of the waves is not so clearly observed at all of these stations which are located along the west coast of Lake Biwa. For this reason, data from these stations are omitted in the present treatment. In order to adjust the calculated values to the observed ones for the said stations, we have to suppose the existence of the superficial layer with a lower velocity overlying the the 1st layer.

2. 2nd layer and 3rd layer

The phase P_3 traveling through the 3rd layer appears as an initial arrival beyond Sikibigahara. The 2nd layer's thickness is computed as 23.0 km and therefore the boundary depth as 28.7 km, using the intercept time of P_3.

The late arrivals observed at Ôharano and Tainohata are explained by the thickening of the 1st layer between $\Delta=180$ km and 250 km, being 15.3 km. The arrival time at Kitaama is anomalously early. It is impossible to interpret this fact only by the decrease in the 1st layer's thickness, so that the discontinuity between the 2nd and 3rd strata is

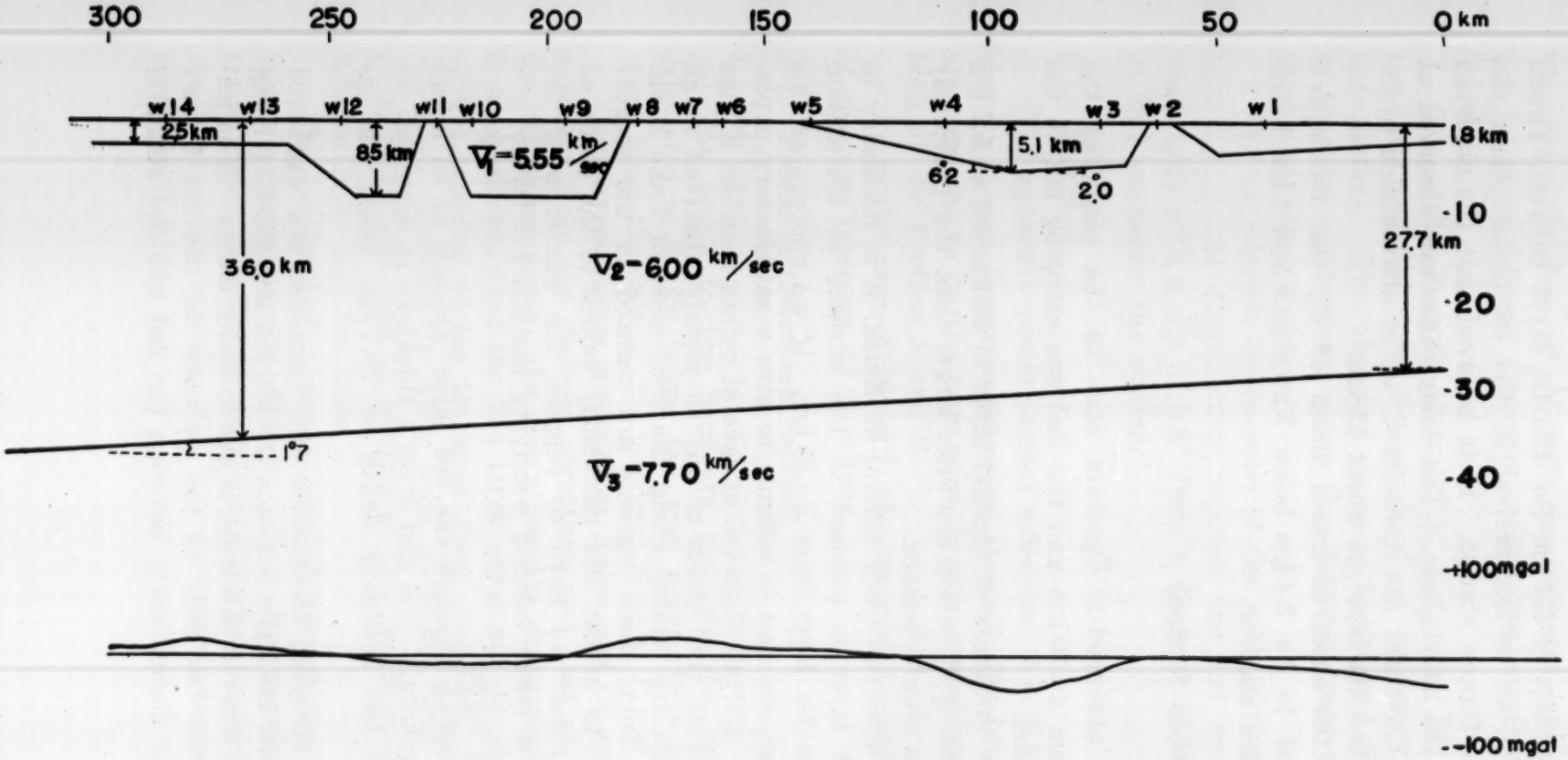

Fig. 8 (a). Crustal structure in the Western profile A. Model I, with Bouguer anomaly of gravity along the profile.

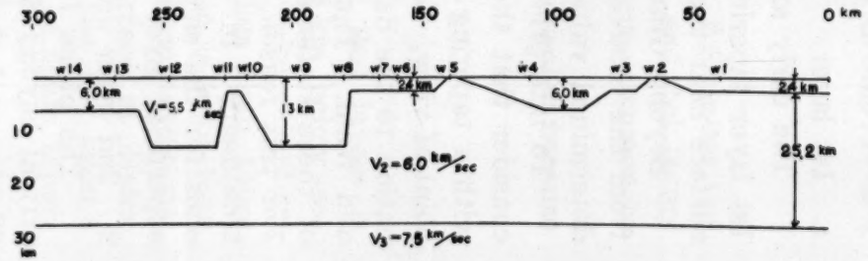

Fig. 8 (b). Crustal structure in the Western profile A. Model II.

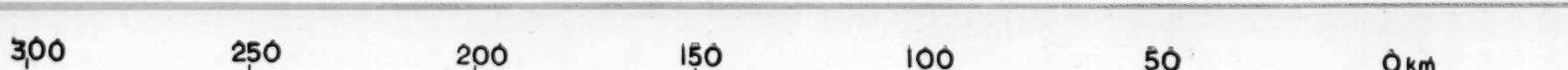

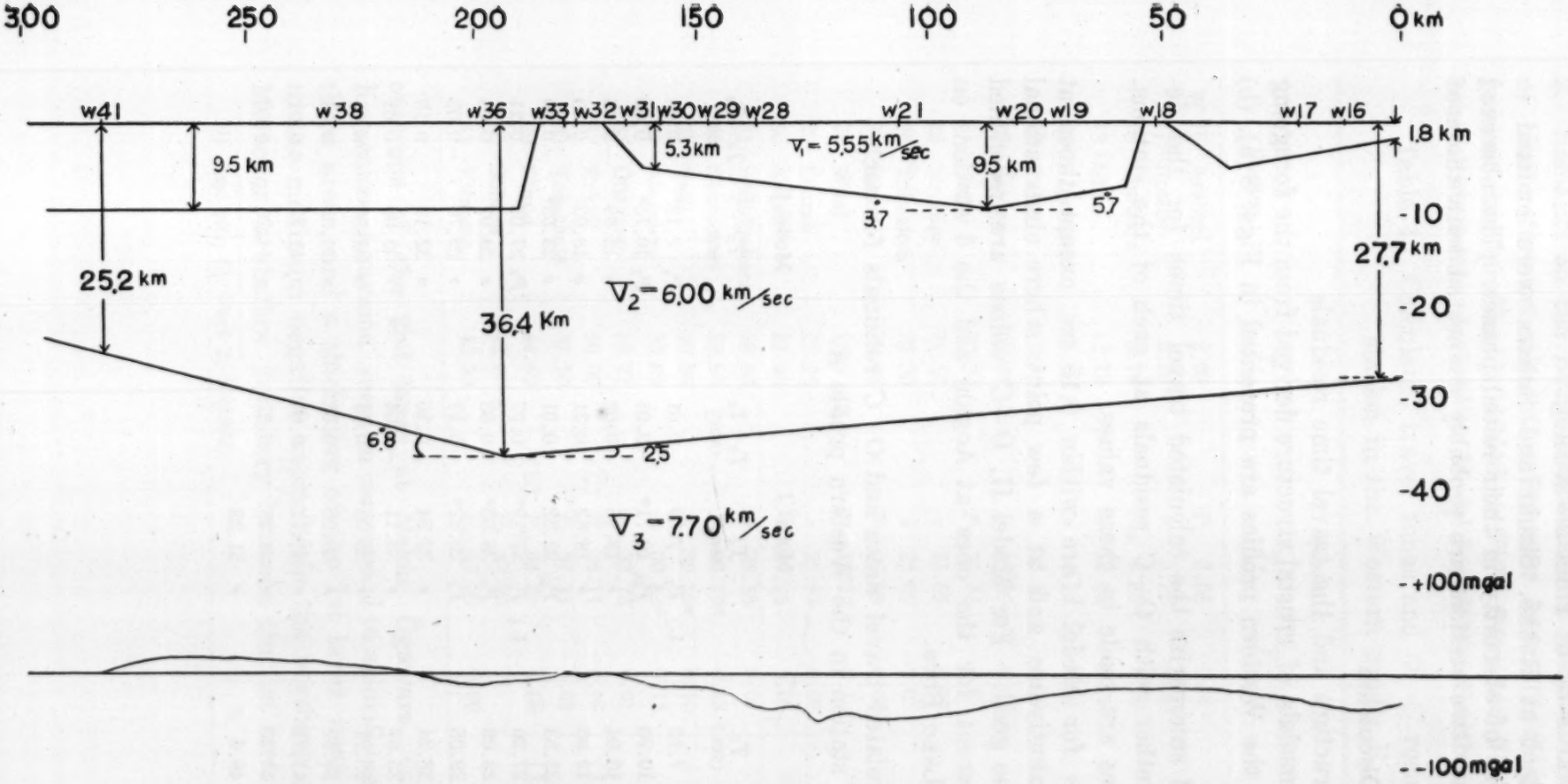

Fig. 9(a). Crustal structure in the Western profile B. Model I, with Bouguer anomaly of gravity along the profile.

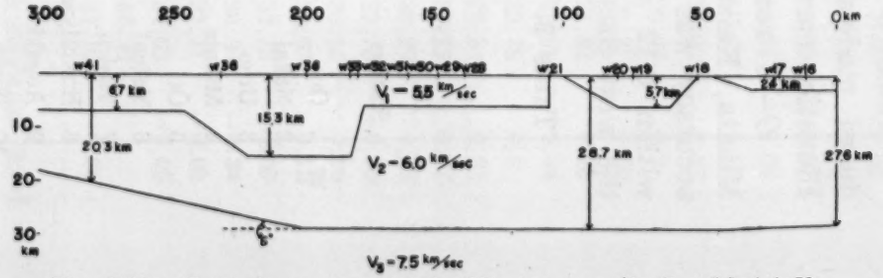

Fig. 9(b). Crustal structure in the Western profile B. Model II.

thought to dip upwards by 6° from $\Delta=200$ km.

The data obtained at Rokkô, Sizuki and Suhara were omitted in this analysis because of obscurity in their initial phases. The observed values at the former two stations are probably connected with those of a later phase.

§ 4. Results and Discussion

1. The derived structure and the travel time residuals

Two probable models of crustal structure derived from the foregoing analysis for both the Western profiles are presented in Figs. 8 (a), (b) and 9 (a), (b).

Tables 3 and 4 summarize the calculated travel times for the deduced models, together with $O-C$ residuals at each of the stations. Elevation corrections are made in these values.

$O-C$ residuals for Model I are within 0.15 sec except those at Mikata, Kaizu, Hukutiyama and at a few points where observational accuracy was not so good. For Model II, $O-C$ values are reconciled within 0.12 sec except for the ones at Aogaki and the 6 stations on the west coast of Lake Biwa.

Table 3. Calculated travel times and $O-C$ residuals for each station in the Western profile A.

	Station		Model I		Model II	
		T_0 (sec)	T_c (sec)	T_0-T_c (sec)	T_c (sec)	T_0-T_c (sec)
W	1 Ôno	7.10	(L) P_1 7.09	−0.01	P_1 7.16	−0.06
	2 Nakai	10.70	P_{21} 10.71*	−0.01	P_2 10.70*	0.00
	3 Utuo	13.04	〃 13.06	−0.02	〃 13.09	−0.05
	4 Mikata	19.03	〃 18.82	0.21	〃 18.93	0.10
	5 Ôi	23.53	P_{22} 23.52	0.01	〃 23.63*	−0.10
	6 Yatuai	27.26	(L) P_3 27.19*	0.07	P_3 27.05	0.21
	7 Yasiro	28.06	P_{22} 28.03*	0.03	〃 28.01	0.05
	8 Hukutiyama	29.65	P_3 29.82*	−0.17	〃 29.70	−0.05
	9 Aogaki	32.34	〃 32.24	0.10	〃 32.19	0.15
	10 Ikuno	35.07	〃 35.11	−0.04	〃 35.08	−0.01
	11 Kawakami	35.91	〃 36.05*	−0.14	〃 35.96*	−0.05
	12 Yamazaki	39.07	〃 39.05	0.02	〃 39.03	0.04
	13 Kamigōri	41.71	〃 41.71	0.00	〃 41.72	−0.01
	14 Yanahara	44.26	〃 44.25	0.01	〃 44.26	0.00
	15 Yakage	49.6 ?	〃 51.23			

2. Remarks on the Bouguer anomaly of gravity

For reference sake, the Bouguer anomaly of gravity[6] along the present two profiles is added to Figs. 8(a) and 9(a). Comparing the crustal structure derived as Model I with the distribution of the anomaly,

Table 4. Calculated travel times and $O-C$ residuals for each station in the Western profile B.

Station	T_0 (sec)	Model I T_c (sec)	Model I T_0-T_c (sec)	Model II T_c (sec)	Model II T_0-T_c (sec)
W 16 Arabuti	2.09	P_1 2.08	0.01	P_1 2.10	−0.01
17 Itosiro	3.73	〃 3.73	0.00	〃 3.76	−0.03
18 Ôgawara	8.74	P_{21} 8.83*	−0.09	P_2 8.74*	0.00
19 Gihu	13.12	〃 13.10	0.02	P_2' 13.05	0.07
20 Kinomoto	14.08	〃 14.12	−0.04	〃 14.04	0.04
21 Kaizu	17.91	〃 18.47	−0.56	〃 17.93*	−0.02
23 Kitoge	19.47	〃 19.40	0.07	〃 18.90	0.57
24 Imazu	20.2	P_{22} 20.44	−0.2	〃 20.03	0.2
25 Sirahige	21.57	〃 21.55	0.02	〃 21.27	0.30
26 Takasima	22.00	〃 22.05	−0.05	〃 21.82	0.18
27 Kido	23.95	(L) P_{21} 23.89	0.06	〃 23.51	0.44
28 Wani	23.9	P_{22} 23.77	0.1	〃 23.75	0.2
29 Bessyo	25.25	〃 25.32	−0.07	〃 25.24	0.01
30 Kyôto	27.20	〃 27.15	0.05	〃 27.13	0.07
31 Sikibigahara	28.40	〃 28.39	0.01	P_3 28.29	0.11
32 Kameoka	29.66	P_3 26.79*	−0.13	〃 29.76	−0.10
33 Taki	30.26	〃 30.16*	0.10	〃 30.16	0.10
34 Abuyama	30.69	〃 30.82*	−0.13	〃 30.57	0.12
36 Ôharano	32.73	〃 32.72	0.01	〃 32.73	0.00
37 Rokkô	36.05	(L) P_{22}' 36.11	−0.06	(L) P_2 36.39	−0.34
38 Tainohata	37.10	P_3 37.11	−0.01	P_3 37.11	−0.01
39 Sizuki	44.60	(L) P_{22}' 44.57	0.03	(L) P_2 44.65	−0.05
40 Suhara	43.9 ?	P_3 42.96		P_3 42.96	
41 Kitaama	43.20	P_{32} 43.20	0.00	P_3' 43.16	0.04

outcrops of the 2nd layer at Nakai, Ôgawara, Ôi—Hukutiyama and Kameoka—Abuyama seem to correspond to a small negative anomaly near these areas, and a thickening of the 1st layer near Mikata and Kitoge to the maximum negative anomaly in the northern part of Lake Biwa. Moreover, a shallow boundary between the 1st and 2nd layers beneath

6) *loc. cit.*, 5), Part 2, 5 (1954).

Kamigōri, and that between the 2nd and 3rd layers below Kitaama are suggestive of a positive anomaly near those regions, respectively.

In other words, it can safely be said that the derived structure corresponds qualitatively to distribution of the Bouguer anomaly.

5. Concluding Remarks

From an analysis of the observed results of seismic waves from the Miboro Explosions, two probable models of crustal structure as shown in Figs. 5, 8 and 9 were derived for the Eastern and Western profiles, respectively.

Final results are as follows.

In the Eastern profile, Model I, the first and second layers indicate a downward warping. The deepest portion of the former occurs near Matusiro and that of the latter in the neighbourhood of the Tyûbu mountain region. Their deepest values are about 9 km and 38 km, respectively. This is a remarkable feature in Model I. This may be as expected hitherto from an isostatic hypothesis.

In Model II of the same profile the mean depth of the second discontinuity is estimated to be about 36 km.

In the Western profiles, Model I, thicknening of the first layer is found to occur in the northern part of Lake Biwa. The boundary surface between the second and third layers descends westwards, but seems to ascend toward Awazi Island. Its deepest value is nearly 36 km.

In Model II of the profiles the mean depth of the said boundary is 27–29 km.

Comparing the results in the two Western profiles, the first layer is thought to taper northwards (toward the Japan-Sea coast) from southern parts of the mentioned regions.

On the whole, no striking conflict exists between the structres over the said three profiles, on view of Model I.

The discontinuity surface between the second and third strata becomes deeper westwards from the Kwantô District with its deepest value in the Tyûbu mountain region, and in turn becomes shallower toward Miboro. This deepens again toward the Kinki District, but seems to be shallower beneath Awazi Island.

It may safely be said that the derived structure corresponds, at least qualitatively, to the Bouguer anomaly of gravity and to the struc-

ture deduced from spectrum of the anomaly[7].

The interface between the second and third strata may be regarded as the Mohorovičić discontinuity. There may be left, however, some doubt in respect to the adopted velocity of 7.70 km/sec being a little smaller for that in the mantle surface.

In order to gain a more precise knowledge of the deeper structure of the crust, it will be necessary in future to observe seismic waves at a longer distance.

Acknowledgement

Finally, we wish to express our heartfelt thanks to the other members of the Research Group for their kind advice. Our thanks are also due to Mrs. T. Huzita for her assistance in preparing this paper.

---

10. 御母衣爆破地震動観測による日本中部の地殻構造
第2部 地殻構造について

京都大学防災研究所 三雲 健
京都大学理学部地球物理学教室 大塚道男
気象庁 宇津徳治
東京大学理学部地球物理学教室 寺島敦
東京大学地震研究所 岡田惇

御母衣爆破地震動の観測資料を解析した結果，東方および西方の二つの測線に対して，第5,8,9図に示されるようなそれぞれ二つの地殻構造の model が得られた．

各観測点で記録された P 波初動の走時曲線はそれぞれ次のようなみかけ速度を示す．

Model I
- 東方測線 : 5.55, 5.86, 6.33, 7.91 km/sec
- 西方測線A : 5.55, 5.92, 6.32, 7.52 〃
- 西方測線B : 5.55, 5.81, 6.16, 7.45 〃

Model II
- 東方測線 : 5.5, 6.0, 7.9 〃
- 西方測線A, B : 5.5, 6.0, 7.5 〃

Model I においては，関東地方ですでに得られた結果を考慮して，これらの資料から 5.55, 6.00 および 7.70 km/sec の速度を持つた3層より成る構造が考えられた．

第1層は中部地方および琵琶湖北部で厚くなつており，約9kmの厚さと推定される．また西方の二つの測線の構造を比較すると，これは南側より北側（日本海側）へ向つて薄くなつていると思われる．第2-3層境界面（恐らく Mohorovičić discontinuity と考えられる）は関東地方より西方へ向つて深くなり，中部山岳地方で約 38 km の深さを持ち，さらに西方へかけてはいつたん浅くなる．御母衣附近で数 28 km である．これは近畿地方へ向つてまた深くなるが，淡路島方面では浅いと考えられる．最深の値は約 36 km である．

Model II の立場に立てば，第2-3層境界面の平均の深さは，中部地方で約 36 km，近畿地方で 27-29 km である．しかしながらこの model においては東西両測線の構造に若干の矛盾を生ずる．

7) T. TOMODA, *Journ. Geod. Soc. Japan*, **6** (1960), 47-55.

地震研究所彙報
第39号(1961) 351-358頁

11. 静岡県御前崎沖(御前岩)における波浪観測 (序報)

地震研究所 高橋龍太郎
羽鳥徳太郎

(昭和 36 年 2 月 28 日発表—昭和 36 年 3 月 31 日受理)

1. 緒　　言

静岡県御前崎より東方約 3km 沖に御前岩といわれる岩礁がある. (Fig. 1) この附近は駿河湾内の清水, 焼津港に通ずる航路近傍に位置し, 貨物, 漁船の往来はげしい所であるので, 過去においてこれら船舶の座礁等の事故が多い. このため海上保安庁灯台部において海難防止対策として, 灯標の建設が計画されていた.

しかし, この附近は常時うねり高く, 何等の遮蔽物もない洋上における灯標建設とて, 多くの困難を伴つたが, 特殊な設計で1959 年 3 月完成した.

灯標建設に対する波浪の基礎資料の一つとして宇野木・中野[1]は, 御前崎測候所において御前崎港内の波浪観測資料[2]から台風時における御前岩附近の最大波浪高の推定値を求

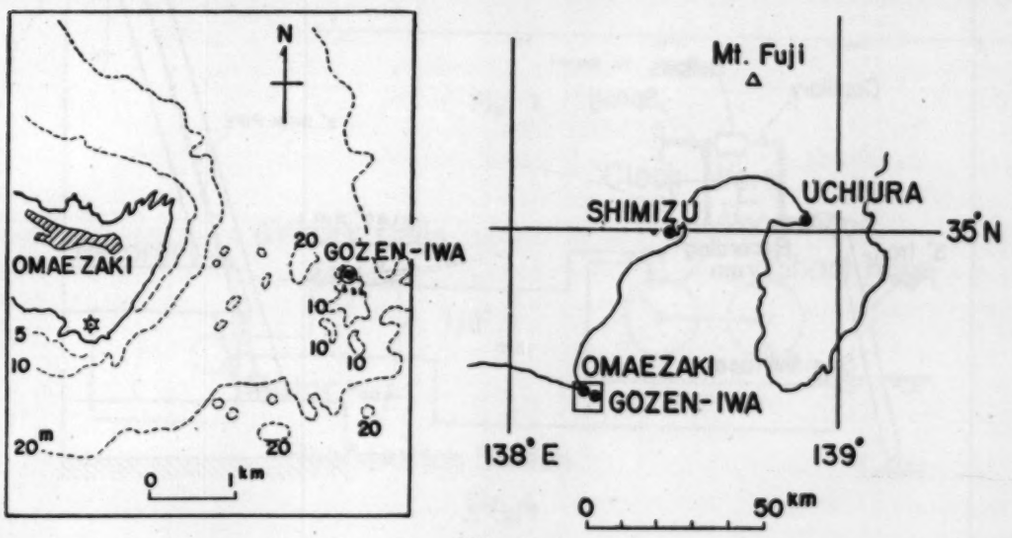

Fig. 1.

めた. しかし港内と御前岩附近の波浪とは平素波の様子が非常に異なり, 御前岩における波浪観測は, かつてなされたことがない.

昭和 33 年度文部省総合研究“海難の研究”による研究の一環として特殊の波浪計を設計製作したが, 今回海上保安庁灯台部の御好意で, 御前岩灯標内にこの波浪計設置の許

1) 宇野木早苗・中野猿人 1958. 台風による御前岩と五島灘の波浪の計算　日本海洋学会誌 14 巻 1 号

2) 太田芳夫 1953 長期捲波浪計の試作—御前崎の波浪について—日本海洋学会誌 9 巻 3-4 号.

可が得られ，観測を開始したのでここに報告する．

観測は May, 7, 1959 に開始されたが，Motor の起動が電接時計によるもので（後述）設置当初は起動の不良で欠測が多かつた．その後，いくつかの改良の結果，Oct. 1960 頃より観測が軌道にのり欠測なく観測出来るようになつたので，この記録と内浦，清水の日平均潮位の変動と比較して，御前岩の波高と湾内の潮位変動の関係を検討した．

2. 波　浪　計

本計器は洋上の波浪観測であるので保守の点を考慮し，器械の構造を簡単にして取扱いの簡易化を計り，圧力式の波浪計としたのである．Fig. 2 に示すごとく，波浪による

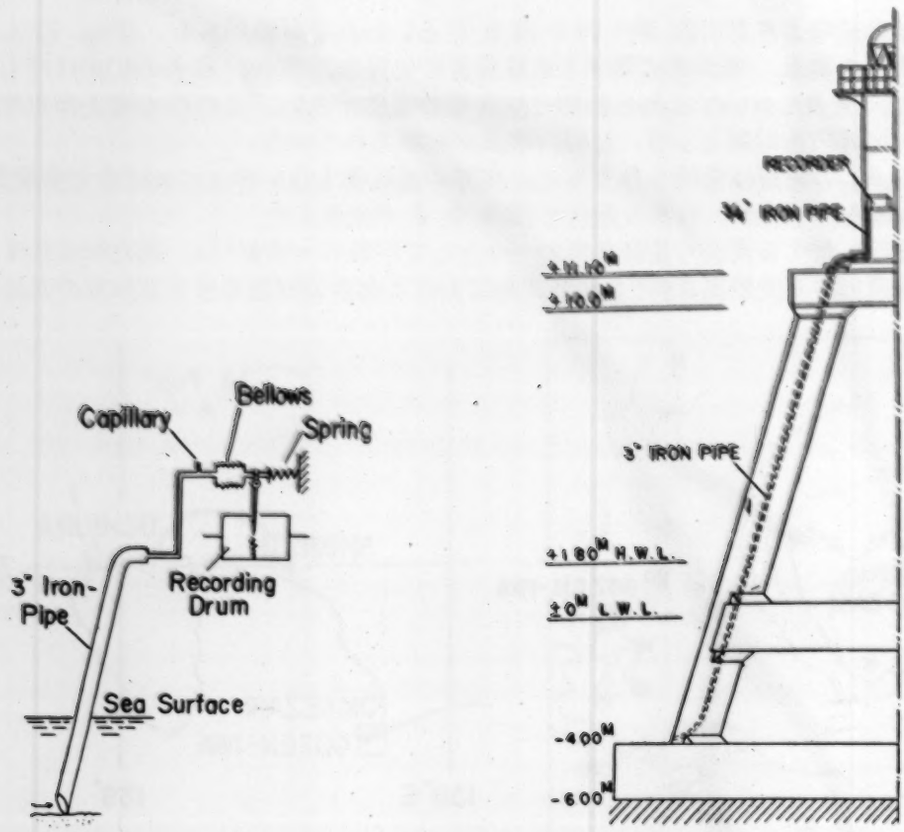

Fig. 2.

海水の圧力は鉄管を通じてベローを伸縮させ，これに倍率をかけて煤書のドラムに記録する．鉄管の途中に毛細漏洩管を設け潮汐を消して波浪のみを記録する．記録部の実際の据付は，灯標内の 2 階に設置し圧力の導管は灯標の三脚柱内，東向の一つに 3 吋の鉄管を埋めこみ，脚柱下部に圧力口を開いている．また灯標内の記録部と灯標脚柱内 3 吋鉄管との間は 3/4 吋ガス管で連結した．

記　録　感　度

ドラムに記録される振巾 1mm は実際の海の波高で 31.8cm に相当する．

波浪高は最大 9m を記録し得る．この波高は御前岩で期待される最高のものである．[1]

記 録 速 度

ドラムの回転速度 1 分間に 20mm 送る.

観 測 時 間

冬期は海上が荒れ, 灯標に登りうる機会は月 1 回位となるのでドラムの取換えは最長 30 日毎とした. 観測時間は 1 日 2 回, 0h, 12h (G.M.T.) に時計装置で電源を断続し, 1 回 15 分間 Motor を回転して 30 日間自働的に観測する. 即ちドラムは 15 分間に半回転し, 12 時間後再び半回転し 1 日に 1 回転する.

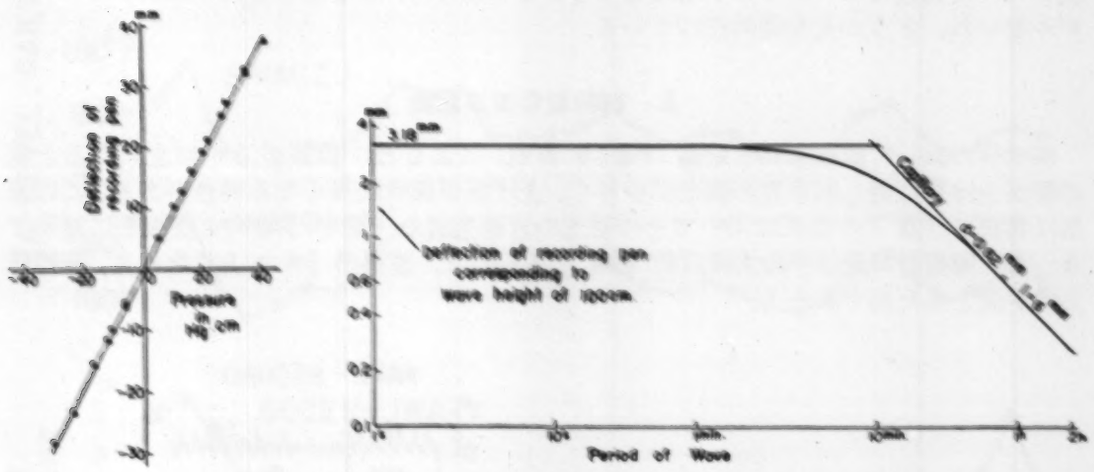

Fig. 3.

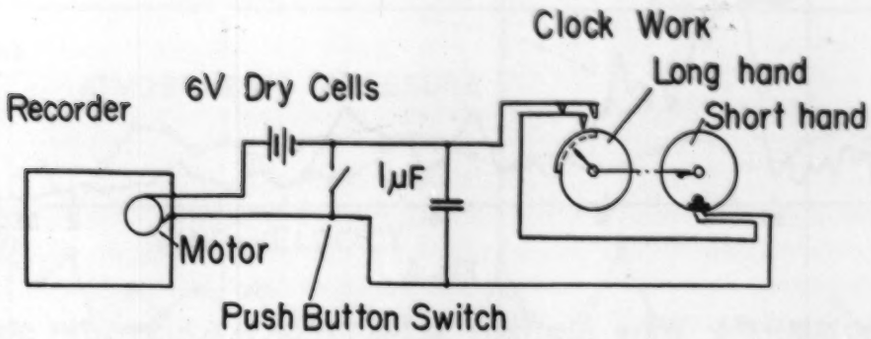

Fig. 4.

記録の送り及び起動装置

ドラムはマイクロモーター (6V, 17mA, 1r.p.m.) の回転を歯車にて減速して廻し, 記録の横送りはペン先がドラムの 1 回転につき 1cm 宛移動するようにした.

マイクロモーターの起動装置は, 30 日捲ゼンマイ時計の短針にアクリル酸樹脂製カムを 2 枚とりつけ, 2 ケのレバーがそれぞれのカムにのり 15 分間導通する. また長針にはアクリル酸樹脂製の円板をとりつけ一部分に真鍮をはめこみ, これもまた 2 本のレバーで接触せしめ, 15~20 分導通せしめる.

以上時計の長短両針の電接の直列組合せで 1 日 2 回, 各 15 分間 Motor を起動せしめる.

なお波高の高いときには灯標は衝撃的振動があるため，時計を Spring で吊し防振装置をほどこした箱に入れてある．

電　　源

平角 5 号乾電池 (3V) を 2 ケ直列に使用，3 ケ月毎に取換える．蓄電池の使用は灯標に登る際に非常な困難が伴うため不適である．

対 湿 装 置

本計器の設置が洋上の灯標内であるため，きわめて湿度高く潮害を防ぐ対策として，器械カバーの周囲にゴムパッキンをほどこし，その他時計，乾電池も木箱に密閉してシリカゲルをいれ，とりかえを随時行つている．

3. 御前岩の波浪記録

御前岩において観測される記録 (Fig. 9 参照) によると，波高が 1m 以上になると波の形が上げ波に対し引き波の振巾が少さく，上げ波が異状に高くなる特色がある．この現象は御前岩灯標下の水深は 6m でその附近の岩礁尖端の一部は干潮時に海面上に露出する．また御前岩周辺の平均水深は約 20m であるので，波高が 1m 以上になると，御前岩で波が盛上るためであろう．

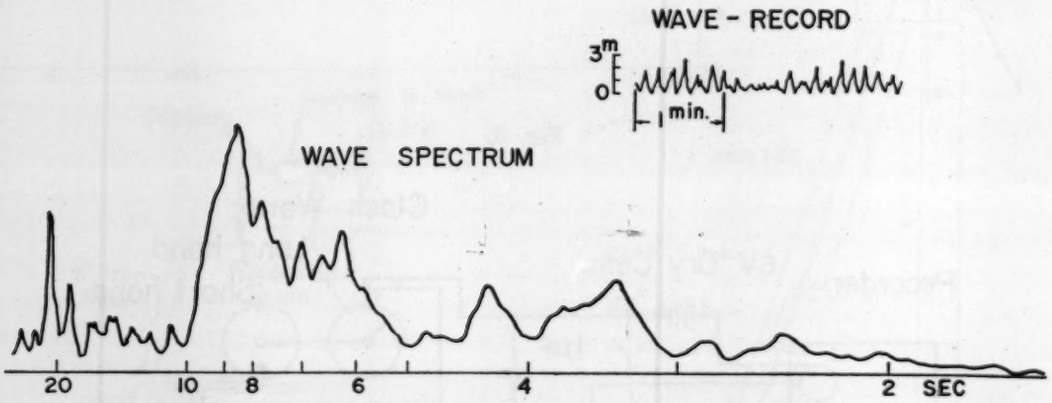

Fig. 5.

次に波の周期分析を Wave Analyzer[3] にかけて行つてみると 9sec, 7sec が卓越し 2 次高調波として 4.5sec, 3.5sec がみられる．その他 12sec があらわれることがある．

4. 御前岩の波高と湾内の潮位変動の関係について

台風に伴う高潮に際し，湾口の波高と湾内の潮位の高まりとの関係を導く基礎資料を得るため，常時観測で湾口の波高と湾内の潮位変動量の関係を求めておくことは高潮の研究上大きな意義がある．

筆者らは Oct. 26—Nov. 24, 1960 年の約 1 ケ月の御前岩の波浪観測記録を用い，気象庁の御好意で提供された湾内の内浦，清水，御前崎の潮位観測値と比較検討した．

まず御前岩の波高で (Fig. 6) Oct. 27 と Nov. 23 に 3m を記録している．前者は台

3) 高橋龍太郎・相田勇　津波スペクトルの研究　地震研究所談話会 (昭和 36 年 2 月 28 日)

風 25 号，後者は移動性低気圧による波浪である．なおこの記録の振巾読みとり値は，9^h と 21^h の観測時における最大波高の平均値である．

御前岩の波浪と湾内の潮位の変動量をさらにみやすくするため，Fig. 7 のごとく潮位の変動量を log 目盛でかき表わすと，かなり点がばらつく．

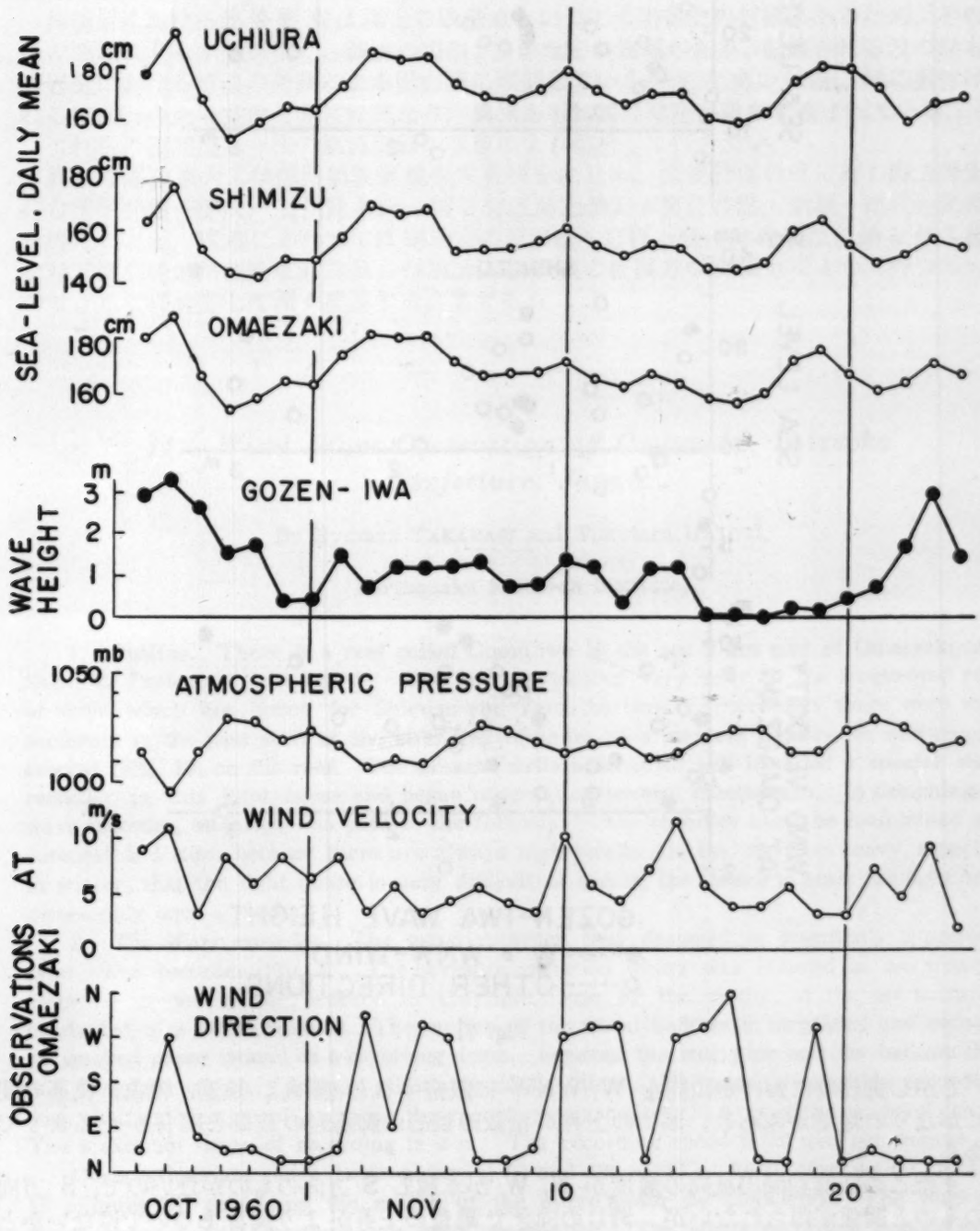

Fig. 6.

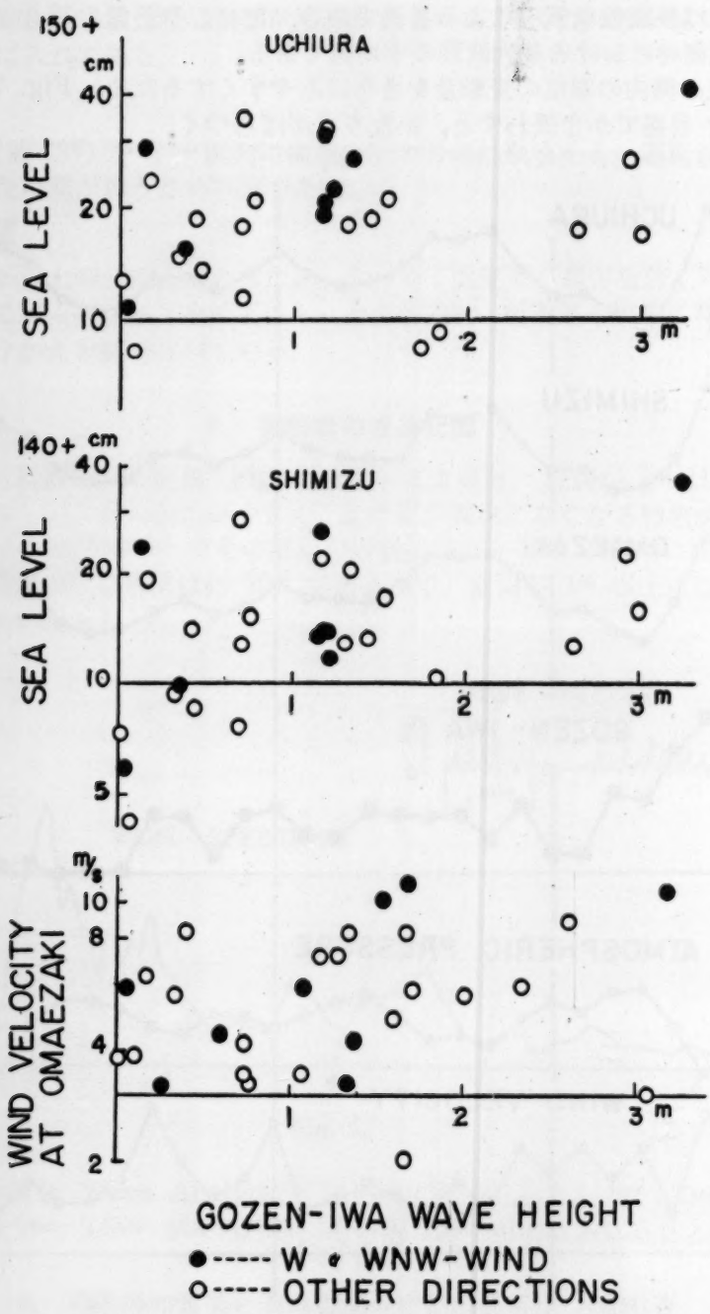

Fig. 7.

しかし御前崎における風向を W, WNW に限定すると（黒丸），風速，潮位，波高の間にかなりの対応がみられ，潮位の上昇が指数函数的に御前岩の波高と関係があるようである．

またこの観測期間の風向の瀕度が N, W が卓越し S 方向のものがないので，S 方向のものと関係が得られないが，湾口の向きで潮位の上昇がより関係あるのではないかと思われる．このことは今後の観測資料の集収にまたねばならない．

次に御前崎における風速の影響による波浪の高まりは，潮位の上昇程関係がみられない．

5. あとがき

御前岩における波浪観測は洋上の観測点といつても岩礁上の灯標にあるため，その近傍の海域よりも水深が浅く，波浪の増巾，変形などの問題があり，記録される波の形も港湾岩壁における波浪の衝激による圧力波に類似しているが港内或いは島，岬に据付けられる波浪計の立地条件と非常に異なり，興味ある特異な問題が数多く含まれている．

これらの諸問題は今後の観測記録の収積により解折して行きたい．

終りに臨み東大工学部船舶教室乾崇夫教授をはじめ，波浪計据付けに対し海上保安庁灯台部平井信一郎氏，石川進六氏，第3管区海上保安本部灯台部，余湖一郎氏の御協力を得たことと，観測にあたつては御前岩の波浪高く灯標上陸には非常な危険を伴う業務を地元御前崎航路標識事務所酒井作恵所長他職員の皆様方の御協力によつて行つているので，ここに特記して深く感謝する次第である．

---

11. Wind Wave Observation off Omaezaki, Shizuoka Prefecture, Japan.

By Ryutaro TAKAHASI and Tokutaro HATORI,

Earthquake Research Institute.

1. *Outline.* There is a reef called Gozen-iwa in the sea 3 km east of Omaezaki-cape, Shizuoka Prefecture (see Fig. 1). The reef is located very near to the frequented route of ships which are bound for Shimizu and Yaizu harbors. Accordingly there were many accidents in the past such as the stranding of ships, so a manless light-house was recently erected (Fig. 10) on the reef. The present writers designed and installed a special wave-recorder in this light house and began observation several months ago. In designing the wave recorder, attention was paid to the following: the recorder must be maintained with sureness and ease, because there are always high swells and the sea is so heavy, especially in winter, that the light house is very difficult of access, the chance to enter the light house comes only once a month.

2. *The Wave recorder.* The wave recorder thus designed is essentially a pressure-type wave recorder (Fig. 8). The pressure variation which was induced in an iron-pipe embeded in one of the pedestal of the light-house by the motion of the sea surface is conducted to a metal bellows. The motion of the metal bellows is magnified and recorded on smoked paper wound on a revolving drum. Between the iron pipe and the bellows there is a slow-leak capillary tube to elliminate tidal motions. The sensitivity of the recorder is such that a deflection of 1 mm on the record corresponds to 31.8 cm of the sea level change. The maximum range of recording is 9 m. The recording speed is 20 mm per minute.

Observations are made twice a day at 0^h and 12^h (GMT). Each observation lasts for 15 minutes by controling the switch of the micro-motor by clockwork. The recording drum makes a half revolution in each observation. The whole recording system works entirely automatically for 30 days (Fig. 4).

As the electric source two 3-volt dry-cells connected in series are used, the whole equipment is provided with a device to protect it from humidity and vibrations.

3. *Results*. According to the record obtained (Fig. 9) when the wave height exceeds 1 m the crest becomes exceedingly steep and high while the trough becomes flat and shallow. This must be caused by the soaring of the wave owing to the sudden depth change, from 20 m to 6 m, in approaching the sunken reef on which the light-house stands. Frequency analysis of the wave records were also made (Fig. 5).

The present writers compared the wave heights at Gozen-iwa thus observed with the daily mean sea levels at Uchiura, Shimizu and Omaezaki to investigate the relation between the fluctuations of the sea level in Suruga Bay and the wave height at the month of the bay. According to the observation made in the last month, there seems to be a linear relation between them, if we take only the days when WNW or W winds are blowing, although the relation becomes somewhat vague when all days were taken into account. Observations are being continued.

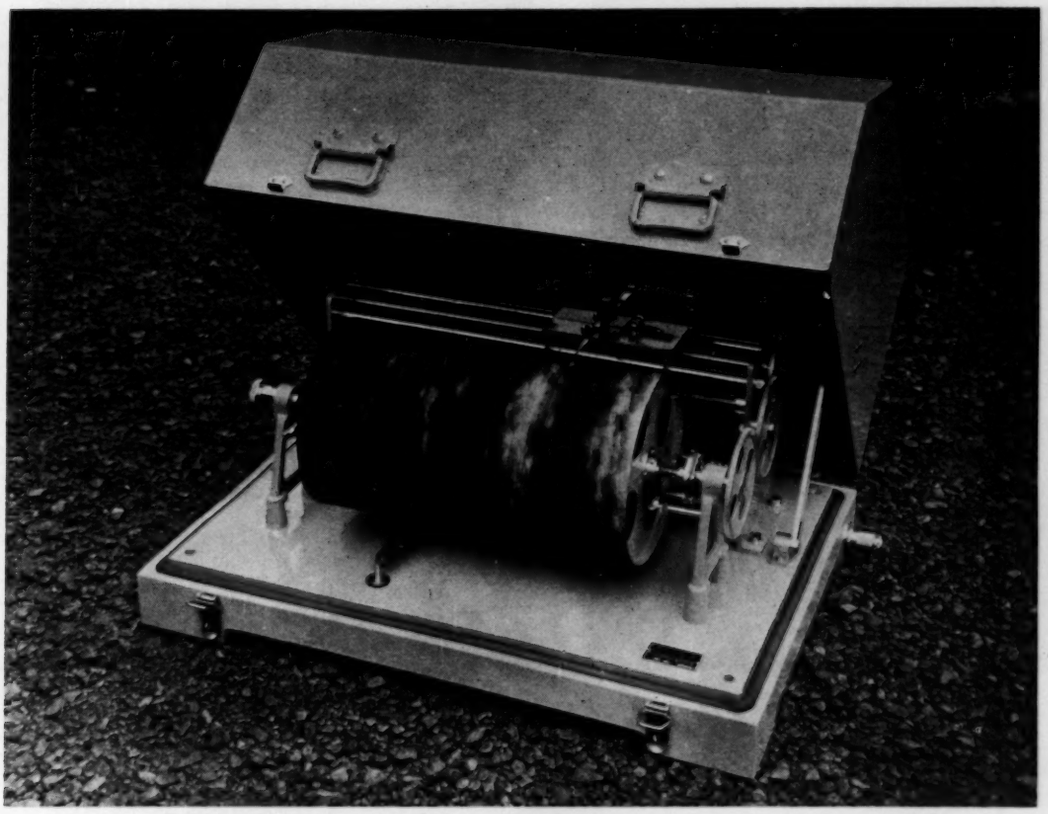

Fig. 8. Recorder for the wave meter.

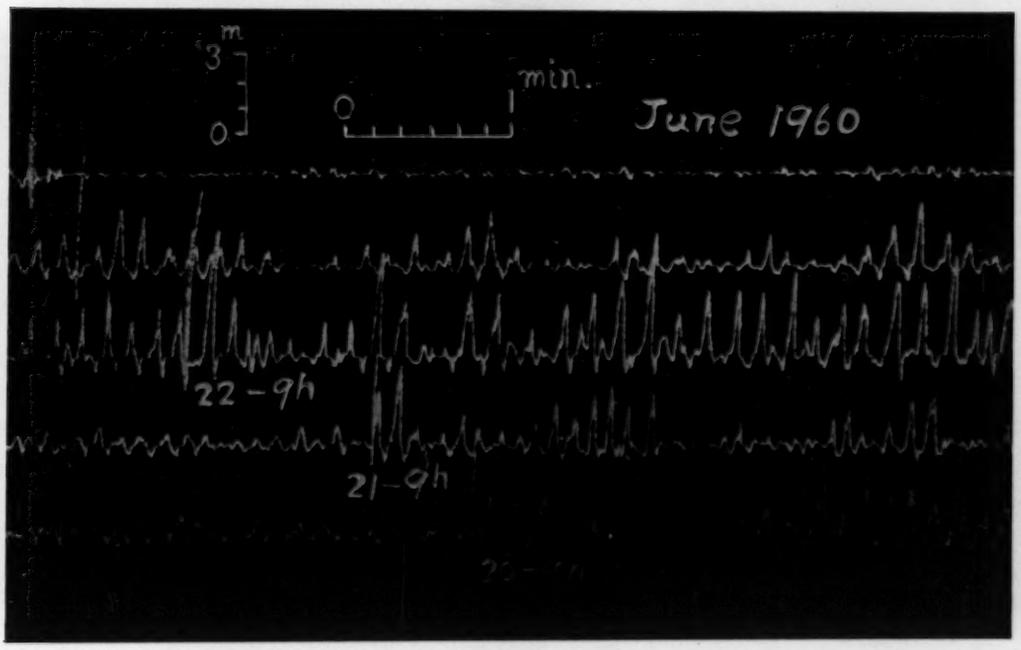

(震研彙報 第三十九号 図版 高橋・羽鳥)

Fig. 9.

Fig. 10. Gozen-iwa light-signal.

Fig. 11.

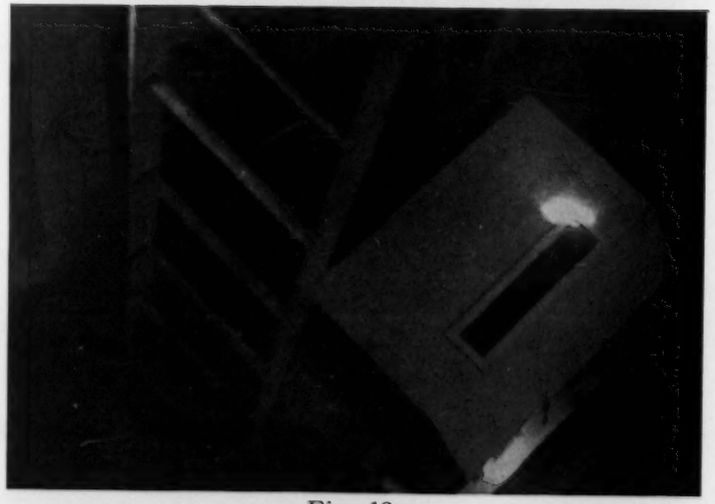

Fig. 12.

——所　　報——

◎談話会記事

第 383 回談話会 (昭和 35 年 12 月 20 日)

1. 水分を含んだ砂粒中の縦波の速度について　桃井高夫
2. コロンビア型地震計による表面波の観測（第 7 報）ラブ波の分散　三東哲夫
3. 火砕流堆積物の機械的組成　村井勇
4. 三原山の地球磁気学的研究（第 9 報）
   1958～1960 年の偏角変化の連続観測プロトン磁力計による三原山の磁気測量　行武毅・棚岡巌
5. 伊豆大島熔岩の古地磁気学的研究による地球磁場の変動　行武毅
6. 降下火山灰の変朽度について　小坂丈予
7. 岩手火山におけるガス及び湧水の化学成分　野口喜三雄・後藤達夫・一国正己
8. 携帯用長周期地震計の試作　序報　辻浦賢
9. 地球熱学　第 7 報
   海底地殻熱流量測定装置の試作と実験　上田誠也・宝来帰一・棚岡巌・友田好文・金森博雄（力武所員紹介）

第 384 回談話会 (昭和 36 年 1 月 24 日)

1. 御母衣爆破地震動の観測（その 1）
   「地震動観測結果」　爆破地震動研究グループ代表者 松沢武雄
2. 御母衣爆破地震動の観測（その 2）
   「日本中央部の地殻構造」　三雲健・大塚道男・宇津徳治・寺島敦・岡田惇
3. 強震時の建物振動性状（序報）　金井清
4. 強震の振動特性 第 2 報
   （アメリカ合衆国における常時微動測定結果との比較）　金井清・田中貞二

第 385 回談話会 (昭和 36 年 2 月 28 日)

1. 静岡県御前崎沖（御前岩）における波浪観測（序報）　高橋竜太郎・羽鳥徳太郎
2. 津浪スペクトルの研究
   1. ウエーブアナライザーの製作
   2. 江の島津浪観測所で観測された津浪及び常時長波の周期分析
   3. 日本各地で観測されたチリ地震津浪の周期分析

   高橋竜太郎・相田勇
3. 南極昭和基地における脈動観測（その 3）　村内必典

4. チリ地震のさいに京都でえられた重力計記録の周期分析 — 西村英一・中川一郎・竹内均・斎藤正徳（萩原所員紹介）

5. レーリー波位相速度法による日本の地下構造の研究 第1報 気象庁ウィーヘルト地震計網による研究 — 安芸敬一

6. 褶曲境界面における弾性波の反射・屈折 その3 P波入射の場合 II — 浅野周三

7. 杭打による地盤震動 — 金井清・田中貞二・吉沢静代

8. 長岡地震調査概報 — 河角広・大沢胖・柴野睦郎

追加 Vibrational Characteristic of a Layer which Has Non-uniform Thickness. — Silva Ainadjian

第 386 回談話会 (昭和 36 年 3 月 28 日)

1. 表面波に関する一つの問題 — 金井清

2. 岩石強度の寸法効果 (岩石と地殻の強度の比較についての一考察) — 茂木清夫

3. 昭和 36 年 2 月 27 日日向灘地震調査概報 — 岸上冬彦・小牧昭三・黒木義弘

4. 1961 年 2 月 27 日日向灘地震に伴つた津浪について — 高橋竜太郎・羽鳥徳太郎

5. 長岡地震における家屋の震害について (その 1 概報) — 大沢胖・山本正勝

追加 均質なマントルとコアよりなる弾性球の振動 第1種の振動 — 佐藤泰夫・松本利松（代読山口林造）

第 387 回談話会 (昭和 36 年 4 月 25 日)

1. 褶曲境界面における弾性波の反射・屈折 その4 SV 波入射の場合 I — 浅野周三

2. 長岡地震における家屋の震害について (その 2) 作用震度の推定 — 大沢胖

3. 海底地震計の設計 — 岸上冬彦・黒木義弘

4. 地震観測用自動利得調整増幅器 — 松本英照

追加 Vibrational Characteristic of a Layer which Has Non-uniform Thickness (Part II). — Silva Ainadjian

第 388 回談話会 (昭和 36 年 5 月 23 日)

1. 表面波に関する一つの問題 (続報) — 金井清

2. 長岡地震による地盤変動 (概報) — 岡田惇

3. 伊豆大島における火山活動と地磁気変化について　上田誠也
4. 岩石の熱衝撃破壊について　上田誠也・藪武夫
5. 爆破点近傍における岩盤の振動　表俊一郎・山崎良雄・小牧昭三・中島直吉・上野昭穂

第 389 回談話会 (昭和 36 年 6 月 27 日)

1. 最小自乗法によつてきめた係数相互の関係について　安芸敬一
2. パンチカードによる観測データの整理について　萩原尊礼・茅野一郎
3. 表面波が同じ分散性を示す地区を見出す一つの試みについて (附. 香港及びハワイで記録されたレーリー波の分散)　三東哲夫
4. 浅発地震と隆起変動　岡田惇
5. 本学構内深井戸の水位変化　山口林造
6. 長岡地震地域の重力測定　実川顕一・田島広
7. 地上及び地下における地震動の比較観測　嶋悦三
8. 建築物の固有周期と減衰係数　金井清・吉沢静代
9. 霧島火山に発生する地震　水上武郎・平士務・宮崎
10. 箱根火山における一, 二の観測　水上武郎・平士務・宮崎

CORRIGENDUM

In the Bulletin of the Earthquake Research Institute, Vol. 39, Part 2, June, 1961;

Page	Line		Read
133	5	Received April 30, 1961	Received March 31, 1961
285	5	Received June 30, 1961	Received March 31, 1961
327	6	Received June 30, 1961	Received March 31, 1961.

正　　誤

地震研究所彙報　第 39 号　第 2 冊　昭和 36 年 6 月で

頁	行	誤	正
133	5	Received April 30, 1961	Received March 31, 1961
285	5	Received June 30, 1961	Received March 31, 1961
327	6	Received June 30, 1961	Received March 31, 1961

に訂正して下さい．

昭和36年8月20日印刷
昭和36年8月25日発行

東京都文京区本富士町一番地
東京大学構内
編纂兼
発行者　東京大学地震研究所

東京都新宿区山吹町一八四番地
印刷者　笠井康頼

東京都新宿区山吹町一八四番地
印刷所　株式会社国際文献印刷社

売捌所
東京都中央区日本橋通三丁目六番地
丸善株式会社

Sold by Maruzen Co., Ltd., Nihonbashi-dôri, Chûô-ku, Tôkyô.
Price of this copy: 783 Yen. (Postage exclusive.)